BIODIESEL PRODUCTION USING SUPPORTED 12-TUNGSTOPHOSPHORIC ACID AS SOLID ACID CATALYSTS

A Thesis Submitted to the College of

Graduate Studies and Research

In Partial Fulfillment of the Requirements

For the Degree of Doctor of Philosophy

In the Department of Chemical and Biological Engineering

University of Saskatchewan

Saskatoon

By

CHINMOY BAROI

PERMISSION TO USE

In presenting this thesis in partial fulfilment of the requirements for a Postgraduate degree from the University of Saskatchewan, I agree that the Libraries of this University may make it freely available for inspection. I further agree that permission for copying of this thesis in any manner, in whole or in part, for scholarly purposes may be granted by Dr. Ajay K. Dalai who supervised my thesis work, or in his absence, by the Dean of the College of Engineering. It is understood that any copying or publication or use of this thesis or parts thereof for financial gain shall not be allowed without my written permission. It is also understood that due recognition shall be given to me and to the University of Saskatchewan in any scholarly use which may be made of any material in my thesis.

Requests for permission to copy or to make other use of material in this thesis in whole or part should be addressed to:

Head of the Department

Department of Chemical and Biological Engineering

University of Saskatchewan

57 Campus Drive

Saskatoon, Saskatchewan

Canada S7N 5A9

ABSTRACT

Biodiesel has achieved worldwide recognition for many years due to its renewability, lubricating property, and environmental benefits. The abstract represents a summary of all the chapters of the thesis. The research chapters are defined as research phases in the abstract. The thesis starts with an introduction followed by literature review. In the literature review, all the necessary data were collected reviewing the literature. Then an artificial neural network model (ANN) was built based on the published research data to capture the general trends or to make predictions. Both catalyst properties and reaction conditions were trended and predicted using the network model. The review study revealed that esterification and transesterification required catalysts with slightly different properties. In the first phase of the study, biodiesel production using 12-Tungstophosphric acid (TPA) supported on SBA-15 as a solid acid catalyst was studied. In this phase of the study, a large number of 0-35% TPA on SBA-15 catalysts were synthesized by impregnation method and the effects of various operating conditions such as– catalyst wt.% and methanol to oil molar ratio on the transesterification of model feedstock Triolein were studied. A 25% TPA loading was found to be the optimum. A 4.15 wt.% catalysts (based on Triolein) and 39:1 methanol to Triolein molar ratio was found to be the optimum reaction parameter combination, when the reaction temperature was kept fixed at 200°C, stirring speed of 600 rpm and 10 h reaction time. The biodiesel yield obtained using this condition was 97.2%. In the second phase of the study, a 12-Tungstophosphoric acid (TPA) was supported by using organic functional group (i.e. 3-aminopropyltriethoxysilane (APTES)) and was incorporated into the SBA-15 structure. A 45 wt.% TPA incorporated SBA-15 produced an ester with biodiesel yield of 97.3 wt.%, when 3 wt.% catalyst (based on the green seed canola (GSC) oil) and 25.8:1 methanol GSC oil molar ratio were used at 200^0C for reaction time of 6.2 h. In the third phase, process sustainability (i.e. process economics, process safety, energy efficiency, environmental impact assessment) studies were conducted based on the results obtained in phase three. Based on the study, it was concluded that heterogeneous acid catalyzed process had higher profitability as compared to the homogeneous acid catalyzed process. Additionally, it was obtained that heterogeneous acid catalyzed process was safe, more energy efficient and more environment friendly than homogenous process. In the fourth phase, the catalytic activity of Tungsten oxide (WO_3) and TPA supported (by impregnation) on H-Y, H-β and H-ZSM-5 zeolite catalysts were tested for biodiesel production from Green Seed Canola (GSC) oil. In this phase

of the study, TPA/H-Y and TPA/H-β zeolite were proved to be effective catalysts for esterification and transesterification, respectively. A 55% TPA/H-β showed balanced catalytic activity for both esterification and transesterification. It yielded 99.3 wt.% ester, when 3.3 wt.% catalyst (based on GSC oil) and 21.3:1 methanol to GSC oil molar ratio were used at 200°C, reaction pressure of 4.14 MPa and reaction time of 6.5 h. Additionally, this catalyst (55% TPA/H-β) was experimented for etherification of pure glycerol, and maximum conversion of glycerol (100%) was achieved in 5 h at 120°C, 1 MPa, 1:5 molar ratio (glycerol: (*tert*-butanol) TBA), 2.5% (w/v) catalyst loading. Later, these conditions were used to produce glycerol ether successfully from the glycerol derived after transesterification of green seed canola oil. A mixture of GSC derived biodiesel, and glycerol ether was defined as biofuels. In the fifth phase, catalytic activity of H-Y supported TPA (using different impregnation methods) was studied in details further for esterification of free fatty acid (FFA) of GSC oil. From the optimization study, 97.2% FFA (present in the GSC oil) conversion was achieved using 13.3 wt.% catalyst, 26:1 methanol to FFA molar ratio at 120°C reaction temperature and 7.5 h of reaction time. In the sixth- and final phase, techno-economic and ecological impacts were compared between biodiesel and combined biofuel production processes based on the results obtained in phase four. Based on the study, it was concluded that, biodiesel production process had higher profitability as compared to that for combined biofuel production process. Additionally, biodiesel production process was more energy efficient than combined biofuel production process. However, combined biofuel production process was more environment-friendly as compared to that for biodiesel production process.

ACKNOWLEDGMENT

This thesis would have not been possible without guidance and assistance of several individuals who one way or the other appreciably contributed to the completion of this thesis.

I would like to convey my earnest and sincere indebtedness to my supervisor, Dr. Ajay K. Dalai not only for his valuable guidance, encouragement, and support but also for giving me an opportunity to produce research work during the course of my Ph.D. program.

I cordially thank my advisory committee members, Dr. J. Soltan, Dr. C. Niu, Dr. R. Evitts, and Dr. S. Foley, for their valuable comments which helped to improve the quality of this thesis. I appreciate technical assistance and precious discussions from visiting professors (Dr. Alberto Navajos, Dr. Kalpana Maheria) and my colleagues at the Catalysis and Chemical Reaction Engineering Laboratories as well as technicians (R. Blondin, H. Eunike) and secretaries (J. Horosko, K. Bader, D. Cekic) in the Department of Chemical and Biological Engineering, University of Saskatchewan.

I would like to thank Dr. X. Cui and Dr. N. Chen (Scientists, Canadian Light Source Inc., Canada) for their guidance, technical help and suggestions in performing the XPS and EXAFS studies.

The financial supports from the Natural Science and Engineering Council of Canada (NSERC), Agriculture and Biomass Innovation Network (ABIN) and Canada Research Chair (CRC) are acknowledged.

My deepest indebtedness goes to my parents for their everlasting love and support that helped me to overcome obstacles during the course of my Ph.D. study. Last but not the least; I warmly thank my wife Smriti for her continuous love and friendship that always rejuvenate my spirit.

TABLE OF CONTENTS

LIST OF TABLES

LIST OF FIGURES

LIST OF ABBREVIATION

ANN	Artificial Neural Network
APTES	3-Amionopropyl trietoxysilane
CCD	Central Composite Design
C_{WP}	Weisz–Prater constant
CRW	Chemical Reactivity Worksheet
DFT	Density Function Theory
DTBG	Di- *tert*- butyl glycerol ethers
DG	Diglycerides
FFA	Free Fatty Acid
F.W.	Formula Weight
FWHM	Full Width Half Maximum
FAME	Different methyl esters (product)
FAME.S	Chemisorbed different methyl esters
G	Glycerol
G.S	Chemisorbed glycerol
GSC	Green seed canola
HAZOP	Hazard and Operability Study
h	Plank constant
HPA	Heteropoly acid
IRR	Internal Rate of Return
M	Reactant species M – methanol
M.S	Chemisorbed M
MTBG	Mono-*tert*- butyl glycerol ethers
NPV	Net Present Value
P&ID	Piping and Instrumentation Diagram
P123	Non-ionic co-polymer
Sh	Sherwood number
TBA	Tertiary Butyl Alcohol
TEOS	Tetra ethyl ortho silicate

TPA	12-Tungstophosphoric acid
TTBG	Tri- *tert*- butyl glycerol ethers
TG	Reactant species triglycerides
TG.S	Chemisorbed triglycerides
TG_i	Reactant species different triglycerides (i.e. Triolein, Linolein)
TG_i.S	Chemisorbed different triglycerides
WAR	Waste Reduction Algorithm
X_{TGi}	Fractional conversion of TG_i
X_G	Fractional conversion of glycerol
θ	Porosity
τ	Tortuosity
k_B	Boltzman constant

NOMENCLATURE

C_{oil}, C_{FAME}	Concentration of oil and FAME (mol/L)
C'_{TG}, C'_{MeOH}	Concentration of TG and MeOH (mol/g cat.)
C_M, C_{TGi}	Concentration of M and TG_i (mol/L)
C_{M0}, C_{TGi0}	Initial concentration of M and TG_i (mol/L)
C_{TGiS}	Concentration of TG_i at solid (catalyst) surface (mol/L)
D	Diametr of the impeller (m)
$D_{oil,MeOH}$	Diffusion coefficient of oil in Methanol (m^2/s)
D_P	Diameter of catalyst particle (m)
$D_{TGi,M}$	Diffusion coefficient of TG_i in M (m^2/s)
D_e	Effective diffusivity (m^2/s)
$\Delta G^{\ddagger}$	Gibb's free energy of activation (kJ/mol)
$\Delta H^{\ddagger}$	Enthalpy of activation (kJ/mol)
K_1	Equilibrium constant for adsorption of TG_i on the catalyst surface (L/mol)
K_2	Equilibrium constant for adsorption of M on catalyst surface (L/mol)
K_{SR}	Equilibrium constant for surface reaction (dimensionless)
k_{SR}	Surface reaction rate constant for forward reaction (g. Cat^2/mol. L. s)
k'_{SR}	Surface reaction rate constant for reverse reaction (g. Cat^2/mol. L. s)
K'_{ME}	Equilibrium constant for desorption of ME on catalyst surface (mol/L)
K_{ME}	Equilibrium constant for adsorption of ME on catalyst surface (L/mol)
K'_G	Equilibrium constant for desorption of G on catalyst surface (mol/L)
K_G	Equilibrium constant for adsorption of G on catalyst surface (L/mol)
kc_{TGi}	Mass transfer coefficients (m/s)
k_1	Forward reaction rate
k_2	Backward reaction rate
K	Equilibrium constant (dimensionless)
kc_{oil}	Mass transfer coefficients (m/s)
K_1	Equilibrium constant for adsorption of TG on catalyst surface (g cat./mol)
k_S	Surface reaction rate constant for forward reaction (g cat./mol. s)
K_G	Equilibrium constant for adsorption of G on catalyst surface (L/mol)
N	Rotational speed of the impeller (rps)

R_p	Radius of catalyst particle (m)
$-r_{TGi}$	Rate of disappearance of TG_i (mol/L. s)
r_{obs}	Observed rate of reaction (mol /L. s)
R_p	Radius of catalyst particle (m)
$-r_{oil}$	Rate of disappearance of oil (mol/L. s)
$-r'_{oil}$	Rate of disappearance of oil (mol/g cat. s)
$-r''_{oil}$	Rate of disappearance of oil (mol/m^2. s)
$\Delta S^{\ddagger}$	Entropy of activation (J/mol. K)
w	Catalyst loading (g cat./L of liquid phase)
W_{TGir}	Molar flux of triglycerides (mol/m^2. s)
W_{oil}	Molar flux of oil (mol/m^2. s)
ρ_p	Density of catalyst particle (g/cm^3)
μ	Viscosity of reaction mixture (kg/m.s)

CHAPTER 1: INTRODUCTION AND RESEARCH OVERVIEW

1.1 Introduction

Biodiesel is a renewable, diesel substitute fuel. This fuel is produced from triglycerides (major constituents of oils or fats) using lower alcohol through transesterification reaction. The other name of transesterification is alcoholysis because in this process one alcohol is replaced by another i.e. the higher alcohol (glycerol) present in the triglyceride (TG) is replaced by a lower alcohol (e.g. methanol, ethanol). The resultant monoalkyl esters (i.e. methyl ester) of fatty acids are called biodiesel.

Biodiesel is produced from vegetable oils and fats (e.g. rapeseed, soybean, sunflower, coconut, palm oil). Biodiesel yet cannot compete with the diesel because of its higher production price. The higher price is associated with the production cost, and 88% of the total production cost is related to the feedstock price (Kulkarni and Dalai, 2006; Marchetti and Errazu, 2008). The biodiesel production cost can be optimized by exploring cheap and low quality feedstocks (e.g. used cooking oil, yellow grease, green seed canola oil), which contain considerable amounts of free fatty acids (FFA) (4-40 wt.%). Acid catalysts catalyze esterification along with the transesterification reaction to produce similar type of esters from free fatty acids using alcohol.

Homogeneous acid catalysts can be used for this purpose, but solid acid catalysts are favored over those for waste minimization and easy product recovery (Kulkarni et al., 2006). Mesoporous solid acids catalysts with a moderate to strong acid sites and a hydrophobic surface are desireable for the biodiesel preparation (Lotero et al., 2005; Kiss et al., 2006).

Among the solid acids, heteropoly compounds show strong Brønsted acidity which are commonly known as heteropoly acids (HPA) (Busca, 2007; Okuhara et al., 2000), especially, $H_3PW_{12}O_{40}$ (TPA) possesses strong Brønsted acidity and higher thermal stability as compared to other HPA compounds (Kozhevnikov, 2007). The disadvantages of using this heteropoly acid are lower surface area (1 – 10 m^2/g) and polar solvent solubility (Kulkarni et al., 2006). These problems may be bypassed supporting $H_3PW_{12}O_{40}$upon various carriers. Details of TPA structure, supports, catalyst structure, and reaction conditions of biodiesel production are discussed in literature review section of the thesis.

1.2 Research overview

The overall objective of the Ph.D research was to develop TPA based heterogeneous (solid) acid catalysts to produce biodiesel. Different TPA based heterogeneous (solid) acid catalysts were synthesized with the help of different supports (e.g. SBA-15, zeolites) and their structure was analyzed. Besides, the reaction parameters effects on biodiesel production processes were also analyzed and optimized. In one of the studies, the biodiesel production process has been extended to the combined biofuel (biodiesel + glycerol-ether as fuel additives) production. Additionally, process economics, process safety, environmental impact and process energy efficiency of each process were assessed. The overall research is divided into six phases which are discussed in chapter 3 to chapter 8. In the chapter 3, Triolein (a model compound representation oil) was exploited to analyze the catalytic activity of SBA-15 supported TPA as a solid acid catalyst. This was a base-line study. In the Chapter 4, the feasibility of simultaneous esterification, transesterification and chlorophyll removal were studied using novel catalysts. In the Chapter 5, process sustainability (i.e. process economics, process safety, energy efficiency, environmental impact) of heterogeneous and homogeneous acid catalyzed simultaneous esterification, transesterification and chlorophyll removal were studied and compared. In the Chapter 6, catalytic activity of different acidic zeolite catalyzed combined biofuel (biodiesel + glycerol-ether as an additive) production process was studied. In Chapter 7, the catalytic activity of H-Y zeolite in esterification of FFA was studied. In the Chapter 8, techno-economic and ecological impacts were compared between biodiesel and combined biofuel production processes. The major conclusions from the entire research work are given in chapter 9.

CHAPTER 2: LITERATURE REVIEW

A version of this chapter has been published in the following journal and presented in the following conference:

- Chinmoy Baroi, Ajay K. Dalai. Review on biodiesel production from various feedstocks using 12-Tungstophosphoric acid (TPA) as a solid acid catalyst precursor. Industrial and Engineering Chemistry Research, July 2014.
- Chinmoy Baroi, Ajay K. Dalai.Data Mining Study of 12-Tungstophosphoric Acid (TPA) Precursored Solid Acid Catalyzed Biodiesel Production. 64th Canadian Chemical Engineering Conference. Niagara Falls, Ontario, Canada, 19-22 October, 2014.

Contribution of the Ph.D. Candidate

The literature review and the Artificial Neural Network (ANN) model development were conducted by Chinmoy Baroi. The content in this chapter was written by Chinmoy Baroi with discussions and suggestions provided by Dr. Ajay Dalai.

Contribution of this Chapter to the Overall Ph.D. Research

This chapter contains the literature review and the results obtained through the Artificial Neural Network (ANN) model. The ANN model results helped to develop the overall research (see section 1.2) and to predict the catalytic activity of different TPA based catalysts both in esterification and transesterification.

2.1 Abstract

Solid acid catalysts are an important class of catalysts due to their applications in various organic reactions. A 12-Tungstophosphoric acid (TPA) is a member of heteropoly acid (HPA) compounds, which grabbed attentions due to its low volatility, low corrosivity, higher activity and acidity compared to sulfuric acid. However, the major problems of using TPA are its solubility in polar media and its lower surface area. Therefore, various techniques are applied to use it as heterogeneous catalysts. Biodiesel is a diesel replacenment fuel, which is produced from various renewable feedstocks through transesterification and/ or esterification reactions. Acid catalysts can be utilized to catalyze both transesterification and esterification reactions. For this

reason, research has been conducted to study various TPA precursory heterogeneous (solid) acid catalysts catalytic activity for biodiesel production. In this review paper, a pattern recognition technique has been applied to extract valuable information from the previously published literature. For this purpose an Artificial Neural Network (ANN) model has been developed using the published data to capture the general trends or to make predictions. Both catalyst properties and reaction conditions are trended and predicted using the network model.

2.2 Introduction

The near zero sulfur content and renewability make vegetable oils an excellent source of diesel substitute renewable fuel feedstock. Vegetable oils have higher viscosity, flash points, cloud points and pour points due to their large molecular structure (Srivastava and Prasad, 2000). Vegetable oils mainly consist of esters. These esters are odorless and nonvolatile, but possess all the characteristic properties of general ester compounds. Vegetable oil esters are composed of trihedral alcohol-glycerol combined with organic fatty acids, which belong to the aliphatic straight-chain type, with few exceptions. These organic acids have an even number of carbon atoms per molecule, usually in the range between 8 and 24. In addition to these esters, there are some minor constituent present which are phospholipids, sterols, vitamins, antioxidants, pigments, free fatty acids and hydrocarbons. The other name of oil is triglyceride, because, in the oil, glycerol is esterified with three equivalents of fatty acids. These fatty acids may be of the same acid or three different acids attached with the same molecule of glycerol. In the fats or oils, glycerol may be esterified with one or two equivalents of fatty acids called mono or di-glycerides. Vegetable oils are mixtures of mixed triglycerides (one molecule of glycerol is attached with three different fatty acids) (Eckey and Millar, 1954). Fatty acid present in the triglyceride are of different types. These naturally occurring fatty acids may be saturated or unsaturated. Fatty acids having one or more double bond in their structure are called unsaturated fatty acids. Generally, these fatty acids are expressed in terms of shorthand notation (x: y system); where x represents the carbon atom numbers present in the acid chain and y represents the number of double bond present in the carbon chain (Hoffman, 1989).

The higher viscosity, molecular weight and bulky chemical structure of vegetable oil limits its application as a diesel engine fuel. Thus, vegetable oil is used as a feedstock for

producing renewable fuels including biodiesel, whose properties are similar to those for diesel fuel.

2.3 Biodiesel production process

Biodiesel is produced from different vegetable oils mainly through transesterification. The other name of transesterification is alcoholysis because in this process one alcohol is replaced by another i.e. the higher alcohol (glycerol) present in the triglyceride (TG) is replaced by a lower alcohol (i.e. methanol, ethanol) and the resultant monoalkyl esters of long carbon chain fatty acids are called biodiesel. Three consecutive and reversible reaction steps are believed to occur in the transesterification process. The first step of transesterification is to convert the triglycerides (TG) into diglycerides (DG), then to convert the diglycerides (DG) to monoglyceride (MG), and of monoglyceride to glycerol, which generates three moles of methyl ester from one mole of triglyceride (Abbaszadeh et al., 2012). The detailed reaction is given in equations 2.1-2.3 (Gerpen and Knothe, 2005).

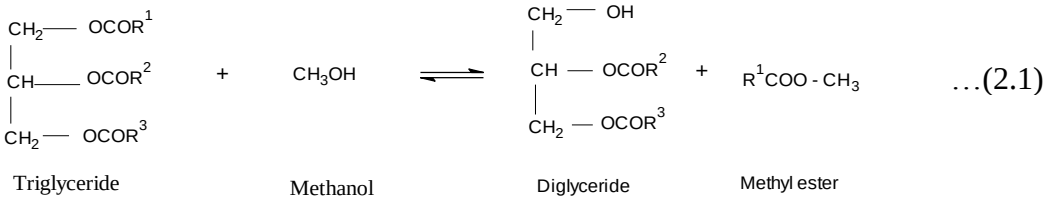

…(2.1)

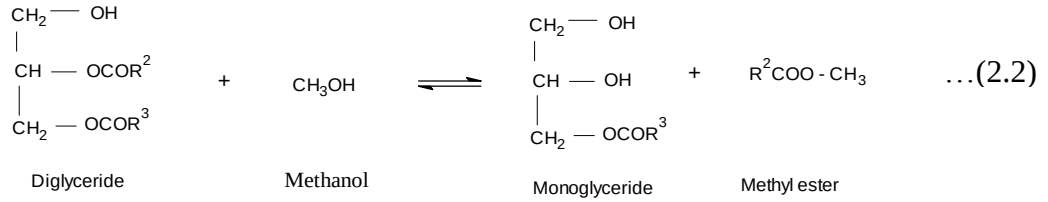

…(2.2)

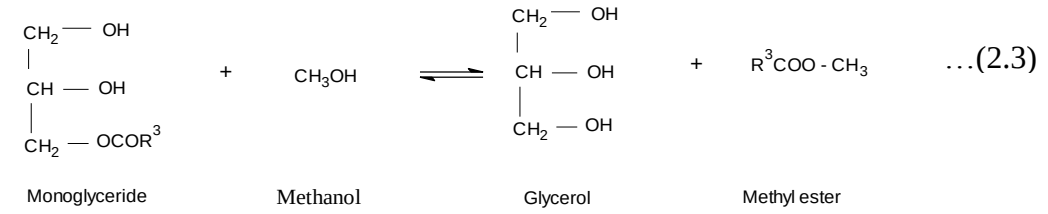

…(2.3)

As the stepwise reactions are reversible, a molar excess of alcohol is utilized to shiftthe equilibrium towards the ester formation according to the Le Chatellier's principle (Veljkovic, 2012). Although transesterification is a reversible reaction, in the final step when glycerol is

formed, the reverse reaction does not take place or is very negligible because it is not miscible with the product biodiesel.Thus, glycerol formation creates a two-phase system (Gerpen and Knothe, 2005).

Most of the commercial transesterification reaction is conducted with homogeneous alkaline catalysts, because of their faster reaction ratesas compared to the homogeneous acid catalyzed reaction (Srivastava and Prasad, 2000). One of the problems of the base catalyzed reaction is the soap formation as an undesired reaction between free fatty acids (FFA) and bases, which consumes some of the base. Thus, the base available for catalyzing the reaction is reduced. The biodiesel production processis not affected significantly upto the 3% FFApresence in the feedstock but if the oil contains more than 5% FFA, the separation of glycerol from the methyl esters is inhibited by soap (Gerpen and Knothe, 2005). The main problem of commercial biodiesel production is the high price of treated feedstock or pretreatment of the feedstock that causes a higher price of the biodiesel. Estimation depicts that approximately 88% of the total production cost is associated with the feedstock (Marchetti and Errazu, 2008). This cost can be reduced by using cheaper feedstocks i.e. used cooking oil, yellow grease, etc. which contain high free fatty acids. Enzyme catalysts and acid catalysts can play a significant role in biodiesel production process. These enzyme or acid catalysts can catalyze esterification reaction using alcohol to produce similar type of ester from free fatty acids, which is depicted in equation 2.4 (Gerpen and Knothe, 2005).

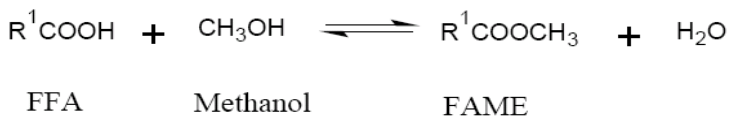

…(2.4)

Enzymes are bio-catalysts, which offer a biological route of biodiesel production. The major problems of enzyme-catalyzed biodiesel production process are high cost of enzymes, low conversion efficiency, rapid deactivation of enzymes and thermal instability of enzymes (Christopher, 2014).

Acid catalysts are free from these problems. Though homogeneous acid catalyst can serve this purpose, it causes severe corrosion problem to the equipment, and also lead to environmental problems. Thus, solid acid catalysts are point of interests in producing biodiesel from different feedstocks as they can catalyze esterification and transesterification reactions in producing biodiesel (Kulkarni et al., 2006). The overall reaction mechanism of heterogeneous

(solid) acid catalyzed esterification and transesterification reaction are depicted in Figure 2.1. The free fatty acids (RCOOH) and methanol (CH_3OH) take part in esterification reaction, whereas glycerides (RCOOR') and methanol take part in the transesterification reaction. The carbonyl oxygen of free fatty acid or glyceride interacts with the acidic site of the catalyst to form carbocation. Then a tetrahedral intermediate is produced by the nucleophilic attack of alcohol to the carbocation. In the esterification reaction, this tetrahedral intermediate formation generates one mole of water during rearrangement and formation of one mole of ester ($RCOOCH_3$), and in case of transesterification the tetrahedral intermediate only rearranges and forms one mole of similar ester to that of the esterification reaction (Kulkarni et al., 2006). It is found that esterification reactions are faster than transesterification reaction (Ataya et al., 2007). Water is one of the products of the esterification reaction.

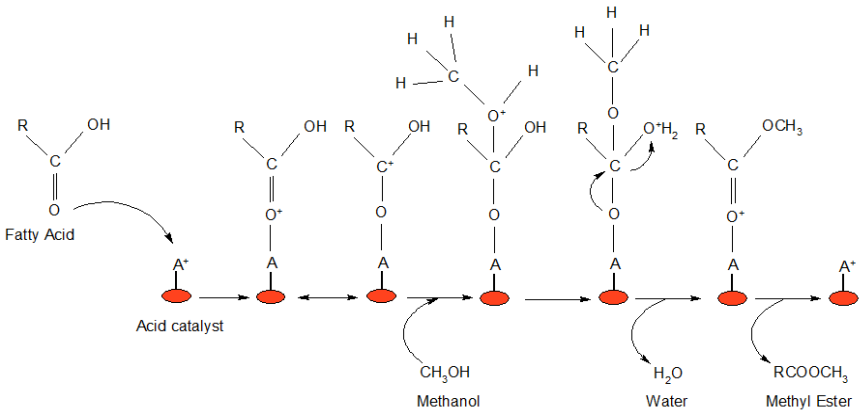

Fig. 2.1(a) Reaction mechanism of acid catalyzed esterification reaction

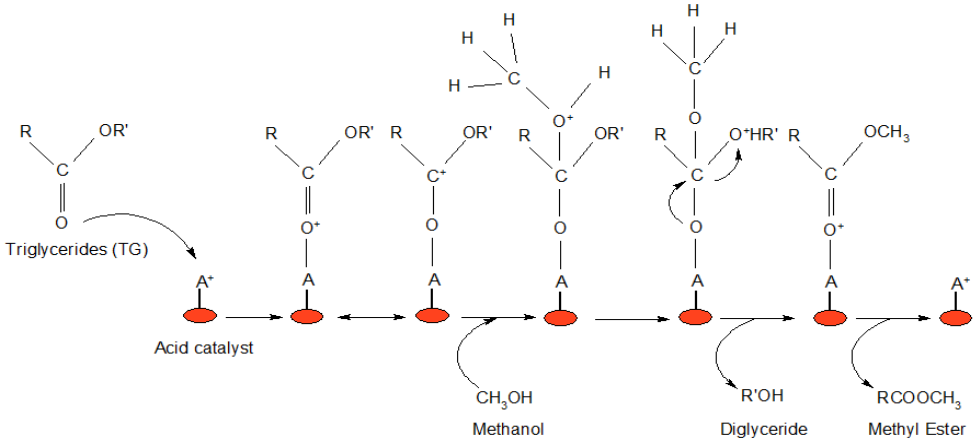

Fig. 2.1(b) Reaction mechanism of acid catalyzed transesterification reaction

According to Lotero et al. (2005), the presence of water molecules affects the TG accessibility to the catalysts and inhibits the reaction (Di Serio et al, 2007). It is found that homogeneous Brønsted acid catalysts are mainly active in the esterification and homogeneous Lewis acid catalysts are mainly active in the transesterification (Di Serio et al, 2007). In the case of heterogeneous catalysts, support structure, active species concentration, support-active species interaction determines the catalytic activity and acidity.

2.4 TPA (12-Tungstophosphoric acid) as heterogeneous catalysts precursor

A 12-Tungstophosphoric acid (TPA) belongs to the heteropoly acid (HPA) compounds. HPA compounds may have different structures. However, the most of the catalytic applications use Keggin structure type HPA compounds for acid catalysis. The Keggin HPAs consists of heteropoly anions of the formula $[XM_{12}O_{40}]^{n-}$, where X represents the heteroatom (P^{5+}, Si^{4+}, etc.) and M represents the adjunct atom (Mo^{6+}, W^{6+}, etc.). The Keggin anion structure is composed of a central tetrahedron XO_4 surrounded by 12 edge- and corner-sharing metal-oxygen octahedral MO_6 (Kozhevnikov, 2007; Kozhevnikov, 2009). Heteropoly acids show strong Brønsted acidity (Busca, 2007; Okuhara et al., 2000), especially, 12-Tungstophosphoric acid (TPA) which possesses super acidity (Brønsted acidity) and higher thermal stability as compared to other HPA (Kozhevvnikov, 2007). In TPA the Keggin structure is consists of a central PO_4 tetrahedron, surrounded by 12 WO_6 octahedra (Fig. 2.2). The formula of the heteropoly anion in TPA is $[PW_{12}O_{40}]^{3-}$. The net -3 charge of heteropoly anion requires three cations for electroneutrality. The Brønsted acidity arises when the three protons (H^+) neutralize the net -3 charge of the heteropoly anion by acting as cations (Yadav, 2005).

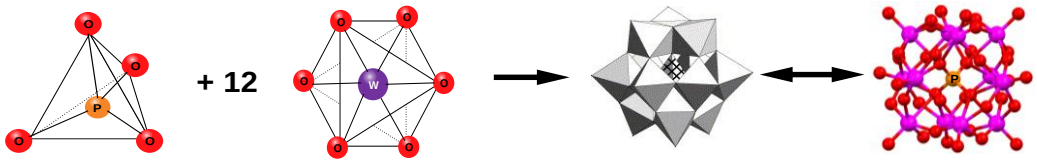

Fig. 2.2 Keggin structure of heteropoly anion $(PW_{12}O_{40})^{3-}$ of TPA

Generally, TPA exists in hydrate form with a chemical formula of $H_3PW_{12}O_{40}.nH_2O$. The physisorbed water (Fig. 2.3) from TPA is removed, when it is heated to 100°C, and the removal process is reversible. This heating leaves 6 moles of water (n=6) per Keggin unit, and the TPA exists in the pseudo-liquid phase (Kozhevnikov, 2007; Kozhevnikov, 2009; Uchida et al., 2000).

At this point, all the Keggin units are equally hydrogen bonded by $H_5O_2^+$ cations (Fig. 2.3). If the heating is continued, when $n \leq 1.5$, all the Keggin units are equally hydrogen bonded by H_3O^+ cations instead of by $H_5O_2^+$cations (Uchida et al., 2000). All the crystal water is removed ($n = 0$) at 200°C, causing 3 acidic protons per Keggin unit, and the pseudo-liquid phase to disappear. All these acidic protons are removed at 450°C, leaving anionic heteropoly Keggin unit. Finally, this Keggin structure decomposes into tungsten oxide (WO_3) and phosphorus pentoxide (P_2O_5) (Kozhevnikov, 2007; Kozhevnikov, 2009).

The disadvantages of using TPA in its bulk form are that they are soluble in polar media-creating problems related to homogeneous catalysis, and they have a lower surface area (1 – 10 m^2/g) (Kulkarni et al., 2006; Yadav, 2005). This lower surface area reduces the accessibility of the protons to the reactants, especially if the reactants are non-polar.

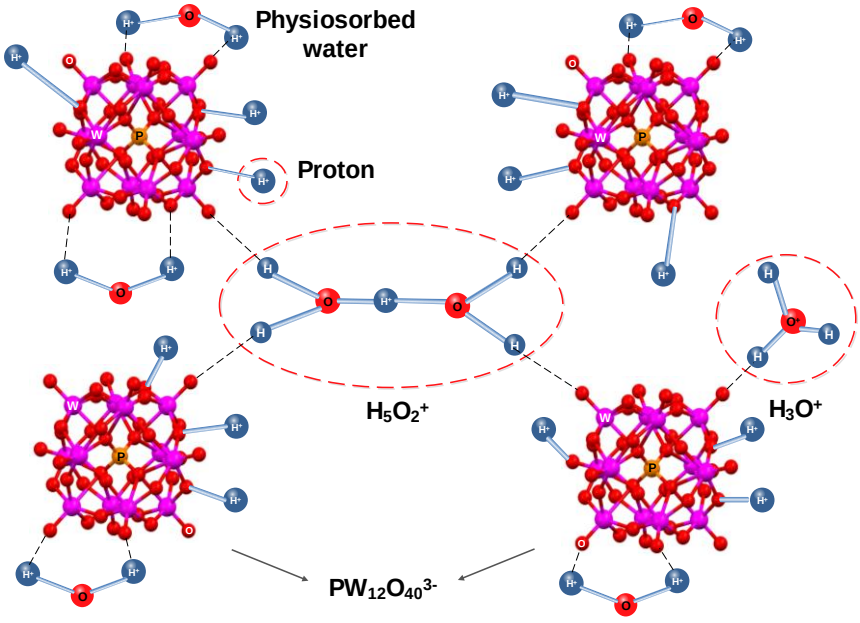

Fig. 2.3 Protonic species present in $H_3PW_{12}O_{40}.nH_2O$

The problems associated with using bulk form TPA can be avoided by supporting $H_3PW_{12}O_{40}$ on various support carriers. The protons of TPA interact with the support surface hydroxyl groups either by ligand exchange mechanism (Fig. 2.4a) or forming surface complex by hydrogen bonding (Fig. 2.4b), once the physisorbed waters are removed at 100°C (Yadav, 2005; Wu et al., 1996).

In the ligand exchange mechanism, surface hydroxyl group (M-OH) reacts with the proton to produce water (eqn.2.5-2.7).

$$H_3PW_{12}O_{40} \rightarrow H^+ + (H_2PW_{12}O_{40})^{-1} \quad \ldots(2.5)$$

$$M\text{-}OH_{(s)} + H^+ \rightarrow MOH_2^+ \quad \ldots(2.6)$$

$$MOH_2^+ + (H_2PW_{12}O_{40})^{-1} \rightarrow MH_2PW_{12}O_{40} + H_2O \quad \ldots(2.7)$$

TPA interacts with supports such as MgO through this mechanism. However, strong interaction leading to loss of all protons may lead catalytic inactivity in some cases (Kulkarni et al., 2006; Herrera et al., 2008: Khder et al., 2008). Another mechanism involves hydrogen bonding of protonated surface hydroxyl groups with the Keggin anion to form a surface complex (eqn.2.8).

$$MOH_2^+ + (H_2PW_{12}O_{40})^{-1} \rightarrow MOH_2^+ (H_2PW_{12}O_{40})^{-1} \quad \ldots(2.8)$$

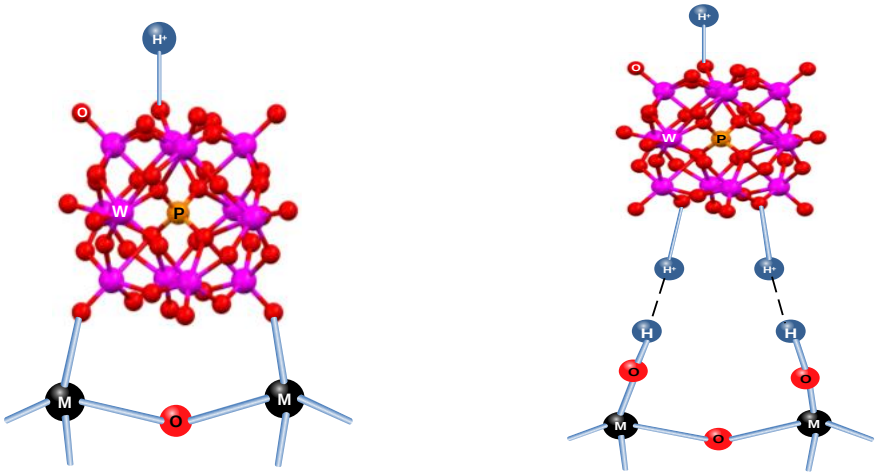

(a) Exchange mechanism (b) Hydrogen bonding mechanism

Fig. 2.4 Support-TPA interaction mechanisms

The surface complex acid strength depends on the firmness of the immobilization of the TPA with the support and the cation present in TPA. The firmness of the immobilization depends on the concentration of the TPA, concentration of the hydroxyl group and pH of the TPA containing solution (Wu et al., 1996). At a lower TPA loading, strong interactions (following exchange mechanism) between the support and Keggin ions may lead to a reduction in HPW acid (Brønsted) strength. However, if the TPA loading is increased, if exists as a mono/multi-layer and the Keggin anions are hydrogen bonded through H_3O^+ cations even at higher temperature (300°C) (McCormick et al., 1998; Thomas et al., 2005).

In some cases, the firmness of the TPA immobilization on the support is increased by a binder (e. g. zirconia, titania). In this method, the support surface is coated with a binder, which binds the TPA through weak chemical interaction (Herrera et al., 2008). Weak organic bases (e.g. APTES) are used as the binders to minimize the loss TPA acidity during immobilization (Inumaru et al., 2007).

Another approach of solving the problems of lower surface area and solubility in polar media involves converting TPA into Keggin anion water insoluble salts of large cations (e.g. Cs^+, K^+, NH_4^+ etc.), obtained by precipitation from $H_3PW_{12}O_{40}$ aqueous solution. The common formulae of these salts are $M_xH_{3-x}PW_{12}$ (M = Cs^+, K^+, NH_4^+ etc.), and these salts are micro/mesoporous solids having larger surface area (200 m^2/g) (Busca, 2007). However, the salt particles form a colloidal solution in a highly polar medium and are difficult to separate (Inumaru, 2007). This problem is avoided by entrapping the TPA salt into the support structure matrix or supporting the TPA salts on various support carriers (Yadav, 2005; Izumi, 1997; Yadav et al., 2003).

2.5 Pattern recognition algorithm for knowledge extraction

Pattern Recognition algorithm (Pattern recognition) is a branch of computer science used to extract useful information or knowledge which is very difficult to observe (Gunay and Yildirim, 2013). The purpose of the pattern recognition algorithm is to convert the real-world data into a model and analyzing the pattern using the model (Ohrenberg et al., 2005; Tally et al., 2010). The algorithm includes collection of raw data, processing of raw data, pattern discovery using algorithm (model building) and visualization of the data (Fig. 2.5) (Rothenberg, 2008).

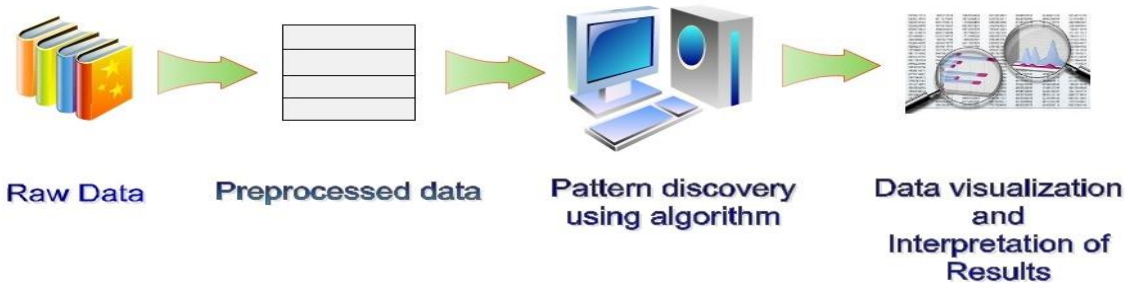

Fig. 2.5 Pattern recognition algorithm

An example of the algorithm is, a credit card issuer can collect credit and demographic data about the population of a certain geographic area. Using the historical data of the customer's

credit history, the credit card issuer can build a model of the attributes associated with "good" customers (e.g., customers that generate high profits for the credit card issuer) and seek to target new potential customers by identifying prospects with attributes similar to the good customers (Talley et al., 2010). The model can be simple linear models, such as Partial Least Square (PLS) regression or non-linear models, for example Artificial Neural Network (ANN). The ANN model can handle complicated systems, but they are "Black-Box" models. The ANN often used, when the input and output relationship is complex and difficult to explain in terms of "correlation" (Rothenberg, 2008).

2.6 Use of TPA as a solid acid catalyst precursor for biodiesel production: a pattern recognition approach

Research has been conducted for biodiesel production from various feedstocks composed of different triglycerides and fatty acids using different alcohols. TPA has been tested as a solid acid catalyst precursor to produce biodiesel from various feedstocks using different reaction conditions. However, the variations of TPA precursory catalysts, fatty acid compositions, and reaction conditions create difficulties to understand the effects of type of supports, support properties, TPA-support interactions, TG carbon chain lengths (which depends on the carbon number), TG unsaturation, FFA carbon chain lengths (which depends on the carbon number), FFA unsaturation, and reaction conditions on the biodiesel production process.

For pattern recognitionpurposes, all the literature mentioning TPA in any form as heterogeneous (solid) acid catalysts used to producevarious oils or free fatty acids derived biodiesel were outlined (Table 2.1). The least carbon number in the oil is 8 (i.e. C_8), however, in the literature review Synopsis, research with various model compounds containing carbon number from 2 (i.e. C_2) are considered to increase reliability in predictions for oils and FFAs with different carbon chain lengths (e. g. C_8, C_{10}, C_{12}), for which the research has not been conducted yet using the TPA based catalysts. While summarizing, it was found that the variation from case to case were diversified, which made the pattern recognitioncomplicated. To avoid this complex issue, based on the data outlined in Table 2.1, the support structure, TPA state, feedstock structures were converted and expressed in some sort of common mathematical formulation which was gathered in Table 2.2.

Table 2.1: Synopsis of the published research works using TPA as heterogeneous acid catalysts (cont'd)

Case No.	Support	TPA precursor	TPA loading (wt%)	Calcination Temperature (°C)	Feedstock		FFA Conc. (wt%)	Alcohol	Alcohol To feedstock ratio	Time (h)	Reaction Temperature (°C)	Cat. wt%	Conv.%[a]/Yield%[b]		Ref:
					Oil (TG)	FFA							Ester.[a]	Trans[b]	
1	HZSM-5	TPA	15	120	-	Levulinic	100	MeOH	8	4	78	4	94	0	Nadiwalea et al., 2013
2	H-β	TPA	30	100	-	Oleic	100	MeOH	20	6	60	3.54	84	0	Patel et al., 2012
3	Nb_2O_5	TPA	25	400	-	Oleic	100	MeOH	14	6	65	1.65	100	0	Srilatha et al., 2012a
4	MCM-41	$CsH_2PW_{12}O_{40}$	19.4	350	-	Palmitic	100	MeOH	15	4	85	12	92	0	Trakarnpruk, 2013
5	-	$CsH_2PW_{12}O_{40}$	-	120	-	Oleic	100	MeOH	14	4	65	5.35	92	0	Srilatha et al., 2012b
6	ZrO_2	TPA	20	300	-	Palmitic	100	MeOH	14	4	65	20	98	0	Srilatha et al., 2011
7	K-10	TPA	20	100	-	Acetic	100	BuOH	3	12	150	3.33	88	0	Bhorodwaj et al., 2011
8	Nb_2O_5	TPA	25	400	U. Oil	-	100	MeOH	18	20	200	3	0	92	Srilathaet al., 2010
9	-	$Ag_{0.5}H_2PW_{12}O_{40}$	-	120	Triacetin	-	100	MeOH	29	3	50	8.33	0	80	Zieba et al., 2010
10	-	TPPS-TPA	-	100	-	Acetic	100	BuOH	1.2	1.5	150	11	97	0	Zhang et al., 2009
11	Ta_2O_5-R	TPA	12	100	Soybean	Mystric	20	MeOH	90	24	65	2	100	100	Xu et al., 2009a
12	-	TEAPS3-TPA	-	100	-	Acetic	100	BuOH	1.2	1.5	110	11	95	0	Leng et al., 2009
13	-	TEAPS3-TPA	-	100	-	Acetic	100	EtOH	1.2	1.5	90	11	84	0	Matachowski et al., 2009
14	-	$Cs_{2.5}H_{.5}PW_{12}O_{40}$	-	120	Triacetin	-	100	EtOH	29	3	50	4.95	0	21	Matachowski et al., 2009
15	Nb_2O_5	TPA	25	400	-	Palmitic	100	MeOH	13.7	4	65	10	97	0	Srilatha et al., 2009

[a]Conversion in esterification; [b]Yield in transesterification

Table 2.1: Synopsis of the published research works using TPA as heterogeneous acid catalysts

Case No.	Support	TPA precursor	TPA loading (wt%)	Calcination Temperature (°C)	Feedstock		FFA Conc. (wt%)	Alcohol	Alcohol To feedstock ratio	Time (h)	Reaction Temperature (°C)	Cat. wt%	Conv.%[a]/Yield%[b]		Ref:
					Oil	FFA							Ester.[a]	Tran[b]	
16	Ta_2O_5-R	TPA	10	45	Soybean	Mystric	20	MeOH	15	6	170	5	100	98	Xu et al., 2009b
17	K-10	TPA	20	100	Sunflower	-	100	MeOH	29	3	65	8.33	0	37.8	Bokade and Yadav, 2009
18	-	$K_2HPW_{12}O_{40}$	-	100	Castor	-	100	MeOH	20	5	200	3	0	32	Zieba et al., 2009
19	ZrO_2	TPA	15	750	Sunflower	-	100	MeOH	15	8	170	5	0	86	Sunita et al., 2008
20	K-10	TPA	20	100	Sunflower	-	100	MeOH	30.4	24	60	0.2	100	0	Bokade and Yadav, 2007
21	-	$Cs_{2.3}H_{.7}PW_{12}O_{40}$	-	100	Tributylen	-	100	MeOH	30.4	24	60	0.2	0	82.3	Narasimharao et al., 2007
22	-	$Cs_{2.3}H_{.7}PW_{12}O_{40}$	-	100	-	Palmitic	100	MeOH	9	10	200	3	100	0	Xu et al., 2008
23	ZrO_2	TPA	20	300	GSC oil	Oleic	10	MeOH	3	3	78	3.4	100	0	Xu et al., 2008
24	Ta_2O_5	TPA	11	100	-	Lauric	100	EtOH	24	6.5	200	3.04	99.5	0	Kulkarni et al., 2006
25	SBA-15	TPA	25	450	GSC oil	Oleic	4.25	MeOH	25.84	6.25	200	2.96	92.6	97.3	Baroi and Dalai, 2013
26	H-β	TPA	55	450	GSC oil	Oleic	4.25	MeOH	21.3	6.5	200	3.3	91.9	99.4	Baroi et al., 2014

[a]Conversion in esterification ; [b]Yield in transesterification

Table 2.2: Converted published research data for ANN model building(cont'd)

Case No.	Support Tag	Flow path	CationTag	Cation No.	TPA loading (wt%)	Calcin. Temp. (°C)	FFA		Oil		FFA Conc. (wt%)	Alc. Tag	Alc. ratio	Time (h)	Temp.(°C)	Cat. wt%	Conv.%/Yield%	
							No. of Carbon	No. of Unsat.	No. of Carbon	No. of Unsat.							Ester.[a]	Trans[b]
1	0.476	3	1	3	15	120	5	2	0	0	100	1	8	4	78	4	94	0
2	0.476	3	1	3	30	100	18	1	0	0	100	1	20	6	60	3.54	84	0
3	0.699	1	1	3	25	400	18	1	0	0	100	1	14	6	65	1.65	100	0
4	0.47	2	132.9	1	19.4	350	16	0	0	0	100	1	15	4	85	12	92	0
5	1	1	132.9	1	100	120	18	1	0	0	100	1	14	4	65	5.35	92	0
6	0.74	1	1	3	20	300	16	0	0	0	100	1	14	4	65	20	98	0
7	0.63	1	1	3	20	100	2	0	0	0	100	4	3	12	150	3.33	88	0
8	0.699	1	1	3	25	400	0	0	18	1	0	1	18	20	200	3	0	92
9	1	3	107.87	0.5	100	120	0	0	2	0	0	1	29	3	50	8.33	0	80
10	1	3	556.43	3	100	100	2	0	0	0	100	4	1.2	1.5	150	11	97	0
11	0.59	2	1	3	12	100	14	0	18	1	20	1	90	24	65	2	100	100
12	1	3	224	3	100	100	2	0	0	0	100	4	1.2	1.5	110	11	95	0
13	1	3	224	3	100	100	2	0	0	0	100	2	1.2	1.5	90	11	84	0
14	1	1	132.9	2.5	100	120	0	0	2	0	0	2	29	3	50	4.95	0	21
15	0.699	1	1	3	25	400	16	0	0	0	100	1	13.7	4	65	10	97	0

Table 2.2: Converted published research data for ANN model building

Case No.	Support Tag	Flow path	CationTag	Cation No.	TPA loading (wt%)	Calcin. Temp. (°C)	FFA		Oil		FFA Conc. (wt%)	Alc. Tag	Alc. ratio	Time (h)	Temp.(°C)	Cat. wt%	Conv.%/Yield%	
							No. of Carbon	No. of Unsat.	No. of Carbon	No. of Unsat.							Ester.[a]	Trans[b]
16	0.59	2	1	3	10	45	14	0	18	1	20	1	15	6	170	5	100	98
17	0.63	1	1	3	20	100	0	0	18	2	0	1	29	3	65	8.33	0	37.8
18	1	3	40	2	100	100	0	0	18	1	0	1	20	5	200	3	0	32
19	0.74	1	1	3	15	750	0	0	18	2	0	1	15	8	170	5	0	86
20	0.63	1	1	3	20	100	0	0	18	2	100	1	30.4	24	60	0.2	100	0
21	1	1	132.9	2.3	100	100	0	0	4	0	0	1	30.4	24	60	0.2	0	82.3
22	1	1	132.9	2.3	100	100	16	0	0	0	100	1	9	10	200	3	100	0
23	0.74	1	1	3	20	300	18	1	18	1	10	1	3	3	78	3.4	100	0
24	0.81	1	1	3	11	100	12	0	0	0	100	2	24	6.5	200	3.04	99.5	0
25	0.47	2	1	3	25	450	18	1	18	1	4.25	1	25.84	6.25	200	2.96	92.6	97.3
26	0.476	3	1	3	55	450	18	1	18	1	4.25	1	21.3	6.5	200	3.3	91.9	99.4

Usually, the supportsdon't act as catalysts themselves. This was confirmed reviewing the literature, from where the data were collected for ANN model building. The support and solid acid catalyst precursor (TPA) together are called catalysts. Different types of supports (i.e. silica, ZrO_2, zeolite) were used to immobilize TPA on them. However, this support name could not be used in the ANN model building. For this reason, the supports were tagged as the wt. fraction of the surface active species of support (i.e. the wt. fraction of Si in SiO_2 or MCM-41 or SBA-15 is 0.47, which was the support tag for pure silica-based materials). The surface active species (i.e. represented by M in eqn. 2.6-2.8) decides how strongly TPA will interact with the support. The unsupported TPA salts were assumed to have hydrogen as their support, thereby support tag 1 (e.g. case number 5, column 2 in Table 2.2). Support structure can be different even if the constituent materials are same (i.e. MCM-41, SBA-15, SiO_2 are made of silica). To distinguish them, the structure identification tag was required. Some literature expressed structural properties with the help of support surface area, pore diameter, pore volume, whereas many literature did not mention anything about them, which made it difficult to accept these properties into the ANN model building. This problem was avoided by considering the reactant and product flow paths through the pores of the support structures. Traditional/readily available porous supports have irregular pore systems with one end closed, and such pore systems are known as one-dimensional (Chung et al., 2013). Thus, the flow paths for these kinds of supports were assigned to be one (Scheme 1). On the contrary, template assisted synthesized supports have well-defined pore systems with either two ends open (two-dimensional pores) or two pores connected by another pore (known as three-dimensional pore systems) (Wagner et al., 2013; Thommes et al., 2000; Zhao et al, 2013). Thus, the flow paths for these kinds of supports were assigned to be two and three respectively (Scheme 1). In the case of catalysts with no pores, the active sites are believed to be exposed outside (Wong and Wales, 1998) and, therefore, the flowpath was considered to be three dimensional (Scheme 1). The metal oxide supports reviewed in this study (case numbers 3, 6-8, 11, 15, 16, 17, 19, 20, 23, 24) were readily available supports or synthesized as simple metal oxides following standard synthesis procedures (Christopher et al., 2014; Srilatha et al., 2012a; Srilatha et al., 2012b; Bhorodwaj et al., 2011; Srilatha et al., 2010; Xu et al, 2009a; Xu et al, 2009b; Bokade and Yadav, 2009; Zieba et al, 2009; Bokade and Yadav, 2007; Narasimharao et al., 2007; Baroi and Dalai, 2013). Therefore, it was appropriate to assign flow path 1 for these supports (column 3 of Table 2.2). Silica based MCM-41 and SBA-15

(case number 4, 25) were synthesized using templates following well established procedures, for which the two-dimensional pore systems were confirmed (Trakarnpruk, 2013; Zhang et al, 2013; Okuhara and Nakato, 1998). The zeolite supports reviewed in this study (case number 1, 2, 26) were commercial supports or synthesized following well established conditions (Nadiwalea et al, 2013; Baroi et al., 2014), for which the pore systems are three dimensional (Haber et al, 2005). Therefore, it was appropriate to assign flowpath 2 for SBA-15, MCM-41 and flow path 3 for HZSM-5, H-β zeolites (column 3 of Table 2.2). Most of the TPA salts reviewed in this study (case number 5, 18, 21, 22) were porous (Srilatha et al., 2012b; Sunita et al., 2008; Bokade and Yadav, 2007; Haber et al., 2005; Moradi et al., 2013). However, Ag, TPPS and TEAPS3 salts (case number 9, 10, 12, 13) were non-porous (zieba et al., 2010; Zhang et al., 2009; Leng et al., 2009; Matachowski et al., 2009). Thus, it was appropriate to assign flow path 1 and 3 respectively for these (column 3 of Table 2.2).

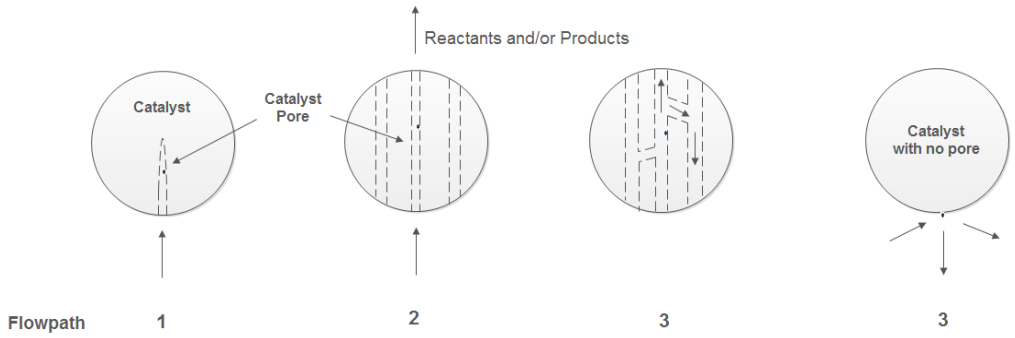

Scheme. 1 Flow path systems in different catalysts

In the case of various TPA salts (e.g. $CsH_2PW_{12}O_{40}$), the metal or organic cations (e.g. Cs for $CsH_2PW_{12}O_{40}$) were tagged by their molecular weight in that salt (e.g. molecular wt. of Cs is 132.9 in $CsH_2PW_{12}O_{40}$ salt), and the numbers of cations (e.g. number of cation (Cs) in $CsH_2PW_{12}O_{40}$ is 1) were also considered during model building (case number 5, columns 4 and 5 in Table 2.2). However, for TPA form, proton (H^+) was treated as cation. The atomic weight of the proton is 1, and pure TPA has 3 acidic protons. Thus, TPA form was tagged by cation tag 1 and cation number 3 (e.g. case number 2, columns 4 and 5 of Table 2.2). The TPA loading for unsupported TPA salts was considered to be 100%, because the Keggin anion ($PW_{12}O_{40}^{-3}$) of TPA does not change because of the salt formation (e.g. case number 18, column 6 of Table 2.2). The calcination temperatures were used as it is from Table 2.1 to Table 2.2. Various feedstocks

(i.e. oil and FFAs) were used by various research groups. All these feedstocks (both TG and FFA) were identified in terms of their major constituent fatty acid carbon numbers and number of unsaturation bonds in their structure. For example, the major constituent of canola oil is Triolein (glycerol ester of oleic acid) (Baroi et al, 2014), and the fatty acid of Triolein can be expressed as 18:1 (following x: y system) – where 18 represents carbon numbers, and 1 represents one double bond in the structure. Thus, in Table 2.2, the canola oil was represented by TG carbon number 18 and number of unsaturation 1 (e.g. case 25, columns 10 and 11). Similarly, the FFA were tagged with the help of their chemical structure following x: y system (columns 8 and 9 of Table 2.2). If the feedstock was pure fatty acid (FFA), then TG carbon number and number of double bonds were set to 0 (e.g. case 21) and when the feedstock was pure triglycerides then FFA carbon number and FFA double bond number were set to 0 (e.g. case number 8). The feedstock was considered to be a mixture of oil (Triglycerides-TG) and fatty acids (FFA). In pure/refined vegetable oil (e.g. edible canola oil, soybean oil), fatty acid content is 0%. For the crude/used vegetable oil, if the fatty acid content is 60% the rest 40% is triglycerides (Scheme 2). If the feedstock is a pure fatty acid, i.e., fatty acid (FFA) content is 100% obviously the triglyceride content in the feedstock is 0% (Scheme 2). Thus, FFA of 100% represented only fatty acids as feedstocks.

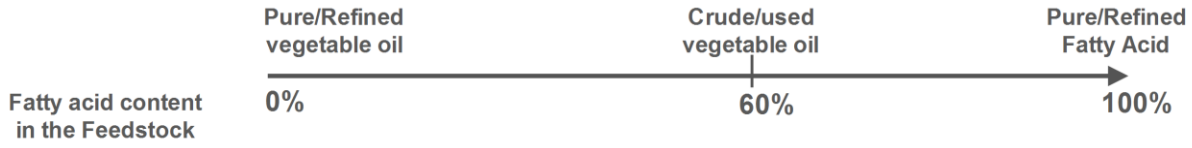

Scheme. 2 Fatty acid content in the feedstock

Similarly, various alcohols were identified in terms of their carbon numbers. For example, carbon number in ethanol is 2 (i.e. C_2); thus ethanol was tagged as 2 in case 13 (column 13 of Table 2.2). The alcohol ratio, catalyst wt.%, time (h) and temperature (°C) were used as is from Table 2.1 to Table 2.2.

The ANN is a powerful and complex mathematical modeling tool that can be applied to quantify a non-linear relationship between independent variables (input) and dependent variables (output) by means of iterative training of data. The network is composed of single computational

units (neurons), which are attached through a parallel structure.These structures are inspired by human brain biological neurons (Soleimani et al., 2013). There are different network types in ANN. The multi-layer perceptron (MLP) is the most commonly used because of its strong learning capability and good model performance (Soleimani et al., 2013; Abbasi and Mahlooji, 2012). In an MLP, the inputs form the first layer and the outputs from the last layer. The intermediate layers are the hidden layers, where the processing takes place. In the hidden layers, in each neuron, the input is multiplied by the parameters (weight) and then added with another parameter (bias). This sum is pass through to a function (transfer or activation function), and finally output is generated (Soleimani et al., 2013; Shimizu et al., 2008). Generally, in an MLP network, the data sets are divided into three subsets. The first dataset is the training dataset, which takes part in the training and updating the network weights and biases. The second subset is the validation data set, which takes part in the training, used to prevent overfitting of the data. The third subset is the test dataset, which is not used during the training, but is used to check the reliability of the model and also to compare the performances of different models (Abbasi et al., 2012). The performance of the ANN is determined by the sum of square error (SSE), which tries to minimize the squared error between the output and the target.

The ANN model was developed using Data mining tool available in STATISTICA 12 software. A multi-layer perceptron (MLP) method was used to correlate the inputs and outputs. For the network build-up, 1000 iterations were used with an initial guess of hidden units or neurons between 5 to 16. The optimal MLP structure obtained was with 3 layers (Fig.2.6): the first layer with 16 inputs, the second layer with 16 hidden units and the third layer with 2 outputs. During the ANN model build-up, the test data and validation data were picked up randomly by the software. The correlation co-efficient (R) for validation of data was found to be 0.99, which indicated that the optimal MLP was reached.

Once the ANN model was built, the reliability of the model was verified by comparing the experimental results (published in different journals-which were not used in the modeling) with the predicted one (see appendix A). The model predicts similar results as published in the literature. This validated the model well.

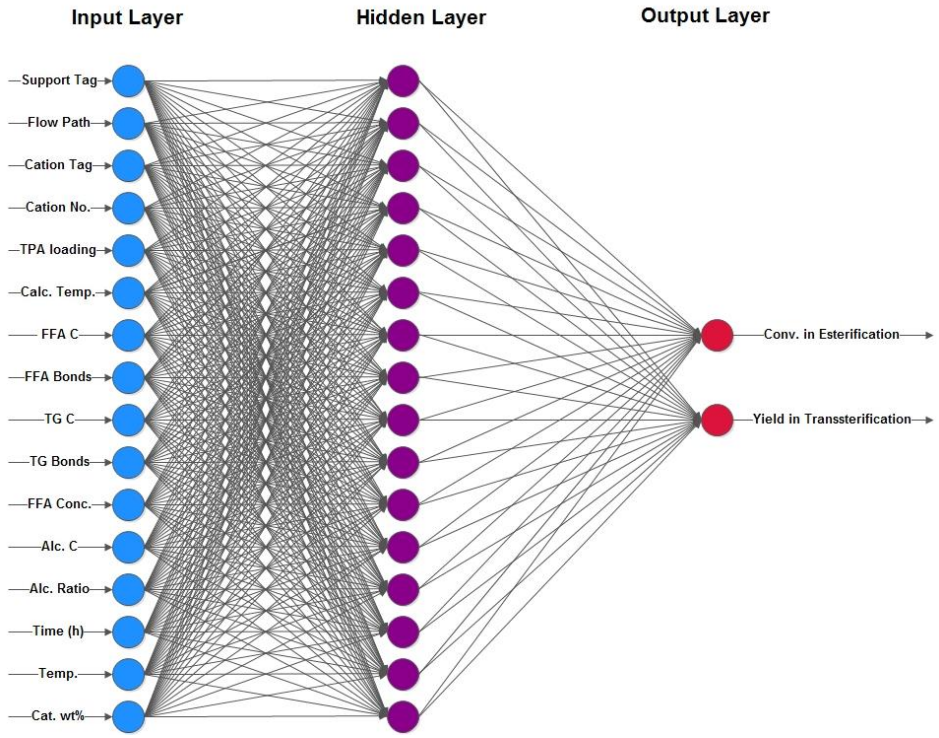

Fig. 2.6 Artificial Neural Network (ANN) with Multilayer Perceptrons (MLP)

The model is built based on the following assumptions:

- Support has no or negligible catalytic activity
- The results obtained from the literature were not affected by internal or external mass-transfer limitations
- All the reactors used in the literature were ideal

To analyze the effect of different variable on the esterification and transesterification conversion, Design of Experiments (DOE) was exploited to vary a pair of variables, keeping other variables constant. Central Composite Design (CCD) was used for this purpose. The effect of a single variable on the esterification and transesterification conversion was analyzed by performing the experiments of varying the variable were performed manually. "Custom Prediction" option of the software was used to obtain the results of the experiments.

The effects of supports can be described by support tag and flow path. The support tag referred to the wt. fraction of the surface active species of support (represented by M in eqn 2.6-2.8). These surface active species determine how densely TPA will be attached with support

oxygen. The wt. fraction of the surface active species represents the concentration of these species in the support. Catalytic activity also depends on the reactants and products mass-transfer rate. These rates depend on the pore systems, which are defined by flow path (Scheme 2). Thus, the support tag and support flow path were varied keeping other variables constant. The active species (TPA) acid strength depends on the type of cations (M^+), and the number of cations present in TPA (after support-TPA interaction and acidic cation-proton (H^+) replacement by cation (M^+)). The Brønsted acidity strength depends on the number of acidic cation-proton (H^+) present in TPA (Okuhara et al., 2000). The Brønsted acidity strength decreases with a decrease in protons. However, depending on the type of proton substituting cations and support-TPA interactions, Lewis acidity increases, and its strength increase with the increase of the number of cations (Ataya et al., 2007; Khder 2008; McCormick et al., 1998; Molnar et al., 1998; Haber et al., 2003). The type of cation was defined by the atomic wt. of the cation (i.e. for H^+ it is 1), which is used as cation tag. Thus, the cation tag and cation number were varied keeping other variables constant. The formation of mono/multilayer of active species (TPA) and availability of cations depend on calcination temperature and TPA loading. The calcination temperature and TPA loading were varied keeping other variables constant. The effect of feedstock (i.e. oil (TG) type, FFA type) depends on the fatty acid carbon number and the number of double bonds present in it. Thus, the TG carbon number and number of double bonds were varied keeping other variables constant to analyze the effect of the oil (TG) type on transesterification. Similarly, FFA carbon number and number of double bonds were varied to analyze the FFA type effects on the esterification. The FFA content in the feedstock was varied from 10 to 90% with a 10% FFA content increment keeping all other variables constant. The effect of alcohol depends on alcohol carbon number and alcohol ratio. Thus, these two parameters were varied keeping all other variables constant. The effects of time (h), reaction temperature (°C), catalyst wt.% were analyzed by varying one variable at a time within the range of 3-24 h, 50-200°C, and 0-12 wt.% respectively.

2.7 Effects of different parameters on the catalytic activity

2.7.1 Effects of different supports and their structural properties

Different support materials have different structural properties. These structural properties along with support pore structure contribute to the esterification and

transesterificationactivity. Transesterification of canola oil prefers oxide supports which consist of materials with lower atomic weight metals (i.e. silica based SiO_2, SBA-15, MCM-41, zeolites) as compared to materials with higher atomic weight metals (i.e. Nb_2O_5, Ta_2O_5, ZrO_2). Esterification of FFA prefers no support (Fig. 2.7). Support structural three-dimensional pore system provides the highest catalytic activity, rather than irregular one-dimensional pore systems for both transesterification and esterification (Figures 2.7).

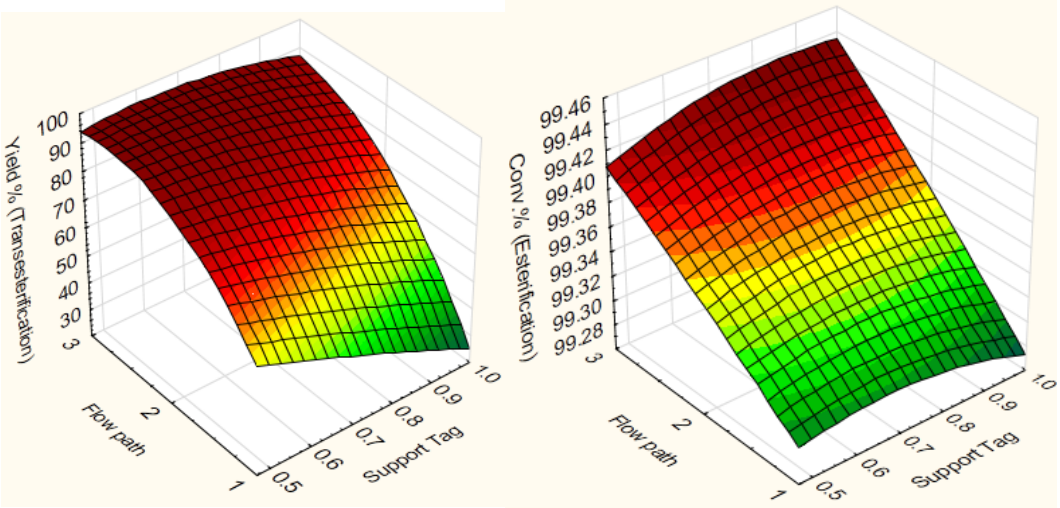

a) Transesterification b) Esterification

Fig. 2.7 Effects of supports and its pore system in the a) transesterification, b) esterification reaction (0.10% $H_3PW_{12}O_{40}$ loading, 100°C calcination temperature, canola oil, 10 wt% catalyst, 3:1 methanol molar ratio, 120°C, 6 h)

An unsupported TPA depicts only Brønsted acidity (Di Serio et al., 2008). Acidic or neutral supports like silica based materials (i.e. SiO_2, SBA-15, MCM-41) attach to TPA through hydrogen bonding mechanism or weak interaction (through ion-exchange mechanism), in which no or minimal acidic protons (H^+) of TPA are lost (Wu et al., 1996; Baroi and Dalai, 2012). This phenomena restores the acidity of TPA in both Brønsted and Lewis form and causes higher activity in esterification and transesterification as Brønsted and Lewis acidity are mainly active for esterification and transesterification respectively (Ataya et al., 2007; Di Serio et al., 2008; Busca, 2007; Okuhara et al., 2000; Shi et al., 2012).

2.7.2 Effects of cations types and number of cations

The catalytic activity in the transesterification reaction increases with an increase in lower molecular/atomic weight cations (Fig. 2.8).

On the contrary, the catalytic activity in the esterification increases with a decrease in higher atomic/molecular weight cations (Fig. 2.8).

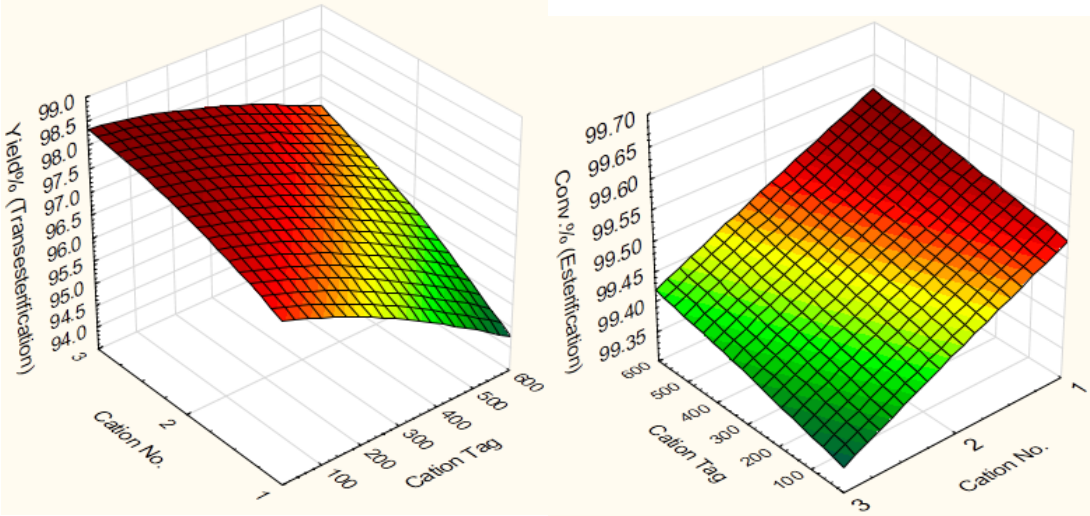

a) Transesterification b) Esterification

Fig. 2.8 Effects of cation type and number of presence of cation number in the a) transesterification, b) esterification reaction (Support Tag:0.47, flow path 3, 0.1% loading, 100°C calcination temperature, canola oil, 10 wt.% catalyst, 3:1 methanol molar ratio, 120°C, 6 h)

Cation exchanged TPA contains both Lewis and Brønsted acidity. Lower atomic/molecular weight cations generate moderate Lewis acidity, whereas higher atomic/molecular weight cations generate moderate to strong Lewis acidity (Shi et al., 2012). Combination of moderate Lewis acidity along with moderate Brønsted acid sites of catalysts are responsible for higher activity towards transesterification, whereas strong Brønsted acid sites or combination of moderate Brønsted acid sites and strong Lewis acid sites of catalysts are accountable for higher activity towards esterification (Shi et al., 2012).

2.7.3 Effects of TPA loading and calcination temperature

The calcination temperature and TPA loading affect the mono/multilayer formation of TPA, the presence of the crystal water and protons. The catalytic activity in transesterification increases with a decrease in TPA loading and the activity increases with the calcination

temperatures (Fig. 2.9). It indicates that lower TPA loading and higher calcination temperature provides more moderate acid sites, which favor transesterification reaction, as mixture of moderate Lewis acid sites and Brønsted acid sites of catalysts are responsible for higher activity towards transesterification (Park et al., 2012). The catalytic activity in esterification is highest around 50% TPA loading and the activity increases with the calcination temperature (Fig. 2.9).

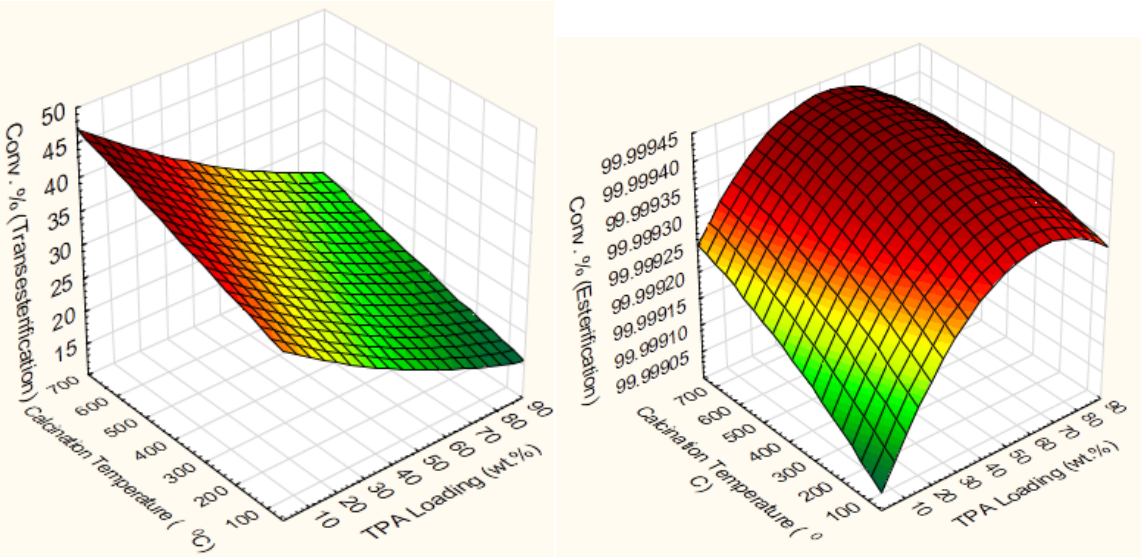

a) Transesterification b) Esterification

Fig. 2.9 Effects of $H_3PW_{12}O_{40}$ loading and calcination temperature in the a) transesterification, b) esterification reaction (Support Tag: 0.47, flow path 3, 10 wt.% catalyst, 3:1 methanol to canola oil molar ratio, 120°C, 6 h)

It implies that excess TPA loading provides more active sites, which speeds up the esterification and produces water within a short period and may deactivate the catalysts. TPA Keggin structure decomposes to WO_3 above 600 °C (Kozhevnikov, 2007). Decomposition of one TPA Keggin unit yields 12 WO_3. Supported WO_3 exhibits both Brønsted and Lewis acidity (Park et al., 2012), which might be responsible for catalytic activity both in esterification and transesterification even if the TPA based catalysts are calcined above 600°C.

2.7.4 Effects of reactant properties on the catalytic activity

The catalytic activity for transesterification is optimum with feedstocks having carbon atom numbers between C_{16}-C_{20}. The catalytic activity is also favored by the absence of any unsaturation double bond (Fig. 2.10).

From previous studies through kinetic and thermodynamic properties measurement it was observed that there might be an optimum combination of carbon atom number and number of double bonds for which the formation of activation complex is fastest and the activation complex is readily decomposed (Nadiwalea et al., 2013; Choi et al., 2011).

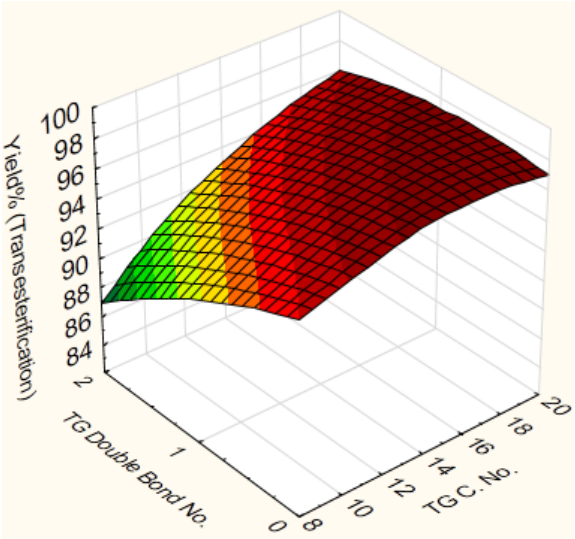

Fig. 2.10 Effects of TG carbon number and number of unsaturation on the transesterification reaction (Support Tag: 0.47, flow path 3, 0.1% $H_3PW_{12}O_{40}$ loading, 100°C calcination temperature, 10 wt.% catalyst, 3:1 methanol to canola oil molar ratio, 120°C, 6 h)

The catalytic activity for esterification is high with feedstocks having low carbon numbers and higher unsaturation (Fig. 2.11). Similar trend of results were observed in other studies (Cardoso et al., 2008; Cardoso et al., 2009). However, in both studies, the effects of carbon number and number of double bonds were considered negligible.

The FFA presence in the feedstock oil reduces the catalytic activity in transesterification. On the contrary, the catalytic activity in esterification increases with the increase in FFA content (Fig. 2.12). TPA contains Brønsted acidity, which is mainly active in the esterification reaction. Esterification reaction is a faster reaction as compared to transesterification reaction (Ataya et al., 2007). The presence of water (by-product from esterification) which restricts TG accessibility (Ataya et al., 2007) may cause this catalytic behavior towards esterification and transesterification reaction.

The catalytic activity in the transesterification increases with the alcohol molar ratio increase and the catalytic activity is relatively insensitive with the alcohol carbon chain number

(Fig. 2.13). Transesterification is a reversible reaction (Gerpen and Knothe, 2005), thus, an excess alcohol moves the transesterification reaction towards equilibrium.

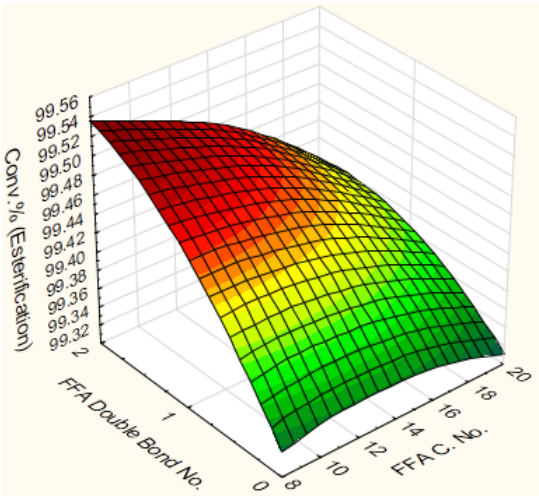

Fig. 2.11 Effects of FFA carbon number and number of unsaturation bonds in the esterification reaction (Support Tag: 0.47, flow path 3, 0.1% $H_3PW_{12}O_{40}$ loading, 100°C calcination temperature, 10 wt.% catalyst, 3:1 methanol to oleic acid molar ratio, 120°C, 6 h)

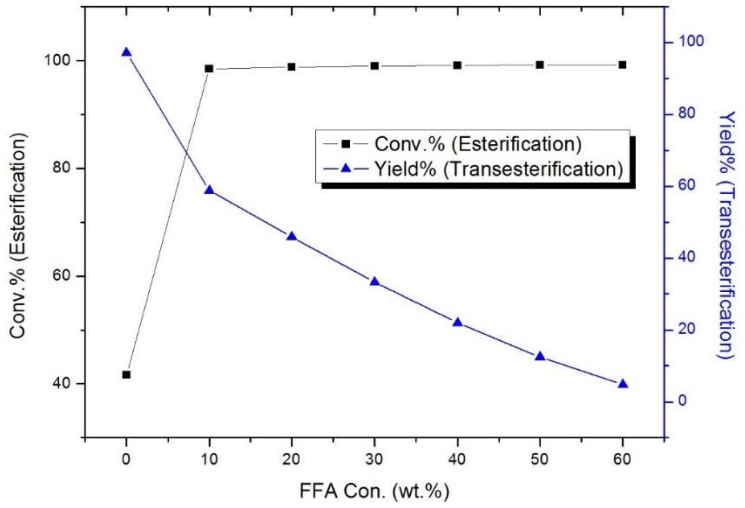

Fig. 2.12 Effects of FFA concentration in oil in esterification and transesterification reaction (Support Tag: 0.47, flow path 3, 0.1% $H_3PW_{12}O_{40}$ loading, 100°C calcination temperature, 10 wt.% catalyst, 3:1 methanol ratio, 120°C, 6 h)

The catalytic activity in esterification increases with a decrease in the alcohol carbon number and increase in alcohol ratio (Fig. 2.13). High bulk hindrance occurs on the hydroxyl group, for alcohols with higher carbon numbers which reduces the attack efficiency to the carbonyl carbon of the fatty acids (Cardoso et al., 2008). Esterification is a reversible reaction (Gerpen and Knothe, 2005). Thus, excess alcohol moves the esterification reaction towards

equilibrium (Lavarez et al., 2009). Besides, increasing alcohol amount decreases the reaction mixture viscosityand therefore the rate of mass-transfer increases. As a result, the conversion of FFA increases (Gan et al., 2012).

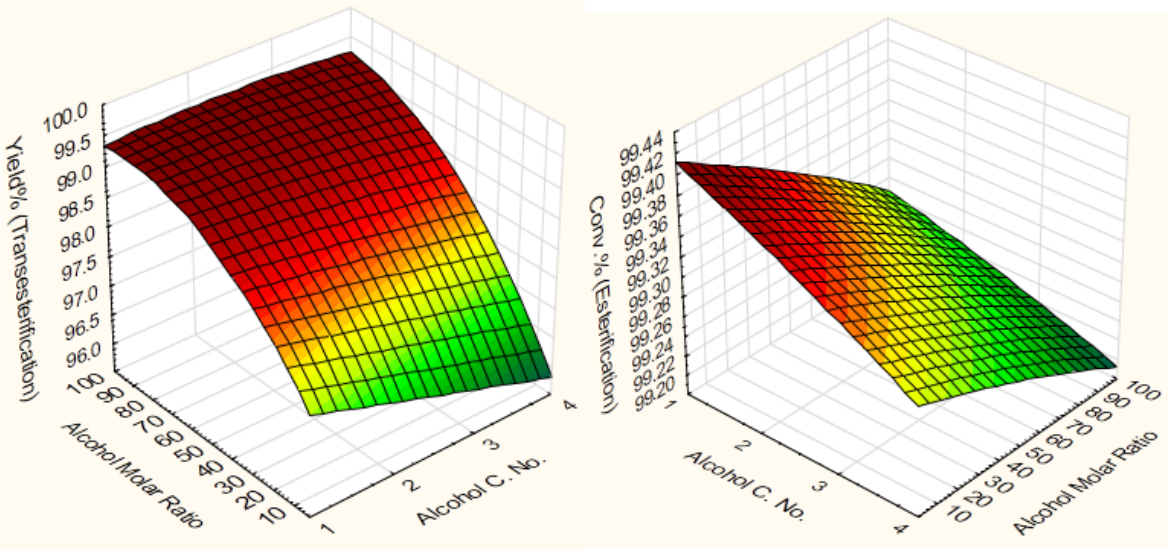

a) Transesterification b) Esterification

Fig. 2.13 Effects of alcohol carbon number and alcohol to oil molar ratio on the a) transesterification, b) esterification reaction (Support Tag: 0.47, flow path 3, 0.1% $H_3PW_{12}O_{40}$ loading, 100°C calcination temperature, 10 wt.% catalyst, 120°C, 6 h)

2.7.5 Effects of reaction parameters on the catalytic activity

The catalytic activity for both esterification and transesterification decreases with an increase in catalyst loading (Fig. 2.14). More catalyst loading provides more active sites, which speeds up the esterification and transesterification and produces water and glycerol respectively within a short period of time. These may deactivate the catalysts.

The catalytic activity for both esterification and transesterification reaction increases with the increase in the reaction temperature (Fig. 2.15), which is expected as both the reactions are endothermic in nature (Baroi et al., 2013). The catalytic activity for both transesterification and esterification increases with the increase in the reaction time (Figure not depicted).

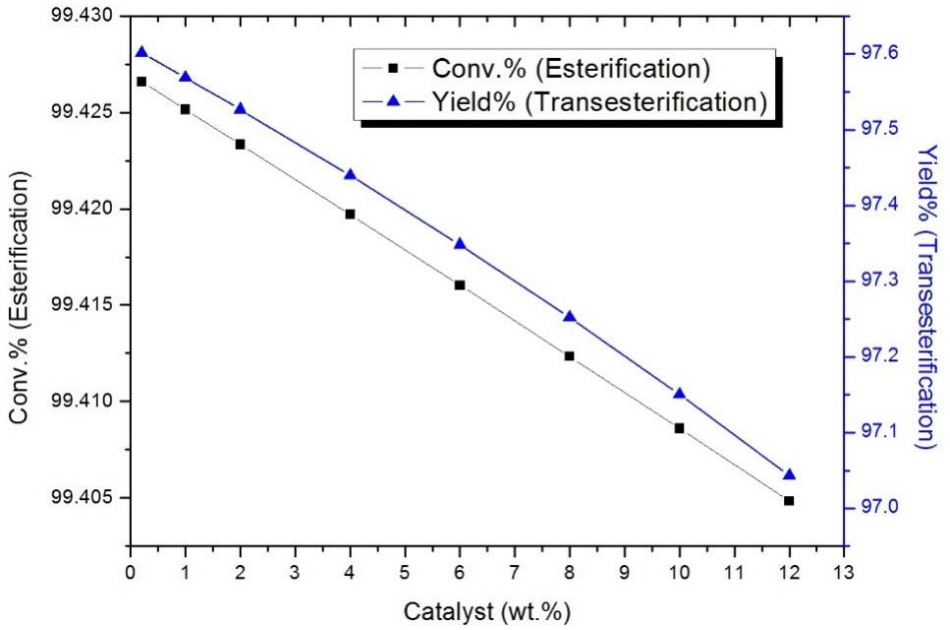

Fig. 2.14 Effects of catalyst loading (wt.%) in the esterification and transesterification reactions (Support Tag: 0.47, flow path 3, 0.1% $H_3PW_{12}O_{40}$ loading, 100°C calcinations temperature, 3:1 methanol ratio, 120°C, 6 h)

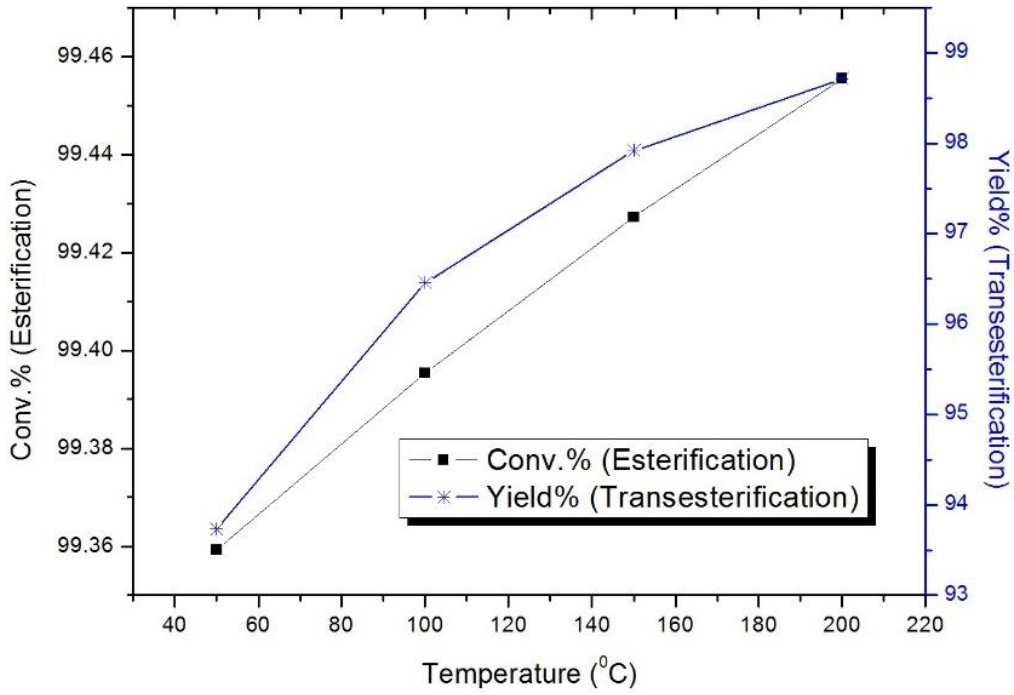

Fig. 2.15 Effects of reaction temperature in the esterification and transesterification reactions (Support Tag: 0.47, flow path 3, 0.1% $H_3PW_{12}O_{40}$ loading, 100°C calcination temperature, 10 wt.% catalyst, 3;1 methanol ratio, 6 h)

2.8 Conclusions

The pattern recognition of the literature review indicates that esterification and transesterification reactions require catalysts with slightly different properties. Supported/unsupported TPA, different type of proton exchange cation and different cation numbers are preferred for optimum activity in transesterification and esterification reactions. The feedstock properties, reaction conditions also affect the esterification and transesterification reaction activity. The catalytic activity in the transesterification decreases with an increase in the feedstock FFA content and decreases with the increase in the TPA loading. Alcohol ratio, reaction temperature and time affect the transesterification and esterification reaction activityin the similar manner. Thus, depending on the properties of the feedstocks, optimization of the catalyst properties (i.e. catalyst support, cation type, cation numbers, TPA loading) should be carried out in order to get balanced catalytic activity in both transesterification and esterification.

CHAPTER 3: CATALYTIC ACTIVITY OF TPA SUPPORTED ON SBA-15 FOR THE BIODIESEL PRODUCTION

A version of this chapter has been published in the following symposium series and presented in the following conferences:

- Chinmoy Baroi, Ajay K. Dalai. TPA supported on SBA-15 as solid acid catalysts for the biodiesel production. ACS symposium series, issue: Nanocatalysis for Fuels and Chemicals, 1092 (2012), 93-109.
- Chinmoy Baroi, Ajay K. Dalai. Biodiesel production using solid acid catalysts. 22nd North American Catalysis Society Meeting (NAM 22), Detroit, Michigan, USA - June 5-10, 2011.
- Chinmoy Baroi, T. Issariyakul, K. Srilatha, Ajay K. Dalai. Biodiesel production using solid acid catalysts. Agriculture and Biomass Innovation Network (ABIN) conference, London, Ontario, Canada, January 9-11, 2011.
- Chinmoy Baroi,T.Issariyakul, K. Srilatha, Ajay K. Dalai. Biodiesel production using solid acid catalysts. The 2010 International Chemical Congress of Pacific Basin Societies (Pacifichem), Honolulu, Hawaii, USA, December 15 - 20, 2010.
- Chinmoy Baroi, Ajay K. Dalai. Biodiesel Production Using Solid Acid Catalysts. 60th Canadian Society for Chemical Engineering (CSChE) conference. Saskatoon, SK, Canada, October 24-27, 2010.
- Chinmoy Baroi, Ajay K. Dalai. Biodiesel production from Triolein using solid acid catalysts. Agriculture and Biomass Innovation Network (ABIN) conference, London, Ontario, Canada, March 23-25, 2010.

Contribution of the Ph.D. Candidate

Experiments were conducted by Chinmoy Baroi. The content in this chapter was written by Chinmoy Baroi with discussions and suggestions provided by Dr. Ajay Dalai.

Contribution of this Chapter to the Overall Ph.D. Research

Triolein is one of the major triglycerides of vegetable oils. The research work of this chapter can be considered as a base-line study. The aim of this chapter is to illustrate how the

presence of free fatty acids (FFA) and water can affect the catalytic activity in transesterification of Triolein. This chapter also illustrates what should be the desired characteristics be of a heterogeneous (solid) acid catalyst for both transesterification and esterification of crude vegetable oils, such as green seed canola oil.

3.1 Abstract

Biodiesel has gained worldwide recognition for many years due to its renewability, lubricating property and environmental benefits. This research is focused on the synthesis of SBA-15 supported 12-Tungstophosphoric acid (TPA) as a heterogeneous (solid) acid catalyst for the model feedstock Triolein derived biodiesel production. A large number of SBA-15 supported 0-35% TPA catalysts was synthesized by impregnation method and the catalysts were characterized using BET, XRD, FTIR, and ICP-MS. These catalysts' catalytic activity was tested by transesterification of Triolein using a stirred tank reactor. The effect of operating conditions for example catalyst concentration and methanol to Triolein molar ratio on the transesterification of Triolein was studied exploting response surface methodology (RSM). A 25% TPA is identified as the optimum catalyst loading on SBA-15 by impregnation. From the optimization study of 25% TPA impregnated SBA-15 using RSM model, 4.15 wt% catalyst (based on Triolein) and 39:1 methanol to Triolein molar ratio is found to be the optimum reaction conditions, when the reaction temperature is kept fixed at 200°C, stirring speed at 600 rpm and allowing 10h of reaction time. Predicted ester yield at the above condition is 97.4%, and the actual (experimental) yield is 97.2%.

3.2 Introduction

The other name of transesterification is alcoholysis because in this process one alcohol is replaced by another, i.e., the higher alcohol (glycerol) present in the triglyceride is replaced by a lower alcohol (e.g., methanol, ethanol) and the resultant monoalkyl esters of fatty acids are called biodiesel. Alcohols (e.g., methanol, ethanol) and oils or fats (edible and non-edible) are used as reactants in the transesterification reaction. Transesterification of triglycerides with methanol produces fatty acid methyl esters (FAME) and glycerol. Diglycerides and monoglyceride are the intermediates in thetransesterification. The overall equation of transesterification is given in equation 3.1.

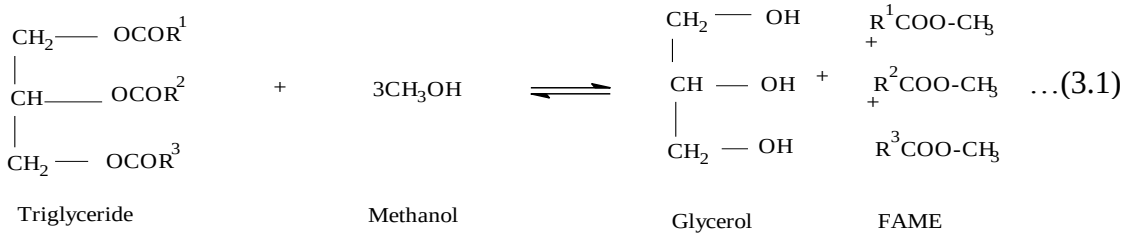

…(3.1)

Transesterification reaction can proceed either in the presence of catalysts at lower temperature, pressure or in the absence of catalysts. Catalyst assisted transesterification reaction is preferred in biodiesel production process because of the moderate reaction conditions. Most of the commercial transesterification reaction is conducted with homogeneous alkaline catalysts because homogeneous base catalyzed transesterification reaction is 4000 times faster than the homogeneous acid catalyzed reaction (Srivastava and Prasad, 2000). One of the problems associated with the base catalyzed reaction is the formation of soap as an undesired reaction between free fatty acids (FFA) and bases, which consumes some of the base catalyst. Thus, the base available for catalyzing the reaction is reduced. The biodiesel production process is not affected significantly upto the 3% FFA presence in the feedstock but if the oil contains more than 5% FFA, the separation of glycerol from the biodiesel is inhibited by soap (Gerpen and Knothe, 2005). The main problem of commercial biodiesel production process is the high price of treated feedstock or pre-treatment of the feedstock which leads to the higher price of the biodiesel. Estimation depicts that approximately 88% of the total production cost is associated with the feedstock (Marchetti and Errazu, 2008). This cost can be reduced by using cheaper feedstocks, e.g., used cooking oil, yellow grease. Acid catalysts can catalyze both esterification reaction and transesterification reaction to produce similar type of ester from free fatty acids using alcohol, which is depicted by equation 3.2 (Gerpen and Knothe, 2005).

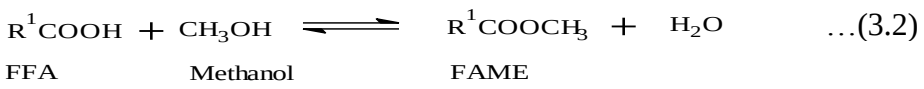

…(3.2)

Though homogeneous acid catalyst can serve this purpose, it causes severe corrosion problem to the equipment and also leads to the environmental problem (Kulkarni et al., 2006).

Therefore, solid acid catalysts are now point of interests in producing biodiesel from different feedstocks. Among the solid acids, heteropoly compounds show strong and pure Brønsted acidity which are commonly known as heteropoly acids (HPA) (Busca, 2007; Okuhara et al., 2000), especially, $H_3PW_{12}O_{40}$ (TPA) possesses super acidity (Brønsted acidity) and higher thermal stability as compared to other HPA compounds (Kozhevnikov, 2007). The disadvantages of using this heteropoly acid are lower surface area (1 – 10 m^2/g) and polar solvent solubility (Kulkarni et al., 2006). These problems may be bypassed supporting $H_3PW_{12}O_{40}$upon various carriers. Silica based mesoporous materials fully satisfy all the desired criteria as a support for these types of reactions (Wong and Knowles, 1998). Especially SBA-15, a silica-based mesoporous material is an attractive support for its higher hydrothermal stability and a low carbon deposition tendency compared to other silica based mesoporous supports (Herrera et al., 2008). There is no literature available so far; on the TPA supported SBA-15 catalyzed transesterification. Thus, it can be considered as a baseline study to understand the catalytic activity of SBA-15 supported TPA in the transesterification reaction for biodiesel production.

3.3 Experimental

3.3.1 Reagents

Triolein, Methanol (99.9%), P123 and TEOS (Tetraethyl orthosilicate) were purchased from Sigma-Aldrich, Oakville, Ontario, Canada. 12-Tungstophosphoric acid (TPA) was purchased from Alfa-Aesar, MA, USA.

3.3.2 Catalyst preparation

SBA-15 was synthesized by utilizing amphiphilic triblock copolymer poly (ethylene glycol)-block-poly (propylene glycol)-block- poly (ethylene glycol), which is commonly known as P123. The typical synthesis procedure for SBA-15 is as follows: 13.38 g of P123 was dissolved in 396 g water plus 25.11 g HCl solution by stirring for 2-3 hours at 40°C. Thereafter, 30 g of Tetra Ethyl Orthosilicate (TEOS) was added into the aquous solution with stirring at 40°C. The mixture solution was stirred at 40°C for 24 h and thereafter, the solution mixture was aged in a Teflon bottle at 110°C for 24 h. The solids from the mixture were recovered by

filtration. These were washed with water and then dried overnight at 100°C. Finally, the powder was calcined in a 550°C for 6 h.

TPA impregnated on SBA-15 was prepared as follows: Calcined SBA-15 was added into the solution of calculated amount of TPA. After stirring, the sample was oven dried at 110°C for 24 h and calcined at 300°C for 2 h. TPA loading of 5, 15, 25 and 35 wt.% supported on SBA-15 were prepared and used in the catalytic studies. These catalysts were designated as X%TPA/SBA-15, where X represents wt.% loading.

3.3.3 Catalyst characterization

The synthesized catalysts BET surface area and pore size analysis were performed using Micrometrics adsorption equipment (Model ASAP 2000). The catalysts wereheated at 200°C in a vacuum of 5×10^{-4} atm before the analysis. The surface area was calculated from the isotherms using Brunauer-Emmett-Teller (BET) method. The pore diameter and pore volume was calculated using BJH method from desorption branch of the isotherms. For XRD analysis, a small amount of each sample was placed on a standard Goniometer head and the sample was set at the center of the Diffractometer. Diffraction data were collected with a Bruker Smart 6000 CCD detector on a Goniometer. The X-ray radiation source was Cu-K_α (1.54 A°) X-ray tube fitted with pinhole Collimator. The sample to detector distance was 29.48 cm. The catalysts FTIR spectra were recorded through Perkin Elmer FTIR spectrum GX equipment. For the FTIR analysis, sample pallets were prepared by pelleting a well mixed 3 mg of catalyst powder with 200 mg of KBr. The Brønsted and Lewis acid sites of the catalysts were differentiated by in situ infrared (FTIR) spectroscopy with chemisorbed pyridine. The catalyst sample was heated in a designed cell from room temperature to 300°C in a flowing stream of pure Helium. The cell was heated at 300°C for 2 h and then cooled to 100°C. Pyridine vapour was introduced along with the flowing helium and the spectra were recorded from 1400–1600 cm^{-1}. The Tungsten (W) content in the prepared catalysts and biodiesel were determined by ICP-MS.

3.3.4 Transesterification of Triolein

Transesterification of Triolein (a model compound representing oil) using supported TPA was conducted in a 450 mL Parr reactor (Parr Instrument Co., ILL, USA). Initially, 100 g of

Triolein was taken into the reactor and preheated to 60°C with stirring at 600 rpm. The stirring speed was optimized to eliminate the mass transfer limitation effect and the results are depicted in the section 3.4.2. Catalysts and methanol were then added to the reactor. Depending on the reaction temperature, the reactor was pressurized to ensure the liquid phase of the reactants. Preliminary catalyst screening experiments were carried out using reaction conditions of 200°C, 4.14 MPa, 9:1 methanol to oil (Triolein) molar ratio, 1.5 wt.% catalyst (based on the wt. of Triolein). These preliminary reaction conditions were chosen based on the previous research work by Kulkarni et al. (2006). Central Composite Design (CCD) was utilized to design the experiments and Design Expert 6.1 software was used for this purpose. The ester phase (after separation of the catalyst by filtration and separation of the glycerol phase) was analyzed utilizing High-performance liquid chromatography (HPLC). The ester phase collected from each experiment was analyzed for its ester content utilizing a Hewlett-Packard 1100 series HPLC. Two Phenogel 100°A 300X7.80 mm 5 micron columns in series protected with guard column were exploited to separate different components of the samples during analysis. THF was used as a mobile phase at 1 mL/min for 25 min. The operating parameters were of sample injection volume 5 μL, detector temperature of 35°C, and column temperature of 24°C. Standard chemicals including methyl oleate, triolein, diolein, and monoolein were used for the HPLC calibration (see Appendix B). The ester yield (wt.%) was calculated according to the equation 3.3.

$$\text{Ester yield (wt\%)} = (\text{wt. of the methyl ester in the ester phase})/(\text{wt. of the oil phase}) \times 100 \quad \ldots(3.3)$$

Biodiesel water content was determined by Karl-Fisher titration method (Fischer, 1935) and the acid value of the produced biodiesel was determined according to the AOCS-D6751 method.

3.4 Results and Discussion

3.4.1 Catalyst characterization

The catalysts textural properties are outlined in Table 3.1. The table depicts that the introduction and increase in the loading of TPA decrease the BET surface area, pore volume and

pore size compared to that of pure SBA-15. Similar types of results were observed by Tropecelo et al. (2010).

Table 3.1: Textural property of various catalysts

Catalyst	Surface area[a] (m^2/g)	Pore[b] volume (cc/g)	Average pore diameter (nm)	Theoretical loading	Actual loading[c]
SBA-15	821±41	1.26±0.26	6.10±0.36	0	0
5% TPA/SBA-15	796	1.04	5.72	5	5
15% TPA/SBA-15	749	0.97	5.61	15	15
25% TPA/SBA-15	744	0.97	5.56	25	25
35% TPA/SBA-15)	729	0.91	5.01	35	35

[a]Surface area calculated by BET method
[b]Pore volume obtained from the desorption branch of the isotherm by BJH method
[c]Calculated based on the Tungsten (W) content of the catalyst using ICP-MS

For the catalysts the SBA-15 structure is affirmed by a XRD pattern made of a strong peak (at 2θ around 0.8°) along with two small peaks (at 2θ around 1.6° and 1.8°) (Tropecelo et al., 2010; Yang et al., 2005). These weak peaks appeared as broad peaks with the increase of the TPA loading on SBA-15, indicating a loss of structure (Fig. 3.1).

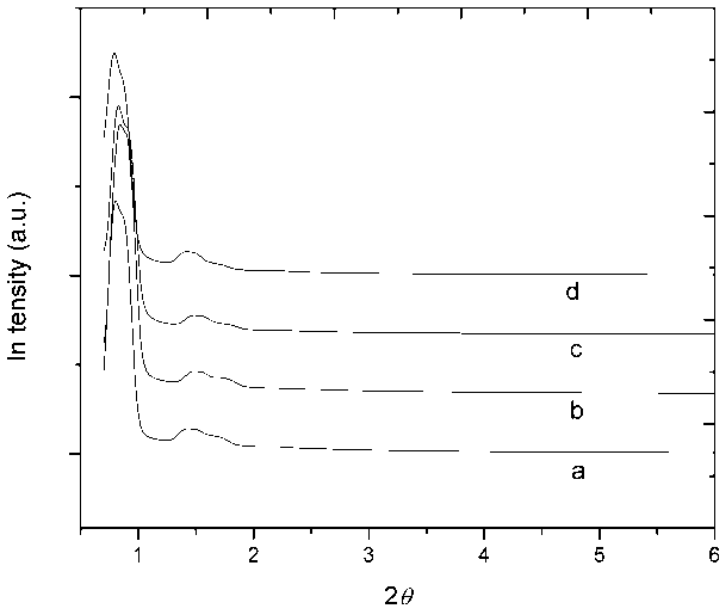

Fig. 3.1 XRD patterns of different TPA loading on SBA-15: (a) SBA-15, (b) 5% TPA/SBA-15, (c) 15% TPA/SBA-15 and (d) 25% TPA/SBA-15

Pure TPA depicts IR peaks approximately at 1081 (P-O in the central tetrahedron), 989 (terminal W=O), 898 and 806 (W-O-W) cm^{-1} indicating asymmetric vibration of Keggin ion (Tropecelo et al.2010; Satishkumar et al., 2006; Damyanova et al., 2003). The IR peaks at approximately 989, 898 and 806 cm^{-1} are intensified significantly with the increase of TPA loading on SBA-15 (Fig. 3.2).

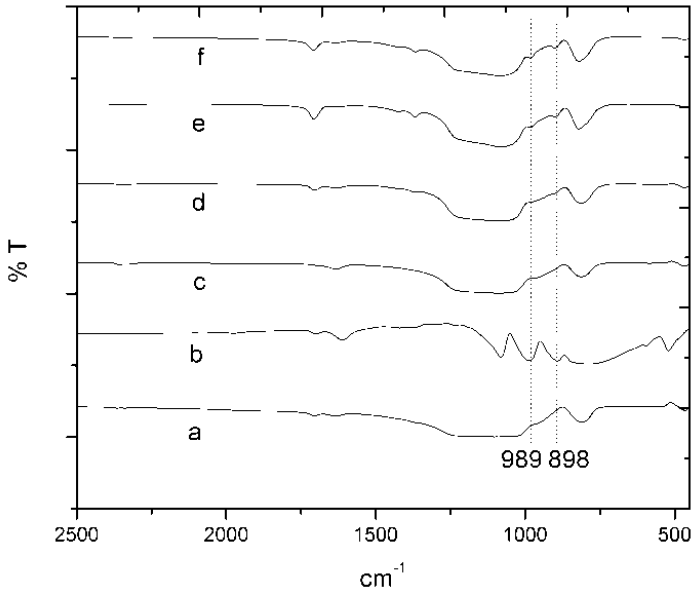

Fig. 3.2 FTIR spectra of different TPA loading on SBA-15: (a) SBA-15, (b) TPA, (c) 5% TPA/SBA-15, (d) 15% TPA/SBA-15, (e) 25% TPA/SBA-15 and (f) 35% TPA/SBA-15

The FTIR spectra of thepyride adsorbed catalysts are depicted in Figure 3.3. The FTIR spectra of the pyridine adsorbed catalysts depict intense bands at 1563 and 1585 cm^{-1}assigned as Brønsted acid sites. The intense band at 1485 cm^{-1} is assigned as both Lewis and Brønsted acid sites. Also, strong bands are observed at 1441 cm^{-1}which arise due to the presence of Lewis acid sites (Kulkarni et al., 2006).

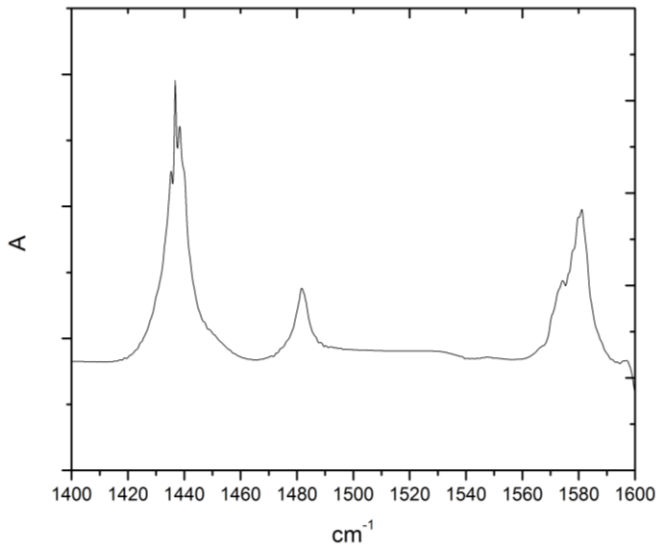

Fig. 3.3 FTIR spectra of pyridine absorbed on 25% TPA/SBA-15

3.4.2 Effect of mixing intensity and external mass transfer resistance

Figure 3.4 depicts that 600 rpm is the optimum stirring speed beyond which there is no increase in the ester yield (wt.%). Thus, 600 rpm was chosen as the optimum stirring speed.

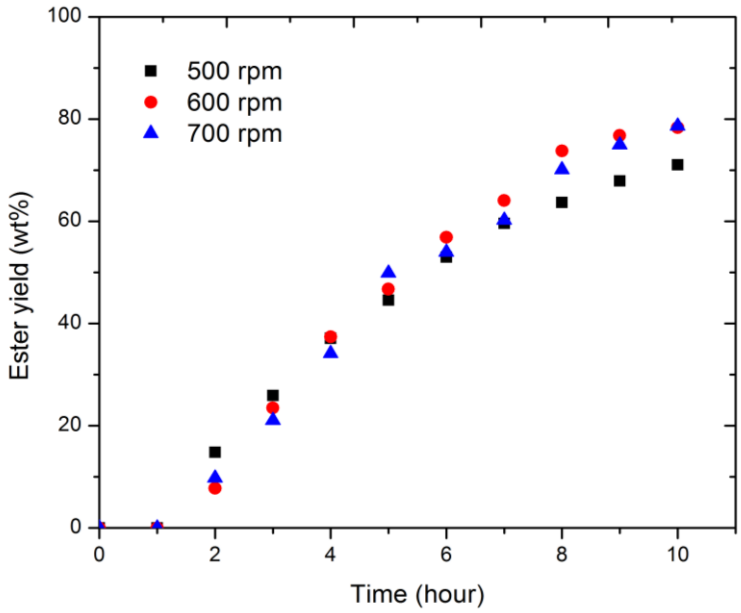

Fig. 3.4 Optimization stirring speed for transesterification (1.5 wt% catalyst, 25% TPA loading, 9:1 methanol to Triolein molar ratio, 200°C, 4.14 MPa and 10 h)

The intensity of mixing in the reactor can be expressed by the Reynold's number

$$Re = \frac{D^2 N \rho}{\mu} \qquad \ldots(3.4)$$

Where, N is the rotational speed of the impeller, D is the diameter of the impeller, ρ is the density and μ is the viscosity of the fluid respectively. The Reynold's number for the optimized stirring speeds used in the transesterification reaction was 27041. This is an indication that the flow in the reactor was turbulent using those impeller speeds.

The catalyst inter-particle mass transfer resistance was calculated exploiting the Wilke–Chang equation and Sherwood number. The diffusivity of the limiting reactant (Triolein/oil) $D_{oil,MeOH}$ was calculated from Wilke–Chang equation given by $D_{Oil,MeOH} = 7.4 \times 10^{-10} \times (\psi . M_{MeOH})^{0.5} \times T/\mu \times (V_{Oil})^{0.6}$, where $\psi = 1.9$ (the association factor for methanol), M_{MeOH} molecular weight of methanol, T reaction temperature in K, μ viscosity of liquid medium, V_{Oil} molar volume of oil(Satterfield, 1970). The value $D_{oil,MeOH}$ calculated to be $9.35 \times 10^{-12} m^2/s$. The value

of mass transfer co-efficient for the limiting reactant kc_{oil} was calculated from Sherwood number $Sh = kc_{oil} \times D_p / D_{oil,MeOH}$ and the value was found to be 8.5×10^{-7} m/s. Assuming the extreme case, the Sherwood number was taken to be 2. The mass transfer flux of GSC oil is given by $W_{oil} = kc_{oil}.C_{oil}$ and the value obtained was 6.17×10^{-4} mol/m^2.s. The initial rate (r''_{oil}) was found to be 8.21×10^{-12} mol/m^2.s. It confirms that the mass transfer rates were much higher than rates of reaction and hence speed of agitation had no influence on reaction rate.

3.4.3 Effect of intra-particle diffusion resistance

The influence of the internal (intra-particle) diffusion resistance was assessed exploiting Weisz – Prater criterion (Fogler, 2006). The Weisz–Prater criterion is a dimensionless parameter $\{C_{WP} = r_{obs} \times R_p^2/De_{oil}\ [C_{oil}]\}$ that represents the ratio of the intrinsic reaction rate to the intra-particle diffusion rate. This ratio can be estimated based on the observed rate of reaction, the particle radius (R_p), effective diffusivity of the limiting reactant (D_{eoil}) and [C_{oilS}] concentration of the reactant at the external surface of the particle. The effective diffusivity of GSC oil $De_{oil}$was calculated by utilizing bulk diffusivity ($D_{Oil,MeOH}$), porosity (θ) and tortuosity (τ).The average values of porosity and tortuosity were taken as 0.4 and 3, respectively, as a conservative estimate. The effective diffusivity of GSC oil (De_{oil}) was obtained to be1.25×10^{-12} m^2/s. In the present phase, the highest value of C_{WP} wasestimated as 1.22×10^{-3}, which is much less than 1 (Fogler, 2006; Yadav and Manyar, 2003). Hence, there was no intra-particle diffusion resistance.

3.4.4 Catalytic activity

Figure 3.5 depicts that 25% TPA/SBA-15 produced the highest ester yield of 80.2±1.45 wt.% (at 95% confidence interval) as compared to that using 35% TPA/SBA-15, when 1.5 wt.% catalyst (based on Triolein) and 9:1 methanol to Triolein molar ratio were used at 200°C, 4.14 MPa reaction pressure and 10 h reaction time as an initial reaction condition, and further increase in loading results in almost same amount of ester formation. This 25% TPA loading also produces almost same ester yield (15.1±1.2% at 95% confidence level) compared to that of 35% TPA loading (15.2%), when 3.25 wt% catalyst (based on Triolein) and 10.5:1 methanol to Triolein molar ratio are used at 150°C, 1.38 MPa reaction pressure and 10 h reaction time. Thus, 25% TPA/SBA-15 was considered as the optimum catalyst composition.

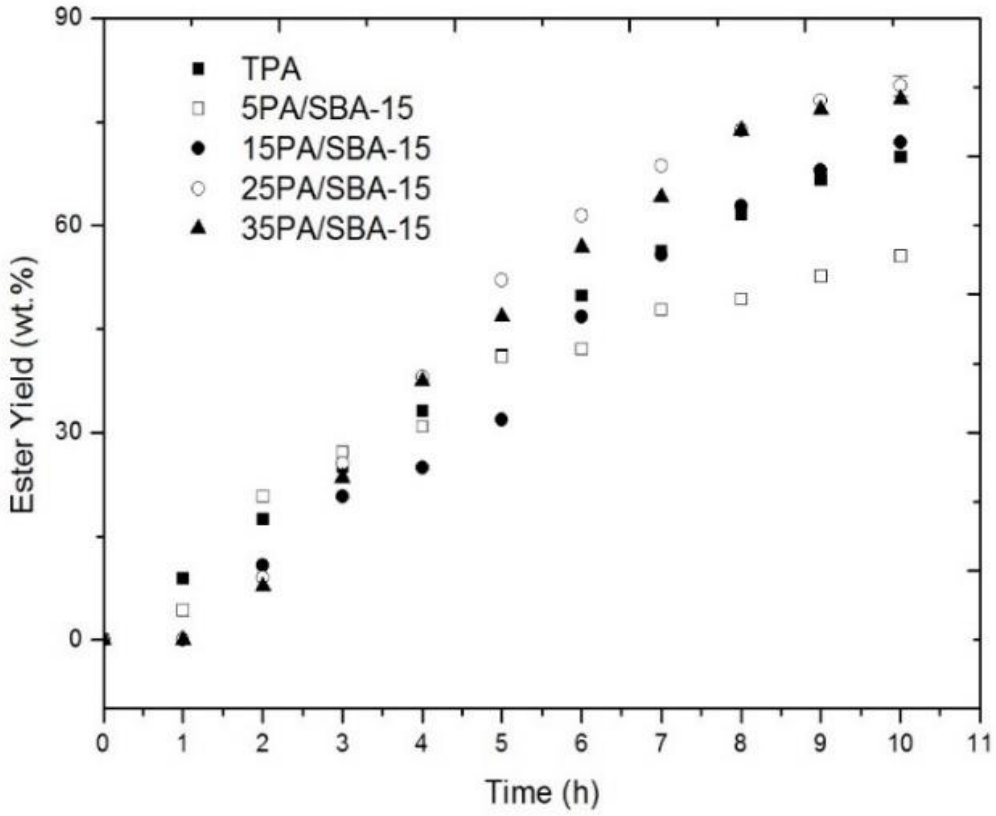

Fig. 3.5 TPA loading screening (1.5 wt% catalyst, 9:1 methanol to Triolein molar ratio, 200°C, 4.14 MPa and 10 h)

3.4.5 Experimental design, statistical analysis and optimization

In the first stage, the range of experimental parameters studied are: (1) catalyst wt.: 1.5 -5 wt.% (2) Methanol to oil molar ratio: 6:1-15:1 and (3) Reaction temperature: 100-200°C. A three-factor two level design was used to perform 20 experiments. From the experiments, it was found that reaction temperature is the most important factor, which affected the ester yield positively without the interaction of other parameters. These experiments also showed that the % ester yieldincreased with the increase in values of other two parameters. Similar results were found using homogeneous acid catalyst in another study by Canakci and Gerpen (1999). According to their study, reaction temperature dominates the reaction rate and the conversion increases with increasing the temperature of the reaction, increasing methanol to oil molar ratio and increasing acid catalyst concentration. The nitrogen pressure used in the experiments according to the reaction temperature and the pressure requirement increases exponentially with the reaction temperature (i.e. for the reaction temperature 240°C, pressure requirement is 7.72

MPa). Thus, the reaction temperature was kept fixed at 200°C for energy saving to analyze the effects of catalyst wt.% and methanol to Triolein molar ratio on the ester yield. Later in the second stage, the catalyst weight was varied from 1.5 to 8.5 wt.% and the methanol to Triolein molar ratio from 19.4:1 to 40.6:1. A two-factor two level designs was used to perform the experiments. Figure 3.6 depicts the effects of methanol to oil molar ratio on the ester yield (wt. %). This figure depicts the optimum region of parameter combinations for obtaining the highest ester yield. From the experiments, a second-order polynomial equation is developed to fit the experimental data.

Ester yield% = 47.95+1.21×Cat.wt%+2.39×Methanol to Triolein molar ratio-0.48×Cat. wt%^{2}-0.03×Methanol to Triolein molar ratio^2 +.072×Cat.wt%×Methanol to Triolein molar ratio

…(3.5)

From the above model, Cat.wt%, Methanol to Triolein molar ratio, Methanol to Triolein molar ratio^2 are found to be the significant factors.

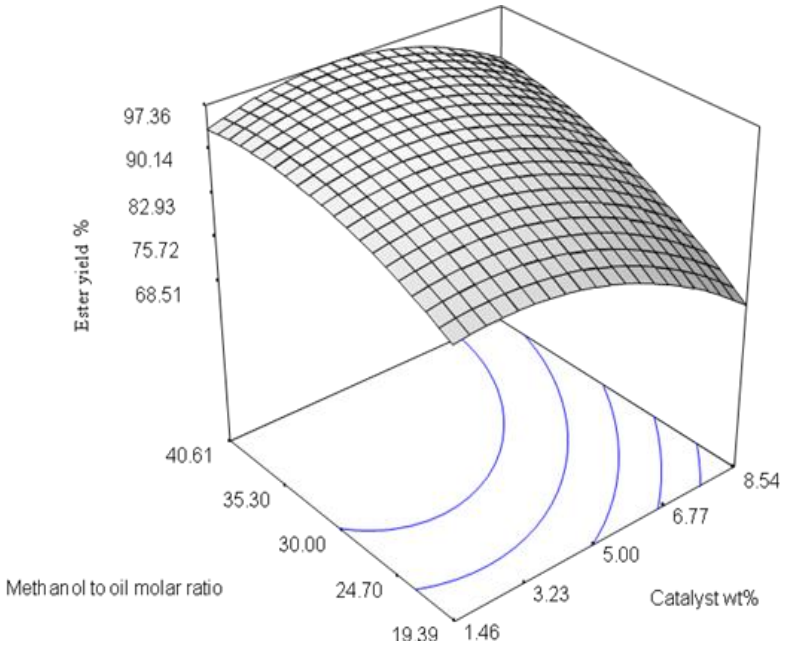

Fig. 3.6 Effects of methanol to oil (Triolein) molar ratio and catalyst wt.% (based on Triolein) on Ester yield%

From the optimization, 4.15 wt.% catalyst (based on Triolein) and 39:1 methanol to Triolein molar ratio are found to be the optimum reaction conditions, when the reaction temperature is kept fixed at 200°C, stirring speed at 600 rpm and allowing 10 h of reaction time. Predicted ester yield using the above condition is 97.4 % and the actual (experimental) yield is 97.2%, which indicates that the model prediction is validated well. In the second stage of the experiments, reaction temperature, residence time and reaction pressure are kept constant (all experiments were conducted at fixed temperature, time and reaction pressure). Thus for the above polynomial model three fixed reaction parameters are 200°C reaction temperature, 10 h reaction time, and 4.14 MPa reaction pressure.

3.4.6 Catalyst deactivation and reusability study

For catalystsreusability study, the catalyst was separated from the reaction mixture by filtration.The separated spent catalyst was washed with hexane and methanol to remove non-polar and polar compounds (e.g. methyl esters, glycerol) present on the surface and dried at 100°C for 1 h. Finally, the dried catalyst was used for transesterification. The study was done using the center point reaction condition of the optimization study. Table 3.2 depicts the catalytic activity (in term of ester yield) of fresh and spent catalyst. It depicts that the activity of the spent catalyst decreased with the usage.

Table 3.2: Catalytic activity of fresh and spent catalyst (5 wt.%, 25% TPA/SBA-15 at 200°C, 4.14 MPa, 600 rpm, 10 h and using 30:1 methanol to triolein molar ratio

Run no.	Ester yield (wt.%)
1 (Fresh)	93.9
2	87.2
3	59.7
4	56.9

This loss in catalytic activity of the spent catalyst is due to the leaching of the active acid species, which is confirmed by pyridine adsorption study and W content of the biodiesel and the catalysts in the successive runs (Fig. 3.7, Tables 3.3 and 3.4).

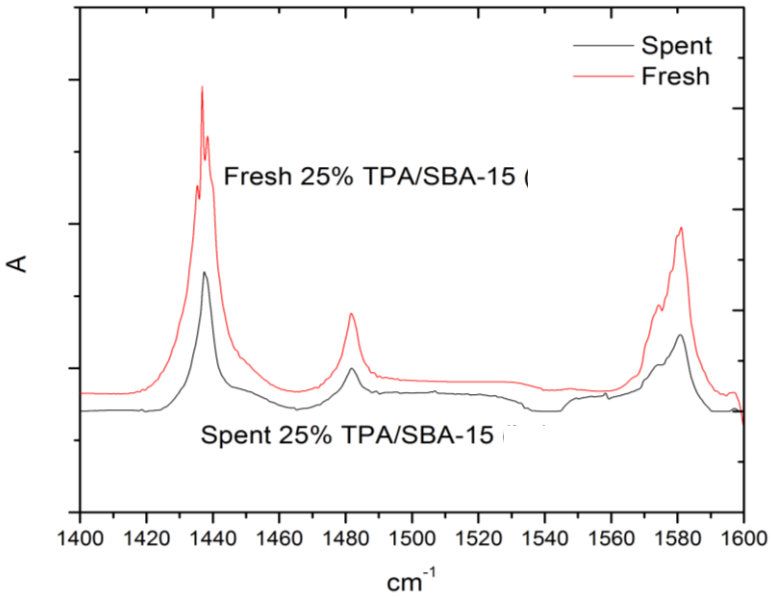

Fig. 3.7 FTIR spectra of the pyridine absorbed fresh and spent catalysts (25%TPA/SBA-15)

Table 3.3: Metal content in Triolein and biodiesel samples in successive runs

Sample	Metal (W) content/ppm
Triolein	<0.03
Run 1	3.20
Run 2	18.6
Run 3	13.8
Run 4	2.60

Table 3.4: TPA content of the fresh and spent catalysts

Run No.	TPA content in the catalyst (wt.%)[a]
1 (Fresh)	25
2	10.86
3	4.78
4	4.41

[a]calculated based on the Tungsten content (W) of the catalyst using ICP-MS

Table 3.3 indicates that with a higher yield, less TPA is present in the ester (biodiesel) phase, whereas at a lower yield higher amount of TPA is present in the biodiesel (ester) phase. The surface area, pore volume and pore diameter of the spent catalyst (25% TPA/SBA-15) are found to be 570 m^2/g, 0.73 cc/g and 5 nm respectively, which are almost same as those of fresh catalysts (Table 3.1), that indicating that there was no structural change in the catalyst 25% TPA/SBA-15.

3.4.7 Effect of presence of water

For this study 0-2 wt.% water was mixed with the Triolein. Figure 3.8 depicts the effect of the presence of water in the feedstock on the ester yield%. It depicts that the ester yield % dropped from 93.9% to 56.8% with the presence of 1wt% water and this ester yield further decreased to 51.3% with the presence of 2 wt.% water in the feedstock.

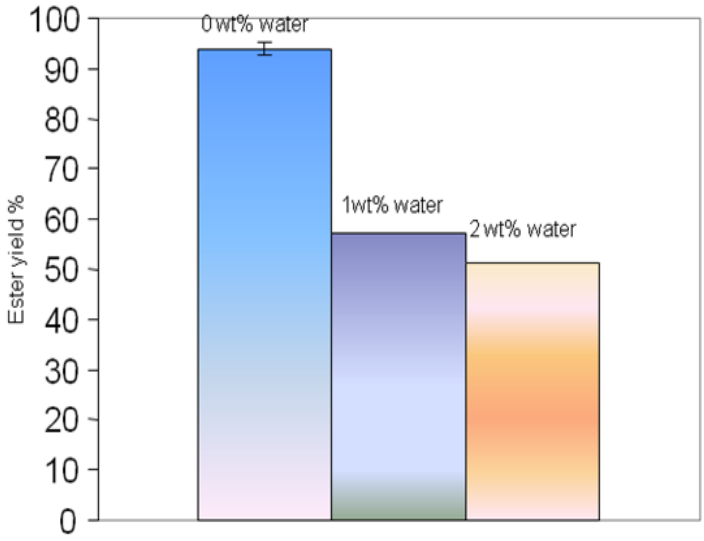

Fig. 3.8 Effect of presence of water in Triolein on ester yield% (5wt% catalyst 25% TPA/SBA-15 at 200°C, 4.14 MPa, 600 rpm, 10 h and using 30:1 methanol to oil molar ratio)

Similar result was found using homogeneous catalyst by Canakci and Gerpen (1999). Increasing the concentration of water can give rise to water-rich clusters around protons and can block it from triglyceride molecules, inhibiting reactions. On the other hand, free fatty acid (FFA) with its polar carboxyl group can interact easily with the water molecules through hydrogen bond, and esterification reaction can continue in the presence of water (Lotero et al., 2005).

3.4.8 Effect of free fatty acids (FFA)

For this study 0-35 wt.%, oleic acid was mixed with the Triolein. Figure 3.9 depicts the effect of free fatty acid on the catalytic activity. It depicts that the ester yield decreases to 64.7±3.21 wt.% (at 95% confidence interval) with the presence of 5 wt.% free fatty acid (FFA) in the Triolein and again increases with the increase in the FFA content in the Triolein (for 15% FFA the ester yield increases to 71.94±1.58 wt.% (at 95% confidence interval). Figure 3.9 depicts that the water content is the highest in the biodiesel (0.4±.01 wt.% at 95% confidence interval) when the Triolein contains 5% FFA. Further increase in FFA, the water content in the biodiesel is less compared to that of 5% FFA, whereas the water contents of the Triolein (containing 0% FFA) and corresponding biodiesel is 0.01 and 0.09 wt.% respectively. Figure 3.10 depicts that with the increase of the FFA in the feedstock Triolein, the acid value of the product biodiesel increased, whereas the acid value of the Triolein containing 0% FFA and corresponding biodiesel was 1.3 and 0.83±.02 mg KOH/g sample (at 95% confidence interval) respectively.

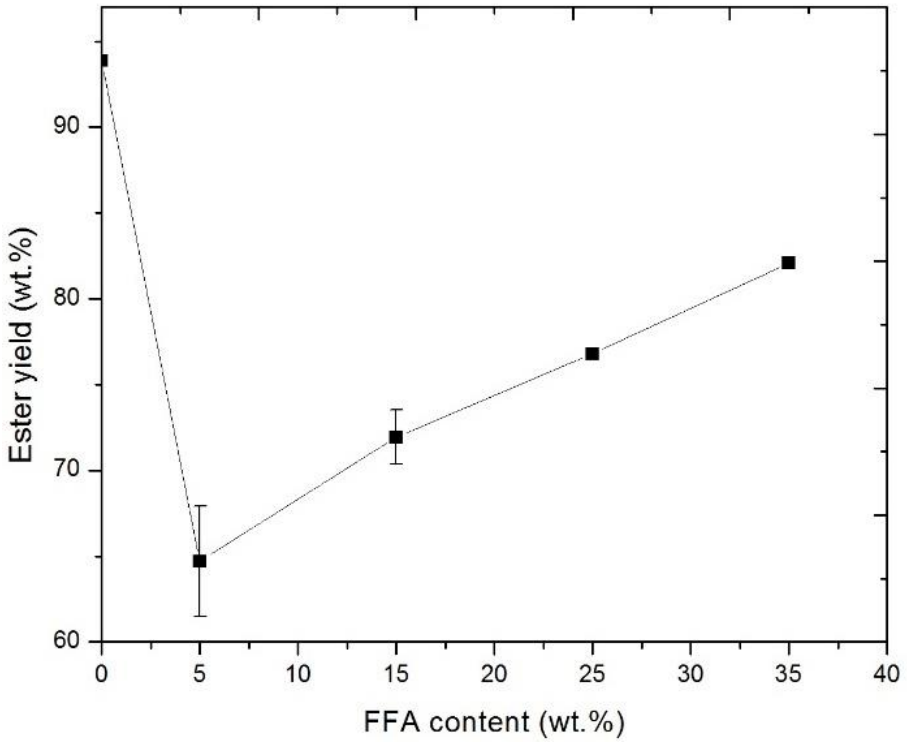

(a)

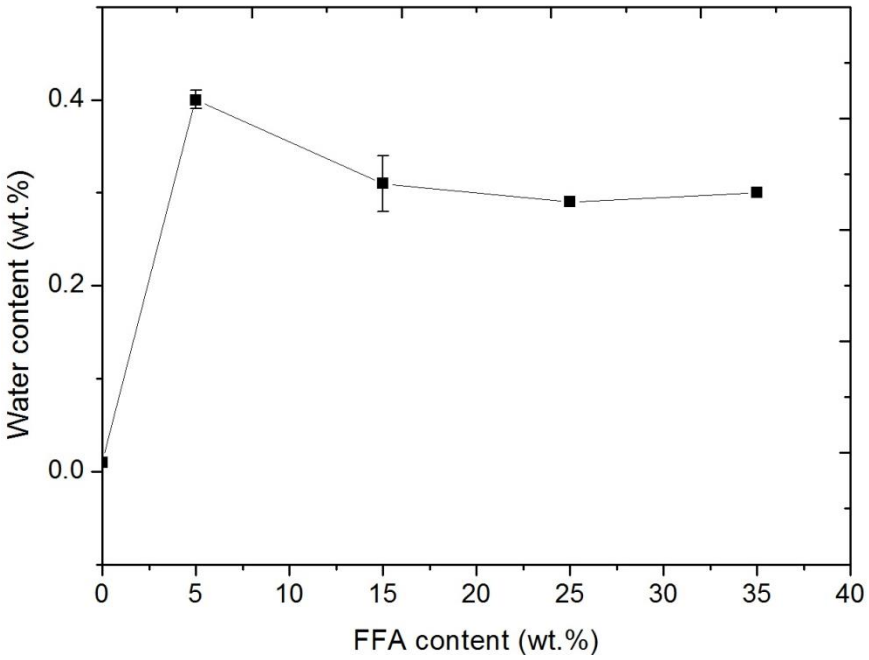

(b)

Fig. 3.9 Effect of presence of (a) free fatty acids (FFA) in Triolein on ester yield% and (b) water content (5wt% catalyst 25% TPA/SBA-15 at 200°C, 4.14 MPa, 600 rpm, 10 h and using 30:1 methanol to oil molar ratio)

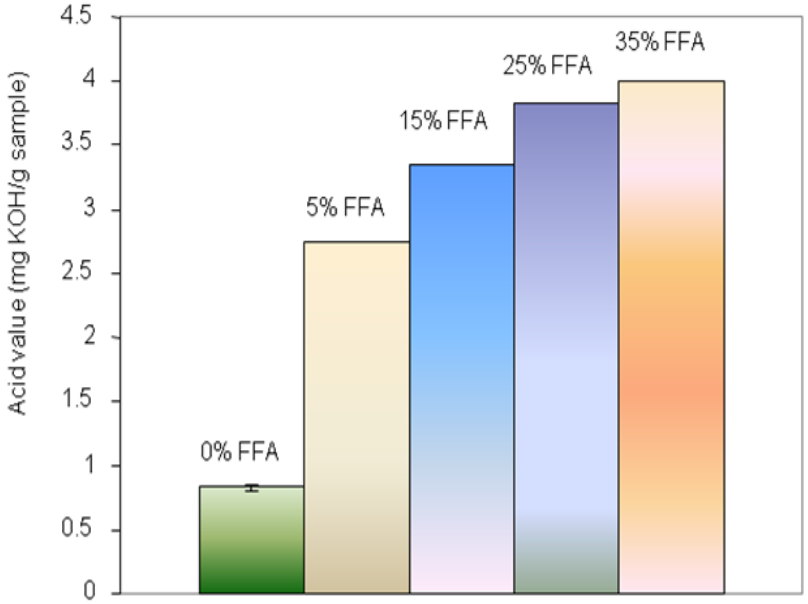

Fig. 3.10 Effect of free fatty acids in Triolein on acid value (mg KOH/g sample) in the produced biodiesel

The sudden decrease of the ester yield in presence of 5% FFA can be explained based on the water content in the biodiesel and the acid catalyzed transesterification and esterification reaction mechanism (Fig. 3.9 and 3.11). The overall reaction mechanism of solid acid catalyzed transesterification and esterification reaction is depicted in Figure 3.11. The free fatty acids (RCOOH) and methanol (CH_3OH) take part in esterification reaction, whereas glycerides (RCOOR') and methanol take part in the transesterification reaction. The carbonyl oxygen of free fatty acid or glyceride interacts with the acidic site of the catalyst to form carbocation. Then a tetrahedral intermediate is produced by the nucleophilic attack of alcohol to the carbocation.

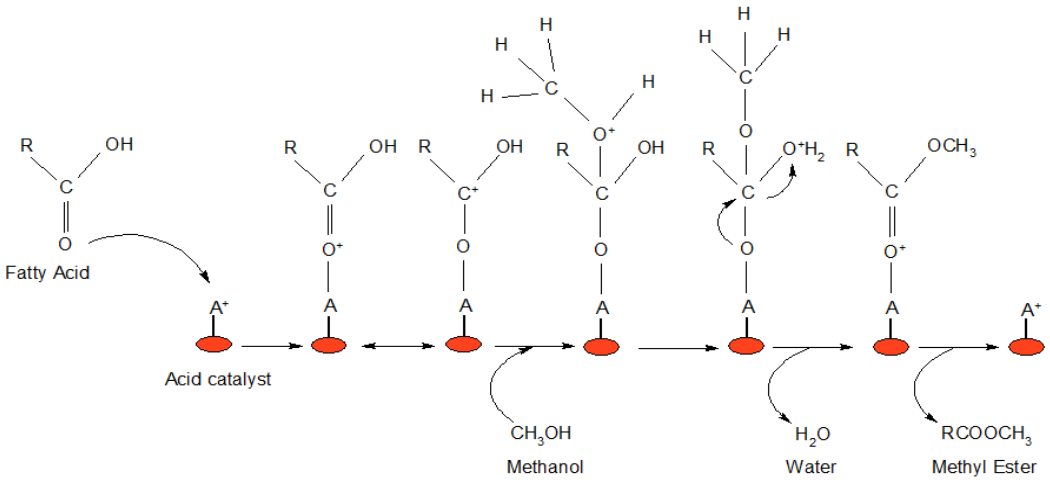

a) Esterification

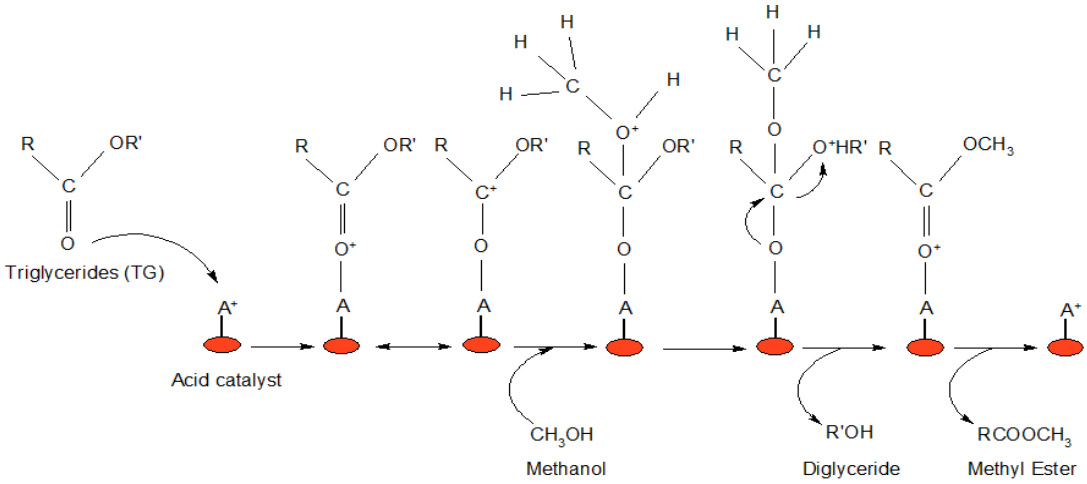

b) Transesterification

Fig. 3.11 Reaction mechanism of acid catalyzed a) esterification and b) transesterification reaction

In the esterification reaction, this tetrahedral intermediate formation generates one mole of water during rearrangement and formation of one mole of ester ($RCOOCH_3$), and in case of transesterification the tetrahedral intermediate only rearranges and forms one mole of similar ester to that of the esterification reaction (Kulkarni et al., 2006). In studies it was found that esterification reactions are faster than transesterification reaction (Ataya et al, 2007; Lopez et al., 2008). Water is one of the products of the esterification reaction. According to Lotero et al.'s findings, the water molecules affect the TG molecules accessibility to the catalyst and inhibit the reaction (Lotero et al., 2005).

The higher water content in the produced biodiesel from the feedstock containing 5% FFA indicated that, in that case, the catalyst initially catalyzes the esterification reaction than transesterification reaction. The esterification reaction product water later worked as a poison for the transesterification reaction, which was already evident from the effect of the presence of water study. The lower acid value of biodiesel in absence of FFA (Fig. 3.10) indicated that 25% TPA/SBA-15 mainly catalyzes the transesterification reaction for biodiesel production.

3.5 Conclusions

This research can be considered as a baseline study to understand the catalytic activity of SBA-15 supported TPA in the transesterification reaction for biodiesel production. Based on the study, 25% TPA is identified as the optimum catalyst loading on SBA-15 by impregnation method for biodiesel production from Triolein. From the optimization study using RSM model, 4.15 wt% catalyst (based on Triolein) and 39:1 methanol to Triolein molar ratio are found to be the optimum reaction conditions, when the reaction temperature is kept fixed at 200°C, stirring speed at 600 rpm and allowing 10 h of reaction time. Predicted ester yield at the above condition is 97.4%, whereas the actual (experimental) yield is 97.2%. The catalyst suffers from poor reusability characteristics due to the leaching of the active species and the catalytic activity is reduced in the presence of FFA and by-product water.

CHAPTER 4: SIMULTANEOUS ESTERIFICATION, TRANSESTERIFICATION AND CHLOROPHYLL REMOVAL FROM GREEN SEED CANOLA OIL USING SOLID ACID CATALYSTS

A version of this chapter has been published in the following journal and presented in the following conference:

- Chinmoy Baroi, Ajay K. Dalai. Simultaneous esterification, transesterification and chlorophyll removal from green seed canola oil using solid acid catalysts. Catalysis Today, 2013, 207, 74-85.
- Chinmoy Baroi, Titipong Issariyakul, Ajay K. Dalai. Simultaneous esterification, transesterification and chlorophyll removal of green seed canola oil using solid acid catalysts. 61st Canadian Society for Chemical Engineering (CSChE) conference, October 23-26, 2011, London, Ontario, Canada.

Contribution of the Ph.D. Candidate

Experiments were conducted by Chinmoy Baroi. The content in this chapter was written by Chinmoy Baroi with discussions and suggestions provided by Dr. Ajay Dalai.

Contribution of this Chapter to the Overall Ph.D. Research

Green seed canola oil is a low price feedstock. In this phase of the study a new method of catalyst preparation (Cat-2) has been developed. This catalyst is proved to be effective to produce biodiesel from different fatty acids (i.e. oleic acid). On the other hand, TPA doped SBA-15 (Cat-3-45-450) is proved to be an effectual catalyst for transesterification, esterification and chlorophyll removal in a single step to produce high-quality biodiesel from GSC oil. The concept of the chlorophyll removal, esterification, transesterification using a heterogeneous (solid) catalyst in a single step is novel.

4.1 Abstract

Green Seed Canola (GSC) oil is a non-edible potential feedstock for biodiesel production. In this work, 12-Tungstophosphoric acid (TPA) was supported by using organic functional group

(i.e. APTES) and was incorporated into the SBA-15 structure. The catalysts were characterized by BET, XRD, FTIR, Raman, TPD and ICP-MS analysis techniques. The catalytic activity of these catalysts was tested using a stirred tank reactor. From the study, organic functional group anchored TPA on SBA-15 showed higher catalytic activity for esterification of free fatty acid (FFA), whereas TPA incorporated into SBA-15 showed higher catalytic activity for transesterification, for biodiesel production from waste green seed canola oil. A 45 wt.% TPA incorporated SBA-15 produced the ester yield of 97.3 wt.%, when 2.96 wt.% catalyst (based on green seed canola oil) and 25.8:1 methanol to Green Seed Canola (GSC) oil molar ratio were used at 200°C for reaction time of 6.25 h. Besides, the catalyst also improved the quality of the biodiesel by adsorbing chlorophyll from the feedstock (75.6 % chlorophyll removal), during the transesterification reaction. Kinetic study showed that the formation of Methyl Oleate was the slowest, compared to other fatty acid methyl ester (FAME) formation. The thermodynamic property values also agreed with this result.

4.2 Introduction

The limited stock of fossil fuels and environmental pollution from the use of these fuels has intensified the need for research on producing renewable fuels. Biodiesel is a renewable diesel substitute fuel. This fuel is produced from triglycerides using lower alcohol through transesterification reaction. The other name of transesterification is alcoholysis because in this process one alcohol is replaced by another i.e. the higher alcohol (glycerol) present in the triglyceride is replaced by a lower alcohol (e.g. methanol, ethanol) and the resultant monoalkyl esters of fatty acids are called biodiesel. Biodiesel is produced are vegetable oils and fats e.g. rapeseed, soybean, sunflower, coconut and palm oil. Biodiesel can also be produced from free fatty acids though esterification reaction. However, the existence of pure fatty acid is rare, as they exist in the form of triglyceride (oil) in nature, and production of pure free fatty acids (FFA) for biodiesel production is not economically feasible. Most of the conventional feedstocks for transesterification are food crops, which creates controversy of creating world food crisis by using those for biodiesel production. Besides, the biodiesel yet cannot compete with the petro-diesel because of its higher price, which is associated with the production cost (Kulkarni and Dalai, 2006). Estimation depicts that approximately 88% of the total production cost is associated with the feedstock (Marchetti and Errazu, 2008). This cost can be reduced by using

cheaper feedstocks, e.g., used cooking oil, yellow grease. Acid catalysts can catalyze esterification reaction along with transesterification reaction to produce similar type of esters from free fatty acids. Homogeneous acid catalysts can serve this purpose, but solid acid catalysts are preferred over those for waste minimization and easy product recovery (Kulkarni et al., 2006). Mesoporous solid acids catalysts with a moderate to strong acid sites and a hydrophobic surface are desireable for the biodiesel preparation (Lotero et al., 2005; Kiss et al., 2006).

Green seed canola oil is one of the low-grade oils available in huge quantity in Western Canada. The raw green seed canola oil are not edible because of the presence of the higheramount of chlorophyll (Abraham and DeMan, 1986). The higher chlorophyll content also reduces the oxidation stability of the oil (Rawks and Santen, 1970). However, the green seed canola oil processing cost for edible purpose is high (Kulkarni et al., 2006). Untreated green seed canola oil has poor oxidation stability due to the presence of the higher amount of chlorophyll. However, this can be improved by pre-treating the green seed canola oil with the mixture of mineral acids and/or using acid treated adsorbents, which can reduce the chlorophyll to a significant amount, and the pretreated oil can produce biodiesel with improved oxidation stability similar to that of canola biodiesel following traditional base catalyzed reaction (Kulkarni et al., 2006; Bahmaei et al., 2005).

Heteropolyacids (HPA) depicts strong and pure Brønsted acidity (Devassy and Halligurdi, 2005; Busca, 2007; Okuhara et al., 2000). A 12-Tungstophosphoric acid (TPA)with a Keggin structure has higher thermal stability and depicts superior acidity as compared to other HPA compounds (Kozhevnikov, 2007). Heteropolyacid compounds have lower surface area (1 – 10 m^2/g) and they are soluble in polar media (Kulkarni et al., 2006). These problems can be avoided by supporting $H_3PW_{12}O_{40}$ on various carriers. Silica based mesoporous materials fully satisfy all the desired criteria as a support for reactions involving polar solvents (Wong and Wales, 2006). SBA-15, a silica-based mesoporous material can be an ideal support due to its higher hydrothermal stability and the low carbon deposition tendency compared to other silica based mesoporous supports (Herrera et al., 2008). Possible pathways for preparation of TPA supported SBA-15 catalysts are direct incorporation of TPA into SBA-15 structure and use of organosilane compounds as an anchoring agent of TPA on the silica surface. In a previous work (Inumaru et al., 2007) TPA was supported on SBA-15 with the help of 3-Aminopropyl triethoxysilane (APTES) and the surface was made hydrophobic with the help of *n*-

octyltriethoxysilane. That catalyst was used for the hydrolysis reaction, and the SBA-15 surface was modified with APTES and *n*-octyltriethoxysilane by post-synthesis method (Inumaru et al., 2007). Incorporating TPA into SBA-15, as well as template removal, was performed by varying the sequence of addition and composition of components such as templates, HCl, TEOS and TPA precursor (Yun et al., 2004; Yang et al., 2005; Dufaud et al., 2009; Guo et al., 2008; Galarneau et al., 2001; Gagea et al., 2009; Shi et al., 2005; Wang et al., 2006; Zhang and Yang, 2008). All these catalysts were tested in different reactions other than transesterification reaction. In this work for the first time, APTES and *n*-octyltriethoxysilane were directly incorporated into the SBA-15 structure, and TPA was loaded on SBA-15 with the help of APTES. Moreover, a different catalyst was prepared by direct incorporation of TPA into SBA-15 structure following a modified composition of components (template/HCl/TPA/TEOS) and modified synthesis steps without using organic functional groups.

The overall objective of this work was for the first time to explore the possibility of using untreated green seed oil for esterification, transesterification and chlorophyll removal in a single step to produce high quality biodiesel using acid catalysts.

4.3 Experimental

4.3.1 Reagents

Unrefined green seed canola oil (4.25 wt.% FFA) was obtained from Milligan Biotech Inc., Foam Lake, Saskatchewan, Canada. Methanol (99.9%), P123 and TEOS (Tetraethyl orthosilicate) were purchased from Sigma-Aldrich, Oakville, Ontario, Canada. 12-Tungstophosphoric acid (TPA) was purchased from Alfa-Aesar, MA, USA.

4.3.2 Catalyst preparation

Cat-1:

For this catalyst the following composition was used (mole basis): TEOS: APTES: P123: HCl: H_2O= 0.098612: 0.001388: 0.0014: 0.585: 16.2. The synthesis procedure for Cat-1 is as follows: 14.58 g of P123 was dissolved in 426 g water plus 85 g HCl solution by stirring for 2 hours at 35°C. Thereafter, 30 g of Tetra Ethyl Orthosilicate (TEOS) was added to the aquous solution with stirring at 35°C. After 1 hour .324 mL APTES was added into the solution, as it

was found previously that hydrolysis of TEOS is completed within 1 hour and adding APTES thereafter doesn't negatively affect the SBA-15 structure (Wang et al., 2004; Wang et al., 2005). The resulting mixture was stirred at 35°C for 20 h and thereafter, the mixture was aged in a Teflon bottle at 110°C for 48 h. The solid product was filtered and washed several times with water. Refluxing ethanolfor 48 h (40 mL ethanol per 1 g of material) was used to remove the template from the material and then the material was dried overnight at 110°C. The resultant material was treated with HCl solution for 24 h. The treated material was filtered out, water washed, and dried overnight. The material was immerged into the TPA solution and dried at 110°C overnight.

Cat-2:

For this catalyst the following composition was used (mole basis): TEOS: APTES: P123: HCl: H_2O = 0.098612: 0.001388: 0.0014: 0.585: 16.2. The synthesis procedure for Cat-1 is as follows: 14.58 g of P123 was dissolved in 426 g water plus 85 g HCl solution by stirring for 2 hours at 35°C. Thereafter, 30 g of TEOS was added to the aquous solution with stirring at 35°C. After 1 hour 0.324 mL APTES was added into the solution, as it was found previously that hydrolysis of TEOS is completed within 1 hour and adding APTES thereafter does not negatively affect the SBA-15 structure (Wang et al., 2004; Wang et al., 2005). Then after another 1 h calculated amount of TPA was added. The resulting mixture was stirred at 35°C for 20h and thereafter, 6 mL *n*-octyltriethoxysilane was added into the mixture and was stirred at 35°C for another 20 h. The mixture was aged in a Teflon bottle at 110°C for 48 h. The solid product was filteredout and water washed several times. Refluxing ethanolfor 48 h (40 mL ethanol per 1 g of material) was used to remove the template from the material and then the material was dried overnight at 110°C.

Cat-3:

For this catalyst the following composition was used (mole basis): TEOS: P123: HCl: H_2O= 0.1 0.0014: 0.585: 16.2. The synthesis procedure for Cat-4 is as follows: 14.58 g of P123 was dissolved in 426 g water plus 85 g HCl solution by stirring for 2 hours at 35°C. Thereafter, calculated amount of TPA was added in an aqueous solution form (dropwise). After 1 h, 30 g of

TEOS was added to the solution with stirring at 35°C. The resulting mixture was stirred at 35°C for 20 h and thereafter, the mixture was aged in a Teflon bottle at 110°C for 48 h. The solid product was filtered out, water washed and dried overnight at 110°C. The catalysts were calcined at 350°, 450°, 550° and 650°. The catalysts were designated as Cat-3-X-T, where X represents the loading and T represents the calcination temperature.

4.3.3 Catalyst characterization

The synthesized catalystsBET surface area and pore size analysis were performed using Micrometrics adsorption equipment (Model ASAP 2000). The catalysts were heated at 200°C in a vacuum of 5×10^{-4} atm before the analysis. The surface area was calculated from the isotherms using Brunauer-Emmett-Teller (BET) method. The pore diameter and pore volume was calculated using BJH method from desorption branch of the isotherms. Temperature programmed desorption of ammonia (TPD) was carried out on a Micrometrics equipment using a TCD detector. In a typical experiment, at first 75 mg of the each sample was pretreated in He (Helium) at 400° C for 1 h with a flow rate of helium of 20 mL/min. The sample was exposed to NH_3 at 100° C for 0.5 h (half hour) and then was purged by helium for 1 hour. Then the spectra was recorded between 100° C to 750° C, with a temperature ramp of 10 °C /min. The X-ray diffraction (XRD) patterns of the samples were collected on a Bruker D8 Advance diffractometer using Cu $K\alpha$ radiation (λ = 1.5418 A). The catalysts FTIR spectra were recorded through Perkin Elmer FTIR spectrum GX equipment. For the FTIR analysis, sample pallets were prepared by pelleting a well mixed 3 mg of catalyst powder with 200 mg of KBr. Raman spectra of the catalyst were recorded at room temperature with a Renishaw system 2000 spectrometer (785 nm). The W (Tungsten) and Mg (Magnesium) was determined by ICP-MS.

4.3.4 Catalytic activity testing

The catalytic activity of the prepared catalysts was tested through transesterification of green seed canola oil. The reactions were conducted in a 450 mL Parr reactor (Parr Instrument Co., ILL, USA). Initially, 100 g of GSC oil was taken into the reactor and preheated to 60°C with optimized stirring at 600 rpm. Methanol and catalysts were then added to the reaction vessel. Preliminary catalyst screening experiments were conducted at a reaction temperature of

150°C, 20:1 methanol to oil molar ratio, 3 wt.% catalyst (based on the wt. of Green seed canola oil). Central Composite Design (CCD) was utilized to design the combination of experiments analyzing the effect of reaction parameters and Design Expert 6.1 software was used for this purpose. The biodiesel phase (after separation of the catalyst by filtration and separation of the glycerol phase) was analyzed utilizing High-performance liquid chromatography (HPLC). The sample collected from each experiment was analyzed for its ester content utilizing a Hewlett-Packard 1100 series HPLC. Two Phenogel 100°A 300X7.80 mm 5 micron columns in series protected with guard column were exploited to separate different components of the samples during analysis. THF was used as a mobile phase at 1 mL/min for 25 min. The operating parameters were of sample injection volume 5 μL, detector temperature of 35°C, and column temperature of 24°C. Standard chemicals including methyl oleate, triolein, diolein, and monoolein were used for the HPLC calibration (see Appendix B). The ester yield (wt. %) was calculated according to the equation 4.1.

Ester yield (wt. %) = (wt. of the methyl ester in the ester phase)/ (wt.. of the oil phase) ×100 …(4.1)

An Agilent make Gas Chromatography system (model 7890A) along with flame ionization detector (FID, 260 °C) and capillary column DB-23 (dimensions: 60 m length, 0.25 mm ID, 0.25 μm film) was used for the analysis of different fatty acids in methyl ester (FAME). Throughout the experimentation, the GC was operated at constant conditions (Carrier: hydrogen gas with flow rate 20 cm/min & 0.16MPa pressure; Oven: 140 to 240 °C at 4 °C/min. and Injection: 1 μl sample, 260 °C & split: 20:1). The acid value, cloud point and pour point of the biodiesel product was determined according to the ASTM D6751 methods. A UV-260 Shimadzu spectrometer was exploited to determine the amount of chlorophyll. Chlorophyll content in the feedstock Green Seed Oil and biodiesel was calculated according to the method described by Lichtenthaler (1987). The free fatty acid conversion was calculated based on the initial and final acid value.

4.4 Results and discussion

4.4.1 Catalyst characterization

The catalysts textural properties are depicted in Table 4.1. It depicts that, introduction of *n*-octyltriethoxysilane reduces the surface area, pore diameter and pore volume (Cat-2 compared to Cat-1). Table 4.1 also depicts that for Cat-3, with the increase in the calcination temperature up to 450°C, surface area, pore diameter and pore volume increase and decrease thereafter, whereas the Keggin anion density increases. These facts can be explained as an incomplete removal of the template at 350°C and start of sintering beyond 450°C (Guo et al., 2008; Berube and Kaliaguine, 2007; Sawant et al., 2008). For all the catalysts, the actual loading is in good agreement compared to that of theoretical loading (25%), except for Cat-2. While preparing Cat-2, another approach was taken, where APTES and *n*-octyltriethoxysilane was directly incorporated, followed by post grafting of TPA. The theoretical loading for this catalyst was 25 wt.% and the actual loading obtained was 5.63 wt.%, which indicates the presence of *n*-octyltriethoxysilane has a negative impact on the TPA loading. However, following a new method during Cat-2 preparation, the TPA loading can be improved. For Cat-1, 2 and 3 the Keggin anion density was calculated following the method described by Chai et al. (2008). It is observed from Table 4.1 that Keggin anion density increases with the decrease of the pore diameter, surface area and pore volume and vice versa.

Table 4.1: Textural property of different catalysts

Sample	TPA Loading (wt.%)	BET Surface area (m^2/g)	Pore Volume (cc/g)	Average Pore diameter (nm)	d spacing d_{100}/°nm[1]	Pore Wall thickness nm[2]	Keggin-anion density (HPA nm^{-2})
Cat-1	26.21	534	0.67	3.98	5.86	2.79	0.10
Cat-2	16.5	496	0.57	3.49	5.86	2.79	0.07
Cat-3-25-350	-	318	0.53	5.74	5.87	1.04	0.17
Cat-3-25-450	25.98	344	0.55	6.15	5.86	0.62	0.16[3]
Cat-3-25-550	-	305	0.49	5.69	5.86	1.07	0.18[3]
Cat-3-25-650	-	283±51	0.32±0.09	4.90±0.39	5.86	1.87	0.2[3]

[1] d_{100} was calculated using Bragg's law

[2] Pore wall thickness = a-pore dia ($a=2d_{100}/3^{1/2}$)

[3] Assuming the intact Keggin-structure

Table 4.2 depicts the acid strength of different catalysts. It depicts that Cat-3-25-450 has the highest acidic strength.

Table 4.2: Acid strength distribution of different catalysts

Sample	Acidity ($\times 10^4$ mol/g of catalyst)	
	weak	moderate/strong
Cat-1	1.14	-
Cat-2	4.97	-
Cat-3- 25- 350	8.47	1.79
Cat-3- 25- 450	9.88	1.80
Cat-3- 25- 550	5.83	2.54
Cat-3- 25- 650	4.02	0.47

Table 4.3 depicts textural properties of different loadings of Cat-3-X-450. It depicts that, with the increase of TPA loading, surface area, pore diameter and pore volume decrease, which indicates the presence of TPA on to the pore wall rather than buried inside the pore wall of SBA-15 (Gagea et al., 2009).

Table 4.3: Textural property of various TPA loading on Cat-3-X-450

TPA loading (wt. %)	BET surface area (m^2/g)	Pore volume (cc/g)	Average Pore diameter (nm)
25	343.9	0.55	6.12
35	310.4	0.51	5.63
45	272.7	0.46	5.14
55	265.9	0.36	4.52

For the catalysts, the SBA-15 structure is decided by a XRD pattern made of a strong peak (at 2θ around 0.8°) along with two small peaks (at 2θ around 1.6° and 1.8°) (Fig. 4.1) (Yang et al., 2005; Tropecelco et al., 2010).

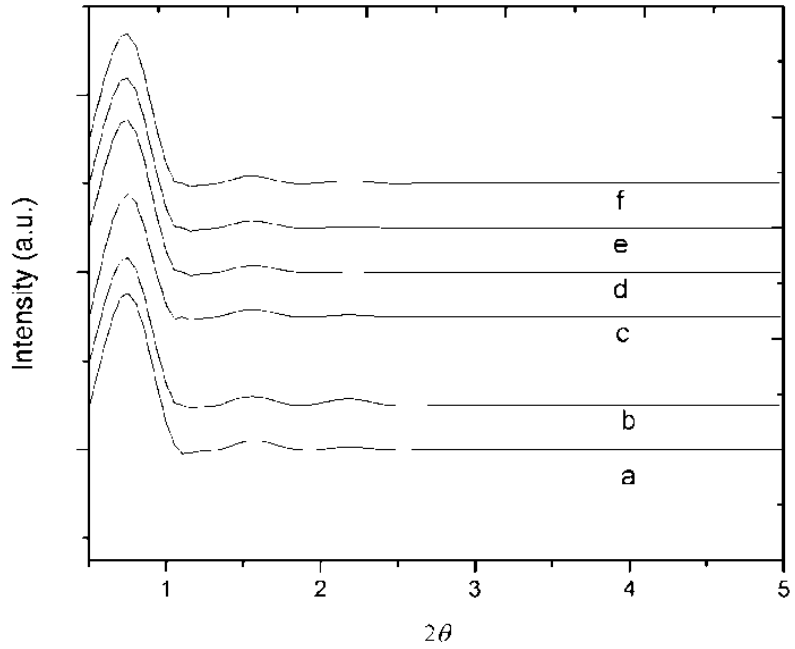

Fig. 4.1 Low angle XRD of different catalysts: (a) Cat-1, (b) Cat-2, (c) Cat-3-25-350, (d) Cat-3-25-450, (e) Cat-3-25-550, (f) Cat-3-25-650

The IR bands approximately at 690 cm^{-1} (N-H bending) and a very weak peak at 1510 cm^{-1} (-NH_2 bending) confirm the presence of APTES in Cat-1 and Cat-2 (Fig. 4.2) (Wang et al., 2005).

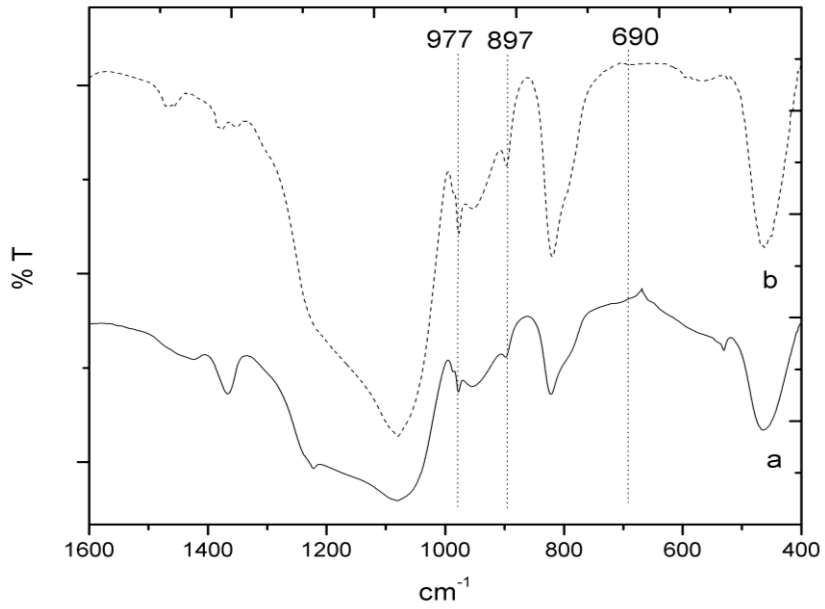

Fig. 4.2 FTIR spectra of (a) Cat-1 (b) Cat-2

The IR band approximately at 970 cm^{-1} is associated with the Si-OH vibration (Ming et al., 2010). In Cat-1 and Cat-2, this band is shifted to 954 cm^{-1}, which indicates strong interaction between the Si-O-C_2H_5 of APTES and the Si-OH of the support and the peak at 2928 cm^{-1} indicates strong interaction between TPA and APTES (Wang et al., 2005; Ming et al., 2010). The presence of *n*-octyl triethoxysilane in Cat-2 was confirmed by IR bands approximately at 2968 cm^{-1} (C-Hstretching;-CH_3) and 2875 cm^{-1} (C-H stretching; -CH_2-) (Fig. 4.3) (Wang et al., 2005; De Prado et al., 2010; Sun et al., 2011).

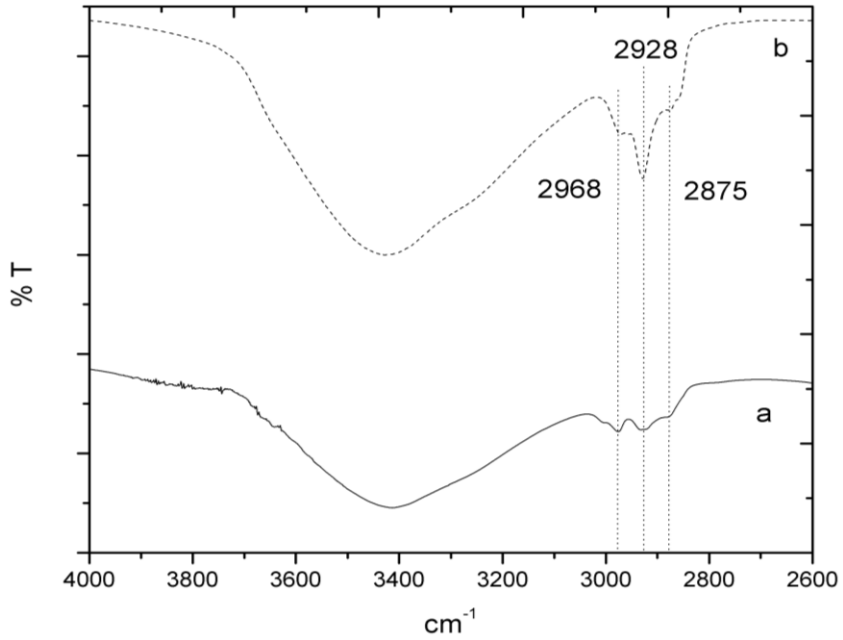

Fig. 4.3 FTIR spectra of (a) Cat-1 (b) Cat-2

Pure TPA depicts IR peaks approximately at 1081 (P-O in the central tetrahedron), 976-995 (terminal W=O), 890-900 and 805-810 (W-O-W) cm^{-1} refers to asymmetric vibration of the Keggin ion (Tropecelo et al., 2010; Satish kumar et al., 2006; Damyanova et al., 2003; Yun and Kubara et al., 2004). The IR peaks at approximately 1081, 977, 897 and 816 cm^{-1} are observed for Cat-1 and Cat-2, which confirms the preservation of Keggin structure (Fig. 4.2). From Figure 4.4 it is observed that, the IR bands of P-O in the central tetrahedron moves to the higher energy region (1080→1091) and that of terminal W=O approximately at 977 cm^{-1} weaken with the increase of calcination temperature in Cat-3-25%. Figure 4.4 also depicts that IR band approximately at 970 cm^{-1} associated with the Si-OH vibration moved towards 951 cm^{-1} with the increase of calcination temperature. IR bands moving towards lower wave number (energy)

indicative of increase in interaction and vice versa (Lopez-Salinas et al., 2000; Touvenot et al., 1984), confirms strong interaction of terminal W=O of TPA structure with SBA-15, with the increase in calcination temperature.

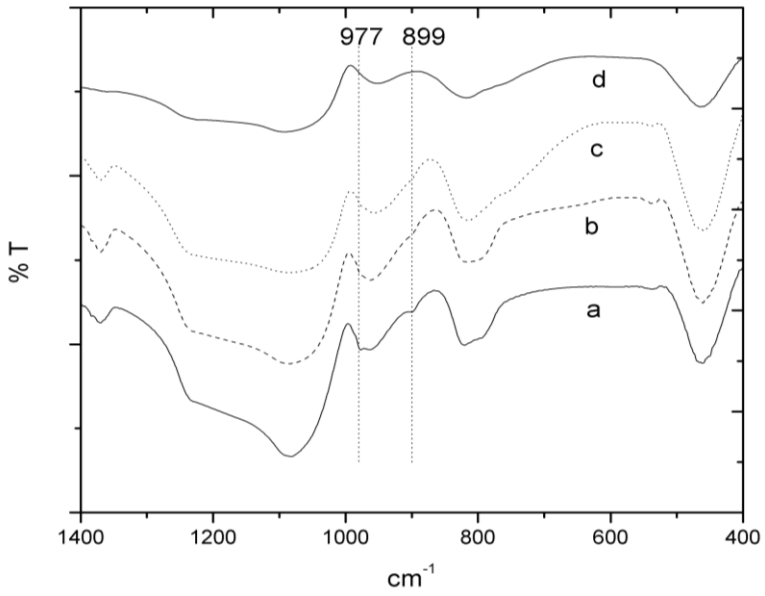

Fig. 4.4 FTIR spectra of Cat-3 calcined at different temperature: (a) Cat-3-25-350 (b) Cat-3-25-450 (c) Cat-3-25-550 (d) Cat-3-25-650

The IR peak at 1370 cm^{-1} is assigned to the C-O-C stretch of P123 (Wang et al., 2005), which are found to be diminished with an increase of the calcination temperature (Fig. not depicted). Raman scattering peaks between 1100-900 cm^{-1} are assigned as to the Keggin unit of TPA (Guo et al., 2008; Thouvenot et al., 1984). Figure 4.5 depicts the Raman spectra of Cat-3 at different calcination temperatures. It depicts that the Keggin structure is present up to 450°C, by showing characteristic Raman scattering approximately at 1007 cm^{-1} (P-O in the central tetrahedron) and 994 cm^{-1} (terminal W=O). Figure 4.5 also depicts that beyond calcination temperature of 450°C, Raman scattering at 1007 cm^{-1} (P-O in the central tetrahedron) and 994 cm^{-1} (terminal W=O) completely disappears and two strong bands approximately at 802 cm^{-1} (shifting of terminal W=O from 994 cm^{-1}) and 715 cm^{-1} (shifting of W-O-W from 912 cm^{-1}) appears. These shifting of the peak positions confirms strong interaction between SBA-15 and the terminal W=O of TPA (Guo et al., 2008).

Figure 4.6 depicts wide angle XRD pattern of different catalysts. It depicts that TPA is highly dispersed in Cat-1, Cat-2, Cat-3-25-350 and Cat-3-25-450 (Dufaud et al., 2009; Gagea et

al., 2009). However, in Cat-3-25-450 and Cat-3-25-550, characteristic peaks of crystalline Tungsten oxide (23.06°, 23.54° and 24.34°) is observed, which indicates that TPA structure has been destroyed (Yang et al., 2008; Bordoloi and Hallligudi, 2008; Zhang et al., 2009).

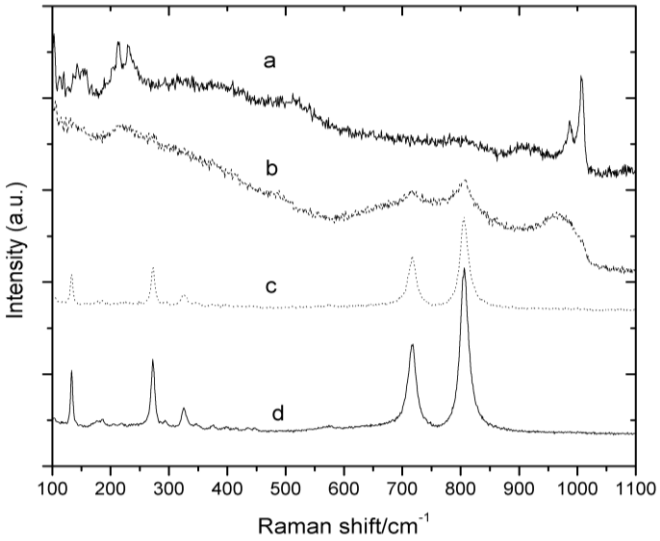

Fig. 4.5 Raman spectra of Cat-3 calcined at different temperature: (a) Cat-3-25-350 (b) Cat-3-25-450 (c) Cat-3-25-550 (d) Cat-3-25-650

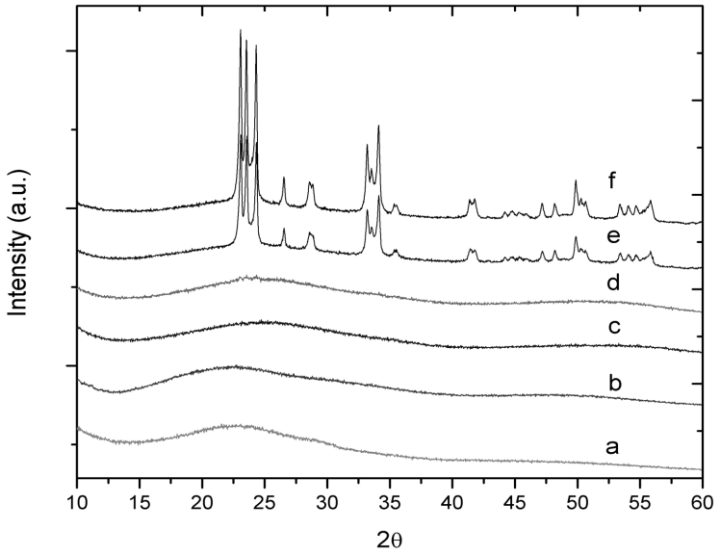

Fig. 4.6 Wide angle XRD pattern of different catalysts: (a) Cat-1 (b) Cat-2 (c) Cat-3-25-350 (d) Cat-3-25-450 (e) Cat-3-25-550 (f) Cat-3-25-650

4.4.2 Postulated synthesis mechanism for Cat-3

Figure 4.7 depicts the postulated synthesis mechanism of the TPA incorporated into SBA-15. According to the postulation, the hydrophilic ethylene oxide (EO) of the surfactant, Pluronic 123 ($EO_{20}PO_{70}EO_{20}$) associates with hydronium ions as $PO_m[(EO).H_3O+)]_{x....}xCl^-$, in presence of HCl. After addition of TPA the Keggin anion of TPA ($PW_{12}O_{40}^{3-}$) substitutes the Cl^- anions leading to strongly attached on the P123 micelle before the silica source addition. TEOS as $(SiO_4H_5)^+$ cations interacts with the anionic side of the P123 micelles (Dufaud and Lefebvre, 2010). After hydrothermal treatment (aging), the silica network traps Keggin anions between P123 and the silica. The P123 are removed by washing, filtration and calcinations, and the TPA would attach on the silica pore wall.

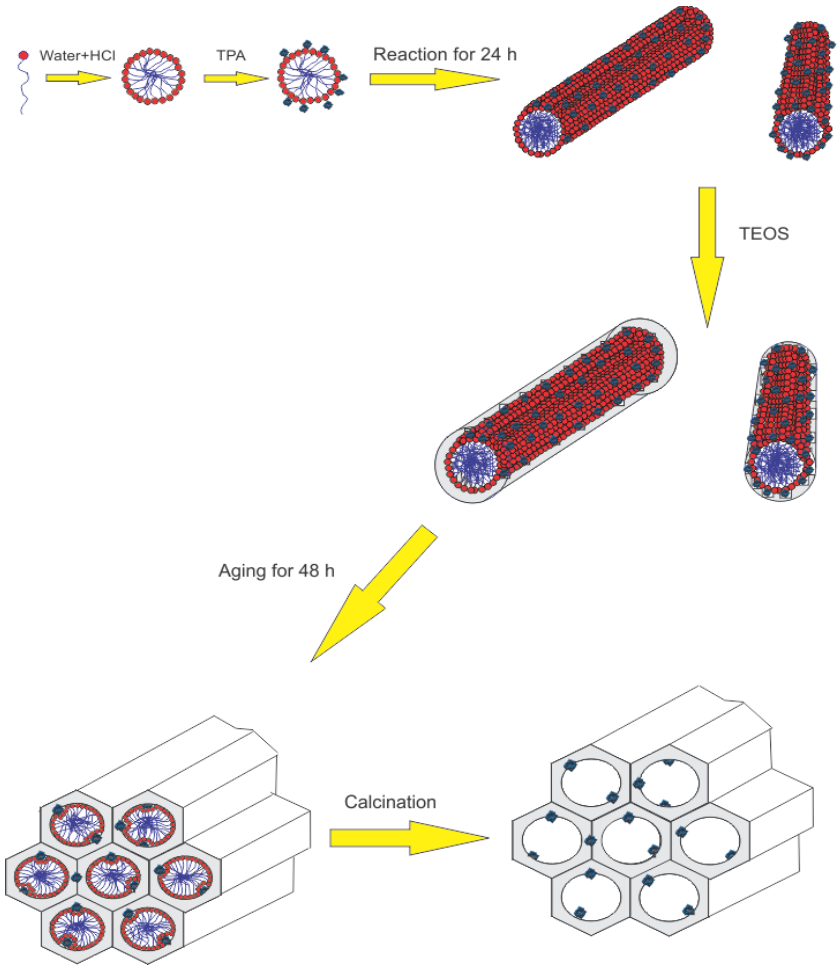

Fig. 4.7 Postulated synthesis mechanism for Cat-3

4.4.3 Catalytic activity

The absence of external and internal mass transfer resistance was confirmed by the Reynolds number of the reaction mixture, mass-transfer flux, reaction rate and Weisz-Prator criteria (see appendix C). Figure 4.8 depicts catalytic activity of different catalysts. It depicts that Cat-1 and Cat-2 were less catalytically active compared to that of Cat-3 calcined at different temperatures. The reasons might be due to the weak acidity and lower loading as compared to that for Cat-3. However, Cat-2 was found to be more active than that of Cat-1 instead of having lower TPA loading, which might be the contribution of hydrophobic surface and also due to the higher acidity. Figure 4.8 also depicts that Cat-3-25-450 had the highest catalytic activity (ester yield of 29±0.15% at 95% confidence interval using 10 h reaction time), which might be because of the highest and optimum surface area, pore diameter, pore volume and highest acidity among the prepared catalysts.

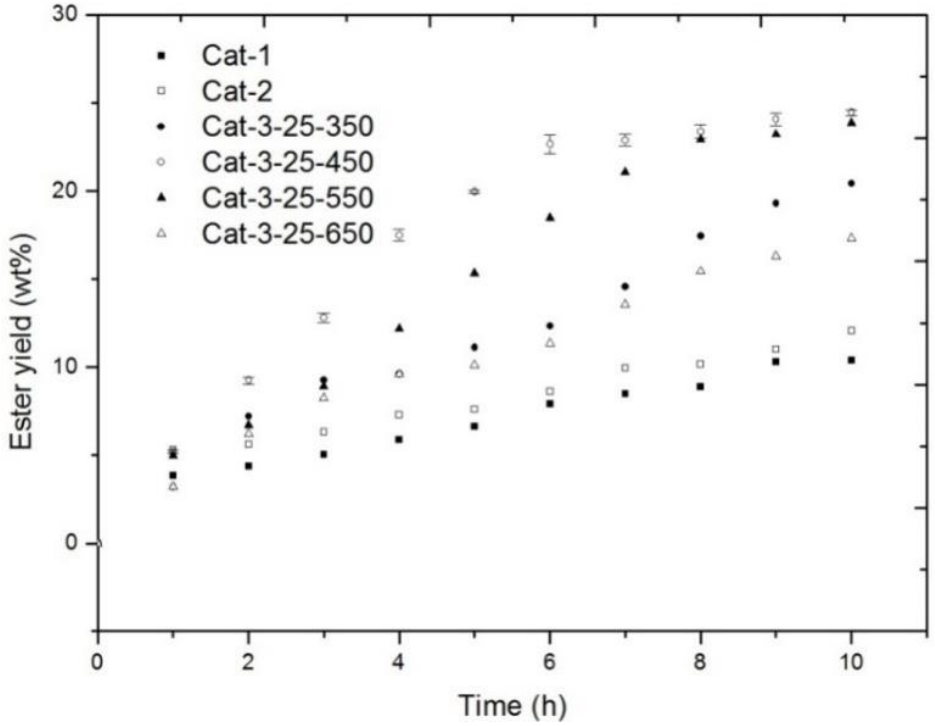

Fig. 4.8 Catalyst screening study (3 wt.% catalyst, 20:1 methanol to GSC oil molar ratio, 150°C and 10 h)

Figure 4.9 depicts the catalytic activity of Cat-2 and Cat-3-25-450 in the FFA (present in the GSC oil) esterification. It depicts that Cat-2 is more catalytically active (96.7±2.3% at 95% confidence level) in esterification reaction than Cat-3-25-450 (70.2±1.6% at 95% confidence

level). This fact can be explained with the help of Brønsted and Lewis acidity. Brønsted acid catalysts are mainly active in the esterification reaction and Lewis acid catalysts are mostly active in the transesterification reaction (Di Serio et al., 2008). Previously it was found that APTES attaches the TPA by co-valent bond, therefore the Brønsted acidity of TPA is retained (Inumaru et al., 2007), whereas, in TPA incorporated SBA-15, TPA is attached to the silica surface by strong electrostatic bond (by calcination), as a result the Lewis acidity may arise from the Brønsted acidity (Yori et al., 2005).

Figure 4.10 depicts catalytic activity of different loading of TPA in Cat-3-X-450. It depicts that catalytic activity increase with the increase of the TPA loading up to 45% and there is no further increase in the catalytic activity beyond that loading thereafter. Similar result was acquired by Caetano et al. (2008). According to their explanation, catalytic activity increases with the increase of the TPA loading by kinetic effect, and catalytic activity decreases with higher loading due to the internal diffusion limitation inside the pores of the catalyst.

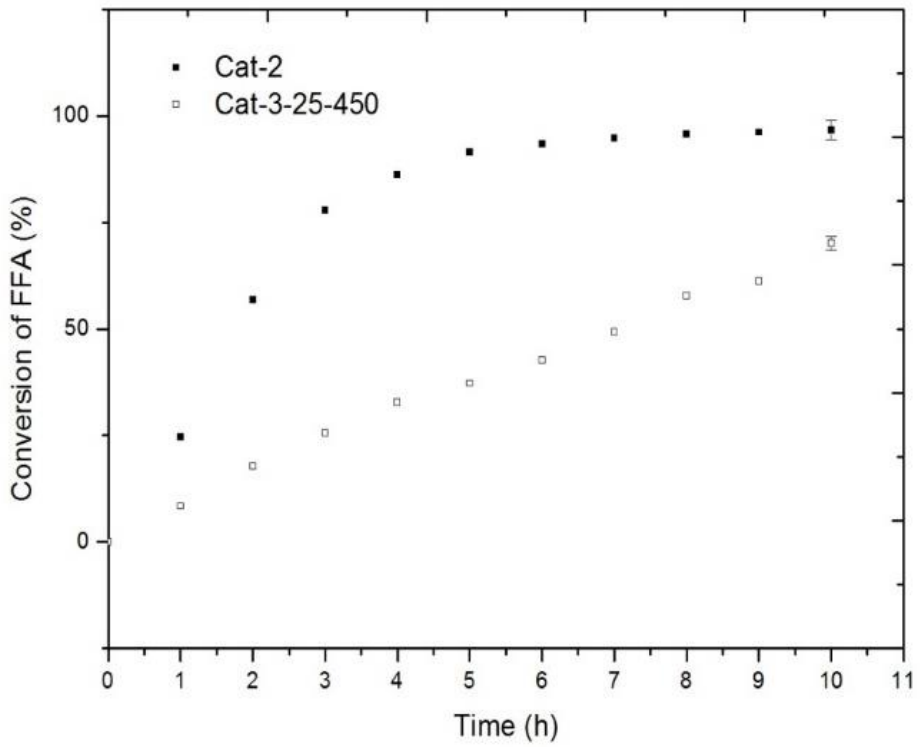

Fig. 4.9 Catalytic activity study different catalyst in esterification of FFA present in the oil (3 wt.% catalyst, 20:1 methanol to GSC oil molar ratio, 150°C and 10 h)

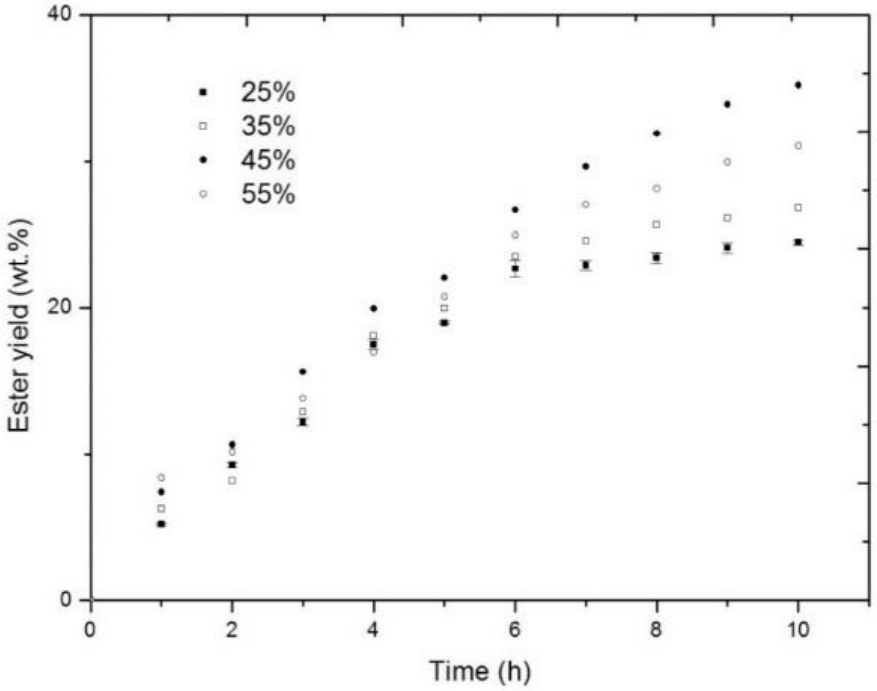

Fig. 4.10 Cat-3-X-450 loading screening study (3 wt.% catalyst, 20:1 methanol to GSC oil molar ratio, 150°C, and 10 h)

4.4.4 Effect of reaction parameters

From the preliminary experiments, reaction temperature was found to be the most important factor, which affected the ester yield without the interaction of other parameters. For this, the reaction temperature effect on ester yield was analyzed keeping the catalyst concentration at 3 wt.% (based on the wt. of oil), 20:1 methanol to GSC oil molar ratio and 10 h of reaction time. Figure 4.11 depicts that ester yield increases with the increases in the reaction temperature (the reproducibility of the data at 200°C was found to be ±0.67 error at 95% confidence level). Similar result was obtained by Canakci and Gerpen (1999). According to their findings, reaction temperature dominates the rate of reaction and the conversion increases with an increasing reaction temperature. However, exceptional results were also found by Melero et al. (2010) and Alba-Rubio AC et al. (2010), where optimum reaction temperature is found, beyond which catalytic activity decreases. The reason for these is, in their studies, organic sulfonic acid functional group (similar kind of functional groups used in Cat-1 and Cat-2, having temperature tolerance below 200°C) was used as active acid sites, which breaks down beyond the optimum (maximum tolerable) temperature. As a result the catalyst surface acidity reduces, the active species leach out and the acid value of the biodiesel increases.

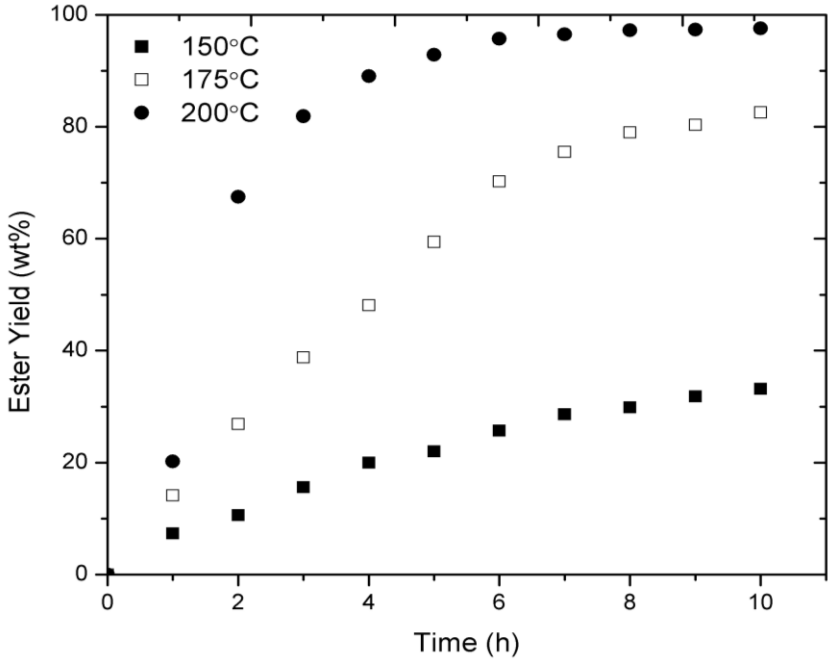

Fig. 4.11 Effect of reaction temperature on catalytic activity (3 wt.% catalyst, 20:1 methanol to GSC oil molar ratio and 10 h)

To grasp the effects of other reaction parameters, the catalyst weight was varied from 0 to 6 wt%, the methanol to GSC oil molar ratio from 10:1 to 30:1 and reaction time from 4 to 10 h. A thee-factor two level design was used to perform the experiments. Figures 4.12, 4.13 and 4.14 depicts the effects of methanol to oil molar ratio, catalyst wt.% and reaction time on the ester yield (wt.%). These figures show the optimum region of parameter combinations for obtaining the highest ester yield.

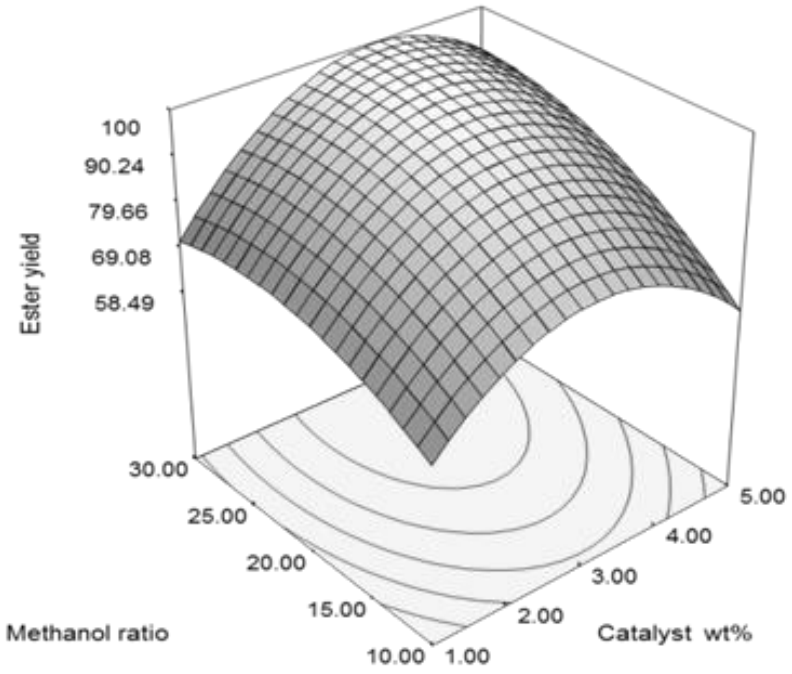

Fig. 4.12 Effect of catalyst wt.% and methanol ratio on the ester yield

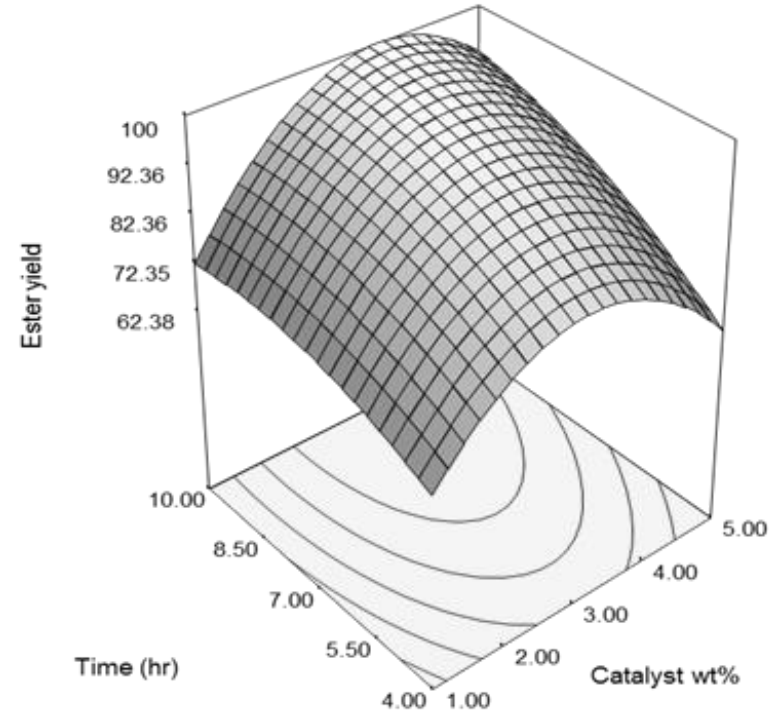

Fig. 4.13 Effect of catalyst wt.% and reaction time on the ester yield

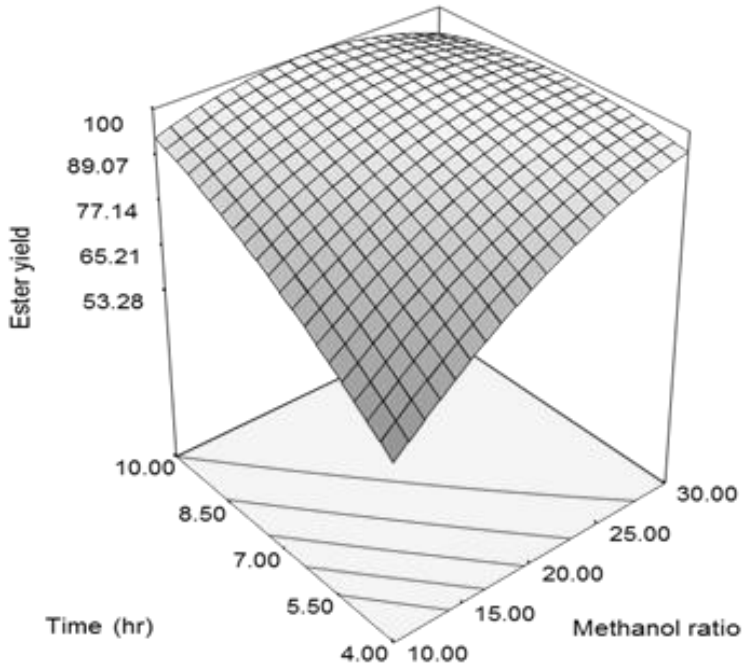

Fig. 4.14 Effect of methanol ratio and reaction time on the ester yield

From the experiments, a second-order polynomial equation is developed to fit the experimental data.

Ester yield (wt.%) = -67.84 + 20.36× Catalyst wt.% + 5.67× Methanol ratio + 14.65 × Time (h) - 4.76× Catalyst wt.%^{2} - 0.07× Methanol ratio^2 - .48× Time (h)^2 + 0.26×Catalyst wt.% ×Methanol ratio + 0.87 × Catalyst wt.% × Time (h) - 0.37 × Methanol ratio × Time (h) …(4.2)

From the above model both linear and quadratic terms of cat.wt.%, Methanol to GSC oil molar ratio, reaction time are found to be the significant factors. Besides, the interactions between cat. wt.%, methanol to GSC oil molar ratio and the reaction time are found to be significant. Figure 4.15 depicts the Perturbation plot, which implies the effect of individual reaction parameter on ester yield (wt. %), keeping the other parameters constant, using the same design range. It exhibits that ester yield (wt.%) increases with the increase of the catalyst wt.% up to a certain limit, then decreases. It also exhibits that ester yield (wt.%) increases with the reaction time, which is found to be similar to another study by Kaufuku et al. (2010). The ester yield (wt.%) is found to be same after increasing the methanol to GSC oil molar ratio to a certain

limit, that means the reaction mixture was not affected by the solubility of the glycerol, which was found to be a problem with the increase of the methanol ratio, thereby decrease in ester yield in another study by Kaufuku et al. (2001).

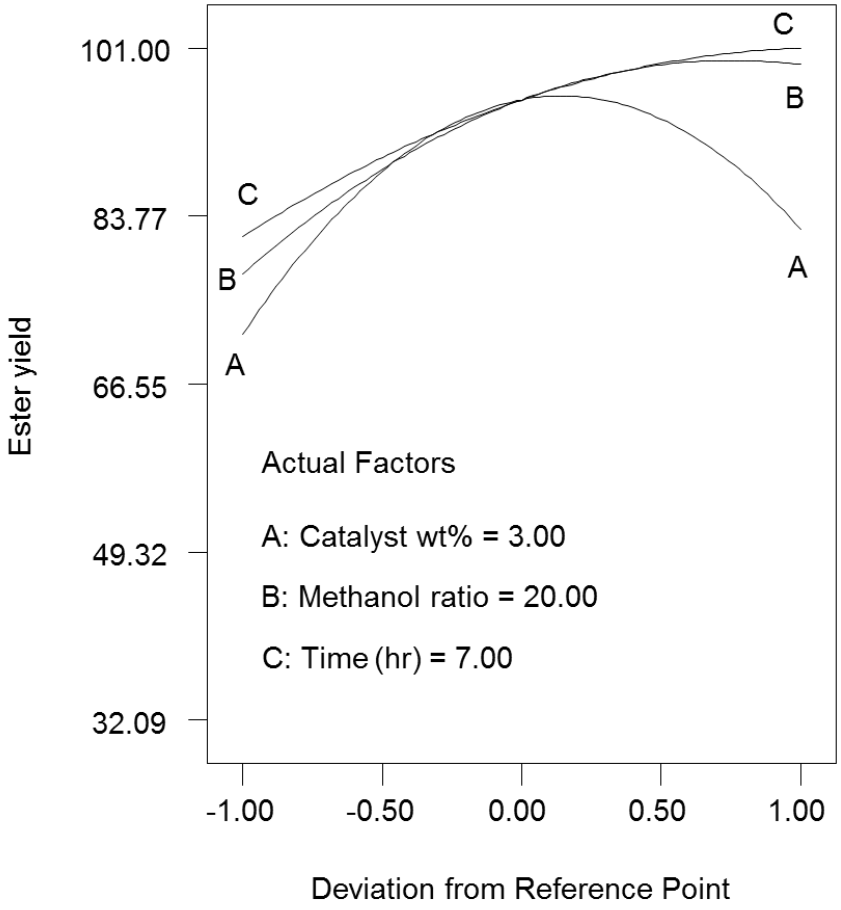

Fig. 4.15 Perturbation plot

From the optimization, 2.96 wt% catalyst (based on GSC oil) and 25.8:1 methanol to GSC oil molar ratio and 6.25 hour are found to be one of the optimum reaction conditions. The predicted yield using the conditions is 97.6 wt% and the actual yield is 97.3 wt%, which validates the model well. Besides, 92.6% of FFA conversion to ester was obtained using the optimized reaction condition. The 6.25 h reaction time required to reach 97.3% ester yield can be explained with the help of the transesterification reaction chemistry. Transesterification is an equilibrium reaction and after reaching a certain yield or conversion, the reaction becomes slow; which is also evident from Figure 4.11. Similar results were found by Boocok et al. (1998), where 90

wt.% ester was obtained fast; thereafter the reaction took a long time to reach the final equilibrium. That is the reason many papers limit their study up to this point to show the novelty of the catalytic activity, which is misleading. Many papers report catalytic activity for biodiesel production through transesterification reaction in terms of conversion of triglycerides, which does not confirm formation of methyl ester. Transesterification reaction is a thee-step reaction, where diglycerides and monoglyceride are the reaction intermediates. Thus, conversion of triglycerides includes mono and diglycerides along with methyl ester.

4.4.5 Development of the kinetic model of the fatty acid methyl ester (FAME) compounds

The optimized reaction condition was exploited to develop the kinetic model of transesterification of triglycerides. In transesterification reaction, triglycerides (TG_i) and methanol (M) react to produce methyl ester (ME) and glycerol (G). It was presumed that different triglycerides (TG_i, i.e. glycerol trioleate, glycerol linoleate) and methanol (M) were weakly adsorbed on the catalyst (Yadav et al., 2012). Adsorption of different triglycerides (TG_i) on a vacant site is given by

$$TG_i + S \overset{K_1}{\Leftrightarrow} TG_i.S \quad \ldots(4.3)$$

Adsorption of Methanol (M) on a vacant site is given by

$$M + S \overset{K_2}{\Leftrightarrow} M.S \quad \ldots(4.4)$$

Surface reaction of TG_i.S and M.S leading to the formation of methyl ester (ME_i.S) and glycerol (G.S) on the site

$$TG_i.S + M.S \overset{K_{SR}}{\Leftrightarrow} ME_i.S + G.S \quad \ldots(4.5)$$

Desorption of different methyl esters (ME_i) and glycerol (G) is given by

$$ME_i.S \overset{K'_{ME}}{\Longleftrightarrow} ME_i + S \quad \ldots(4.6)$$

$$G.S \overset{K'_G}{\Leftrightarrow} G + S \quad \ldots(4.7)$$

If the surface reaction (4.5) is the rate limiting step, then the rate of reaction of TG_i is given by

$$-r_{TG_i} = -\frac{dC_{TG_i}}{dt} = k_{SR}C_{S.TG_i}.C_{M.S} - k'_{SR}C_{S.ME_i}.C_{G.S} \quad \ldots(4.8)$$

The reaction is far away from equilibrium, as initial rate data were used. Thus, reverse reaction cane be neglected (Yadav et al., 2012).

$$-\frac{dC_{TG_i}}{dt} = \frac{k_{SR}\left\{K_1K_2C_{TG_i}C_M - \left(K_{ME}K_GC_{ME_i}C_G/K_{SR}\right)\right\}C_t^2}{\left(1+C_{TG_i}K_1+K_2C_M+K_{ME}C_{ME_i}+K_GC_G\right)^2} \quad \ldots(4.9)$$

$$-\frac{dC_{TG_i}}{dt} = \frac{k_rwC_{TG_i}C_M}{\left(1+C_{TG_i}K_1+K_2C_M+K_{ME}C_{ME_i}+K_GC_G\right)^2} \quad \ldots(4.10)$$

Where

$k_rw = k_{SR}K_1K_2C_t^2$; w = catalyst wt.If the adsorption constants are very small (Yadav et al., 2012), then the above equation reduces to

$$-\frac{dC_{TG_i}}{dt} = k_rwC_{TG_i}C_M \quad \ldots(4.11)$$

As a large molar excess of methanol was used in the reaction. Therefore, $C_M \cong C_{M,o}$ can be assumed in this reaction. Therefore, the above equation can be rewritten in terms of fractional conversion as follows,

$$\frac{dX_{TG_i}}{dt} = k'(1 - X_{TG_i}) \quad \ldots(4.12)$$

Where,

$$k' = k_rwC_{M_o}$$

Integrating the above equation and for constant initial triglyceride concentration, the final expression is

$$-\ln(1 - X_{TG,i}) = k't \quad \ldots(4.13)$$

Thus a plot of $-\ln(1 - X_{TGi})$ against time at different temperatures gave the values of the reaction rate constants of different fatty acid methyl ester (FAME) at different temperatures (Table 4.4). The reaction rate constants for different temperatures were calculated and based on the values an Arrhenius plot was exploited to estimate the apparent activation energy of the reaction (Table 4.4).

Table 4.4: Reaction rate constants and Activation energy of different fatty acid methyl ester (FAME)

Fatty acid methyl ester structure	Reaction rate constant (k') 1/sec			Activation Energy, E_a (kJ/mole)
	180°C	190°C	200°C	
C15:0	2.00×10^{-5}	2.24×10^{-5}	9.03×10^{-5}	133.4
C18:1	3.80×10^{-5}	4.03×10^{-5}	8.19×10^{-5}	67.9
C18:2	1.00×10^{-5}	2.01×10^{-5}	7.95×10^{-5}	184.2
C18:3	2.43×10^{-5}	3.58×10^{-5}	7.81×10^{-5}	103.7

From the kinetic model results, it is obtained that the reaction rate constant increases with the temperature for all the fatty acid methyl ester (FAME) compounds, indicating the reaction is endothermic (Table 4.4). It also depicts that the activation energy of Methyl Oleate formation is the least (67.9 kJ/mole) and is highest (184.2 kJ/mole) for methyl linoleate formation. Table 4.5 depicts that reaction rate constant per unit initial reactant concentration increases in the order of Linolinate>Linoleate>Pentadecyclate>Oleate. These phenomena can be explained with the help of a double bond numbers and the carbon atom numbers in the fatty acids. Higher the double bond numbers and/or lower the carbon atom numbers in the fatty acids, faster the reaction rates (Choi et al., 2011). The enthalpy of activation ($\Delta H^{\ddagger}$), and the entropy of activation ($\Delta S^{\ddagger}$) wereevaluated using Eyring equation (Eyring, 1935):

$$\ln\frac{k'}{T} = -\frac{\Delta H^{\ddagger}}{R}.\frac{1}{T} + \ln\frac{k_B}{h} + \frac{\Delta S^{\ddagger}}{R} \qquad \ldots(4.14)$$

Where, k_B is the Boltzmann constant and h is the Plank constant. Gibbs energy of activation ($\Delta G^{\ddagger}$) was calculated using the following equation:

$$\Delta G^{\ddagger} = \Delta H^{\ddagger} - T.\ \Delta S^{\ddagger} \qquad \ldots(4.15)$$

Table 4.5: Reaction rate constants and Activation energy of different fatty acid methyl ester (FAME)

Fatty acid methyl ester structure	Reaction rate constant per unit initial reactant concentration L/mol. sec		
	180°C	190°C	200°C
C15:0	4.00×10^{-4}	4.48×10^{-4}	1.80×10^{-3}
C18:1	6.33×10^{-4}	6.72×10^{-4}	1.37×10^{-3}
C18:2	5.00×10^{-4}	1.01×10^{-3}	3.98×10^{-3}
C18:3	4.05×10^{-3}	5.97×10^{-3}	1.30×10^{-2}

Table 4.6 depicts the thermodynamic property values of individual fatty acid methyl ester (FAME). It depicts that enthalpy of activation is the least and the entropy of activation is far negative for Methyl Oleate as compared to other fatty acid methyl ester (FAME) compounds. This indicates that least energy input from an external source is required to transform the Triolein into transition state (activation) complex. The far negative value of entropy of activation of Methyl Oleate activation complex indicates that the reactant species joined together to form activation complex through association mechanism. Therefore, the activation complex has a more ordered or more rigid structure than the reactants in the ground state, which makes the rate of reaction of the reactant triolein the fastest (Ong et al., 2013). The positive nonzero values of Gibb's free energy for all the compounds indicate that the transesterification reaction is non-spontaneous.

Table 4.6: Thermodynamic properties data of different fatty acid methyl ester (FAME)

Fatty acid methyl ester structure	$\Delta H^{\ddagger}$ kJ/mol	$\Delta S^{\ddagger}$ J/mol. K	$\Delta G^{\ddagger}$ kJ/mol
C15:0	129.6	-54.1	155.2
C18:1	64.1	-192.4	155.1
C18:2	180.3	53.1	155.3
C18:3	99.9	-116.8	155.1

4.4.6 Chlorophyll removal and catalyst reusability testing

The % of chlorophyll removal by different catalysts using the catalysts screening reaction condition is depicted in Table 4.7. It depicts that, Cat-2 removes the least amount of chlorophyll from the reaction mixture containing produced biodiesel. Previous studies show that higher acidity improves chlorophyll adsorption (Mokaya et al., 1993; Didi et al., 2009). It is also proven from the previous work that, the chlorophyll is adsorbed on the acid sites by chemisorption. Weak acid sites chemisorb chlorophyll, whereas strong acid sites convert chlorophyll (aand b) into phaeophytin (a and b) by replacing magnesium ion of the chlorophyll with two hydrogen, and the phaeophytin is also found to be chemisorbed on the weak acid sites (Didi et al., 2009; Giler and Tunc, 1993; Sabah, 2007; Manna et al., 2009). The trend of presence of chlorophyll in the reaction mixture containing produced biodiesel using different catalysts indicates that, the lowest TPA content of Cat-2 among the prepared catalysts, therefore, lowest loading is responsible for lowest chlorophyll adsorption. Besides, in Cat-2, the losses of weak acid sites by replacing silanol groups with alkyl chains are responsible for the least phaeophytin adsorption.

Table 4.7: Chlorophyll removal from the reaction mixture containing produced biodiesel using different catalysts

Sample	Ch A (ppm)	Ch B (ppm)	Ph A (ppm)	Ph B (ppm)	Total (ppm)	% removed[1]
GSC oil	21.5	3	53.26	0	77.7	-
Cat-1	9.15	6.41	21.36	0	36.9	52.5
Cat-2	11.94	12.15	24.33	0	48.3	37.9
Cat-3-25-450	9.35	14.06	16.89	5.15	45.4	41.5

[1] Reaction condition: 3 wt.% catalyst, 20:1 methanol to GSC oil molar ratio, 150°C and10 h

For the catalyst reusability study, the catalyst was separated from the reaction mixture by filtration.The separated catalysts was washed with THF to remove non-polar, polar compounds and chlorophyll, as THF was found to be an effective solvent for chlorophyll removal from the adsorbent in a previous study (Issariyakul and Dalai, 2010). The catalyst was then dried and finally regenerated by calcination, to remove the residual organic compounds. Table 4.8 depicts that, the catalyst strong acid sites are still active and reusable in presence of chlorophyll after several reaction cycles. It also depicts that the chlorophyll adsorption increases with the

temperature (Tables 4.7 and 4.8), which is due to an increase in adsorption capacity with the increase of temperature (Didi et al., 2009). The adsorption of chlorophyll (a and b) by the catalysts was confirmed by the presence of Mg in the regenerated catalyst and the amount of TPA found in the reaction mixture was very negligible (0.009 wt.%).

Table 4.8: Catalyst reusability and chlorophyll removal from produced biodiesel using Cat-3-45-450

Sample	Ester yield%[1]	Ch A (ppm)	Ch B (ppm)	Ph A (ppm)	Ph B (ppm)	Total (ppm)	% removed
GSC oil	-	21.5	3	53.26	0	77.7	-
Run 1	97.3	4.15	10.75	4.1	0	19	75.5
Run 2	94.8	4.45	8.02	8.31	4.94	25.7	66.9
Run 3	92.1	6.67	4.96	14.64	0	26.3	66.2
Run 4	90.8	6.2	6.32	14.22	0	26.7	65.6

[1] Reaction condition: 2.96 wt.% catalyst, 25.84:1 methanol to GSC oil molar ratio, 200°C and 6.25 h

4.4.7 Properties of the biodiesel

The quality and properties, such as an acid value, cloud point, cloud point of the produced biodiesel were assessed according to ASTM D6751 standards. Table 4.9 depicts the biodiesel properties value comparison. It depicts that the produced biodiesel property values are close to those mentioned in the ASTM standard. The fatty acid profile of the produced biodiesel is depicted in Table 4.10. It depicts that the major component of the produced biodiesel is Methyl Oleate, which is also the major component of the commercial grade canola biodiesel.

Table 4.9: Comparison of the biodiesel properties

Properties	Produced biodiesel	ASTM standard
Acid number (mg KOH/g sample)	0.69	0.5
Cloud point	-2°C	-2°C
Pour point	-15°C	-15°C

Table 4.10: Fatty acid profile of the biodiesel

Structure	Compound name	wt.%
C15:0	Methyl pentadecyclate	35.80
C18:1	Methyl Oleate	45.79
C18:2	Methyl linoleate	13.96
C18:3	Methyl linolenate	4.45

4.5 Conclusion

This research work reveals that solid acid catalysts are able to remove chlorophyll while catalyzing simultaneous transesterification and esterification reactions. Therefore, solid acid catalysts allow using unrefined waste grade feedstock such as GSC oil as a direct feedstock for biodiesel production and reduce pre-treatment costs of the feedstock. While conducting this study, a new method of catalyst preparation (Cat-2) has been developed. This catalyst is proved to be effectual to produce biodiesel from different fatty acids (i.e. Oleic acid). On the other hand, TPA doped SBA-15 (Cat-3-45-450) is proved to be effectual for simultaneous transesterification, esterification and chlorophyll removal to produce high-quality biodiesel from GSC oil.

CHAPTER 5: PROCESS SUSTAINABILITY OF BIODIESEL PRODUCTION PROCESS FROM GREEN SEED CANOLA OIL USING HOMOGENEOUS AND HETEROGENEOUS ACID CATALYSTS

A version of this chapter has been accepted in the following journal:

- Chinmoy Baroi, Ajay K. Dalai. Process sustainability of biodiesel production process from Green Seed Canola oil using homogeneous and heterogeneous acid catalysts. Accepted in Fuel Processing Technology (2015).

Contribution of the Ph.D. Candidate

Simulation models and analysis were performed by Chinmoy Baroi. The content in this chapter was written by Chinmoy Baroi with discussions and suggestions provided by Dr. Ajay Dalai.

Contribution of this Chapter to the Overall Ph.D. Research

This chapter deals with the process sustainability study of green seed canola biodiesel production processes along with the chlorophyll removal using homogeneous and heterogeneous acid catalysts. This chapter demonstrates the prospects of using heterogeneous acid catalysts in biodiesel production.

5.1 Abstract

In this study, the sustainability of homogeneous and heterogeneous acid catalyzed biodiesel production process from green seed canola (GSC) is evaluated. The term "sustainability" is assessed based on four criteria, e.g. process economics, process safety, environmental impact and process energy efficiency. Based on the assessment, it is concluded that both the processes are economically profitable, when the cost of the feedstock is $ 0.35/kg. Surprisingly, heterogeneous acid catalyzed process depicts higher profitability. Comparatively, heterogeneous acid catalyzed process is a safer process and creates less environmental impact. Additionally, heterogeneous acid catalyzed process is more energy efficient and more environment friendly than homogeneous process.

5.2 Introduction

Biodiesel is an attractive diesel substitute fuel because of its low emission profile and renewability. However, the biodiesel production process profitability is still being challenged due to higher feedstock price. On the contrary, cheaper feedstock is only compatible with acid-catalyzed process because of presence of higher amount offree fatty acid (FFA). Especially, heterogeneous (solid) acid catalysts are desired because of easy product separation and waste minimization (Kulkarni et al., 2006).

Green seed canola oil is one of the low-grade oils available in huge quantity in Saskatchewan, Canada. The raw green seed canola oil are not edible because of the presence of the higher amount of chlorophyll (Abraham and De Mann, 1986; Rawk and Santen, 1970). However, a study showed that high quality biodiesel with improved oxidation stability can be produced from this oil using a novel catalyst, which acts as a chlorophyll adsorbent along with its role as a catalyst (Baroi and Dalai, 2013).

Sustainability is a global and a very important issue for the long-term ecosystem and societal benefit, which demands minimum impact on the ecosystem during the manufacturing of any goods or substances (Gangadharan et al., 2013). As criteria of sustainability assessment (Fig. 5.1), now a day, many researches include ecological and social indicators along with economic studies during the early process development and design stages (Li et al., 2011). From economic point of view, a process with positive or higher number in net present value (NPV) and internal rate of return (IRR) are considered to be economically feasible (Li et al., 2011). Ecological impacts are evaluated based on the environmental impacts and energy efficiency of the process (Fig. 5.1). An algorithm namely, waste reduction algorithm (WAR) is developed by US EPA (Young and Cabezas, 1999) to assess the environmental impact at the manufacturing stage within the overall lifecycle of the chemical production and process. The process energy efficiency can be evaluated based on the energy of the raw materials and the products (Trippe et al., 2013). Social impacts are evaluated based on the possibility of the accident, explosion hazard, occupational diseases, toxicity of the process and materials. All these facts cannot be measured in numbers, however can be correlated with the chemical safety and the process equipment safety. Recently a comprehensive safety analysis method has been developed (Gangadharan et al., 2013) to rank and score the individual equipment and overall chemical process by considering the facts of hazard from individual chemical, reactivity and explosion

from the chemical mixture, flow rates, individual equipment operating capacity, temperature and pressure. Higher score indicates higher risks of accident associated with the process. This method provides detailed process safety information with minimal process information at the initial stage of design. An algorithm of sequential process sustainability study has been depicted by Li et al. (2011). According to the algorithm, economic feasibility is conducted first. If it proves feasible, then the second stage is social impact analysis and the last stage is ecological impact analysis (Fig. 5.2). If all the criteria satisfy, then the new process and its design are finalized over existing conventional process.

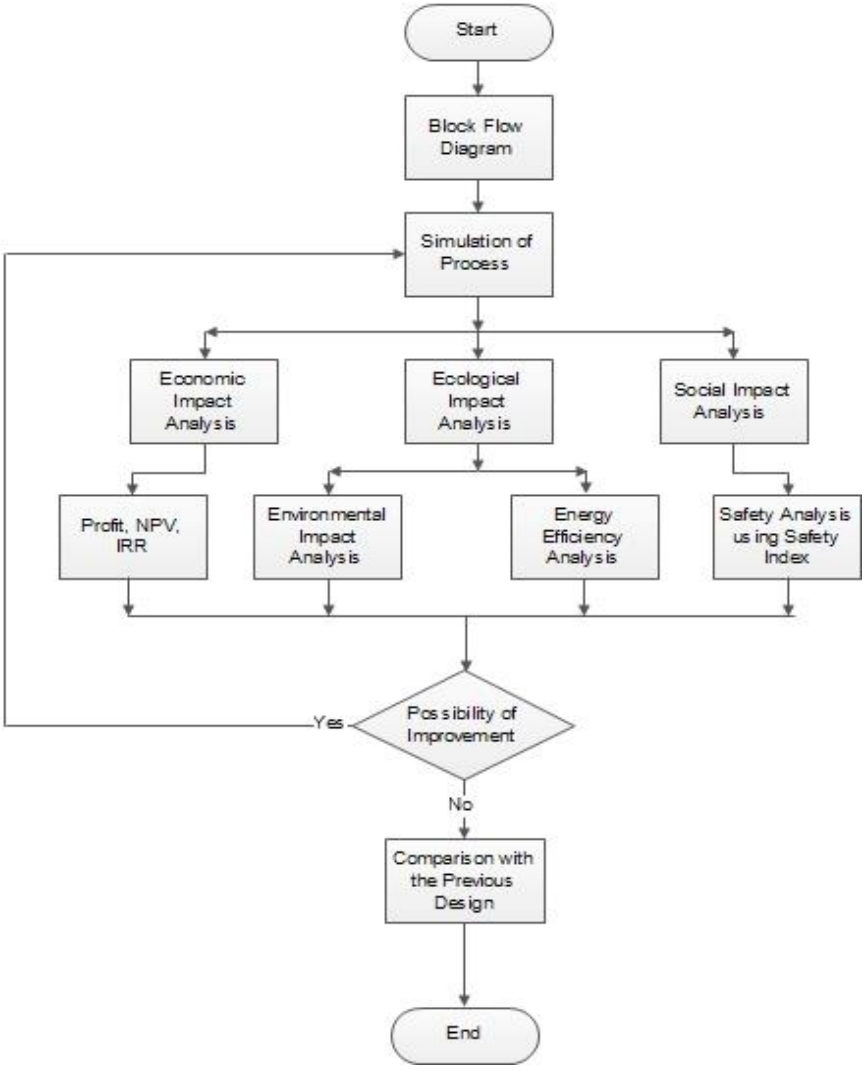

Fig. 5.1 Criteria for sustainability assessment

Previous economic studies on biodiesel process show that one-step homogeneous acid catalyzed process is more profitable than two-step homogeneous acid and base catalyzed process (Zhang et al., 2003; West et al., 2008). It has also been demonstrated that heterogeneous acid catalyzed process is much more profitable as compared to homogeneous acid catalyzed process if the operating conditions are close (West et al., 2008). However, no literature is found on the process sustainability study of the homogeneous and heterogeneous acid catalyzed biodiesel production from the green seed canola oil. This chapter introduces for the first time the process sustainability study of green seed canola biodiesel production processes along with the chlorophyll removal.

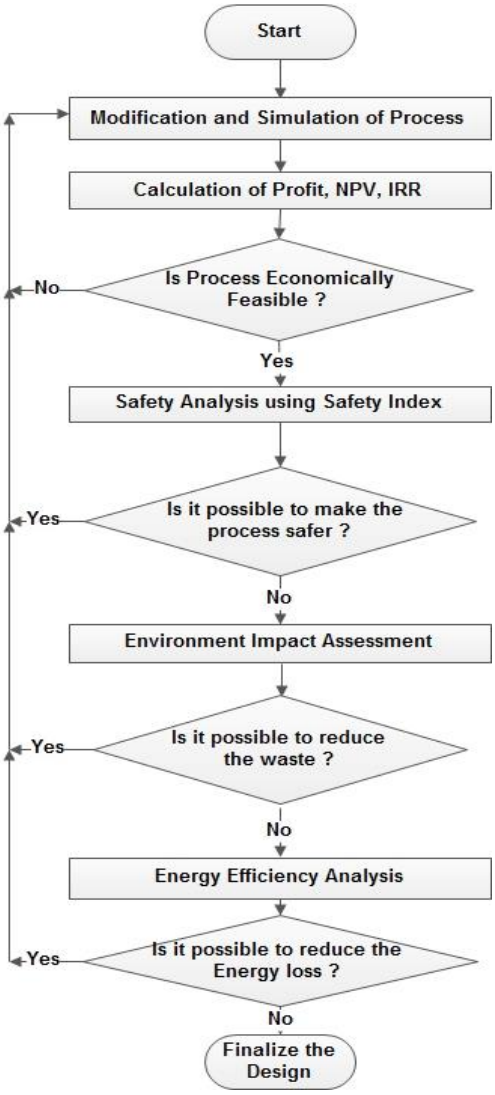

Fig. 5.2 Algorithm for sustainability analysis (redrawn from Gangadharan et al., 2013)

5.3 Development of process models

Aspen HYSYS v.2006 is employed to obtain mass and energy balance for simultaneous esterification, transesterification and chlorophyll removal of GSC oil process using homogeneous and heterogeneous acid catalysts and thereafter sustainability assessment are performed for the same systems. All the unit operations, input conditions and operating conditions are specified during process flow sheet development. Triolein, diolein, monoolein, and oleic acid are selected to represent the triglycerides (TG), diglycerides (DG), monoglyceride (MG) and free fatty acids (FFA) of the GSC oil. In all the previous process feasibility analysis papers, the presence of DG and MG are neglected, even though the MG is present in the case of incomplete conversion. In the process simulation, TG, DG, MG, solid catalysts, CaO, $CasO_4$, chlorophyll A and B (Ch-A and Ch-B) are inserted as hypothetical compounds. Thermodynamic group contribution method is used to develop and define the properties of TG, DG, MG as the hypothetical liquid compounds (Marrero and Gani, 2001; Reid et al., 1987) (see appendix D). Chlorophyll A and B are treated as solids and the properties of solids and thermodynamics are obtained elsewhere (Annamalai et al., 1987; Chen and Cai, 2007) (see appendix D). The properties of other components (e.g. water, oleic acid, methyl oleate, glycerol, methanol) are collected from the HYSYS library. As the simulation involves polar components (glycerol and methanol), non–random two liquid (NRTL) thermodynamic model (West et al., 2008) is chosen as the base model for the biodiesel production process simulation. Since some of the binary interaction parameters are not provided in the databank, theses parameters are estimated using the UNIFAC vapour-liquid equilibrium and UNIFAC liquid-liquid equilibrium model. Plant biodiesel production capacity is taken at 8000 tonnes/year (the same as in Zhang et al., 2003; West et al., 2008). This translates to vegetable oil roughly 1000 kg/h for process configuration. Gravity separation methods are used to separate the salts after neutralization in homogeneous (liquid) acid catalyzed process and to separate the catalysts in the heterogeneous acid catalyzed process. Conversion reactors are used to represent the simultaneous esterification, transesterification and chlorophyll removal and also neutralization of the homogeneous acid catalyst with base. Similarly, conversion reactor is used to represent the simultaneous esterification, transesterification and chlorophyll removal for heterogeneous acid catalyzed process. In the simulation flowsheet, a dummy conversion reactor is used to represent the chlorophyll removal by the catalysts, even though practically transesterification, esterification

reactions and adsorbance occur in a single reactor. The reactors are assumed to operate continuously. For homogeneous acid catalyzed process, sulphuric acid (H_2SO_4) is used as a catalyst. The esterification, transesterification conversions and the chlorophyll removal are taken to be 100%, 97% and 100% respectively. The chlorophyll removal is considered to be conversion of chlorophyll into biodiesel (FAME), as there is no solid adsorbance unit operation is available and removal of chlorophyll helps to increases the methyl ester concentration in the biodiesel. The operating conditions for the above reactions are 80°C. 50:1 methanol to oil molar ratio, 4 h of reaction time, which are taken from a previous literature (West et al., 2008). For heterogeneous acid catalyzed process, the original data mentioned in the paper (Baroi and Dalai, 2013) are converted to conversions for the use in this paper. The reaction conversions for the transesterification, esterification are 99.4% and 92.6% respectively. The chlorophyll removal of 75.6% is considered to be a conversion of chlorophyll into biodiesel (FAME). After the reactions, methanol is retrieved and purified by exploiting a multistage atmospheric distillation column and the purity obtained are 99.96 and 99.92% for homogeneous and heterogeneous processes, respectively. For both the processes, a pressure drop of 20-50 kPa is considered across each vessel (Towler and Sinnott, 2013).

5.4 Process design

The homogeneous acid catalyzed biodiesel production process flowsheet is depicted in Figure 5.3. The process is described with the help of stream numbers, equipment names, and numbers mentioned in Figure 5.3. Both GSC oil (stream no. 106) and H_2SO_4 catalysts (stream no. 104) enter the process at atmospheric pressure and room temperature. However, the methanol (stream no. 101) enters at higher pressure (can be obtained by placing the vessel at a higher elevation) to account for the pressure drop across the heat exchanger E-100 (equipment name and number) (Fig.5.3), through which it exchanges the heat with reactor products and to acquire heat. The methanol stream is selected over other streams for preheating to optimize the cost associated with the heat-exchanger geometry which is determined with the help of HTFS-TASC software. The reaction mixture is then pumped through P-101 (see Fig. 5.3) to obtain the desired pressure of 500 kPa to keep the reactor mixture in the liquid phase inside the reactor. The high-pressure reaction mixture is preheated by exchanging heat with the hot biodiesel product through exchanger E-101. The reaction products are then cooled down by passing through the heat

exchanger E-100, and fed to the neutralizer. In the neutralizer H_2SO_4 catalysts are neutralized with CaO to convert into $CaSO_4$. The neutralized stream (stream no. 112) is then heated using a heater (E-102). The stream is fed to the 3-phase separator (V-100), where methanol are separated as a vapour (114) and $CaSO_4$ is separated in the gravity separator (V-100) by using gravity force. The methanol Vapour (114) is then purified in the distillation column (T-100), cooled down through a cooler (E-103), and then recycled back (details of unit operations are given in Table 5.1). The mainstream is then brought down to lower pressure and sent to another 3-phase separator (V-101) to separate glycerol from biodiesel.

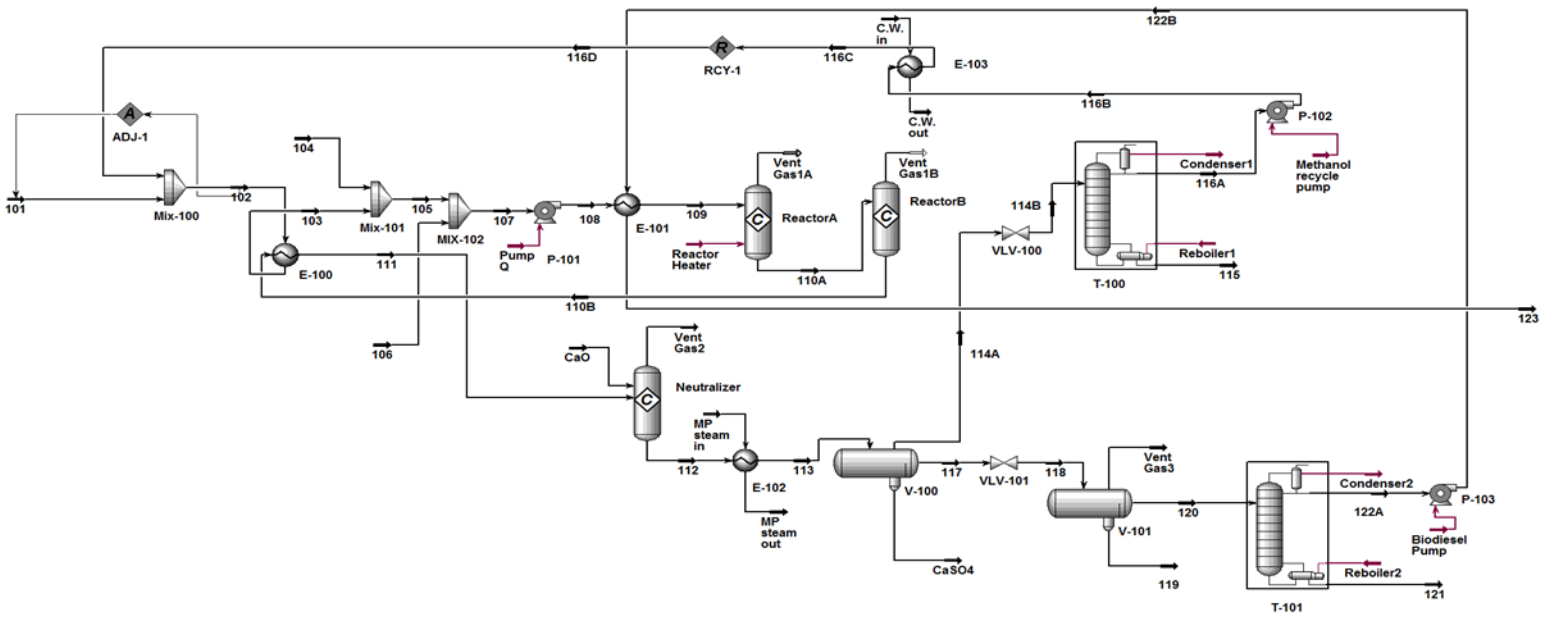

Fig. 5.3 (a) Flowsheet for homogeneous acid catalyzed simultaneous esterification, transesterification and chlorophyll removal process

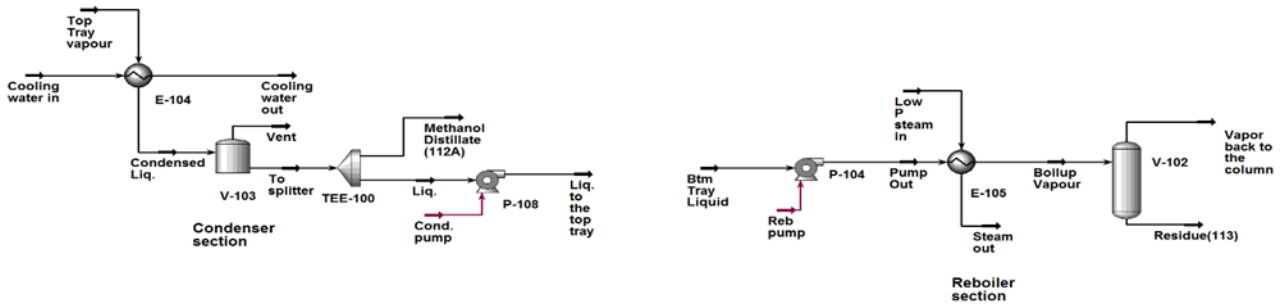

Fig. 5.3 (b) Condenser and reboiler section of methanol recovery unit (T-100)

Table 5.1: Synopsis of the unit operation conditions for each process

	Homogeneous	Heterogeneous
Catalyst	H_2SO_4	Cat-3-45-450
Reactor type	CSTR	CSTR
Temperature (°C)	80	200
Pressure (kPa)	500	4187
Alcohol to oil ratio	50:1	25.84:1
Residence time (h)	4	6.25
Conversion (%) Esterification, Transesterification and chlorophyll removal	100/97/100	92.6/99.40/75.65
Methanol recovery		
Reflux ratio	1	1
Number of stages	12	8
Condenser/reboiler pressure (kPa)	101.3/124.3	101.3/124.3
Type of trays	Sieve	Sieve
Tray spacing	0.61 m	0.61 m
Distillate purity (%)	99.96	99.92
Catalyst Removal		Gravity
Catalyst recovery %		100
Glycerol Separation	Gravity	Gravity
Glycerol purity %	96.52	98.89
Biodiesel Purification		
Reflux ratio	1	4
Number of stages	20	20
Condenser/reboiler pressure (kPa)	10/12	10/12
Type of trays	Valve	Valve
Tray spacing	0.61 m	0.61 m
Biodiesel purity, wt%	99.80	99.84

The product biodiesel stream (stream no. 120) is fed to a vacuum distillation column (T-101), where high purity biodiesel is produced as a top product (stream no.123) (Table 5.2 and Fig. 5.3).

Table 5.2: Feed and product stream information for the homogeneous acid catalyzed process

	101	104	106	119	123
Temperature (°C)	25.0	25.0	25.0	148.3	97.72
Pressure (kPa)	151.3	101.3	101.3	10	101.3
Molar flow (kmol/h)	5.899	1.632	1.355	1.002	3.651
Mass flow (kg/h)	189	160.1	1100	93.44	1007
Component mass fraction					
Methanol	1	-	-	0.0031	0.0002
GSC oil	-	-	0.9574	-	-
DG	-	-	-	-	-
MG	-	-	-	0.0275	0.0007
Free Fatty Acids	-	-	0.0425	-	0.0001
Ch-A	-	-	0.0001	-	-
Ch-B	-	-	0.0000*	-	-
H_2SO_4	-	1	-	-	-
Glycerol	-	-	-	0.9652	0.0011
Water	-	-	-	0.0011	-
FAME	-	-	-	0.0031	0.9980

*Very less amount

The heterogeneous acid catalyzed biodiesel production process flowsheet is depicted in Figure 5.4. The process is described with the help of stream numbers and equipment name and numbers mentioned in Figure 5.4. For heterogeneous acid catalyzed process, both GSC oil (stream number 105) and solid acid catalysts (103) enter the process at atmospheric pressure and room temperature. However, the methanol (101) enters at higher pressure (can be obtained by placing the vessel at an elevation) to account for the pressure drop across the heat exchanger E-100 (equipment name and number) (Fig. 5.4), through which it exchanges the heat with reactor products and to acquire heat. The methanol stream is selected over other streams for preheating to optimize the cost associated with the heat-exchanger geometry which is determined with the help of HTFS-TASC software. The reaction mixture is then pumped through P-101 to obtain the desired pressure of 4187 kPa to keep the reactor mixture in the liquid phase inside the reactor (Baroi and Dalai, 2013). The high-pressure reaction mixture is then preheated by exchanging heat with a hot product biodiesel (stream no. 121B) through exchanger E-101. The reaction products are then cooled down by passing through the heat exchanger E-100, and fed to the 3-

phase separator (V-100), where the catalysts and residual chlorophyll are removed by gravity force. The stream is then brought down to lower pressure and heated to strip off the methanol in the 3-phase separator (V-101). The methanol is then purified in the distillation column (T-100), cooled down (E-103) and then recycled back (details of unit operations are given in Table 5.1). The bottom stream of the separator (V-101) is rich in glycerol and mainstream is rich in biodiesel (stream no. 119). The biodiesel rich stream (119) is fed to the vacuum distillation column (T-101), where high purity biodiesel is produced as a top product (121A) (Table 5.3 and Fig. 5.4). The heated biodiesel is then passed through heat exchangers (E-101) to cool down.

5.5 Equipment sizing

Distillation columns and 3-phase separators are sized using HYSYS sizing utility. Reactors are sized by multiplying volumetric flow rate with the residence time. The residence time for the 3-phase separators are considered to be 0.5 h (Datta, 2008). Table 5.4 summarizes the dimensions of all relevant vessels. All the heat transfer equipments were sized based on the "minimizing cost" criteria using HTFS-TASC software.

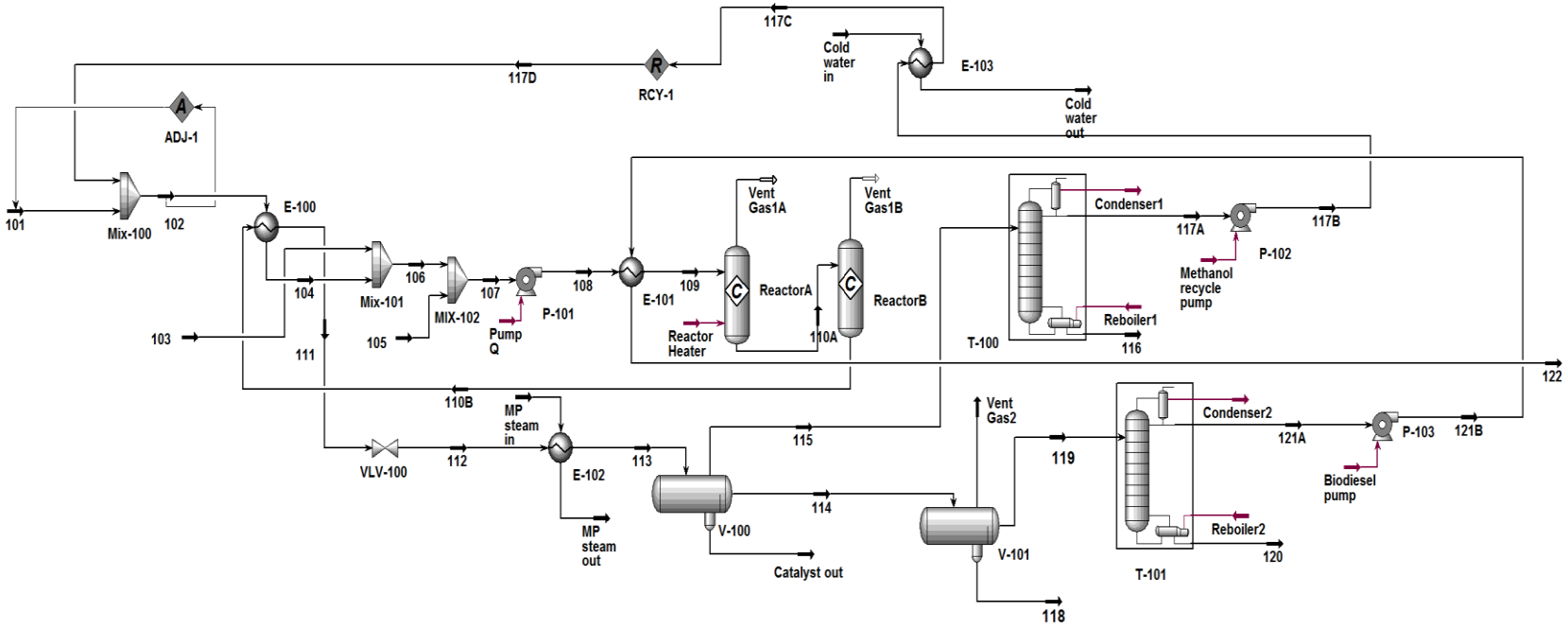

Fig. 5.4 (a) Flowsheet for solid acid catalyzed simultaneous esterification, transesterification and chlorophyll removal process

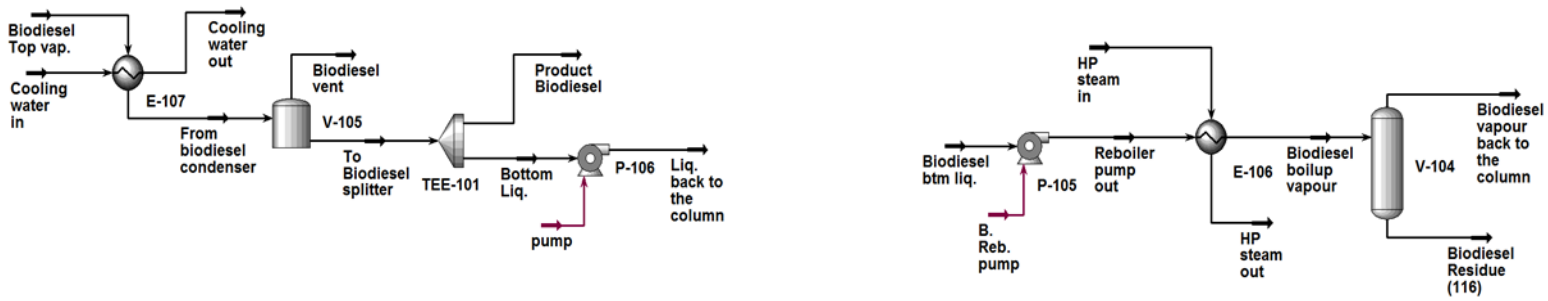

Fig. 5.4 (b) Condenser and reboiler section of biodiesel purification unit (T-101)

Table 5.3: Feed and product stream information for the heterogeneous acid catalyzed process

	101	103	103	118	122
Temperature (°C)	25.0	25.0	25.0	158.9	92.07
Pressure (kPa)	151.3	101.3	101.3	10	101.3
Molar flow (kmol/h)	4.703	0.0167	1.355	0.9341	3.684
Mass flow (kg/h)	150.7	33	1100	86.11	1088
Component mass fraction					
Methanol	1	-		0.0025	0.0002
GSC oil	-	-	0.9574		-
DG	-	-	-		-
MG	-	-	-	0.0057	0.0001
Free Fatty Acids	-	-	0.0425		-
Ch-A	-	-	0.0001		-
Ch-B	-	-	0.0000*		-
Solid acid catalysts	-	1	-		-
Glycerol	-	-	-	0.9889	0.0010
Water	-	-	-	0.0001	-
FAME	-	-	-	0.0028	0.9984

*Very less amount

Table 5.4: Equipment size for various unit operations in the process

Type	Description	Homogeneous	Heterogeneous
Reactor (vertical)*	Esterification, Transesterification and Chlorophyll Removal	2.00 × 6.00	2.33 × 7.00
	Neutralization	1.28 × 3.85	-
Column (vertical)*	Methanol Purification	0.91× 7.3	0.91×4.87
	Biodiesel Purification	1.52× 12.19	1.68× 12.19
Separator (horizontal)**	Solid/Catalyst Separator	0.92× 3.2	0.42 × 2.12
	Glycerol separator	0.92 × 3.2	0.76× 2.67

*Dia×Height (m)

** Dia×Length (m)

5.6 Economic assessment

The plant capacity is assumed to be of 8000 tonnes/year biodiesel production. Operating hours are considered to be 7920h/year (assuming 330 operating days/year). The processes are evaluated based on the net present value (NPV), internal rate of return (IRR) and payback period. The "study estimate", with a range of expected accuracy from +30% to – 20% was used for economic assessment (Turton et al., 2012).

Table 5.5 gives the breakdown of the capital investments of two processes. The equipment prices are estimated using Bare module method (Turton et al., 2012).

The capital cost for the equipments (Table 5.5) depicts that biodiesel distillation column is the most expensive equipment and then reactors are the second highest expensive equipment.

Direct manufacturing expenses are estimated based on the chemical price and utility consumption. The chemical and utility prices are presented in Table 5.6 and material flow information is obtained from HYSYS process flowsheet.

The operating labour cost has been estimated based on the number and types of equipments (Turton et al., 2012). Table 5.7 represents the breakdown of the total manufacturing costs. The detailed direct and indirect manufacturing costs are estimated following the method described elsewhere (West et al., 2008). The net annual profit after tax is calculated assuming an income tax of 42%. The estimated project life is 20 years and the estimated construction period is 2 years. Based on the net present value (NPV), and internal rate of return (IRR), it can be deduced that heterogeneous acid catalyzed process is more economically favorable.

Table 5.5: Major equipment costs, total fixed capital costs and total capital investments (in millions) of the process

Equipment	Description	Homogeneous	Heterogeneous
Reactor	Esterification, Transesterification and Chlorophyll Removal	0.24	0.31
	Neutralization	0.12	-
Column	Methanol Purification	0.38	0.37
	Biodiesel Purification	0.56	0.79
	Solid/Catalyst Separator	0.03	0.03
	Glycerol separator	0.03	0.02
Pump	Reaction mixture pump	0.02	0.04
Heater		0.12	0.12
Cooler		0.12	0.12
Heat Exchangers		0.24	0.24
Total bare module cost, C_{BM}		4.35	4.28
Total module cost, C_{TM}		5.13	5.05
Fixed Capital cost, C_{FC}		6.44	6.33
Working Capital cost, C_{WC}		0.97	0.95
Total Capital Investment, C_{TCI}		7.41	7.28

Table 5.6: Condition for the economic assessment of the process

Item	Specifications	Price ($/kg)	
		Homogeneous	Heterogeneous
Chemicals			
Biodiesel		1	1
Glycerol		0.94	0.94
Methanol	99.9%	0.21	0.21
Green Seed Canola oil	raw	0.35	0.35
Solid acid catalyst	-	-	2.5
H_2SO_4		0.08	-
CaO		0.06	-
$CaSO_4$		0.01	-
Utilities			
Cooling water	25-30°C	$0.0001/kg	$0.0001/kg
Low pressure steam	5 bar, 160°C	$0.03/kg	$0.03/kg
Medium pressure steam	10 bar, 184°C	$0.03/kg	$0.03/kg
High-pressure steam	41 bar, 254°C	$0.03/kg	$0.03/kg
Electricity		$16.8/GJ	$16.8/GJ

Table 5.7: Total manufacturing cost and profit after the tax of the processes

	Homogeneous	Heterogeneous
Direct Manufacturing costs		
Total raw material cost ($ in millions)	4.56	5.00
Total utility cost ($ in millions)	0.03	0.12
Cost of operating labours ($ in millions)	0.16	0.16
Waste Treatment cost ($ in millions)	0.06	0.06
Maintenance and repair(M&R), 6% of C_{FC}	0.38	0.38
Operating supplies, 15% of M&R	0.06	0.06
Lab charges, 15% of operating labour	0.02	0.02
Patents and Royalties	0.11	0.11
Indirect Manufacturing costs		
Overhead packaging and storage	0.09	0.09
Local taxes, 1.5% C_{FC}	0.09	0.09
Insurance, 0.5% C_{FC}	0.03	0.03
Depreciation, 10%	0.64	0.63
Administrative costs	0.02	0.02
Distribution and selling	0.38	0.38
R&D	0.19	0.19
Total Manufacturing costs ($ in millions)	6.85	7.36
Revenue from sales ($ in millions)	9.13	9.73
Net annual profit ($ in millions)	2.28	2.37
Annual taxes, 42%	0.96	0.99
Net annual profit ($ in millions)	1.32	1.37
Net Present Value (NPV) (millions)	4.13	4.37
Internal rate of return (IRR)%	17.99	18.20

5.7 Sensitivity analysis

Figure 5.5 depicts the sensitivity analysis of homogeneous biodiesel production process. It depicts that the maximum price of GSC oil: $0.45/kg and minimum selling price of biodiesel: $0.88/kg are allowable in order to run the process profitable.

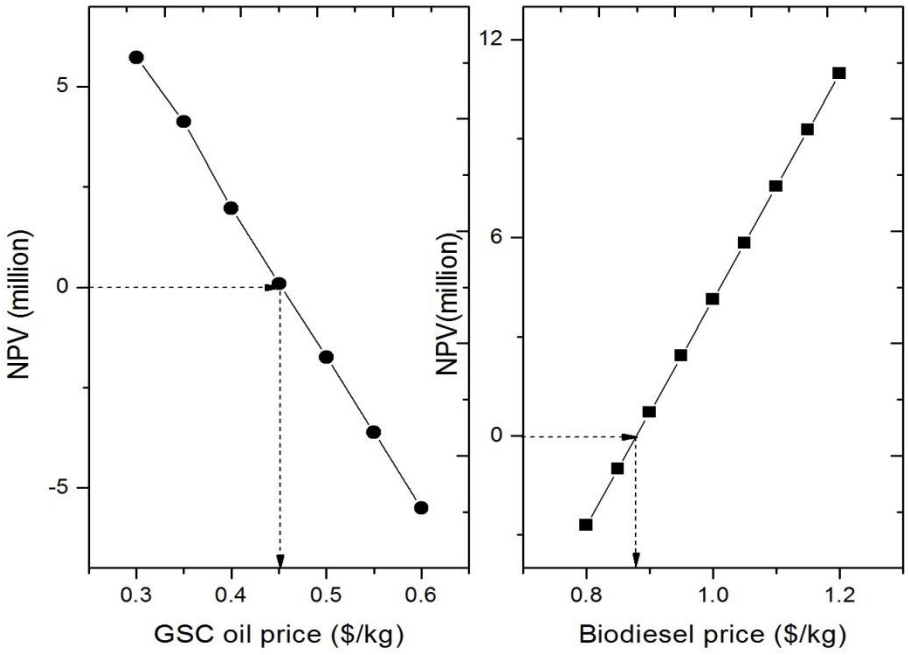

Fig. 5.5 Sensitivity analysis of homogeneous biodiesel production process

Figure 5.6 depicts the sensitivity analysis of heterogeneous biodiesel production process. It depicts that the maximum price of GSC oil: $0.46/kg, solid acid catalysts: $6.1/kg, and minimum selling price of biodiesel: $0.88/kg are allowable in order to run the process profitable.

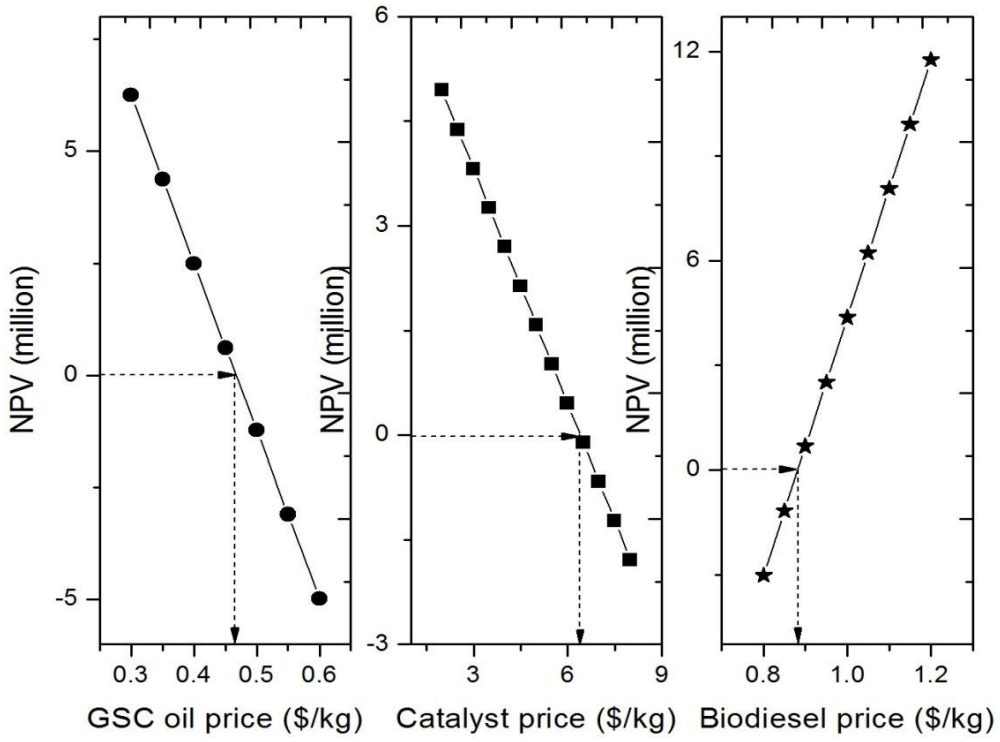

Fig. 5.6 Sensitivity analysis of heterogeneous biodiesel production process

5.8 Social impact assessment

Social impact of the processes was assessed and compared based on the safety index scores. The safety index score encounters chemical hazards associated with individual chemicals, chemical reactivity hazards associated with chemical mixture flowrates, individual equipment safety (capacity, temperature, pressure) and also the connections (i.e. process streamline connecting two equipments) between the equipments.

In a chemical process safety score and individual equipment score are calculated as follows:

At first, the individual component flow rates are calculated around an equipment. Then individual chemical severity index are multiplied with the corresponding component flow rate to give that component severity score. Adding all the component scores give chemical severity score (S_{SCI}) around that equipment. For calculating the chemical reactivity index, the total flow rate around the equipment and the overall mixture are considered. The reactivity of the chemical mixture is predicted by using NOAA's Chemical Reactivity Worksheet (CRW) (NOAA). Based on the prediction, an index score is estimated and multiplied with the total flowrate, which gives chemical reactivity score (S_{SRI}).

S_{CSI} (Chemical Safety score) = S_{SCI} (Chemical Severity Score) + S_{SRI} (Chemical Reactivity Score) …(5.1)

Equipment Safety score (S_{ESI}) are decided based on the capacity, temperature and pressure of the equipment.

S_{IESI} (discrete equipment safety score) = S_{CSI} (Chemical Safety score) + S_{ESI} (Equipment Safety score) …(5.2)

The detailed indexing systems are described elsewhere (Gangadharan et al., 2013). Once the individual equipment index are obtained, the connection (process streamline connecting two equipments) score between the two equipments are estimated as 10% of the summation of the scores of the two equipments (Gangadharan et al., 2013). Then the total process safety score are calcuated as follows:

$S_{total} = \Sigma S_{IESI} + \Sigma$ Connections …(5.3)

The chemical severity index are obtained for all the chemicals are listed in Table 5.8.

Table 5.8: Chemical Severity Index of the chemicals

Chemicals	Chemical Severity Index	Chemicals	Chemical Severity Index
Oil	6	Glycerol	5
FFA	6	Solid acid catalyst	5
FAME	6	Methanol	7
MG	6	H_2SO_4	10
Water	0	CaO	5
$CaSO_4$	3		

The chemical safety index score for the homogeneous and heterogeneous processes indicates that the score are quite high across every equipment probably due to the dealing with highly corrosive and hazardous homogeneous materials. The equipment safety score indicates that reactor and heat exchanger (E-100) of the heterogeneous process have the highest risk because of operating at high temperature, pressure and capacity (Tables 5.9 and 5.10).

The individual equipment safety score (S_{IESI}) indicates that the reactor of homogeneous process is prone to the highest risk and its connecting process streamlines are prone to highest risks compared to any other process streamlines (Fig. 5.7). The overall safety score indicates that heterogeneous catalyzed process is a safer process than that of homogeneous process (Fig. 5.7 and Fig. 5.8).

Table 5.9: Chemical Safety Index scores through individual equipment (Homogeneous Process)

Equipment	Chemical Severity Score (S_{SCI})	Chemical Reactivity score (S_{SRI})	Chemical Safety Index Score (S_{CSI})	Equipment Safety score (S_{ESI})
P-101	23.44	13.76	37.19	2
E-101	29.90	18.06	47.97	3
Reactor	30.63	18.66	49.28	5
E-100	39.02	22.85	61.87	4
Neutralizer	25.46	15.54	41.01	5
E-102	23.09	16.31	39.40	3
V-100	23.09	10.90	33.99	3
T-100	14.16	6.20	20.37	3
P-104	8.68	4.42	13.11	3
E-105	8.68	6.58	15.27	4
V-102	8.68	4.42	13.11	3
E-104	27.4	119.88	147.28	3
V-103	27.4	7.86	35.26	2
P-108	13.69	3.93	17.63	2
P-102	13.70	3.93	17.63	2
E-103	13.70	75.99	89.69	3
V-101	7.18	3.63	10.81	4
T-101	6.59	3.29	9.88	4
P-105	29.19	14.59	43.78	7
E-106	29.19	165.92	195.11	7
V-104	29.19	14.59	43.78	5
E-107	12.93	8.09	21.02	5
V-105	12.93	6.47	19.40	4
P-106	6.47	3.23	9.70	4
P-103	6.47	3.23	9.70	4

Table 5.10: Chemical Safety Index scores through individual equipment (Heterogeneous Process)

Equipment	Chemical Severity Score (S_{SCI})	Chemical Reactivity score (S_{SRI})	Chemical Safety Index Score (S_{CSI})	Equipment Safety score (S_{ESI})
P-101	14.74	6.82	21.56	4
E-101	21.34	10.12	31.46	5
Reactor	21.45	10.18	31.63	7
E-100	23.43	10.60	34.03	5
E-102	14.62	7.91	22.52	4
V-100	14.62	6.82	21.44	4
T-100	7.31	3.16	10.47	3
P-104	13.67	6.07	19.75	3
E-105	13.67	9.31	22.99	4
V-102	13.67	6.07	19.75	3
E-104	22.54	69.11	91.65	3
V-103	22.54	9.66	32.20	2
P-108	15.60	6.69	22.29	2
P-102	6.93	1.98	8.92	1
E-103	6.93	16.39	23.33	2
V-101	7.13	3.56	10.70	4
T-101	6.57	3.28	9.85	4
P-105	64.71	32.35	97.06	5
E-106	64.71	183.68	248.38	7
V-104	64.71	32.35	97.06	7
E-107	32.65	21.73	54.38	4
V-105	32.65	16.32	48.98	4
P-106	26.11	13.05	39.16	4
P-103	6.53	3.26	9.79	4

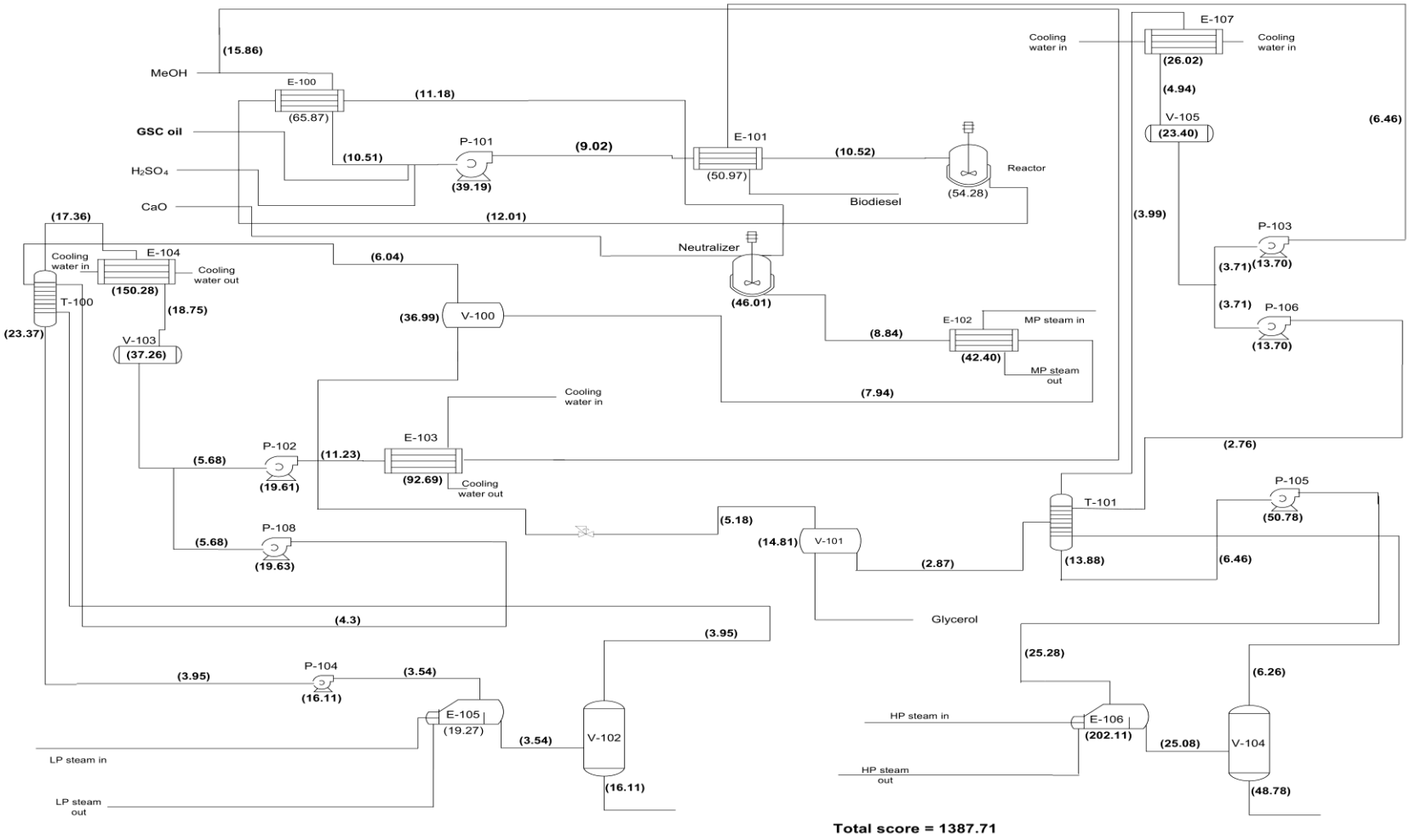

Fig. 5.7 Safety scores across every equipments and connections (Homogeneous process)

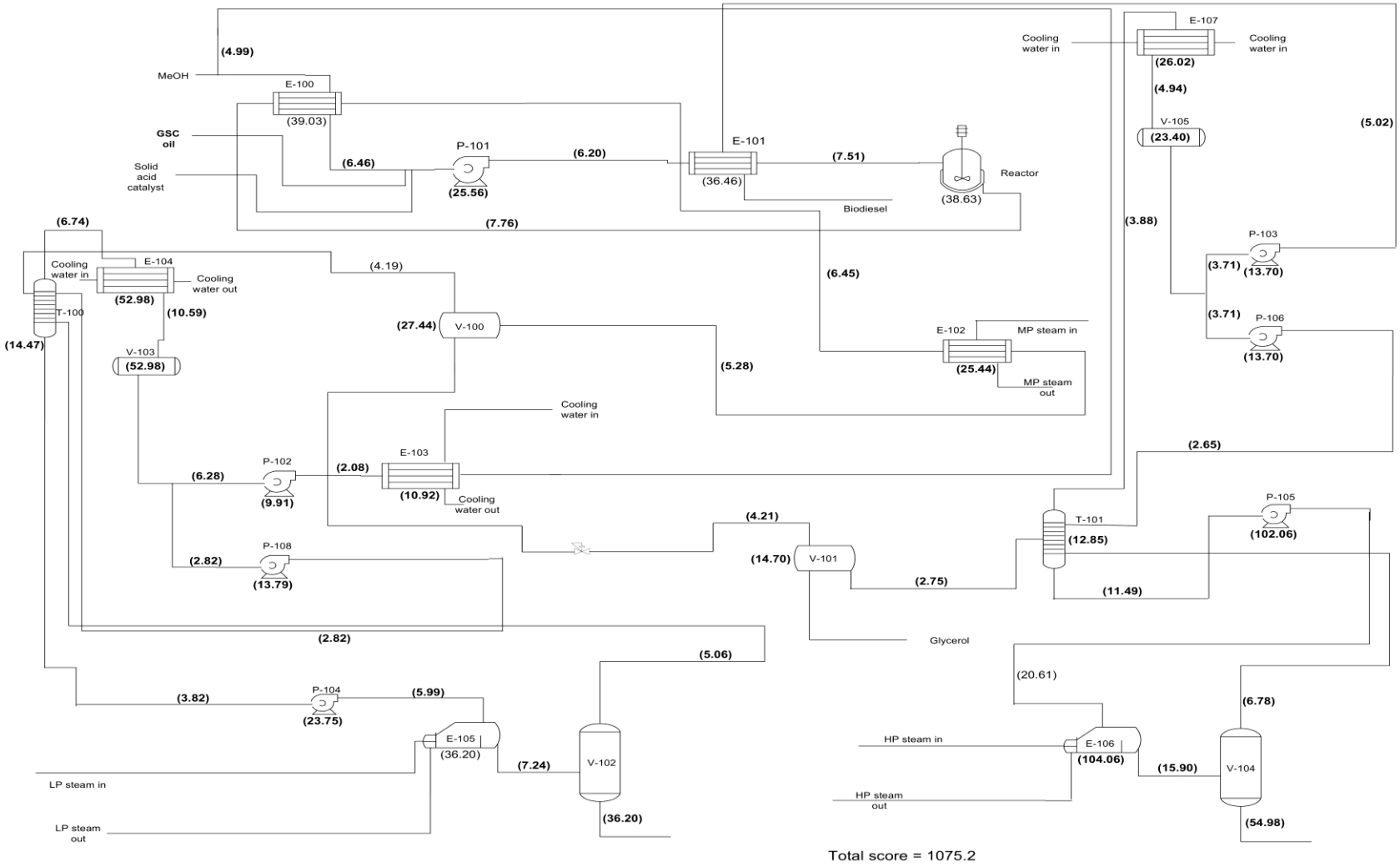

Fig. 5.8 Safety scores across every equipments and connections (Heterogeneous process)

The risk associated with the homogeneous and heterogeneous processes were analyzed further with the help of P&ID diagrams (Fig. 5.9 and 5.10). The pipeline diameters were calculated following two-K method (Datta, 2008), considering the number of fittings and valves. The hydraulics calculation indicates that the pipe segments diameters of homogeneous process are larger than those for heterogeneous process, implying more piping cost for homogeneous process. Additionally, homogeneous process requires more relief valves as compared to heterogeneous process (Fig. 5.9 and 5.10). The pressure relief valves (PRV) were sized based on two-phase (liquid and vapour) flow. The PRV orifice areas of homogeneous and heterogeneous reactors were found to be 127 mm^2 (E-orifice) and 96.77 mm^2 (D-orifice) respectively. The HAZOP studies around the reactors indicate that a homogeneous process require more safeguards than those for heterogeneous process (Tables 5.11 and 5.12).

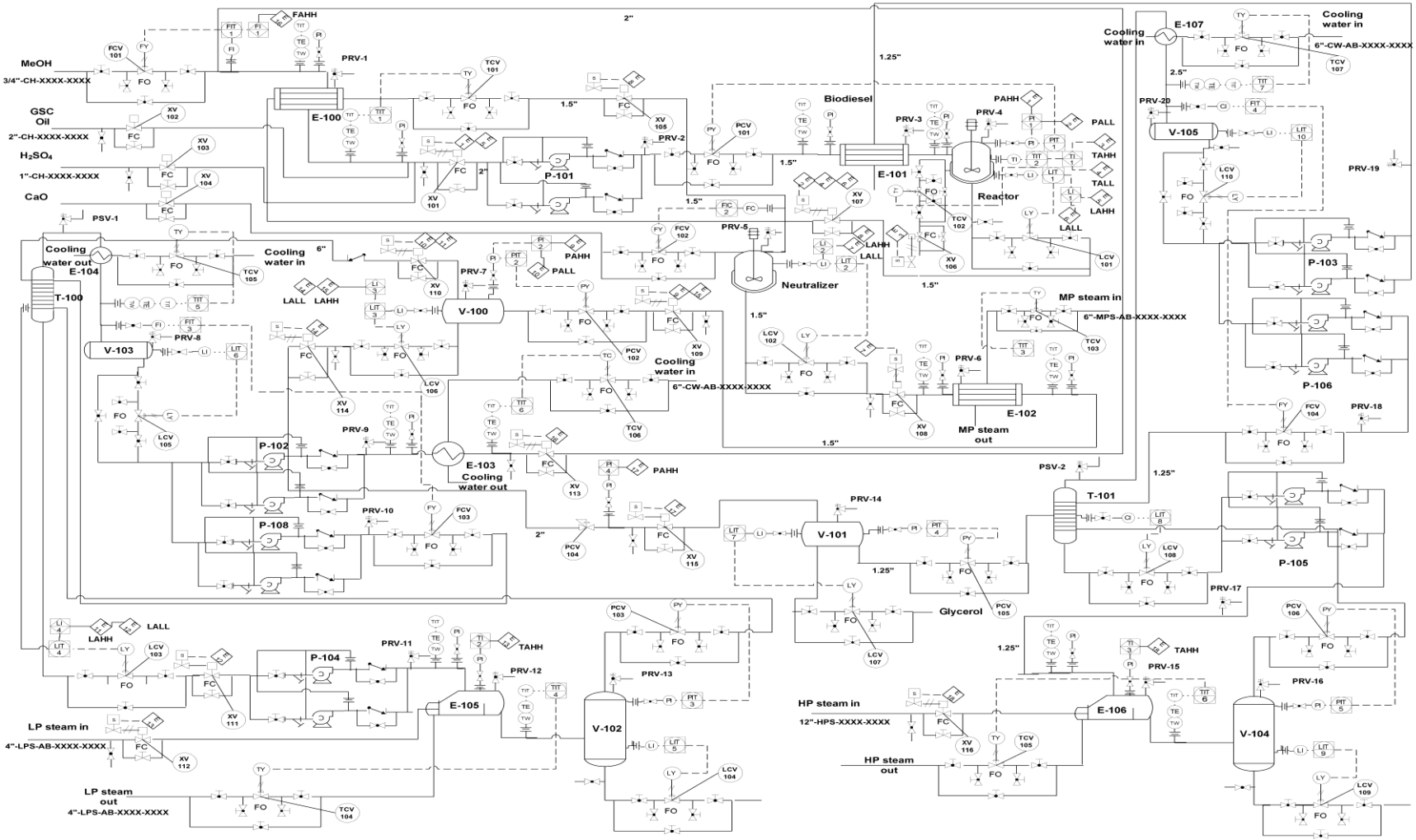

Fig. 5.9 P&ID diagram for homogeneous acid catalyzed simultaneous esterification, transesterification and chlorophyll removal process (homogeneous process)

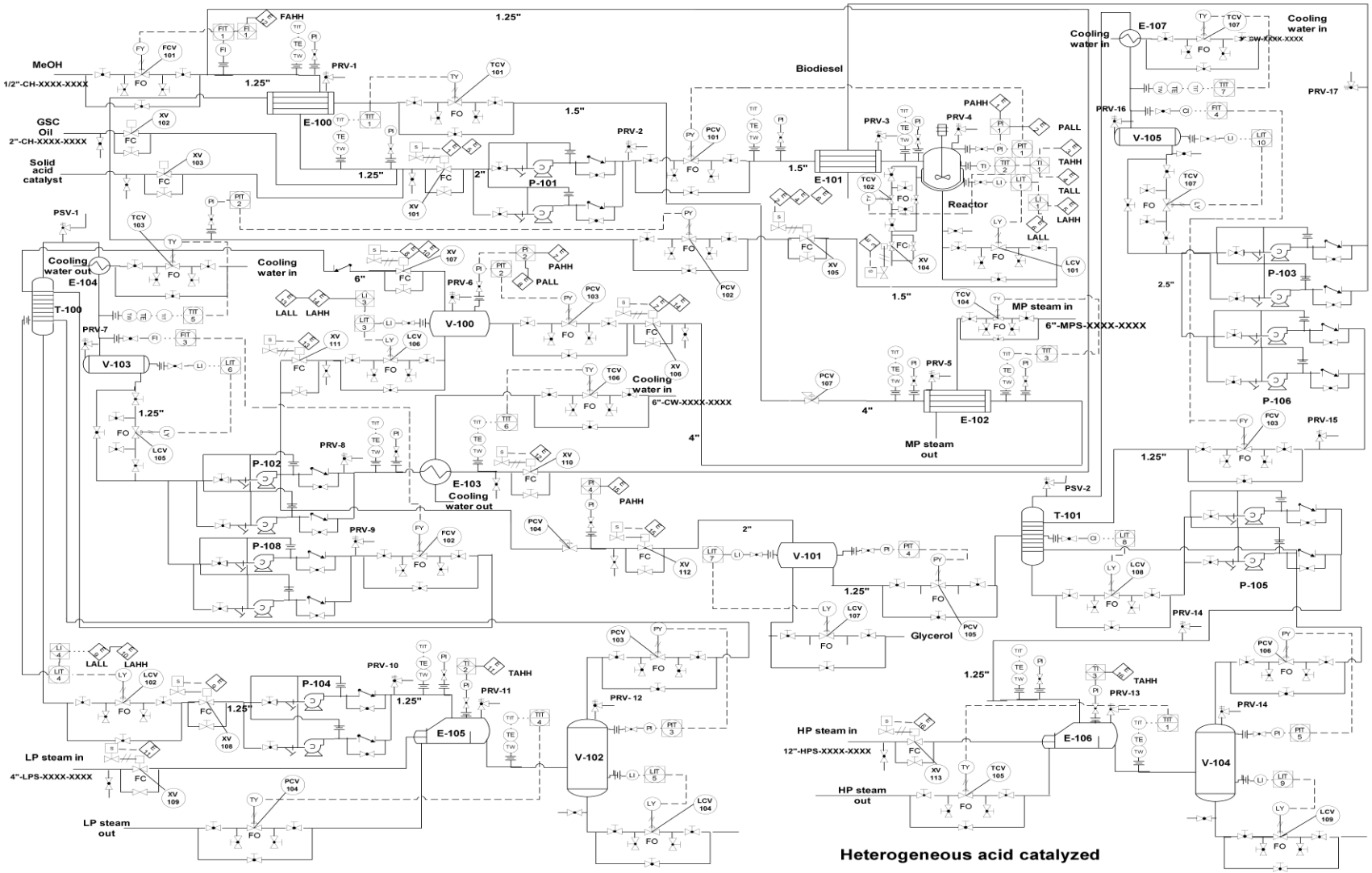

Fig. 5.10 P&ID diagram for solid acid catalyzed simultaneous esterification, transesterification and chlorophyll removal process

Table 5.11: HAZOP study of the homogeneous process

Causes	Consequences	Exist. Safeguards
TCV-101 failed to close or control loop malfunction	Vaporization of the methanol occurs	1. PRV-1 will open 2. XV-101 will shut down
PCV-101 failed to close or control loop malfunction	Vaporization of the reactant mixture occurs	1. PRV-3 will open 2. XV-101 will shut down
FCV-101 failed to close or control loop malfunction	1. Higher reactant volume to the reactor 2. Liquid level High in the reactor	1. PRV-3 will open 2. XV -113 will shut down the recycle line 3. XV-101 will shut down
Pressure in the reactor is very high	Potential explosion risk of the reactor	1. PRV-3 will open 2. XV-101 will shut down
Pressure in the reactor is very low	Vaporization of methanol and incomplete reaction	1. XV-107 will shut down
Temperature in the reactor is very high	1. Runway of the reaction 2. High pressure in the reactor	1. PRV-3 will open 2. XV-106 will shut down
Temperature in the reactor is very low	Incomplete reaction	XV-107 will shut down
Level in the reactor is very low	Improper stirring	XV-107 will shut down
Level in the reactor is very high	1. Possible overflow of the reactor 2. High pressure in the tank	1. PRV-3 will open 2. XV-101 will shut down
Level in the neutralizer is very high	Possible overflow of the neutralizer	1. PRV-4 will open 2. XV-105 will shut down 3. XV-104 will shut down
Level in the neutralizer is very low	Improper stirring	XV-108 will shut down

Table 5.12: HAZOP study of the heterogeneous process

Causes	Consequences	Exist. Safeguards
TCV-101 failed to close or control loop malfunction	Vaporization of the methanol occurs	1. PRV-1 will open 2. XV-101 will shut down
PCV-101 failed to close or control loop malfunction	Vaporization of the reactant mixture occurs	1. PRV-3 will open 2. XV-101 will shut down
FCV-101 failed to close or control loop malfunction	1. Higher reactant volume to the reactor 2. Liquid level High in the reactor	1. PRV-3 will open 2. XV -110 will shut down the recycle line 3. XV-101 will shut down
Pressure in the reactor is very high	Potential explosion risk of the reactor	1. PRV-3 will open 2. XV-101 will shut down
Pressure in the reactor is very low	Vaporization of methanol and incomplete reaction	1. XV-105 will shut down
Temperature in the reactor is very high	1. Runway of the reaction 2. High pressure in the reactor	1. PRV-3 will open 2. XV-104 will shut down 3. XV-101 will shut down
Temperature in the reactor is very low	Incomplete reaction	XV-105 will shut down
Level in the reactor is very low	Improper stirring	XV-105 will shut down
Level in the reactor is very high	1. Possible overflow of the reactor 2. High pressure in the tank	1. PRV-3 will open 2. XV-101 will shut down

5.9 Ecological impact assessment

Ecological impact of the processes were assessed and compared based on the environmental impact and the process efficiency. The environmental impact is expressed in terms of Potential Environmental Impact (PEI/h) and is calculated based on the amount of waste generation (kg/h) from the process. The PEI/h can be calculated based on the equation5.4 (Young et al., 1999; Young et al., 2000).

$$\left(\frac{PEI}{h}\right) = \sum_i^{Env\ cat} \alpha_i \sum_j^{Streams} M_{j,in} \sum_k^{Comps} x_{kj} \psi_{ki}^s \quad \ldots(5.4)$$

Where, ψ_{ki}^s is the specific potential environmental impact of component k, α represents the weighing factor associated with potential environmenta impact, M_j is the mass-flowrate of stream j and $x_{kj}$is the mass-fraction of the component k in stream j. The weighing factor by defaults is considered to be 1, however, depending on the geopraphic location, the weighing factor can be increased for specific potential environmental impact category (Young et al., 1999; Young et al., 2000). The specific environmental impact category fall into two general areas of concern (global atmospheric and global toxicological) with four categories in each area. The four global atmospheric impact categories are: Global Warming Potential (GWP), Ozone Depletion Potential (ODP), Acidification Potential (AP), Photochemical Oxidation Potential (PCOP). The specific potential environmental impact is the normalized score within individual impact category (eqn. 5.5).

$$\psi_{kl}^s = \frac{(Score)_{kl}}{\langle (Score)_k \rangle_l} \quad \ldots(5.5)$$

The $(Score)_{kl}$ represents the value k in some arbitery scale for category l and $<(Score)_k>_l$ represents the average value of all chemicals in category l. The $(Score)_{kl}$ for HTPI and TTP category is calculated by taking the inverse value of LD_{50} of the corresponding chemical.The $(Score)_{kl}$ for ATP category is calculated by taking the inverse value of LC_{50} (any species other than rat). The $(Score)_{kl}$ for HTPE category is calculated based on the time weighted average of Threshold Limit Values (TLV) obtained from occupatioanal safety. The $(Score)_{kl}$ for GWP category is calculated based on the half-life of the chemical. The ODP score is determined by comparing the rate at which a unit mass of chemical reacts with oznoe to form molecular oxygen. The PCOP score is determined by comparing the rate at which a unit mass of chemical reacts with a hydroxyl radical ($OH^{\cdot}$) to the rate at which a unit mass of ethylene reacts with hydroxyl radical ($OH^{\cdot}$). The AP score is determined by comparing the rate of release of H^+ to the atmosphere as compared to the rate of release of H^+ by SO_2 (Young et al., 1999). The PEI index provides a relative indication of the environmental friendliness or unfriendliness of the process across the system boundary. The WAR software is used to calculate the PEI indexes, and the PEI indexes with lower score indicates more environmental friendliness. The impact analysis indicates that heterogeneous acid catalyzed process is more environmentally friendly compared to that for homogeneous process (Table 5.13).

Table 5.13: Toxicity Index comparison of the two processes

	Homogeneous	Heterogeneous
Human Toxicity Potential by Ingestion (HTPI)	7.21	2.18
Human Toxicity Potential by Exposure (HTPE)	2.61	0.66
Terrestrial Toxicity Potential (TTP)	7.21	2.18
Aquatic Toxicity Potential (ATP)	0.18	0.06
Global Warming Potential (GWP)	1.01	0.35
Ozone Depletion Potential (ODP)	3.82×10^{-6}	1.32×10^{-6}
Photochemical oxidation potential (PCOP)	58.1	18.3
Acidification Potential (AP)	10.4	3.6
Total (PEI/h)	86.8	27.3

The process energy efficiency is calculated by dividing the raw materials energy to product energy.

$$\text{Energy Efficiency} = \frac{\text{Energy of the products}}{\text{Energy of the raw materials} + \text{Input energy}} \times 100\% \quad \ldots(5.6)$$

The process efficiency obtained for homogeneous and heterogeneous processes are 18% and 27% respectively. The most of the energy inhomogeneous process is utilized in reactant and product separation and purification as compared to heterogeneous process.

5.10 Discussion

All the assessment results are outlinedand compared between the two processes. Based on the relative comparison, the score 0 or 1 are assigned. Score 0 indicates unfavourable, whereas score 1 indicates favourable. The assessment comparison indicates that the heterogeneous acid catalyzed process is more sustainable than homogeneous acid catalyzed process (Table 5.14).

Table 5.14: Overall comparison of the processes

Assessment Criteria	Scores	
	Homogeneous	Heterogeneous
Profitability (profit, NPV, IRR)	0	1
Process Safety	0	1
Environmental Impact	0	1
Process Efficiency	0	1
Total	0	4

5.11 Conclusions

From the process simulation and sustainability assessment study it is obtained that heterogeneous acid catalyzed process is more sustainable than the conventional homogeneous acid catalyzed process. The profitability of heterogeneous acid catalyzed process is high compared to that of homogeneous process, even though the risk of profitability in heterogeneous process is higher.

CHAPTER 6: COMBINED BIOFUEL PRODUCTION FROM GREEN SEED CANOLA OIL USING ZEOLITES

A version of this chapter has been published in the following journal and presented in the following conference:

- Chinmoy Baroi, Saloni S. Mahto, Catherine Niu, Ajay K. Dalai. Combined biofuel production from green seed canola oil using zeolites. Applied Catalysis A: General, 2014, 469, 18-32.

- Chinmoy Baroi, Ajay K. Dalai. Catalytic behavior of highly active TPA impregnated zeolites in the production of biodiesel from Green Seed Canola (GSC) oil. 22nd Canadian Symposium on Catalysis, Canadian Catalysis Division, May 13-16, 2012, Quebec City, Quebec, Canada.

Contribution of the Ph.D. Candidate

Experiments were conducted by Chinmoy Baroi and Saloni Mahto (under mentorship of Chinmoy Baroi). The content in this chapter was written by Chinmoy Baroi with discussions and suggestions provided by Dr. Ajay Dalai and Dr. Catherine Niu.

Contribution of this Chapter to the Overall Ph.D. Research

In this phase of the research, the interaction of TPA with H-β zeolite has been postulated. Additionally, for the first time the possibility of using the same catalyst for producing value added combined biofuel from GSC oil through three different reactions (transesterification, esterification and etherification) was explored.

6.1 Abstract

Solid acid catalysts are of interests for various organic reactions. Among the solid acids, heteropoly acids (HPA) show strong Brønsted acidity. Especially, 12-Tungstophosphoric acid (TPA) ($H_3PW_{12}O_{40}$) possesses super acidity (Brønsted acidity) and prominent thermal stability as compared to other HPA compounds. The major disadvantages of using this heteropoly acid are their lower surface area (1 – 10 m^2/g) and polar solvent solubility. These problems can be

bypassed by supporting TPA upon various carriers. In this work, Tungsten oxide (WO_3) and TPA was supported on H-Y, H-β and H-ZSM-5 zeolite catalysts. The catalysts were characterized extensively using BET, XRD, FTIR, Raman, XPS, NH_3-TPD and EXAFS. Their catalytic activity was tested by esterification of the free fatty acid (FFA) of the green seed canola (GSC) oil, and transesterification of the GSC oil, using a stirred tank reactor for biodiesel production. In this study, TPA impregnated H-Y zeolite showed higher catalytic activity for esterification, and TPA impregnated H-β zeolite showed higher catalytic activity for the transesterification reaction as compared to other catalysts. A 55% TPA/H-β showed optimum catalytic activity for both esterification and transesterification. It yielded 99.3 wt.% ester, when 3.3 wt% catalyst (based on green seed canola oil) and 21.3:1 methanol to green seed canola oil molar ratio were used at 200°C, reaction pressure of 4.14 MPa (4.14 MPa) and reaction time of 6.5 h. Glycerol is derived from the transesterification of vegetable oils. This catalyst (55% TPA/H-β) was experimented for etherification of pure glycerol, and maximum conversion of glycerol (100%) was achieved in 5 h at 120°C, 1 MPa, 1:5 molar ratio (glycerol: TBA), 2.5% (w/v) catalyst loading. Later, these conditions were used to produce glycerol-ether successfully from the glycerol derived after transesterification of green seed canola oil. A mixture of GSC derived biodiesel and glycerol-ether was defined as biofuels. The properties of biofuels were evaluated and compared to those reported with ASTM standard for pure biodiesel.

6.2 Introduction

Biodiesel is environment friendly because of low carbon monoxide, particulate matter, and unburned hydrocarbon emissions as compared to fossils derived diesel fuel (Agarwal et al., 2006; Reyes and Sepulveda, 2006). Biodiesel is produced through transesterification reaction from triglycerides (oils or fats) using lower alcohol. The other name of transesterification is alcoholysis because in this process one alcohol is replaced by another i.e. the higher alcohol (glycerol) present in the triglyceride is replaced by a lower alcohol (e.g. methanol, ethanol), and the resultant monoalkyl fatty acids esters are called as biodiesel. Biodiesel is produced from vegetable oils and fats (e.g. rapeseed, soybean, sunflower, and palm oil). Biodiesel can also be produced from free fatty acids through esterification reaction. However, the existence of pure fatty acid is scarce, as they exist in the form of triglycerides (oil) in nature, and production of pure free fatty acids (FFA) for biodiesel production is not economically feasible. Biodiesel yet

cannot compete with the diesel because of its higher production price. The higher price is associated with the production cost, and 88% of the total production cost is caused by the feedstock price (Kulkarni and Dalai, 2006; Marchetti and Errazu, 2008). This cost can be reduced by using low quality and cheaper feedstocks such as used cooking oil, yellow grease, green seed canola oil, etc. Acid catalysts catalyze esterification along with the transesterification reaction to produce similar type of esters from free fatty acids using alcohol (Hara, 2010). Homogeneous acid catalysts can be exploited for this purpose, but heterogeneous (solid) acid catalysts are favored over those for waste minimization and easy product recovery (Kulkarni et al., 2006). Mesoporous solid acids catalysts with a moderate to strong acid sites and a hydrophobic surface are desireable for the biodiesel preparation (Lotero et al., 2005; Kiss et al., 2006).

Another approach to improving the economy of the biodiesel market is to find useful application for the co-product i.e. glycerol. Glycerol ethers, a derivative of glycerol, can be used as fuel additives which enhance fuel combustion properties and help in decreasing the cloud point of biodiesel (Klepacova et al., 2003). Glycerol ethers can be produced from etherification of glycerol in the presence of another alcohol and acid catalysts.The acid catalysts initiates the etherification reaction between the two alcohols (Gu et al., 2008). The nature of the reaction is a condensation reaction mainly producing mono glycerol-ether. This mono ether undergoes further etherification to form di and tri glycerol ethers if molar excess of alcohol is present (Fig. 6.1) (Zhao et al., 2013; Da Silva et al., 2009). A *tert*-butyl glycerol ether (TTBG) produced from *tert*-butanol (TBA) and glycerol has a potential for blending with petro-diesel (Wessendorf et al., 1995. Especially, di-*tert*-butyl glycerol ethers (DTBG) and tri-*tert*-butyl glycerol-ether (TTBG) are preferred as additives over mono-*tert*- butyl glycerol-ether (MTBG) because of their higher solubility in diesel/biodiesel compared to that of MTBG (Xiao et al., 2011).

Green seed canola oil is one of the low-grade oils available in huge quantity in North America. The raw green seed canola oil are not edible because of the presence of the higher amount of chlorophyll(Abraham and Man, 1986). The higher chlorophyll content also reduces the oxidation stability of the oil (Rawks and Santen, 1970). However, the green seed canola oil processing cost for edible purpose is high (Kulkarni et al., 2006). Raw green seed canola oil has poor oxidation stability due to the presence of high chlorophyll content. However, this can be improved by pre-treating the green seed canola oil with the mixture of mineral acids and/or using

acid treated adsorbents, which can reduce the chlorophyll to a significant amount, and the pretreated oil can be used to produce biodiesel with improved oxidation stability similar to that of canola biodiesel following conventional base catalyzed reaction (Kulkarni et al., 2006; Bahmaei et al., 2005).

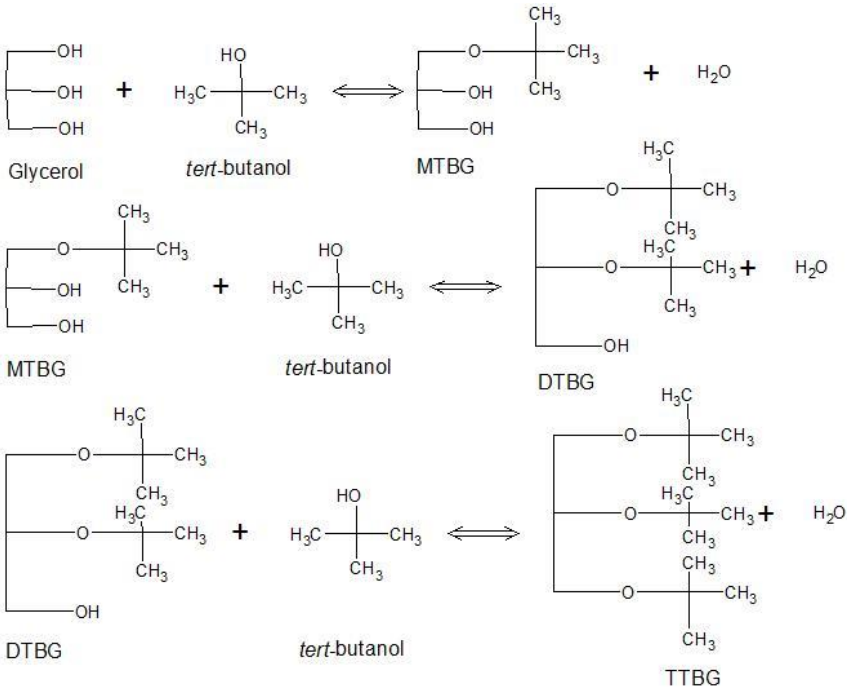

Fig. 6.1 Reaction scheme for the glycerol etherification

Heteropoly acids (HPA) made up of heteropoly anions show strong Brønsted acidity (Devassy and Halligudi, 2005; Busca, 2007; Okuhara et al., 2000). 12-Tungstophosphoric acid (TPA) with Keggin structure is thermally stable and depicts super acidity compared to other HPA compounds (Kozhevnikov, 2007). Heteropoly acids have lower surface area (1 – 10 m^2/g) and are soluble in polar solvents (Kulkarni et al., 2006). These problems can be avoided by supporting TPA on various carriers. Zeolite is a crystalline poroussolid typically made up of Si, Al, and O atoms and a catalytic material with wide industrial applications. Among these, Y, ZSM-5 and β zeolites are the most typical and commercially available zeolites. In all the previous works, TPA has been supported on H-Y, H-ZSM-5 and H-β zeolites, and their catalytic activity was tested in the reactions other than the transesterification of green seed canola oil (Gonzalez et al., 2011; Pain et al., 2000; Atalay and Gunduz, 2011; Prabhakaran and Fereiro,

2011). Moreover, no literature was found to compare the catalytic activity of the H-Y, H-ZSM-5 and H-β zeolites supported TPA.

The first research objective is to compare the catalytic activity of the H-Y, H-ZSM-5 and H-β zeolites supported Tungsten oxide and TPA, in both transesterification and esterification of green seed canola oil to produce high quality biodiesel. The best-performed catalyst in transesterification has been used for etherification of glycerol and for the first time the combined biofuel (GSC biodiesel + GSC glycerol-ether) properties were evaluated and compared against the pure biodiesel ASTM standard. The overall objective was to explore the possibility of using the same catalyst for producing value added combined biofuel from GSC oil through three different reactions (transesterification, esterification and etherification).

6.3 Experimental

6.3.1 Reagents

Unrefined green seed canola oil (4.25 wt% FFA) was obtained from Milligan Biotech Inc., Foam Lake, Saskatchewan, Canada. Commercial grade NH_4-Y, NH_4-β and NH_4-ZSM-5 were purchased from ZEOLYST, PA, USA. A 12 - Tungstophosphoric acid (TPA) and *tert* – Butanol (TBA) were purchased from Alfa-Aesar, MA, USA. Glycerol was purchased from EMD Chemicals, Mississauga, Ontario, Canada.

6.3.2 Catalyst preparation

Commercial grade NH_4-Y, NH_4-β and NH_4-ZSM-5 were calcined at 550°C for 6 h to acquire H-Y, H-β and H-ZSM-5 form. Tungsten oxide (WO_3) and TPA impregnated H-Y, H-β and H-ZSM-5 were prepared as follows: Calcined H-Y, H-β and H-ZSM-5 zeolites were added into the solution of calculated amount of Ammonium Meta Tungstate or TPA. After stirring at room temperature, the samples were oven dried at 110°C for 12 h and calcined at 350°-850°C for 6 h. These catalysts were designated as X%WO_3/S (T) or X%TPA/S (T), where S represents the support, X represents wt% loading and T represents the calcination temperature in degree Celsius. However, throughout the work, symbol X%WO_3/S or X%TPA/S was used for those catalysts, which were calcined at 450°C.

6.3.3 Catalyst characterization

The synthesized catalystsBET surface area and pore size analysis were performed using Micrometrics adsorption equipment (Model ASAP 2000). The catalysts wereheated at 200°C in a vacuum of 5×10^{-4} atm before the analysis. The surface area was calculated from the isotherms using Brunauer-Emmett-Teller (BET) method. The pore diameter and pore volume was calculated using BJH method from desorption branch of the isotherms. The X-ray diffraction (XRD) patterns of the samples were collected on a Bruker D8 Advance diffractometer using Cu $K\alpha$ radiation (λ = 1.5418 A). The catalysts FTIR spectra were recorded through Perkin Elmer FTIR spectrum GX equipment. For the FTIR analysis, sample pallets were prepared by pelleting a well mixed 3 mg of catalyst powder with 200 mg of KBr. Raman spectra of the catalyst were recorded on powder samples at room temperature with a Renishaw system 2000 spectrometer (785 nm). The X-ray photoelectron spectroscopy (XPS) study was carried out at Canadian Light Source. The photon energy used for this study was 235 eV with the total energy resolution of 70 meV. All spectra were collected by Scienta SES100 spectrometer. X-Ray absorption spectra (XAS) were recorded on HXMA beam-line at Canadian Light Source Inc., Canada, utilizing synchrotron radiation of 5-40keV and 100 mA current. W L_{III} data were recorded both in transmission and fluorescence mode employing a Lytle detector typically over 45 min. For EXAFS analysis, the spectra were extracted by utilizing the cubic spline method and normalized to the edge height. The k^3-weighted EXAFS oscillation was Fourier transformed into r space using ATHENA software. Curve-fitting analysis was performed for the W=O and W-O_{ext}-W with the range between r = 1.0 and 2.0 Å using ARTHEMIS software. Temperature programmed desorption of ammonia (TPD) was conducted using Quantachrome (USA) instrument. In a typical experiment, at first 200 mg of each sample was pretreated in He (Helium) at 550° C for 1 h. The sample was later cooled to room temperature in flowing He and saturated with 1% NH_3/N_2 (v/v) mixture at a flow rate of 30 mL/min for 120 min. Then the spectra were recorded between 100° C to 750° C, with a temperature ramp of 10 °C /min.

6.3.4 Postulation of catalyst structure

The strength of interaction of TPA (Terminal W^{6+}) with the β zeolite (Si or Al) was calculated exploiting the Density Functional Theory (DFT) at B3LYP/6-31^{+}G level (Li et al.,

2011). Pseudopotential basis set was used for the tungsten (W) atom in the calculation. A cluster model of H-β zeolite (Papai et al., 1994) was used in the calculation to represent the H-β zeolite structure. All calculations in this work were executed exploiting the Spartan 8 software. The models (schemes) and their structural contributions were selected by matching the calculated IR spectra peaks obtained from the DFT calculations against the experimental IR spectra peaks.

6.3.5 Catalytic activity testing

The catalytic activity of the prepared catalysts was tested through transesterification of green seed canola oil. The green seed canola oil was pretreated with K-10 clay to remove the chlorophyll following the procedure described by Issariyakul and Dalai (2010). The reactions were conducted in a 450 mL Parr reactor (Parr Instrument Co., ILL, USA). Initially, 100 g of GSC oil was taken into the reactor and preheated to 60°C with optimized stirring at 600 rpm. Catalysts and Methanol added to the reactor. Preliminary catalyst screening experiments were conducted at a reaction temperature of 150°C, 20:1 methanol to oil molar ratio and 3 wt% catalyst (based on the wt. of Green seed canola oil). Central Composite Design (CCD) was exploited for designing the experiments to analyze the effects of reaction parameters and Response Surface Methodology (RSM) was exploited for optimizing the reaction parameters. Design Expert 8 software was used for these purposes.The ester phase (after separation of the catalyst by filtration and separation of the glycerol phase) was analyzed utilizing High-performance liquid chromatography (HPLC). The ester phase collected from each experiment was analyzed for its ester content utilizing a Hewlett-Packard 1100 series HPLC.Two Phenogel 5μ 100°A 300X7.80 mm columns in series protected with guard column were exploited to separate different components of the samples during analysis. THF was used as a mobile phase at 1 mL/min for 25 min. The operating parameters were of sample injection volume 5 μL, detector temperature of 35°C, and column temperature of 24°C. Standard chemicals including methyl oleate, triolein, diolein, and monoolein were used for the HPLC calibration (see Appendix B). The ester yield (wt %) was calculated according to the equation 6.1.

$$\text{Ester yield (wt \%)} = \{(\text{wt. of the methyl ester in the ester phase}) / (\text{wt. of the ester phase})\} \times 100 \quad \ldots(6.1)$$

For reaction kinetics analysis, the samples were analyzed utilizing an Agilent 1200 series HPLC. Two PLgel 5μ 50°A 300X7.80 mm columns in series protected with guard column were exploited to separate different components of the samples during analysis. THF was used as a mobile phase at 1 mL/min for 25 min. The operating parameters were of sample injection volume 5 μL, detector temperature of 70°C, and column temperature of 35°C. Standard chemicals including methyl oleate, triolein, diolein, and monoolein were used for the HPLC calibration (see Appendix B). For kinetics analysis, the concentration (C_i=mol/L) of triglycerides (TG), diglycerides (DG), monoglycerides (MG) and free fatty acid (FFA) were converted to equivalent oil concentration as follows (Zheng et al., 2006).

$$C_{oil(t=t)} = C_{TG(t=t)} + 2/3*C_{DG(t=t)} + 1/3*C_{MG(t=t)} + 1/3*C_{FFA(t=t)} \quad \ldots(6.2)$$

The acid value of the produced biodiesel was determined according to the AOCS-D6751 method. The free fatty acid conversion was calculated based on the initial and final acid value.

Etherification of pure glycerol reaction was also performed in the Parr reactor (Parr Instrument Co., ILL, USA) and the inert atmosphere was maintained with N_2 using optimized stirring speed of 800 rpm. The catalyst screening studies were performed with different loadings of TPA in H-β by maintaining the process conditions at 120^0C, 1 MPa, 1:5 molar ratios (glycerol/TBA), 2.5% (w/v) catalyst loading with respect to the reaction volume, and 800 rpm for 5 hours. The effects of various reaction parameters e.g. TPA loading in catalysts, catalyst loading in reaction mixture, temperature and molar ratio (glycerol: TBA) were studied to achieve one of the best conditions for glycerol ether production.

For etherification reaction, TBA was taken in excess in the reaction solution, and the conversion was based on the limiting reactant, glycerol. Samples were analyzed using a GC (Hewlett Packard 5890 series II) equipped with a stabil wax column (length 30 m, internal diameter 0.25mm and width 0.1μm) and a FID detector. The analysis was started at 40^0C, heated up to 240^0C with 20^0C/min ramp rate and kept at 240 for 5 minutes. The injector and detector temperatures were maintained at 280^0C.

$$\% \text{ Conversion of glycerol} = \{(\text{Initial Concentration} - \text{Final Concentration})/ \text{Initial Concentration}\} \times 100\% \quad \ldots(6.3)$$

% Selectivity of Mono, Di or Tri Tert- Butyl Glycerol Ether

= {(Concentration of Mono, Di or Tri ether)/ Concentration of (mono + di + tri) ether} ×100 …(6.4)

Ether Yield = Conversion × Selectivity …(6.5)

Later, this condition was used for etherification of crude glycerol produced from the transesterification of green seed canola oil in the same reactor vessel. In a typical sequential transesterification and etherification reaction, after finishing the transesterification reaction using the optimum reaction conditions, TBA was added for etherification of the glycerol derived from the GSC oil as a byproduct of the methyl ester, and the experiments were performed at the best reaction conditions determined previously. Then the combined biofuel (GSC biodiesel + GSC glycerol-ether) properties were evaluated and compared against the pure biodiesel ASTM standard.

6.4 Results and discussion

6.4.1 Catalyst characterization

The synthesized catalysts textural properties are outlined in Table 6.1. It depicts that there is a decrease in the BET surface area of the H-Y, H-β, and H-ZSM-5, compared with those obtained with the ammonical form analyzed by ZEOLYST. It implies that thermal treatment (calcination) lessened the surface area (Costa et al., 2012). It also depicts that introducing WO_3 and TPA into H-Y zeolite increases the micropore area, BET surface area and decreases total pore volume and pore size compared to that of pure H-Y zeolite. For H-β zeolites, the introduction of WO_3 and TPA decreases the micropore area, BET surface area, pore volume and pore diameter (Table 6.1). For H-ZSM-5 zeolites, the introduction of WO_3 and TPA also decreases the micropore area, BET surface area, total pore volume but increases pore diameter (Table 6.1). The surface density calculation depicts that the values are higher for H-β and H-ZSM-5 containing catalysts compared to those of H-Y (Table 6.1). Both thermal treatment and strong acidity modify the zeolite structure and create secondary pore ranging from 12-300°A. It enables to house 12-Tungstophosphoric acid in spite of having its large size (12 °A) (Pamin et

al., 2000; Olejniczak et al., 2000; Camblor et al., 1998). Especially, H-β is flexible in changing its structure compared to H-Y and H-ZSM-5 (Gonzalez et al., 2011).

Table 6.1: Textural property of various catalysts

Sample	BET surface area (m^2/g)	Pore volume (cc/g)	Micropore area (m^2/g)	Average Pore Diameter nm	Surface density[a] ($/nm^2$)	Crystallinity (%)[b]
H-Y	513	0.49	328	11.39	0	100
H-β	536	0.54	336	11.04	0	100
H-ZSM-5	577	0.71	354	12.05	0	100
25% WO_3/ H-Y	531	0.13	411	4.75	1.22	4.3
25% WO_3/ H-β	299	0.06	202	3.70	2.17	13.6
25% WO_3/ H-ZSM-5	434±23	0.51±0.27	265	13.07±0.42	1.54	10.4
25% TPA/ H-Y	511	0.15	413	5.80	0.10	4.8
25% TPA/ H-β	471	0.14	387	6.13	0.11	7.3
25% TPA/ H-ZSM-5	459	0.55	285	12.54	0.11	13.4

[a]Surface density = [(WO_3or TPA%/100) × 6.023 × 10^{23}]/[F.W. × BET surface area × 10^{18}] (Papai et al. 1994)

[b]Calculated from XRD pattern

Table 6.2 depicts the textural properties of the different loadings of TPA in H-β zeolite. It depicts that with the increase in the loading, the micropore area, BET surface area, pore diameter, pore volume and surface density increase. It also depicts that the normalized BET surface area (per g of β zeolite) changes with the variation of TPA loading, which indicates that, the β zeolite structure changes with the TPA loading (Olejniczak et al., 2000).

Figure 6.2 depicts the XRD patterns of H-β, tungsten oxide and TPA impregnated H-β zeolite. It depicts that the characteristic peak of H-β zeolite structure (appears at 22.44°) diminishes upon tungsten oxide and TPA impregnation, which indicates loss of crystallinity of H-β zeolite structure (Zheng et al., 2011). It also depicts that upon the impregnation, tungsten oxide and TPA have high degree of crystallinity. This high degree of crystallinity arises probably due to high surface density of tungsten oxide and TPA on H- β compared to those for H-Y and HZSM-5 (Table 6.1).

Table 6.2: Textural property of TPA/H-β catalysts

Sample	BET surface area (m^2/g)	Pore volume (cc/g)	Micropore area (m^2/g)	Normalized BET surface area (m^2/g - β)	Average Pore Diameter nm	Surface Density ($/nm^2$)[a]
25% TPA/ H-β	471	0.14	387	628	6.13	0.11
35% TPA/ H-β	233	0.05	168	359	3.82	0.31
45% TPA/ H-β	263	0.06	187	477	4.08	0.36
55% TPA/ H-β	297	0.24	196	661	9.84	0.39
65% TPA/ H-β	334	0.39	211	954	13.0	0.41

[a]Surface density = $[(WO_3\%/100) \times 6.023 \times 10^{23}]/[F.W. \times \text{BET surface area} \times 10^{18}]$ (Papai et al. 1994)

Figure 6.3 depicts the XRD patterns of tungsten oxide and TPA impregnated H-Y zeolite. It depicts that the characteristic peaks of H-Y structure (appear at15.88°, 18.96°, 20.65° and 23.95°) diminish upon tungsten oxide and TPA impregnation, which points to loss of crystallinity of H-Y zeolite structure (Zheng et al., 2011). It also depicts that upon the impregnation, tungsten oxide and TPA are very well dispersed on H-Y zeolite.

Figure 6.4 depicts the XRD patterns of tungsten oxide and TPA impregnated H-ZSM-5. It depicts that the characteristic peak of H-ZSM-5 structure (appears at 22.27°) diminishes upon tungsten oxide and TPA impregnation (Li et al., 2010). It also depicts that upon the impregnation, tungsten oxide and TPA are very well dispersed on H-ZSM-5 zeolite.

The IR bands approximately at 440–463 cm^{-1}, 700–810 cm^{-1} and 1250-950 cm^{-1} are assigned to the T-O_4 (Si or Al) bending vibrations, Si-O symmetrical stretching vibrations and asymmetric stretching vibrations of the tetrahedral Si, Al atoms respectively (Zheng et al., 2011; Morales-Pacheco et al., 2011). Upon tungsten oxide (WO_3) and TPA impregnation on H-β zeolite, stretching vibrations of the tetrahedral Si, Al atoms appear at higher wavenumber (1093 cm^{-1}) compared to those for H-β zeolite (1080 cm^{-1}) (Fig. 6.5). This is an indication of a breakdown of the zeolite framework Si-O-Al bonds (Pamin et al., 2000; Mozgawa, 2000). Figure 6.5 also depicts that upon Tungsten oxide (WO_3) and TPA impregnation the IR band assigned to Si-O symmetrical stretching vibrations appear to lower wavenumber (790 cm^{-1}) compared to those for H-β zeolite (798 cm^{-1}), and the IR bands assigned to the T-O_4 (Si or Al) bending vibrations appear to lower wavenumber (448 cm^{-1}) compared to those for H-β zeolite (459 cm^{-1}).

It indicates a strong interaction of Tungsten oxide and TPA with the H-β zeolite structure network (Lopez-Salina et al., 2000; Thouvenot et al., 1984).

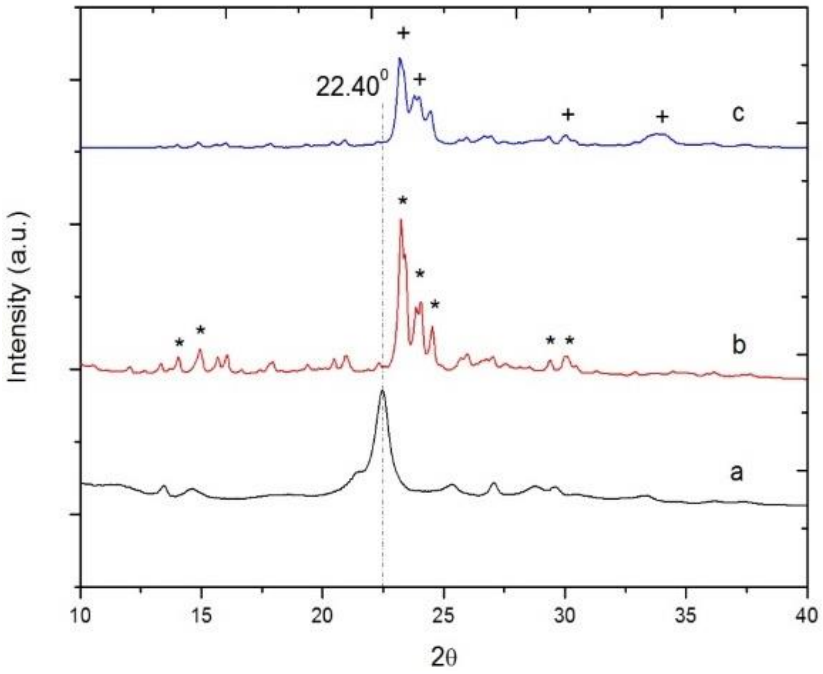

Fig. 6.2 XRD patterns of different β catalysts: (a) H-β, (b) 25%WO_3/H-β and (c) 25%TPA/H-β

(*) Tungsten oxide, (+) TPA

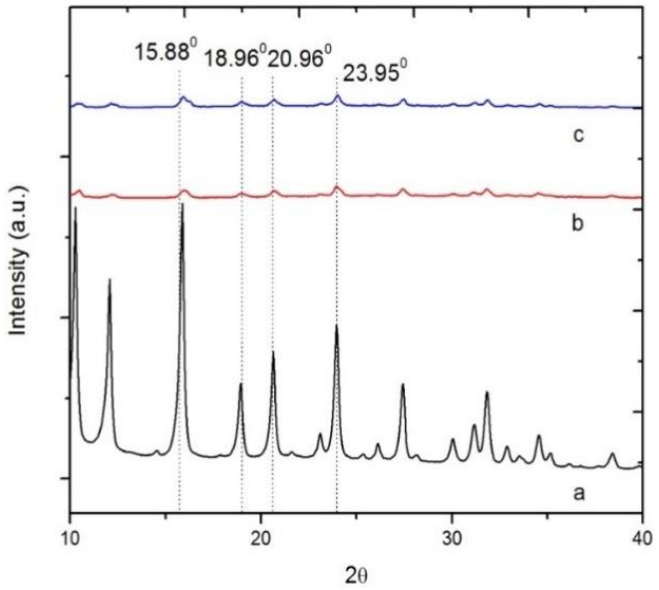

Fig. 6.3 XRD patterns of different Y catalysts: (a) H-Y, (b) 25%WO_3/H-Y and (c) 25%TPA/H-Y

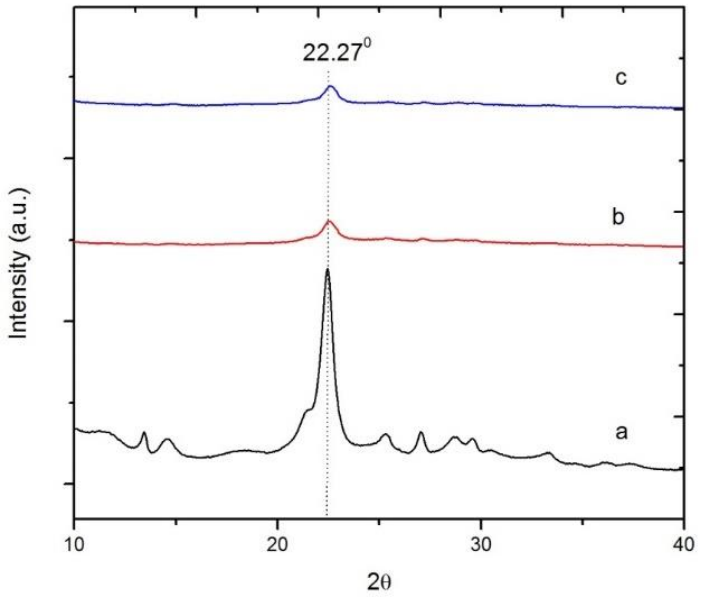

Fig. 6.4 XRD patterns of different ZSM-5 catalysts: (a) H-ZSM-5, (b) 25%WO3/H-ZSM-5 and (c) 25%TPA/H-ZSM-5

Figure 6.6 depicts that upon Tungsten oxide (WO_3) and TPA impregnation, asymmetrical stretching vibrations corresponding to the tetrahedral Si, Al atoms appear at higher wave number (1093 cm^{-1}) compared to those for H-Y zeolites (1050 cm^{-1}). This is an indication of a breakdown of the zeolite framework Si-O-Al bonds (Pamin et al., 2000; Zheng et al., 2011; Mozgawa, 2000). Figure 6.6 also depicts that the IR bands assigned to the T-O_4 (Si or Al) bending vibrations appear at higher wave number (463 cm^{-1}) compared to that of H-Y (455 cm^{-1}) with the impregnation of Tungten oxide and TPA on H-Y zeolite respectively, which indicates weakening of T-O_4 (Si or Al) bond. Pure TPA depicts IR peaks approximately at 1081 (P-O in the central tetrahedron), 976-995 (terminal W=O), 890-900 and 805-810 (W-O-W) cm^{-1} refers to asymmetric vibration of the Keggin anion (Tropecelo et al., 2010; Satishkumar et al., 2006; Damyanova et al., 2003; Yun and Kuabara, 2004). After impregnation of TPA (Fig. 6.6) a new weak band at 900 cm^{-1} appears in the spectrum. This is assigned to W–O–W vibrations of the heteropoly acid.

Figure 6.7 depicts that upon Tungsten oxide (WO_3) and TPA impregnation asymmetrical stretching vibrations corresponding to the tetrahedral Si, Al atoms (Morales-Pacheco et al., 2011; Naskaar et al., 2012), appear approximately at the same wave number (1225 cm^{-1}) compared to that for H-ZSM-5 zeolites (1227 cm^{-1}). Also, no change in the IR bands assigned to the T-O_4 (Si

or Al) bending vibrations (468 cm^{-1}) and Si-O symmetrical stretching vibrations (797 cm^{-1}) is observed upon Tungsten oxide (WO_3) and TPA impregnation.

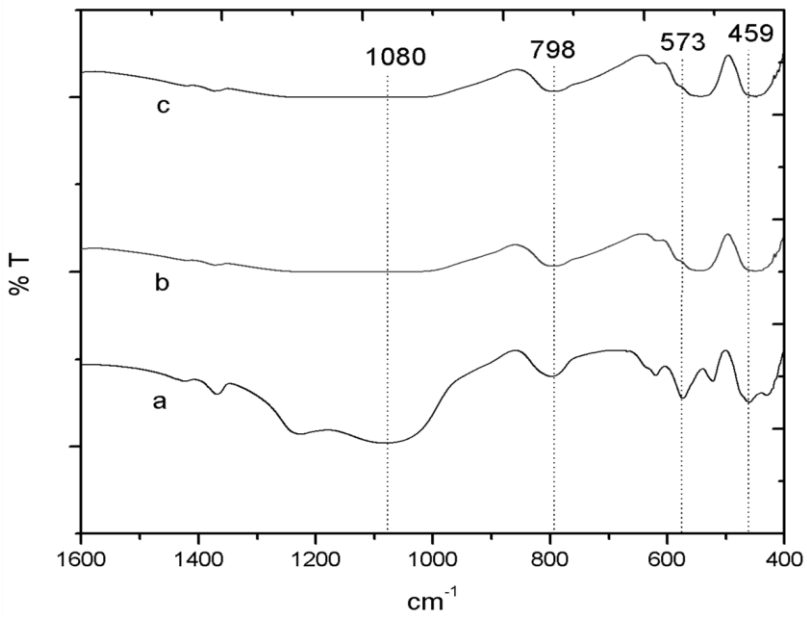

Fig. 6.5 FTIR spectra of different β catalysts: (a) H-β, (b) 25%WO_3/H-β and (c) 25%TPA/H-β

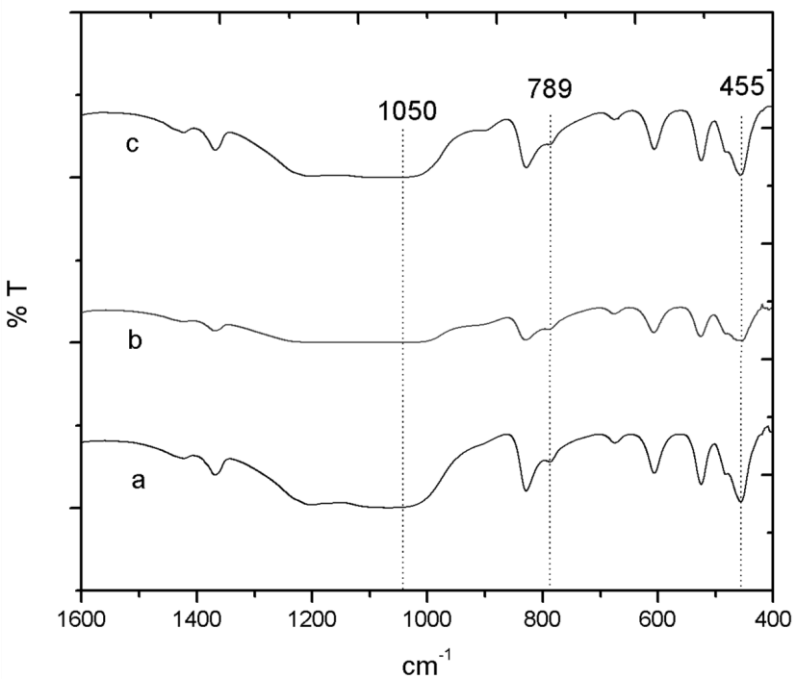

Fig. 6.6 FTIR spectra of different Y catalysts: (a) H-Y, (b) 25%WO_3/H-Y and (c) 25%TPA/H-Y

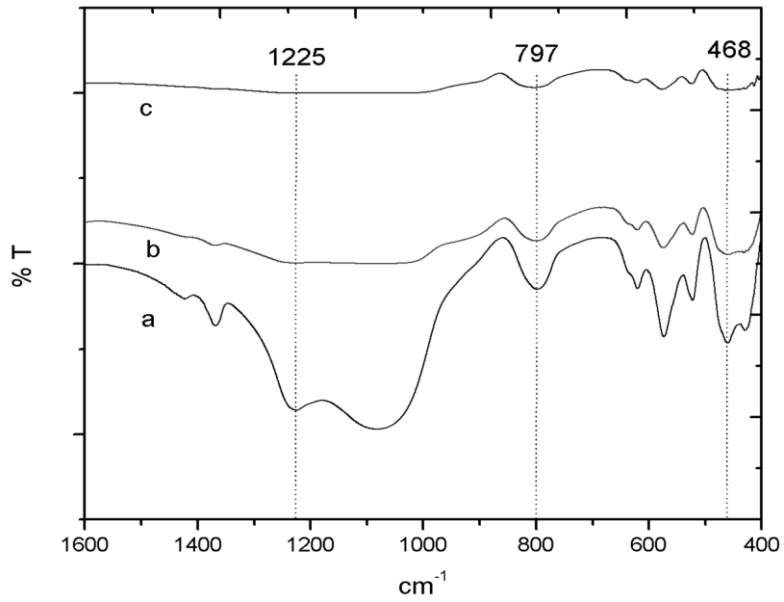

Fig. 6.7 FTIR spectra of different ZSM-5 catalysts: (a) H-ZSM-5, (b) 25%WO_3/H-ZSM-5 and (c) 25%TPA/H-ZSM-5

Figures 6.8 and 6.9 show the Raman spectra of the β zeolite and different loadings of TPA impregnated on H-β zeolite in the Raman shifting range of 100 – 600 cm^{-1} and 600-1100 cm^{-1}respectively. Raman scatterings at 464 cm^{-1}; 340 cm^{-1} (interlayer), 312 cm^{-1} (intralayer) and 396 cm^{-1}, 423 cm^{-1}, represent T-O_4 (T = Si or Al) tetrahedra of the four, five (intra layer and interlayer) and six membered ring of H-β respectively (Moller et al., 2011; Mihailova et al., 2005; Yu et al., 2001). Upon TPA impregnation the peak representing T-O_4 (T = Si or Al) tetrahedra of the four membered ring appears at higher wave number as compared to that for H-β, indicating the weakening the bonds of the 4 membered ring. On the other hand, peaks representing T-O_4 (T = Si or Al) tetrahedra of the five and six membered ring appear at lower wave number as compared to that for H-β, indicating contraction of the bonds of the 5 and 6 membered ring (Fig. 6.8). Figure 6.9 depicts that the Keggin structure of TPA is intact clearly up to 55% loading, when impregnated, by showing signature scattering pattern of TPA approximately at 1010 cm^{-1} (P-O in the central tetrahedron) and 989 cm^{-1} (terminal W=O) (Huang et al., 2008; Guo et al., 2008). It also depicts that up to 55% TPA loading, peak approximately at 805 cm^{-1} (W=O stretching) and 711 cm^{-1} (W-O-W stretching) are observed, which arises probably due to the strong interaction of TPA Keggin structure with the zeolite structural alumina (Herrera et al., 2008). Above 55% loading, very weak intensity of these peaks indicates the absence of strong interaction of TPA Keggin structure with the zeolite structural

alumina. However, in all the cases, signature scattering pattern of TPA approximately at 1010 cm^{-1} (P-O in the central tetrahedron) and 989 cm^{-1} (terminal W=O) are observed (Huang et al., 2008; Guo et al., 2008).

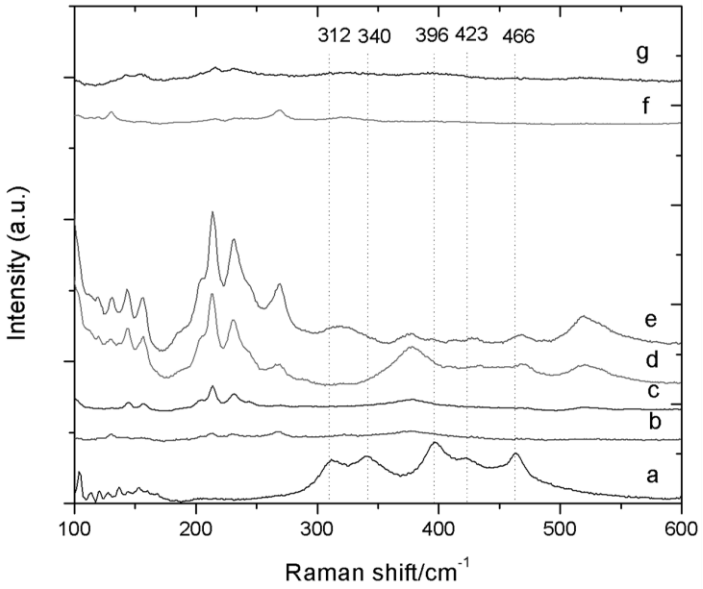

Fig. 6.8 Raman spectra of different amount of TPA loaded β: (a) H-β, (b) 25% TPA/H-β, (c) 35%TPA/H-β, (d) 45% TPA/H-β(e) 55%TPA/H-β, (f) 65% TPA/H-β and (g) 75% TPA/H-β

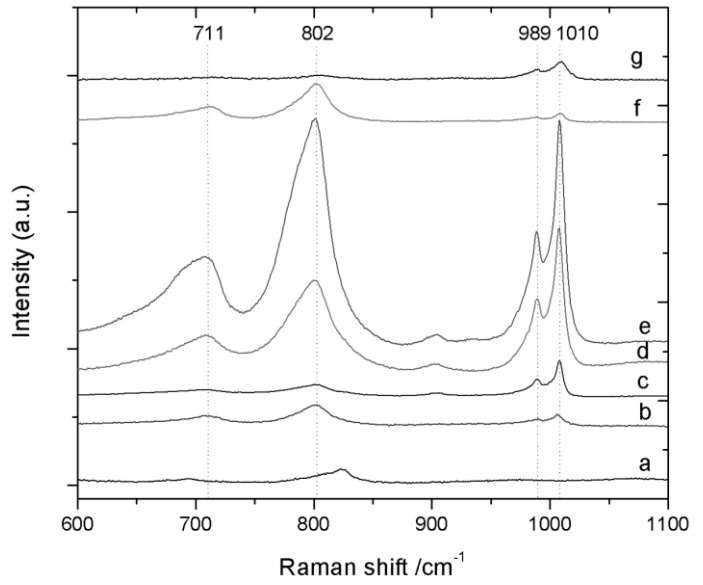

Fig. 6.9 Raman spectra of different amount of TPA loaded β: (a) H-β, (b) 25% TPA/H-β, (c) 35%TPA/H-β, (d) 45% TPA/H-β,(e) 55%TPA/H-β, (f) 65% TPA/H-β and (g) 75% TPA/H-β

Silica 2p depicts the peak to be formed approximately at 104 eV. The movement to higher binding energy refers to the shorter Si-O bonds whereas the lower binding energy refers to the elongated Si-O bonds and in the vicinity to the distorted [AlO_4^-] component of the zeolite framework (Chichova et al., 2009). Upon TPA impregnation, Si (2p) peaks are to be found at around 101 eV and 108 eV (Table 6.3). The Full Width Half Maximum (FWHM) of the peak at 101 eV increases with the TPA loading indicating the creation of more elongated Si-O bonds and in vicinity to the distorted [AlO_4^-] component of the zeolite framework. Besides, the FWHM of the peak at 108 eV decreases with the TPA loading up to 55% TPA, beyond 55% loading, the FWHM of the peak at 108 eV increases (Table 6.3). The Al (2p) binding energy approximately at 74 eV corresponds to Al in IV-fold site β zeolite (Chichova et al., 2009). Upon TPA impregnation, the FWHM of Al (2p) binding energy peak remains almost same up to 55% TPA loading, which increases for 65% TPA loading (Table 6.3). This increase in FWHM is an indication of the existence of the other co-ordination states of alumina when 65% TPA loading is used (Niwa and Katada, 1997).

Table 6.3: The binding energy and FWHM of silica and alumina in the zeolite structure

Sample	Si (2P)		Al (2P)
	FWHM (at 101 eV) (eV)	FWHM (at 108 eV) (eV)	FWHM (at 74 eV) (eV)
H-β	-	6.9	4.1
45% TPA/H-β	1.8	3.3	4.7
55% TPA/H-β	1.9	3.3	4.4
65% TPA/H-β	2.1	4.3	8.6

The coordination number of W=O and W-O_{ext}-W bonds in TPA, 55%TPA/H-β, 65%TPA/H-β are found to be identical (Table 6.4). However, with an increase in TPA loading, the bond length of W=O decreases and the bond length of W-O_{ext}-W increases as compared to pure TPA (Table 6.4). The fitted W L_{III} EXAFS spectra of the 55%TPA/H-β sample is depicted in Figure 6.10. The figure depicts the corresponding radial distribution functions for this material. The pattern of change in bond length is an indication of distortion in TPA kegging

structure with an increase in TPA loading, especially for 65% TPA loading (Yamazoe et al., 2008).

Table 6.4: Structural parameters derived from fitted EXAFS for supported and bulk TPA samples

Samples	Parameters	Coordination environment	
		W=[O]	W-[O_{ext}]-W
Pure TPA	C.N.	1	4
	r (^{0}A)	1.88	1.97
	R-factor	0.008	0.008
55% TPA/H-β	C.N.	1	4
	r (^{0}A)	1.62	1.98
	R-factor	0.01	0.01
65% TPA/H-β	C.N.	1	4
	r (^{0}A)	1.54	2.14
	R-factor	0.04	0.04

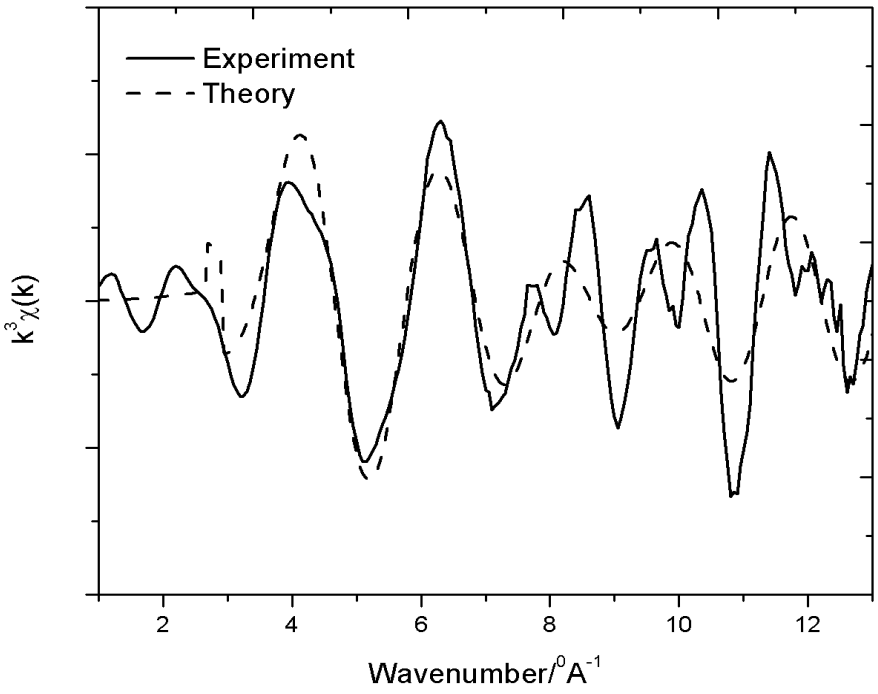

Fig. 6.10 (a) Fitted W L_{III} EXAFS of 55%TPA/H-β

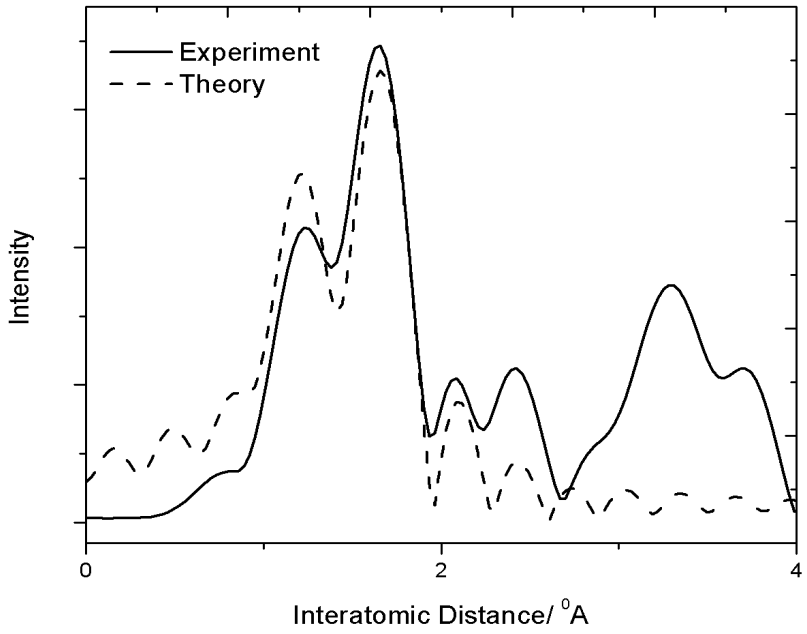

Fig. 6.10 (b) Fitted Redial distribution function (RDF) of55%TPA/H-β

Figure 6.11 depicts the NH_3-TPD results of different loadings of TPA on H-β zeolite. It depicts that the intensity of the low-temperature desorption peak (indicative of weak Brønsted acidity) (Katada and Niwa, 2004; Collignon et al., 2001) increases with the increase in the loading. However, the high temperature peak indicating strong acidity diminishes beyond 55% loading, which is in agreement with the conclusion obtained from the Raman spectra, XPS binding energy pattern and distortion of TPA Keggin structure analyzed through EXAFS analysis.

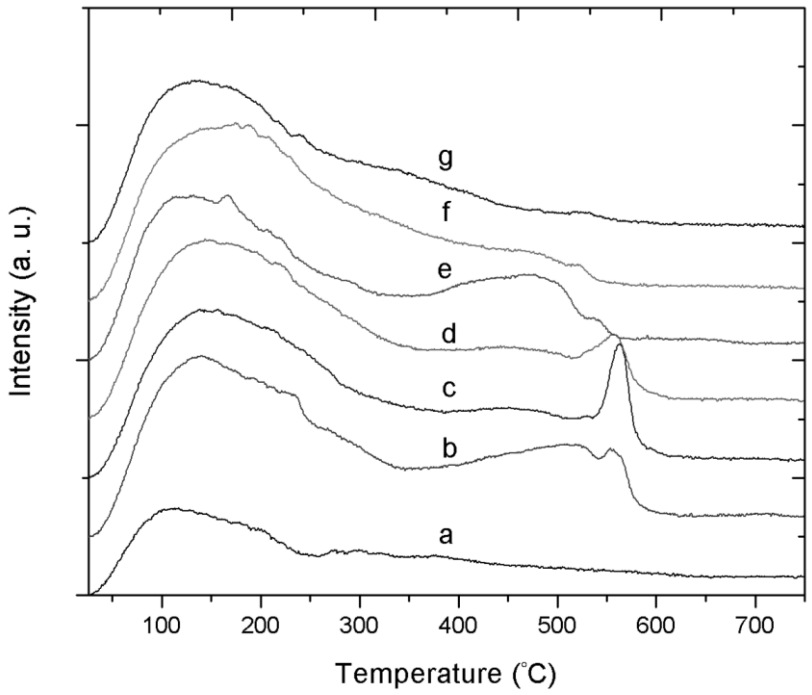

Fig. 6.11 NH_3-TPD of different amount of TPA loaded β: (a) H-β, (b) 25% TPA/H-β, (c) 35%TPA/H-β, (d) 45% TPA/H-β,(e) 55%TPA/H-β, (f) 65% TPA/H-β and (g) 75% TPA/H-β

6.4.2 Postulated catalyst structure

Figure 6.12 depicts the postulated catalyst structure of H-β supported TPA. It depicts that upon the impregnation, TPA attaches to the 4 member structural alumina and silica, and Si-O-Al bond breaks down. This creates a cavity in the structure and mespore. Figure 6.13 depicts 4 different schemes of the interaction of TPA (Terminal W^{6+}) with the H-β zeolite structural IV fold Si or Al.

The cohesive energy can be taken as a measure of the stability with respect to the decomposition. The cohesive energy is given in Equation (6.6) in which i represent the individual atoms that constitute the solid. The higher the cohesive energy of the solid, the more stable it is and more energy is required to decompose the solid (Shetty et al., 2006).

$$E_{coh} = E_{solid} - \sum_i E_i \quad \ldots(6.6)$$

The 55% TPA (55% loading) impregnated H-β having combined higher cohesive energy compared to those for other TPA loading impregnated H-β indicates higher structural stability of the prepared 55% TPA/H-β catalyst (Table 6.5).

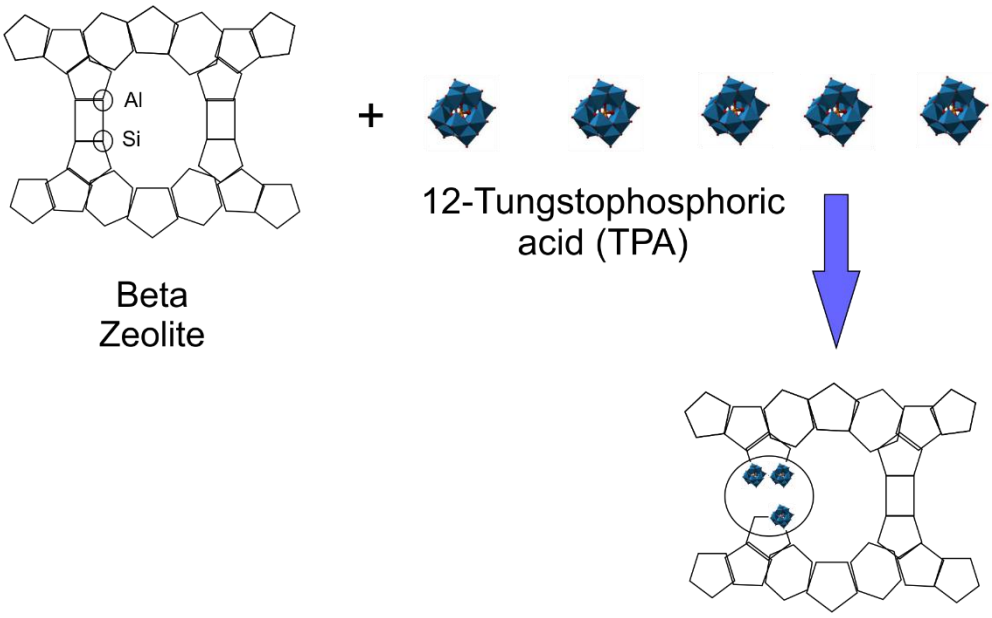

Fig. 6.12 Postulated structure of H-β supported TPA

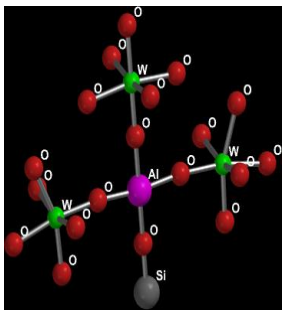

Scheme 1

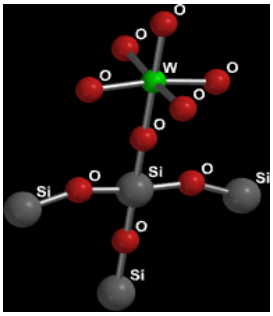

Scheme 2

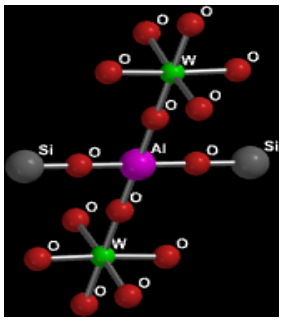

Scheme 3

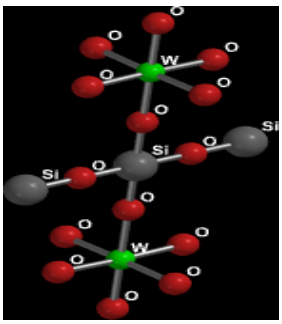

Scheme 4

Fig. 6.13 Different schemes of interaction

Table 6.5: Cohesive energy of different samples

Samples	Scheme No. (see Fig. 6.13)	Contribution of the schemes (%)	Combined Cohesive energy (eV)
45% TPA/H-β	1	25	
	2	25	518.9
	3	50	
55% TPA/H-β	1	40	
	2	20	546.5
	3	40	
65% TPA/H-β	1	40	
	2	20	545.8
	3	20	
	4	20	

6.4.3 Catalytic activity in the transesterification reaction

The absence of external and internal mass transfer resistance was confirmed by the Reynolds number of the reaction mixture, mass-transfer flux, reaction rate and Weisz-Prator criteria (see appendix C). Table 6.6 depicts the catalytic activity of different catalysts. It depicts that 25% WO_3 or TPA impregnated H-Y zeolite depicts higher activity in the conversion of FFA through esterification compared to that for transesterification. It also depicts that 25% WO_3 impregnated H-ZSM-5 zeolite depicts higher activity in the conversion of FFA through esterification and 25% TPA impregnated H-ZSM-5 zeolite depicts optimum catalytic activity both in esterification and transesterification. These implies that higher degree of TPA dispersion favors esterification reaction, whereas, higher degree of crystallinity favors transesterification reaction (Table 6.1). A 25% TPA impregnated β zeolite depicts the optimum catalytic activity in terms of ester yield (wt%) through transesterification and conversion (%) of FFA through esterification, when 3 wt% catalyst (based on the oil), methanol to oil molar ratio of 20:1, reaction temperature of 150°C and reaction time of 10 h are used. This optimum activity might result from an optimum combination of degree of crystallinity and surface density of the TPA (Tables 6.1).

Table 6.6: Catalyst screening experiments (3 wt% catalysts, 20:1 methanol to oil molar ratio, 150°C, 10 h reaction time)

Catalysts	Catalytic activity	
	Ester yield (wt.%)	Conversion of FFA (%)
25% WO_3/H-Y (450°C)	25.9	86.3
25% WO_3/H-Y (850°C)	23.2	74.6
25% WO_3/H-ZSM-5 (450°C)	26.7	78.5
25% WO_3/H-β (450°C)	48.8	55.9
25% WO_3/H-β (550°C)	17.0	-
25% WO_3/H-β (350°C)	37.0	66.9
25% TPA/H-Y (450°C)	34.9±2.7	61.5±4.8
25% TPA/H-ZSM-5 (450°C)	51.7	53.1
25% TPA/H-β (450°C)	67.8	74.3
25% TPA/H-β (550°C)	21.7	77.9
25% TPA/H-β (350°C)	34.9	83.1

Table 6.7 depicts catalytic activity of different loading of TPA in H-β zeolite. It depicts that the catalytic activity (in terms of ester yield wt%) increases with the increase in the TPA loading up to 55%, and there is no further increase in the catalytic activity above that loading. On the other hand, the conversion of FFA decreases with an increase in the loading up to 45% and increases thereafter (Table 6.7). This can be explained with the help of Brønsted and Lewis acidity concept. Børnsted acid catalysts are mainly active in the esterification reaction, and Lewis acid catalysts are mainly active in the transesterification reaction (Di Serio et al., 2008). The ratio of Brønsted to Lewis acid sites is responsible for relative reaction progress between transesterification and esterification. Transesterification reaction requires moderate but more acid sites compared to the strong and fewer acid sites (Kulkarni et al., 2006; Lotero et al., 2005). A 55% TPA loading on β zeolite has moderate, but higher number of acid sites (Fig. 6.11) compared to the other loadings of TPA. This causes the highest activity of 55%TPA/H-β in transesterification reaction and probably a higher relative ratio of Brønstead to Lewis acid sites (Lewis acidity decreases with the increase of TPA loading- obtained from the DFT calculation)

causes an optimum activity in FFA conversion. Thus, considering the fact that esterification reaction rate is faster than that of the transesterification reaction (Ataya et al., 2007), 55% TPA is considered to be the optimum.

Table 6.7: Catalyst loading screening (3 wt% catalysts, 20:1 methanol to oil molar ratio, 150°C, 10 h reaction time)

Catalysts	Catalytic activity	
	Ester yield (wt%)	Conversion of FFA (%)
25% TPA/H-β	67.8	74.3
35% TPA/H-β	86.2	75.7
45% TPA/H-β	94.0	67.3
55% TPA/H-β	95.3	71.8
65% TPA/H-β	67.9	76.1
75% TPA/H-β	55.4	93.6

6.4.4 Effects of reaction parameters in the transesterification reaction

From the preliminary experiments, reaction temperature is found to be the most important factor affecting ester yield. The effects of reaction temperature on ester yield was analyzed keeping the catalyst concentration at 3 wt% (based on the wt. of oil), 20:1 methanol to GSC oil molar ratio and 10 h of reaction time. Figure 6.14 depicts that ester yield increase with the increases in the reaction temperature. It also depicts that at higher temperature (200°C) the initial ester formation is slow compared to those for low temperatures, which can be explained with the help of the transesterification reaction scheme (Fig. 6.15). Transesterification is a three-step reaction. At higher temperature initially the rate of diglyceride and monoglyceride formation (1^{st} and 2^{nd} step) are higher, which leads to complete ester formation later. On the contrary, at lower temperature the three-step transesterification precedes consecutively, which leads constant slow formation of ester (results not depicted). Transesterification reaction is an endothermic reaction, thus reaction temperature has a positive impact on the ester yield (wt.%) (Baroi and Dalai, 2013; Canakci and Van Gerpen, 1999). However, if the catalyst is thermally unstable, catalytic activity

increases up to the temperature of the catalyst stability, beyond which the activity drops because of the loss of active sites (Melero et al., 2010; Alba-Rubio et al., 2010).

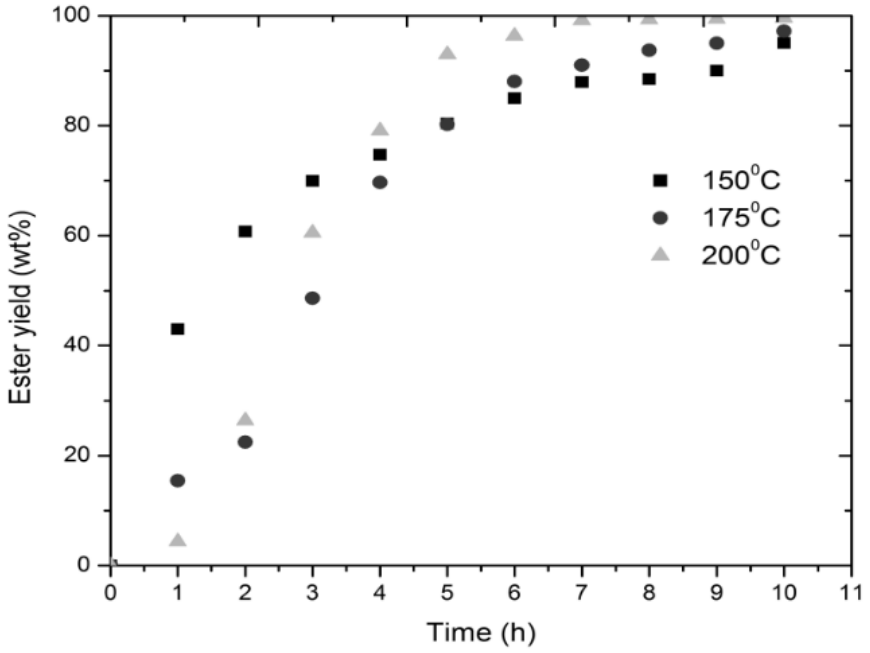

Fig. 6.14 Effect of reaction temperature (55% TPA loading, 3wt% catalyst, 20:1 methanol to GSC oil molar ratio, 4.14 MPa and 10 h)

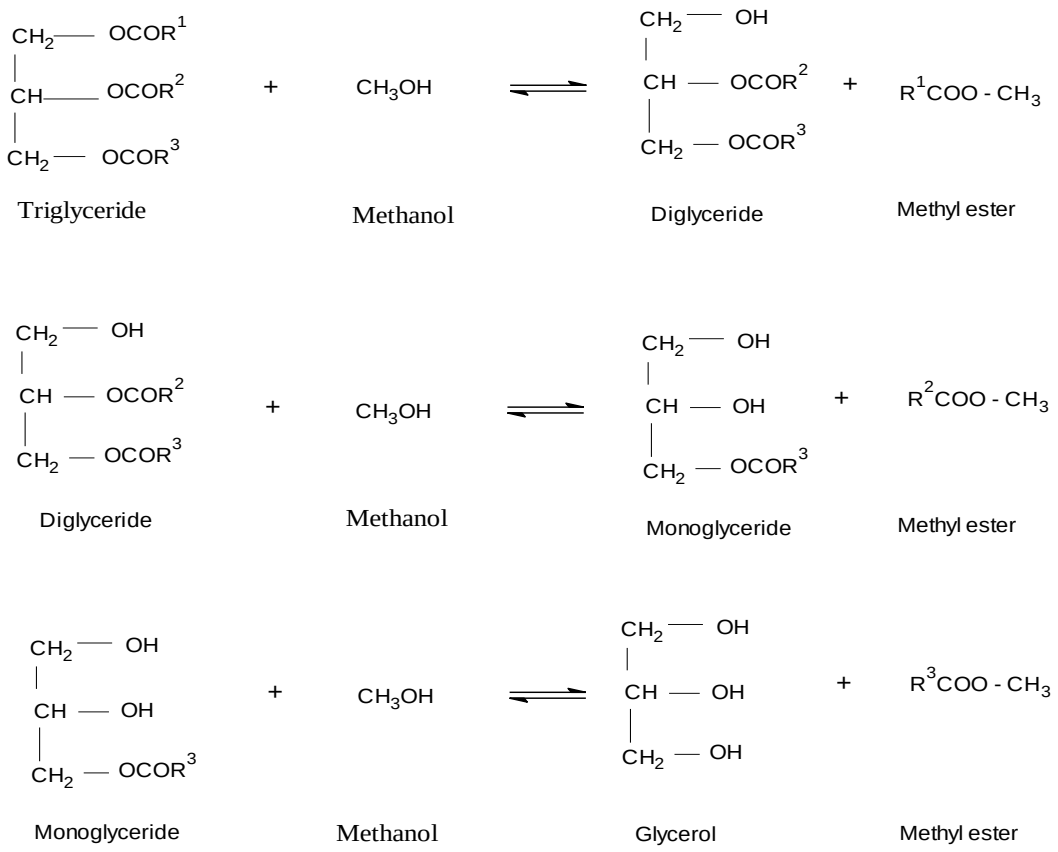

Fig. 6.15 Detailed steps of the transesterification reaction

To understand the effects of other reaction parameters at constant temperature of 200°C, the catalyst weight was varied from 0 to 6 wt%, the methanol to GSC oil molar ratio from 10:1 to 30:1 and reaction time from 4 to 10 h. A three-factor two level design was used to perform the experiments. Figures 6.16, 6.17 and 6.18 show the effects of methanol to oil molar ratio, catalyst wt% and reaction time on the ester yield (wt %). These figures show the optimum region of parameter combinations for obtaining the highest ester yield. Figure 6.16 shows that beyond 4 wt.% catalysts, the ester yield decreases. Exces catalysts concentration provides excess acid sites and therefore promotes the reation rate fatster. As a result, glycerol and water form very fast and may deactivate the catalysts may cause lower yield (Lin et al., 2013). From the experiments, a second-order polynomial equation is developed to fit the experimental data.

Ester yield (wt%) = -83.69 + 36.27× Catalyst wt% + 1.75× Methanol ratio + 22.26 × Time (h) - 4.48× Catalyst wt%^{2} - 0.05× Methanol to oil molar ratio^2 - 1.08× Time (h)^2 …(6.7)

From the above model, both linear and quadratic terms of cat. wt%, methanol to GSC oil molar ratio and reaction time are found to be the significant ($p<0.05$) factors.

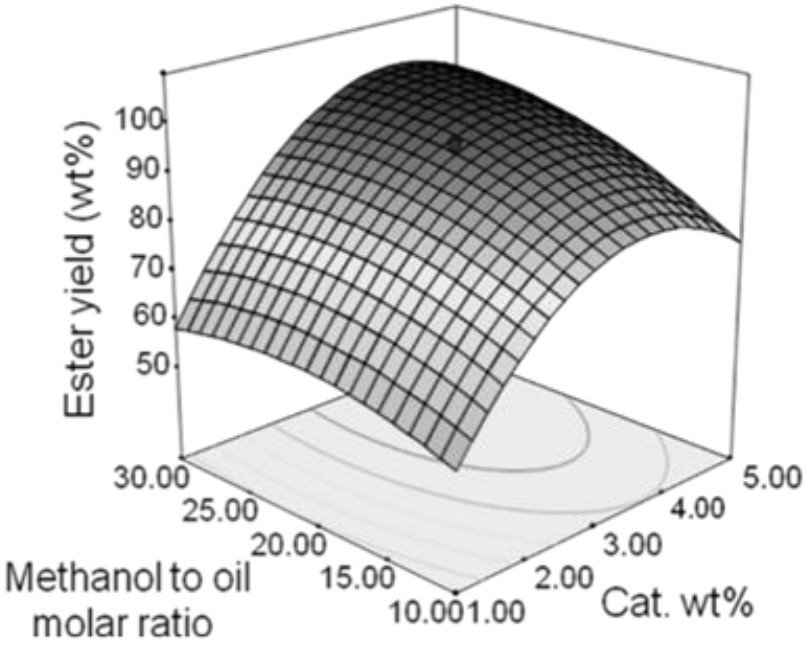

Fig. 6.16 Effect of catalyst wt.% and methanol ratio on ester yield%

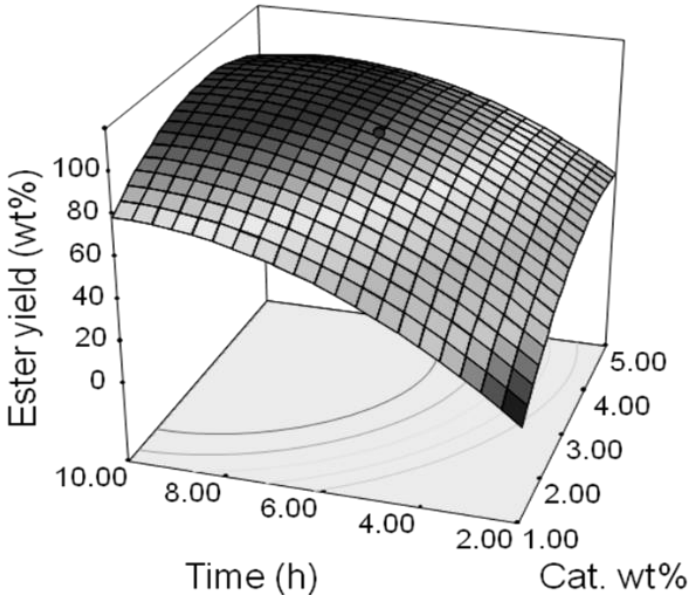

Fig. 6.17 Effect of catalyst wt.% and reaction time on ester yield%

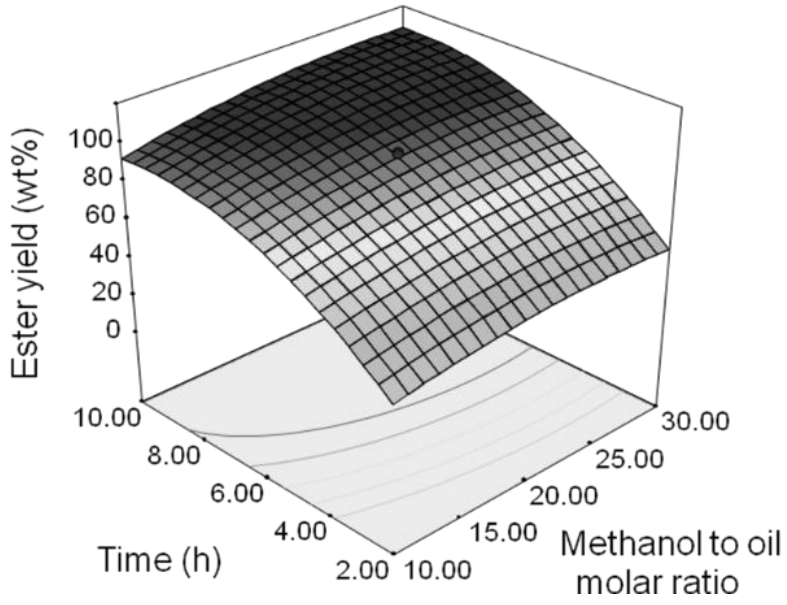

Fig. 6.18 Effect of methanol to GSC oil molar ratio and reaction time on ester yield%

Figure 6.19 depicts the Perturbation plot, which signifies the effect of individual reaction parameter on ester yield (wt %), keeping the other parameters constant, using the same design range. It depicts that ester yield (wt.%) increases with the increase in the catalyst wt% up to a certain limit, then decreases. It also depicts that ester yield (wt. %) increases with the reaction time. The ester yield (wt%) is found to be same after increasing the methanol to GSC oil molar ratio to a certain limit, which implies that the reaction mixture was not affected by the solubility of the glycerol (Baroi and Dalai, 2013). From this study, 3.3 wt% catalyst (based on GSC oil) and 21.3:1 methanol to GSC oil molar ratio and reaction time of 6.5 h are found to be one of the optimum reaction conditions. The predicted yield using the condition is 100 wt% and the actual yield is 99.3 wt%, which validates the model well (see eqn 6.7). The 6.5 h reaction time required to reach 99.3% ester yield can be explained with the help of the transesterification reaction chemistry. Transesterification is an equilibrium reaction and after reaching a certain yield or conversion, the reaction becomes slow (Boocock et al., 1998); which is also evident from Fig. 6.14.

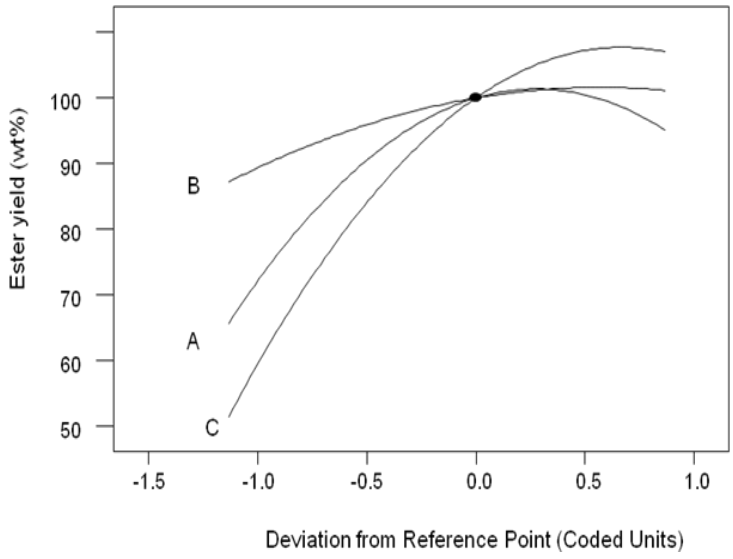

Fig. 6.19 Perturbation plot of the reaction parameters on esters yield.
(A) Catalyst wt%, (B) Methanol to oil molar ratio and (C) reaction period, h

6.4.5 Reusability of the catalysts in the transesterification reaction

For the catalyst reusability study, the catalyst was separated from the reaction mixture and was washed with methanol. It was then dried and finally regenerated by calcination, to remove the residual organic compounds. The ester yield was reduced from 99.3 wt% in experiment one to 91.4 wt.% in experiment three indicating that the catalyst strong acid sites of the catalysts are still active and reusable after at least three reaction cycles.

6.4.6 Catalytic activity in etherification reaction

Table 6.8 depicts the catalytic activity of different loading of TPA in H-β zeolite. It depicts that the conversion of glycerol reaches 100% for 45-65% TPA loading, when the etherification reaction is carried out at 120°C, 1 MPa, 1:5 molar ratio (glycerol: TBA) and 800 rpm for 5 hours. However, 55% TPA loading on H-β produces highest yields of (DTBG+TTBG) compared to those for 45% and 65% TPA loadings. Both the acid site strength and the porosity or pore volume limitation affect the catalytic activity (Melero et al., 2012). A 55% TPA loading on H-β has an optimum combination of acid site strength and porosity compared to those of 45%

and 65% TPA loadings (Table 6.2 and Fig. 6.11) is responsible to obtain the highest combined yield of DTBG and TTBG.

Table 6.8: Effect of TPA loading on etherification reaction (2.5 (w/v)% catalyst, 120°C, 1 MPa, 1:5 molar ratio (glycerol: TBA) and 800 rpm for 5 h)

TPA loading on H-β zeolite (wt%)	Conversion of glycerol (%)	Yield of MTBG (wt%)	Yield of DTBG (wt%)	Yield of TTBG (wt%)	Yield of (DTBG+TTBG) (wt%)
45	100	31.1	40.6	28.3	68.9
55	100	7.9	13.5	78.6	92.1
65	100	23.1	4.6	72.3	76.9

Table 6.9 depicts the effects of catalyst loading on etherification reaction. It depicts that glycerol conversion and yield of (DTBG+TTBG) increase from 1.5 to 2.5 (w/v)% catalyst loading, and above 2.5 (w/v)% both glycerol conversion and combined yield of DTBG and TTBG decrease. It implies that above 2.5 (w/v)% catalyst loading, secondary reactions becomes dominant, as excessive catalyst loading can catalyze dehydration of TBA to isobutylene, etherification of isobutylene to di-isobutylene (DIB) - precursors of gummy products and oligomerization reaction to produce gummy products instead of etherification of glycerol (Da Silva et al., 2009; Frusteri et al., 2012).

Table 6.9: Effect of catalyst loading on etherification reaction (55% TPA/H- β, 120°C, 1 MPa, 1:5 molar ratio (glycerol: TBA) and 800 rpm for 5 h)

Catalyst Loading (w/v)%	Conversion of glycerol (%)	Yield of MTBG (wt%)	Yield of DTBG (wt%)	Yield of TTBG (wt%)	Yield of (DTBG+TTBG) (wt%)
1.5	98.1	45.4	52.6	0.1	52.7
2.5	100	7.9	13.5	78.6	92.1
3.5	86.7	27.5	26.1	43.1	69.2

Table 6.10 depicts the reaction temperature effects on the etherification reaction. It depicts that glycerol conversion increases with the increase in reaction temperature up to 120°C, above which the conversion remains the same. However, above 120°C reaction temperature, the combined yield of DTBG and TTBG drops, as the de-etherification reaction of the product ethers becomes important at high temperature (Frusteri et al., 2012).

Table 6.10: Effect of reaction temperature (2.5 (w/v)% catalyst, 55% TPA/H- β, 1 MPa, 1:5 molar ratio (glycerol: TBA) and 800 rpm for 5 h)

Reaction Temperature °C	Conversion of glycerol (%)	Yield of MTBG (wt%)	Yield of DTBG (wt%)	Yield of TTBG (wt%)	Yield of (DTBG+TTBG) (wt%)
90	84.5	64.6	3.6	16.3	19.9
120	100	7.9	13.5	78.6	92.1
180	100	26.3	39.9	33.8	73.7

Table 6.11 depicts the effect of glycerol to TBA molar ratio on the etherification reaction. It depicts that both the glycerol conversion and yield of (DTBG+TTBG) increase with the increase of the molar ratio up to 1:5, beyond which both the conversion and combined yield of DTBG and TTBG decrease. Excess concentration of *tert*-butanol favors oligomerization reaction to form di-isobutylene, which might lessen the conversion and yield (Liao et al., 2012).

Table 6.11: Effect of Glycerol to TBA molar ratio (2.5 (w/v)% catalyst, 55% TPA/H- β, 1 MPa, 120°C and 800 rpm for 5 h)

Glycerol: TBA ratio	Conversion of glycerol (%)	Yield of MTBG (wt%)	Yield of DTBG (wt%)	Yield of TTBG (wt%)	Yield of (DTBG+TTBG) (wt%)
1:4	96.7	53.1	6.7	36.9	43.6
1:5	100	7.9	13.5	78.6	92.1
1:6	95.8	60.1	5.6	30.2	35.7

The catalyst reusability study was also carried out for etherification reaction. The best-performed catalyst was regenerated using a similar method as in for the transesterification reaction. After three consecutive runs, there was only 2% drop in the conversion of the glycerol.

6.4.7 Development of the kinetic model of the transesterification and etherification

The optimized reaction conditions were exploited to develop the kinetic model of simultaneous transesterification and esterification of GSC oil. At first, simple power law model was exploited calculating the apparent activation energy (Ea) and apparent equilibrium constants (K). The overall reaction was:

$$\text{Oil} + 3\text{MeOH} = 3\text{FAME} + \text{Glycerol} \quad \ldots(6.8)$$

The reaction model form was as follows:

$$-r_{oil} = k_1 C_{oil}^{\alpha} - k_2 C_{FAME}^{\beta} \quad \ldots(6.9)$$

From the power law model, it is observed that the apparent reaction rate constant, equilibrium constant and the reaction order increases with the reaction temperature and is an endothermic reaction (Table 6.12). The fractional reaction order indicates that the overall reaction involves several intermediate reaction steps (DG, MG formation) and the increase in reaction order with temperature indicates that the reaction was in heterogeneous phase (Atkins and De Paula, 2006). The obtained activation energy using the model is 82.5 kJ/mole (Table 6.12).

Table 6.12: Reaction rate constant, equilibrium constant and activation energy of simultaneous esterification and transesterification of GSC oil

Reaction Temperature (°C)	Forward Reaction order (α)	Forward Reaction rate constant k_1	Backward Reaction order (β)	Backward Reaction rate constant k_2	Equilibrium constant (K)	R^2 of fitting	Activation Energy (E_a) kJ/mol	R^2 of fitting
180	0.98	0.02	1.04	0.008	3.25	0.99		
190	0.97	0.03	0.92	0.01	3.33	0.91	82.5	0.85
200	1.6	0.07	2.34	0.019	3.47	0.96		

To understand the simultaneous esterification and transesterification of GSC oil reaction mechanism, severalEley-Rideal (E-R) models was developed using the optimum reaction condition. The following model is obtained after fitting the experimental data:

It is assumed through the mechanism that methanol (MeOH) are weakly adsorbed or not adsorbed on the catalyst. Adsorption of triglycerides (TG) on a vacant site is given by

$$\mathrm{r_{AD_{FFA}}} = \mathrm{FFA + S \Leftrightarrow FFA.S} \quad \ldots(6.10)$$

$$\mathrm{r_{S_{FFA}}} = FFA.S + MeOH \Leftrightarrow FAME.S + H_2O \quad \ldots(6.11)$$

$$r_{\mathrm{AD_{TG}}} = \mathrm{TG + S \Leftrightarrow TG.S} \quad \ldots(6.12)$$

$$r_{\mathrm{S_{TG}}} = TG.S + MeOH \Leftrightarrow FAME.S + DG \quad \ldots(6.13)$$

$$r_{\mathrm{AD_{DG}}} = \mathrm{DG + S \Leftrightarrow DG.S} \quad \ldots(6.14)$$

$$r_{\mathrm{S_{DG}}} = DG.S + MeOH \Leftrightarrow FAME.S + MG \quad \ldots(6.15)$$

$$r_{\mathrm{AD_{MG}}} = \mathrm{MG + S \Leftrightarrow MG.S} \quad \ldots(6.16)$$

$$r_{\mathrm{S_{MG}}} = MG.S + MeOH \Leftrightarrow FAME.S + Glycerol \quad \ldots(6.17)$$

$$r_{\mathrm{D_{FAME}}} = \mathrm{FAME.S \Leftrightarrow FAME + S} \quad \ldots(6.18)$$

At steady-state,

$$r_{AD_{FFA}} = r_{S_{FFA}} = r_{AD_{TG}} = r_{S_{TG}} = r_{AD_{DG}} = r_{S_{DG}} = r_{AD_{MG}} = r_{S_{MG}} = r_{D_{FAME}} = -r'_{oil}$$

If surface reaction of TG (eqn. 6.13) is the rate limiting,

$$-r'_{oil} \approx r_{S_{TG}} = k\mathrm{C_{TG.S}.C_{MEOH}} - k_{\_1}\mathrm{C_{DG}.C_{FAME.S}}$$

$$-r'_{oil} \approx r_{S_{TG}} = k\left(\mathrm{C_{TG.S}.C_{MEOH}} - \frac{\mathrm{C_{DG}.C_{FAME.S}}}{\mathrm{K}}\right) \quad \ldots(6.19)$$

From eqn. (6.10),

$$\mathrm{r_{AD_{FFA}}} = \mathrm{k_{AD_{FFA}}}\left(\mathrm{C_{FFA}.C_S} - \frac{\mathrm{C_{FFA.S}}}{\mathrm{K_{AD_{FFA}}}}\right) \quad \ldots(6.20)$$

At equilibrium, $\frac{\mathrm{r_{AD_{FFA}}}}{\mathrm{k_{AD_{FFA}}}} \approx 0 \Longrightarrow \mathrm{C_{FFA.S}} = \mathrm{K_{AD_{FFA}}C_{FFA}.C_S}$

Similarly, $\mathrm{C_{TG.S}} = \mathrm{K_{AD_{TG}}.C_{TG}.C_S}$; $\mathrm{C_{DG.S}} = \mathrm{K_{AD_{DG}}.C_{DG}.C_S}$; $\mathrm{C_{MG.S}} = \mathrm{K_{AD_{MG}}.C_{MG}.C_S}$;

$$\mathrm{C_{FAME.S}} = \mathrm{K_{D_{FAME}}.C_{FAME}.C_S}$$

Then eqn. (6.19) can be written as,

$$-r'_{oil} \approx r_{S_{TG}} = k\left(\mathrm{K_{AD_{TG}}}.\mathrm{C_{TG}}.\mathrm{C_S}.\mathrm{C_{MEOH}} - \frac{\mathrm{C_{DG}}.\mathrm{K_{D_{FAME}}}.\mathrm{C_{FAME}}.\mathrm{C_S}}{\mathrm{K}}\right) \quad \ldots(6.21)$$

$$-r'_{oil} \approx r_{S_{TG}} = k.\mathrm{K_{AD_{TG}}}.\mathrm{C_S}\left(\mathrm{C_{TG}}.\mathrm{C_{MEOH}} - \frac{\mathrm{C_{DG}}.\mathrm{K_{D_{FAME}}}.\mathrm{C_{FAME}}}{\mathrm{K}.\mathrm{K_{AD_{TG}}}}\right)$$

From acid site balance,

$$\mathrm{C}_t = \mathrm{C_S} + \mathrm{C_{FFA.S}} + \mathrm{C_{TG.S}} + \mathrm{C_{DG.S}} + \mathrm{C_{MG.S}} + \mathrm{C_{FAME.S}}$$

$$\mathrm{C}_t = \mathrm{C_S}(1 + \mathrm{K_{AD_{FFA}}}.\mathrm{C_{FFA}} + \mathrm{K_{AD_{TG}}}.\mathrm{C_{TG}} + \mathrm{K_{AD_{DG}}}.\mathrm{C_{DG}} + \mathrm{K_{AD_{MG}}}.\mathrm{C_{MG}} + \mathrm{K_{D_{FAME}}}.\mathrm{C_{FAME}})$$

$$\mathrm{C_S} = \frac{\mathrm{C}_t}{(1 + \mathrm{K_{AD_{FFA}}}.\mathrm{C_{FFA}} + \mathrm{K_{AD_{TG}}}.\mathrm{C_{TG}} + \mathrm{K_{AD_{DG}}}.\mathrm{C_{DG}} + \mathrm{K_{AD_{MG}}}.\mathrm{C_{MG}} + \mathrm{K_{D_{FAME}}}.\mathrm{C_{FAME}})}$$

Placing into equation (6.21),

$$-r'_{oil} \approx r_{S_{TG}} = \frac{k.\mathrm{K_{AD_{TG}}}.\mathrm{C_t}\left(\mathrm{C_{TG}}.\mathrm{C_{MEOH}} - \frac{\mathrm{C_{DG}}.\mathrm{K_{D_{FAME}}}.\mathrm{C_{FAME}}}{\mathrm{K}.\mathrm{K_{AD_{TG}}}}\right)}{(1 + \mathrm{K_{AD_{FFA}}}.\mathrm{C_{FFA}} + \mathrm{K_{AD_{TG}}}.\mathrm{C_{TG}} + \mathrm{K_{AD_{DG}}}.\mathrm{C_{DG}} + \mathrm{K_{AD_{MG}}}.\mathrm{C_{MG}} + \mathrm{K_{D_{FAME}}}.\mathrm{C_{FAME}})}$$

$$-r'_{oil} \approx r_{S_{TG}} = \frac{k'\left(\mathrm{C_{TG}}.\mathrm{C_{MEOH}} - \frac{\mathrm{C_{DG}}.\mathrm{K_{D_{FAME}}}.\mathrm{C_{FAME}}}{\mathrm{K}.\mathrm{K_{AD_{TG}}}}\right)}{(1+\mathrm{K_{AD_{FFA}}}.\mathrm{C_{FFA}}+\mathrm{K_{AD_{TG}}}.\mathrm{C_{TG}}+\mathrm{K_{AD_{DG}}}.\mathrm{C_{DG}}+\mathrm{K_{AD_{MG}}}.\mathrm{C_{MG}}+\mathrm{K_{D_{FAME}}}.\mathrm{C_{FAME}})} \quad \ldots(6.22)$$

`

Neglecting reverse reaction,

$$-r'_{oil} \approx r_{S_{TG}} = \frac{k'.\mathrm{C_{TG}}.\mathrm{C_{MEOH}}}{(1+\mathrm{K_{AD_{FFA}}}.\mathrm{C_{FFA}}+\mathrm{K_{AD_{TG}}}.\mathrm{C_{TG}}+\mathrm{K_{AD_{DG}}}.\mathrm{C_{DG}}+\mathrm{K_{AD_{MG}}}.\mathrm{C_{MG}}+\mathrm{K_{D_{FAME}}}.\mathrm{C_{FAME}})} \quad \ldots(6.23)$$

Similarly, if adsorption of TG is the rate limiting step, then

$$-r'_{oil} \approx r_{AD_{TG}} = \frac{k'.\mathrm{C_{TG}}}{(1+\mathrm{K_{AD_{FFA}}}.\mathrm{C_{FFA}}+\mathrm{K_{AD_{TG}}}.\mathrm{C_{TG}}+\mathrm{K_{AD_{DG}}}.\mathrm{C_{DG}}+\mathrm{K_{AD_{MG}}}.\mathrm{C_{MG}}+\mathrm{K_{D_{FAME}}}.\mathrm{C_{FAME}})} \quad \ldots(6.24)$$

From eqn. (6.23) and (6.24), if the adsorption co-efficients are very small

$$-r'_{oil} \approx r_{S_{TG}} = k'.\mathrm{C_{TG}}.\mathrm{C_{MEOH}} \quad \ldots(6.25)$$

$$-r'_{oil} \approx r_{AD_{TG}} = k'.\mathrm{C_{TG}} \quad \ldots(6.26)$$

After data-fitting using the above equations,

From eqn. (6.22)

$$-r'_{oil} \approx r_{S_{TG}} = \frac{0.0009\left(C_{TG}.C_{MEOH} - \frac{35.C_{DG}.C_{FAME}}{45\times-1.24\times10^{7}}\right)}{(1 + C_{FFA} + 45C_{TG} + 195C_{DG} + 71C_{MG} + 35C_{FAME})}$$

R^2=0.96; R_{adj}^2 =0.91

From eqn. (6.23)

$$-r'_{oil} \approx r_{S_{TG}} = \frac{0.01C_{TG}C_{MeOH}}{(1+1241C_{TG}+1358C_{FAME}+3426C_{DG}+1.03\times10^{4}C_{MG}+5432C_{FFA})} \quad \ldots(6.27)$$

R^2=0.99; R_{adj}^2 =0.98

From eqn. (6.24)

$$-r'_{oil} \approx r_{S_{TG}}$$

$$= \frac{0.01C_{TG}}{(1 + 1412C_{TG} + 1952C_{FAME} + 2425C_{DG} + 1.03 \times 10^{4}C_{MG} + 1.12 \times 10^{4}C_{FFA})}$$

R^2=0.98; R_{adj}^2 =0.97

From eqn. (6.25)

$$-r'_{oil} \approx r_{S_{TG}} = 0.0005C_{TG}.C_{MEOH}$$

R^2=0.95; R_{adj}^2 =0.95

From eqn. (6.26)

$$-r'_{oil} \approx r_{S_{TG}} = 0.0003C_{TG}$$

R^2=0.95; R_{adj}^2 =0.95

Based on the statistical data-fitting and co-efficient values, eqn (6.23) is found to be the best model, where TG to DG conversion (1st step of transesterification) is the rate-limiting step.

The optimized reaction condition was exploited to develop a kinetic model for etherification of glycerol. In this reaction, glycerol (G) and TBA (T) react to produce MTBG (M) and water (W). Adsorption of glycerol (G) and TBA (T) on vacant site is given by

$$G + S \overset{K_G}{\Leftrightarrow} G.S \quad \ldots(6.28)$$

$$T + S \overset{K_T}{\Leftrightarrow} T.S \quad \ldots(6.29)$$

Surface reaction of glycerol (G) and TBA (T) leads to

$$G.S + T.S \overset{K_s}{\Leftrightarrow} M.S + W.S \quad \ldots(6.30)$$

Desorption of MTGE (M) and Water (W) are given by

$$M.S \overset{K'_M}{\Leftrightarrow} M + S \quad \ldots(6.31)$$

$$W.S \overset{K'_W}{\Leftrightarrow} W + S \quad \ldots(6.32)$$

If the surface reaction (6.26) controls the rate of reaction, then the rate of reaction of glycerol is given by

$$-r_S = k_S C_{G.S} C_{T.S} - \overline{k_S} C_{M.S} C_{W.S} \quad \ldots(6.33)$$

$$-r_S = \frac{k_S C_t^2 (K_G K_T C_G C_T - \frac{K_M K_W C_M C_W}{K_S})}{(1 + K_G C_G + K_T C_T + K_M C_M + K_W C_W)^2} \quad \ldots(6.34)$$

The reaction is far away from equilibrium, as initial rate data were used. Thus, reverse reaction cane be neglected (Yadav et al., 2012)

$$-r_S = \frac{k_S K_T K_G C_t^2 C_G C_T}{(1 + K_G C_G + K_T C_T + K_M C_M + K_W C_W)^2} \quad \ldots(6.35)$$

Assuming the adsorption constants are very small (Yadav et al., 2012), then the above equation reduces to

$$-r_S = k_S K_T K_G C_t^2 C_G C_T$$

Where, $C_t = k_t w$; w=catalyst wt.

$$-r_S = k_S (k_t w)^2 C_G C_T K_T K_G \quad \ldots(6.36)$$

$$-\frac{dC_G}{dt} = -r_S = k_{Ether} w^2 C_G C_T \quad \ldots(6.37)$$

Where $k_{Ether} = k_t^2 . k_s . K_T . K_W$; The above equation can be written in terms of fractional conversion as,

$$\frac{dX_G}{(1 - X_G)(M - X_G)} = k_{Ether} w^2 \, C_{G0} t \quad \ldots(6.38)$$

Where, M is the molar ratio of TBA to glycerol. By integrating the above equation,

$$\ln \frac{(M - X_G)}{M(1 - X_G)} = (M - 1) k_{Ether} w^2 \, C_{G0} t \quad \ldots(6.39)$$

This is an expression of a second-order reaction. Thus a plot of $\ln \frac{(M - X_G)}{M(1 - X_G)}$ vs t at different temperatures gave the values of the reaction rate constants at different temperatures (Table 6.13). The activation energy using the reaction rate constants is 71.3 kJ/mol (Table 6.13).

Table 6.13: Reaction rate constant, equilibrium constant and activation energy of etherification of biodiesel derived glycerol

Reaction Temperature (°C)	Reaction order	Reaction rate constant $k_{Ether}.w^2$ (L/mol).s^{-1}	Activation Energy (E_a) kJ/mol	R^2 of fitting
90	2	3.33×10^{-4}		
100	2	5×10^{-4}	71.3	0.95
120	2	1.1×10^{-3}		

6.4.8 Comparison of biodiesel and combined biofuelproperties

The quality and properties, such as cloud point, cloud point and lubricity (wear and scare μm) of the produced combined biofueland biodiesel were measured according to ASTM D6751 standards. Table 6.14 depicts the comparison of the properties. It depicts that the properties of

the produced biodiesel are close and the combined biofuelproperties are better than those reported by ASTM standards.

Table 6.14: Comparison of the properties of biodiesel and combined biofuelmeasured to those of ASTM standard

Properties	Biodiesel	Biofuel	Biodiesel ASTM standard
Cloud point (°C)	-2	-10	-2
Pour point (°C)	-15	-19	-15
Lubricity (HFRR, μm)	210	≈ 0	314

6.5 Conclusions

From the study, TPA impregnated H-Y zeolite showed higher catalytic activity for esterification, and TPA impregnated H-β zeolite showed higher catalytic activity for the transesterification reaction as compared to other catalysts. A 55% TPA/H-β showed optimum catalytic activity for both esterification and transesterification. This 55% TPA/H-β is proved to be an efficient catalyst producing high-quality biodiesel from green seed canola oil through simultaneous esterification and transesterification reaction. This catalyst is also proved to be an effective catalyst for etherification of glycerol, which enables to use the same catalyst for transesterification of GSC oil and etherification of GSC oil derived the glycerol thereafter. The combined biofuel from green seed canola (GSC) oil depicts better fuel properties compared to those of pure GSC biodiesel and ASTM biodiesel standards.

CHAPTER 7: ESTERIFICATION OF FREE FATTY ACIDS (FFA) OF GREEN SEED CANOLA (GSC) OIL USING H-Y ZEOLITE SUPPORTED 12-TUNGSTOPHOSPHORIC ACID (TPA)

A version of this chapter has been published in the following journal:

- Chinmoy Baroi, Ajay K. Dalai.Esterification of free fatty acids (FFA) of Green Seed Canola (GSC) oil using H-Y zeolite supported 12-Tungstophosphoric acid (TPA), Applied Catalysis A, 2014, 485, 99-107.

Contribution of the Ph.D. Candidate

The experiments were conducted by Chinmoy Baroi. The content in this chapter was written by Chinmoy Baroi with discussions and suggestions provided by Dr. Ajay Dalai.

Contribution of this Chapter to the Overall Ph.D. Research

This chapter contains the catalytic activity of H-Y zeolite supported TPA catalysts, synthesized by different methods in esterification of oleic acid and FFA present in GSC oil.

7.1 Abstract

H-Y is one of the most typical and commercially available zeolites. In this research work, the effect of TPA impregnation in H-Y zeolite has been analyzed. The impregnated catalysts have been characterized in details using TGA, BET, ICP-MS, FTIR, XRD, XPS, NH_3-TPD and EXAFS. The catalytic activity of the prepared catalysts has been tested in esterification of pure oleic acids and free fatty acids (FFA) present in the green seed canola (GSC) oil. A 10.2% actual TPA loading in H-Y zeolite showed optimum catalytic activity in oleic acid esterification. The reaction conversion of 99.3 % (for oleic acid) and 97.2% (for FFA) were achieved, when 13.3 wt% catalyst containing 10.2% TPA and 20:1 methanol to FFA molar ratio were used at 120°C and reaction time of 7.5 h. The catalyst is proved to be reusable. Kinetics study depicts that the activation energy of the esterification reaction is 66.3 kJ/mol.

7.2 Introduction

Biodiesel shows higher promise as a diesel substitute fuel due to its renewability, biodegradability and non-toxicity (Lotero et al., 2005). Alkali catalysts are usually used for transesterification of vegetable oils to produce biodiesel (Encinar et al., 1999). However, higher price of biodiesel is the main problem for its commercialization. The higher price is associated with the production cost, and 88% of the total production cost is related to the feedstock price (Kulkarni and Dalai, 2006; Marchetti and Errazu, 2008). This cost can be reduced by using low quality and cheaper feedstocks such as used cooking oil, yellow grease, green seed canola oil, etc.Acid catalyzed esterification reaction with alcohol produces similar type of esters from free fatty acids (Hara, 2010). Homogeneous acid catalysts can be used for this purpose, but solid acid catalysts are favored over those for waste minimization and easy product recovery (Kulkarni et al., 2006). Brønsted acid sites are highly active in the esterification reaction (Di Serio et al., 2008). Heteropoly acids (HPA) made up of heteropoly anions show strong and Brønsted acidity (Devassy and Halligudi, 2005; Busca, 2007; Okuhara et al., 2000). A 12-Tungstophosphoric acid (TPA) with Keggin structure is thermally stable and depicts super acidity as compared to other HPA compounds (Kozhevnikov, 2007). Heteropoly acids have lower surface area (1 – 10 m^2/g) and are soluble in polar solvent (Kulkarni et al. 2006). These problems can be avoided by supporting TPA on various carriers.Previous study depicts that the H-Y zeolite supported 12-Tungstophoisphoric acid (TPA) has higher activity towards esterification as compared to the transesterification reaction (Baroi et al., 2014). Zeolites are microporous materials with specific pore systems. Acid or thermal treatment creates hierarchical pore (meso/micro) systems in the zeolite structure, which might cause loss of zeolite structural Brønsted acidity (Fig.7.1) (Perez-Ramirez et al., 2008; Zheng et al., 2013). In this paper for the first time, the effect of TPA loading on H-Y zeolite has been examined and the catalytic activity has been tested in esterification of fatty acids (e.g. Oleic acid) and free fatty acids (FFA) present in the GSC oil.

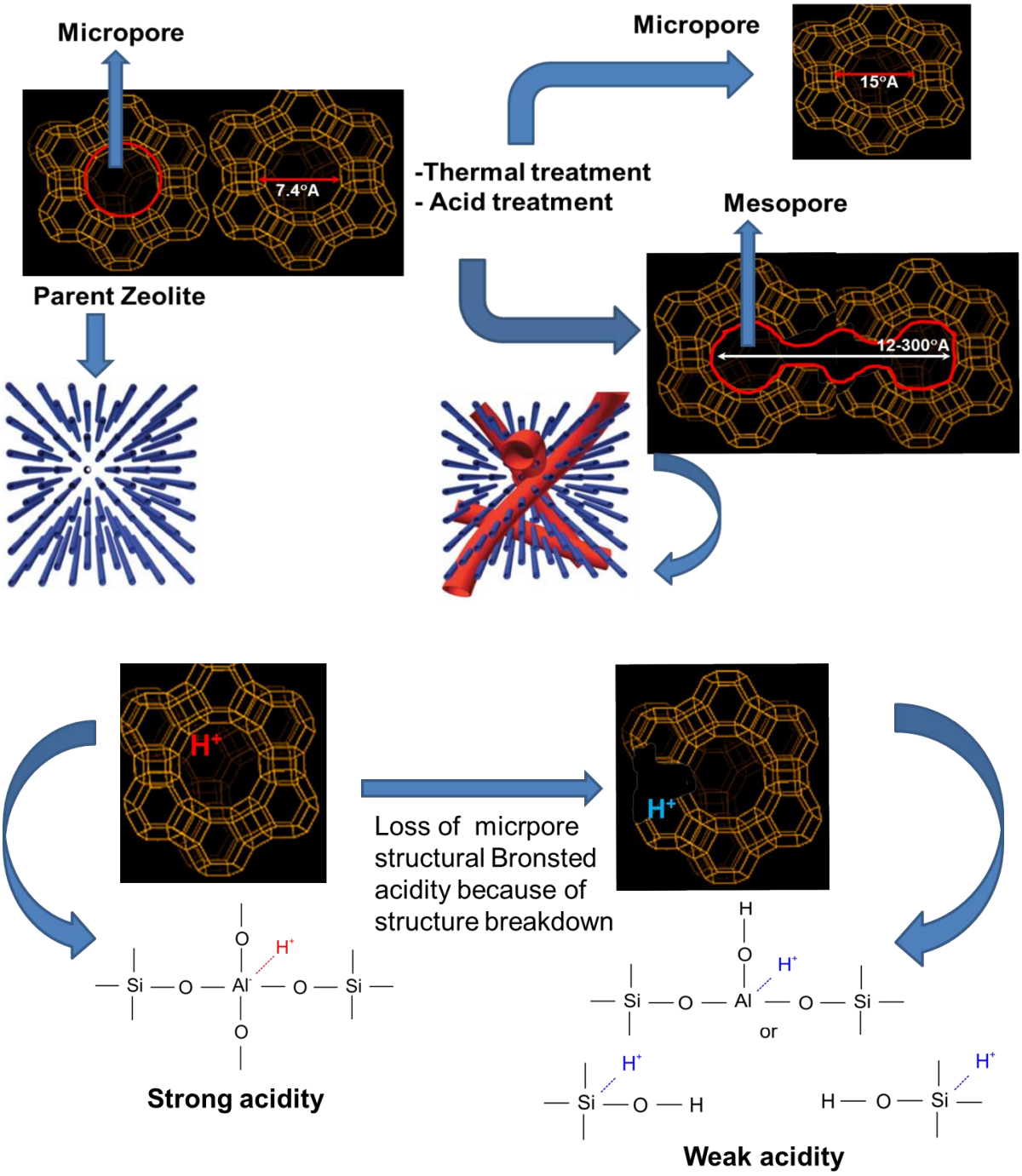

Fig. 7.1 Mespore creation in and loss of acidity in Y zeolite

7.3 Experimental Section

7.3.1 Reagents

Unrefined green seed canola oil (4.25 wt% FFA) was obtained from Milligan Biotech Inc., Foam Lake, Saskatchewan, Canada. Commercial grade NH_4-Y was purchased from ZEOLYST, PA, USA. A 12 - Tungstophosphoric acid (TPA) was purchased from Alfa-Aesar, MA, USA. Oleic acid was purchased from Sigma-Aldrich, Mississauga, Ontario, Canada.

7.3.2 Catalyst preparation

Commercial grade NH_4-Y was calcined at 550°C for 6 h to obtain H-Y form. TPA was impregnated into H-Y following different methods. In method A: calcined H-Y was added into the methanol solution of calculated amount of TPA. Then the solution was dried at 110°C for 12 h. Then the dried solid was washed and filtered with water. Then the solid was dried again at 110°C for 12 h. In method B: all the steps were same as in A except the TPA dissolving solvent was water. In method C, all the steps were same as in A except that TPA washing solvent was methanol. The dried materials were calcined at 250° and 350°C for 6 h. These catalysts were designated as A/B/C-X-T, where A/B/C represents the method name, X represents TPA wt% loading and T represents the calcination temperature in degree Celsius.

7.3.3 Catalyst characterization

Thermo Gravimetric Analyses (TGA) of the prepared catalysts was performed using TGA Q analyzer. The X-ray diffraction (XRD) patterns of the samples were collected on a Bruker D8 Advance diffractometer using Cu $K\alpha$ radiation (λ = 1.5418 A). The synthesized catalystsBET surface area and pore size analysis were performed using Micrometrics adsorption equipment (Model ASAP 2020). The catalysts wereheated at 200°C in a vacuum of 5×10^{-4} atm before the analysis. The surface area was calculated from the isotherms using Brunauer-Emmett-Teller (BET) method. The pore diameter and pore volume was calculated using BJH method from desorption branch of the isotherms. The catalysts FTIR spectra were recorded through Perkin Elmer FTIR spectrum GX equipment. For the FTIR analysis, sample pallets were prepared by pelleting a well mixed 3 mg of catalyst powder with 200 mg of KBr. The X-ray

photoelectron spectroscopy (XPS) study was carried out at Canadian Light Source. The photon energy used for this study was 235 eV with the total energy resolution of 70 meV. All spectra were collected by Scienta SES100 spectrometer. X-Ray absorption spectra (XAS) were recorded on HXMA beam-line at Canadian Light Source Inc., Saskatoon, Canada, utilizing synchrotron radiation of 5-40 keV and100 mA current. W L_{III} data were recorded both in transmission and fluorescence mode employing a Lytle detector typically over 45 min. For EXAFS analysis, the spectra were extracted by utilizing the cubic spline method and normalized to the edge height. The k^3-weighted EXAFS oscillation was Fourier transformed into r space using ATHENA software. Curve-fitting analysis was performed for the W=O and W-O_{ext}-W with the range between r = 1.0 and 2.0 Å using ARTHEMIS software. Temperature programmed desorption of ammonia (TPD) was conducted using Quantachrome (USA) instrument. In a typical experiment, 200 mg of each sample was pretreated in He (Helium) at 550° C for 1 h. The sample was later cooled to room temperature in flowing He and saturated with 1% NH_3/N_2 (v/v) mixture at a flow rate of 30 mL/min for 120 min. Then the spectra were recorded between 100° C to 750° C, with a temperature ramp of 10 °C /min.

7.3.4 Catalytic activity study

The catalytic activity of the prepared catalysts was tested through esterification of oleic acid and FFA of green seed canola oil. The green seed canola oil was pretreated with K-10 clay to remove the chlorophyll following the procedure described by Issariyakul and Dalai (2010), and there was no change in the FFA content (4.25 wt.%) of the oil after pretreatment. The reactions were conducted in a 450 mL Parr reactor (Parr Instrument Co., ILL, USA). Initially, 100 g of oleic acid/GSC oil was taken into the reactor and preheated to 50°C with a stirring speed at 600 rpm. Catalysts and Methanol were then added to the reactor. Preliminary catalyst screening experiments were carried out using reaction conditions of 65°C, 20:1 methanol to oleic acid molar ratio and 5 wt.% catalyst. Artificial Neural Network (ANN) was used to correlate the catalyst structure properties with the catalytic activity in esterification. Central Composite Design (CCD) was exploited for designing the experiments to analyze the effects of reaction parameters and Response Surface Methodology (RSM) was used to optimize the reaction parameters. Design Expert 8 software was used for these purposes. The acid value of the

produced biodiesel was determined according to the AOCS-D6751 method.The free fatty acid conversion was calculated based on the initial and final acid value according to the equation 7.1.

$$\text{Conversion } \% = \frac{\text{Acid value}_{\text{initial}} - \text{Acid value}_{\text{final}}}{\text{Acid value}_{\text{initial}}} \times 100\% \qquad \ldots(7.1)$$

7.4 Results and discussion

7.4.1 Catalyst characterization

The TGA profile of the prepared catalysts (Fig. 7.2) indicates that the maximum weight loss occurs in the range between 100 - 200°C, indicating loss of the physisorbed and crystal water associated with TPA Keggin structure (Kozhevnikov, 2007; Kozhevnikov, 2009; Uchida et al., 2000). The catalyst prepared following method C contains the least amount of crystal/physisorbed water and thermally more stable than those of methods A and B (Fig. 7.2). The synthesized catalysts textural properties are outlined in Table 7.1.

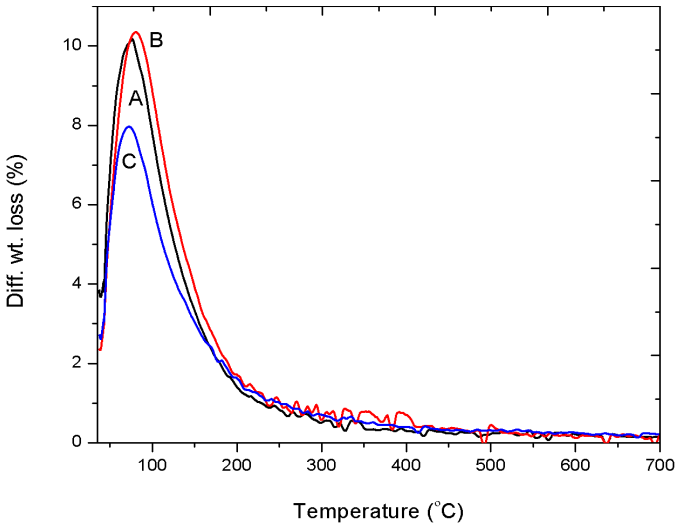

Fig. 7.2 TGA profiles of different catalysts (Cat. A/B/C-25-T)

Table 7.1: Textural property of different catalysts

Sample	TPA Loading (wt%) Actual	Si/Al ratio	BET Surface area (m^2/g)	Pore Volume (cc/g)	Average Pore diameter (nm)	Mesopore Area (m^2/g)	Micropore Area (m^2/g)
H-Y	-	-	910.1±52.6	0.27±.22	6.85±.28	178.9	731.1
Cat.A-25-250	5.6	6.7	863.9	0.25	6.46	159.5	704.4
Cat.B-25-250	4.2	6.6	859.1	0.24	6.68	157.5	701.5
Cat.C-25-250	7.2	6.4	880.1	0.25	6.44	165.64	714.4
Cat.C-25-350	7.2	6.4	742.1	0.23	6.52	133.9	608.2
Cat.C-35-250	9.9	6.4	801.9	0.22	6.45	145.8	655.3
Cat.C-45-250	10.2	6.5	816.8	0.24	6.63	153.5	663.2
Cat.C-55-250	15.4	6.5	780.7	0.19	6.29	139.5	641.3

Increase in TPA loading and micropore surface area improves mesopore area up to a certain range beyond which it decreases (Table 7.1). This indicates that TPA might deposit in mesopores while helping to create it. Increase in TPA loading and pore diameter increase mesopore area up to a certain range and decrease thereafter (Table 7.1). The overall scenario indicates that, while TPA loading creates hierarchal pore (by structural breakdown) in the zeolite structure, it deposits itself at the same time in the pores. Similar result was obtained in a previous study, where impregnation and increase of TPA loading increased mesopore area of support zeolites due to the structural breakdown (Baroi et al., 2014).

Figure 7.3 depicts the XRD patterns of TPA impregnated H-Y zeolite prepared by different methods. It depicts that the characteristic peaks of H-Y zeolite at 15.88°, 18.96°, 20.65° and 23.95° are present upon TPA impregnation, which indicates that the loss of H-Y zeolite crystalline structure is insignificant (Zheng et al., 2011). It also depicts that upon the impregnation, TPA is very well dispersed on H-Y zeolite.

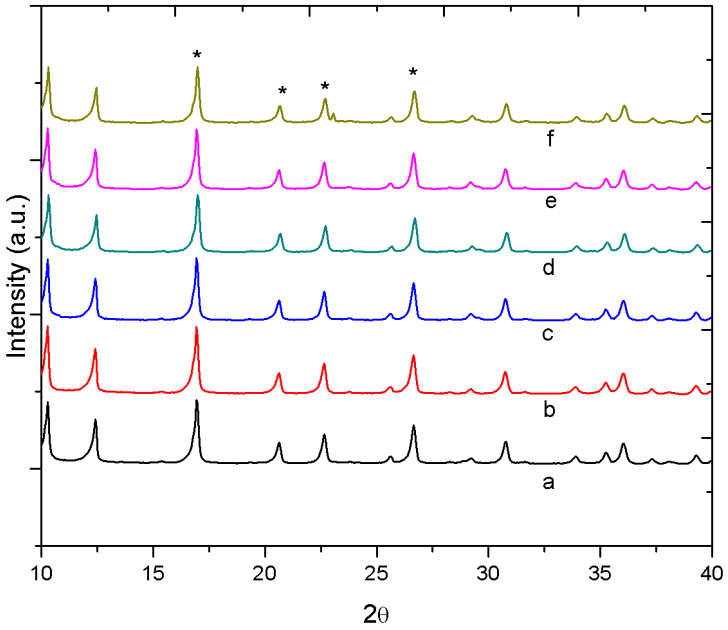

Fig. 7.3 XRD patterns of different catalysts: (a) Cat. A-25, (b) Cat. B-25, (c) Cat. C-25, (d) Cat. C-35, (e) Cat. C-45, (f) Cat. C-55

The IR bands approximately at 1250-950 $cm^{-1}$are referred to the asymmetric stretching vibrations of the tetrahedral Si, Al atoms respectively (Zheng et al., 2011; Li et al., 2010; Morales-Pacheco et al., 2011). Pure TPA depicts IR bands approximately at 1081 (P-O in the central tetrahedron), 976-995 (terminal W=O), 890-900 and 805-810 (W-O-W) cm^{-1} corresponding to asymmetric vibration of the Keggin anion (Tropecelo et al., 2010; Satishkumar et al., 2006; Damyanova et al., 2003; Yun and Kuabara, 2004). After impregnation of TPA (Fig. 7.4) a new weak band at 898 cm^{-1} appears in the spectrum. This is assigned to W–O–W vibrations of the heteropoly acid and no significant change in asymmetric stretching vibrations (at 1206 cm^{-1}) of the tetrahedral Si, Al atoms are observed. The IR band corresponds to the TPA terminal W=O approximately at 989 cm^{-1} and becomes vigilant with the increase in TPA loading (Fig. 7.5).

Tungsten (W) 4f ($4f_{7/2}$ component) binding energy appears at approximately at 35.8 eV for pure TPA. This binding energy shifts to lower energy state for a perturbed tungstate state and to higher energy state (approximately at 37.3 eV) for bulk TPA in presence of water around the Keggin unit of TPA (Lagagneux et al., 2009). For 45% theoretical TPA loading, when the catalyst is calcined at 250°C the TPA kegging structure is present with perturbed tungstate state

(Fig. 7.6). With the increase in TPA loading both bulk and perturbed tungstate states are observed (Fig. 7.7).

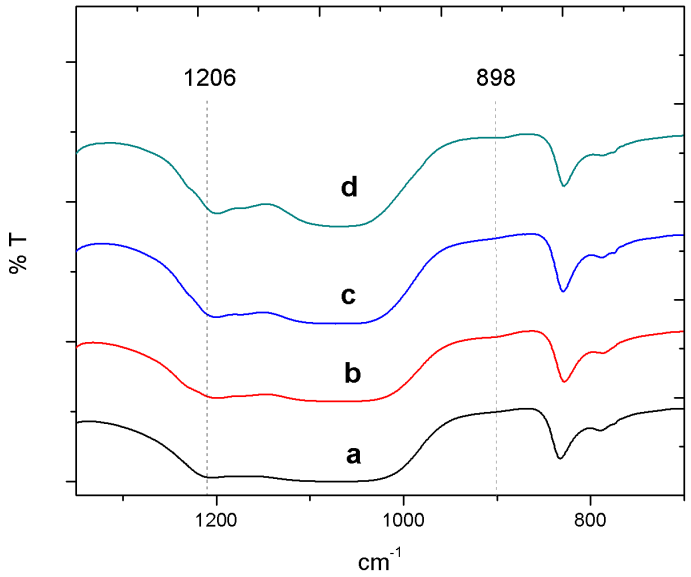

Fig. 7.4 FTIR spectra of different catalysts:(a) H-Y, (b) Cat. A-25, (c) Cat. B-25, (d) Cat. C-25

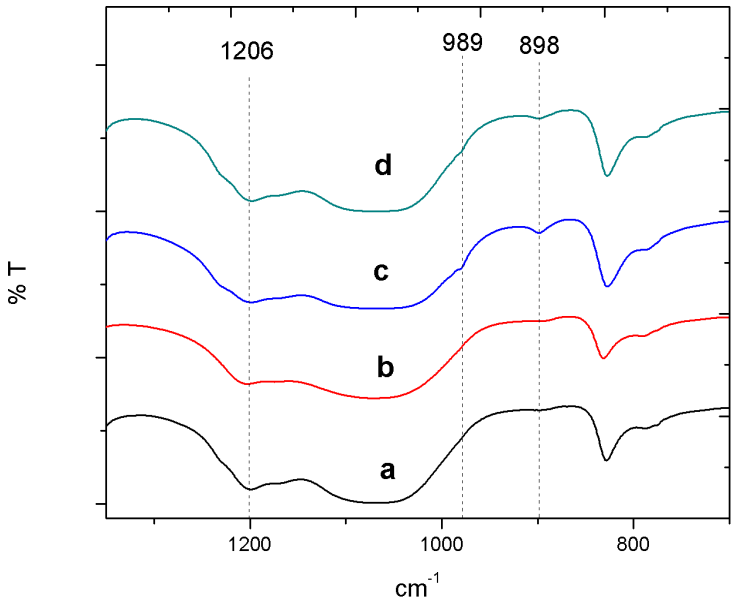

Fig. 7.5 FTIR spectra of different amount of TPA loaded Cat. C: (a) Cat. C-25, (b) Cat. C-35, (c) Cat. C-45, (d) Cat. C-55

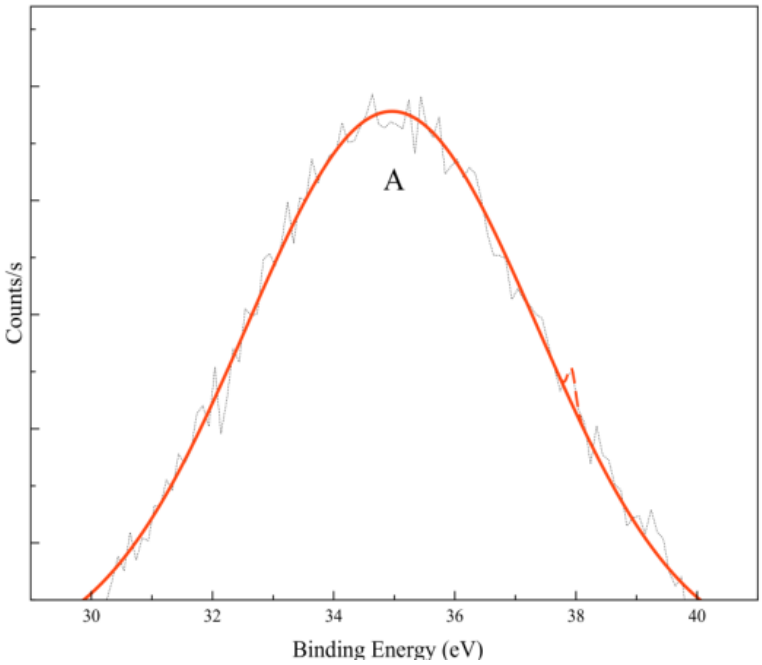

Fig. 7.6 XPS pattern of 45% TPA-Y (A) 34.8 eV

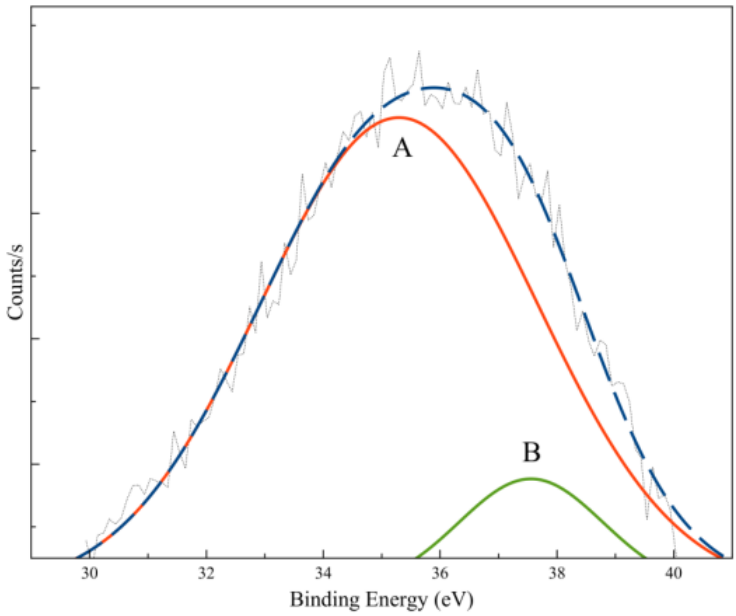

Fig. 7.7 XPS pattern of 55% TPA-Y (A) 34.8 eV, (B) 37.3 eV

The coordination number of W=O and W-O_{ext}-W bonds in TPA, 45%TPA/H-Y, 55%TPA/H-Y are found to be identical (Table 7.2). However, with an increase in TPA loading, the bond length of W=O decreases for 45% TPA loading and increase thereafter and the bond

length of W-O_{ext}-W decreases as compared to pure TPA (Table 7.2). The fitted W L_{III} EXAFS spectra of the 45%TPA/H-Y sample depicted in Fig. 7.8, indicates the corresponding radial distribution functions for this material. The pattern of change in bond length is an indication of distortion in TPA kegging structure with an increase in TPA loading, especially for 55% TPA loading (Yamazoe et al., 2008).

Table 7.2: Structural parameters derived from fitted EXAFS for bulk and supported TPA samples

Samples	Parameters	Coordination environment	
		W=[O]	W-[O_{ext}]-W
Pure TPA	C.N.	1	4
	r (^{0}A)	1.88	1.97
	R-factor	0.008	0.008
45% TPA/H-Y	C.N.	1	4
	r (^{0}A)	1.49	1.89
	R-factor	0.007	0.007
55% TPA/H-Y	C.N.	1	4
	r (^{0}A)	1.93	1.90
	R-factor	0.001	0.04

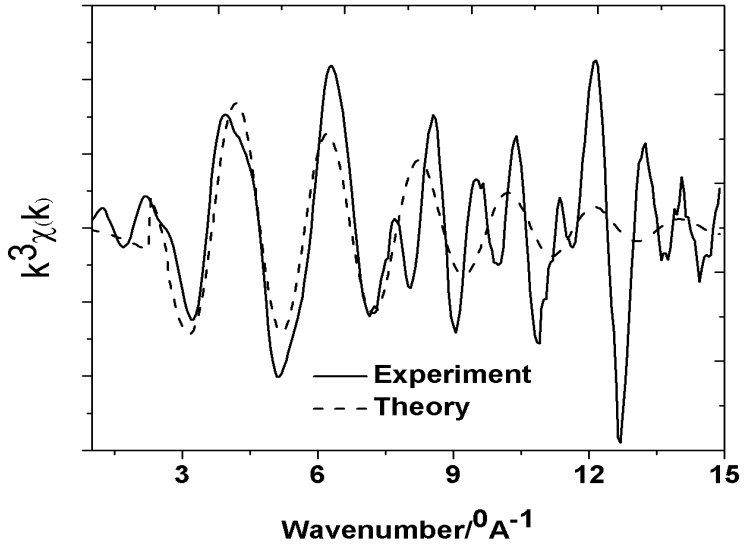

Fig. 7.8 Fitted W L_{III} EXAFS of 55%TPA/H-Y

The NH_3-TPD results of different loadings of TPA on H-Y zeolite (Table 7.3) indicate that the weak acidity decreases with an increase in the loading. However, strong acidity reduces to moderate acidity beyond 45% loading, which is in agreement with the conclusion obtained from the XPS binding energy pattern and distortion of TPA Keggin structure analyzed through EXAFS analysis.

Table 7.3: Acid strength of the catalysts obtained by NH_3-TPD analysis

Samples	Acidity (mmole NH_3/g sample)		
	Weak	Moderate	Strong
H-Y	3.3×10^4	7.6×10^4	-
45% TPA/H-Y	1.3×10^4	4.0×10^4	1.0×10^4
55% TPA/H-Y	1.4×10^4	3.8×10^4	4.5×10^3

7.4.2 Catalytic activity in the esterification reaction

Table 7.4 depicts the catalytic activity of different catalysts. It depicts that 45% TPA (theoretical loading) impregnated H-Y zeolite depicts higher activity for the conversion of oleic acid through esterification.

Table 7.4: Catalytic activity of different catalysts (65°C, 20:1 methanol to oleic acid molar ratio, 5 wt% catalysts, 6 h)

Sample	Conversion %
H-Y	66.7
Cat. A-25-250	68.5
Cat. B-25-250	68.4
Cat. C-25-250	71.7± 1.2
Cat. C-25-350	72.1
Cat. C-35-250	72.3
Cat. C-45-250	77.3
Cat. C-55-250	72.7

To understand the impact of catalyst structural properties on catalytic activity an artificial neural network (ANN) model was developed with the help of STATISTICA 12 software. To analyze the effect of different variable on the esterification and transesterification conversion, Design of Experiments (DOE) was used to vary a pair of variables, keeping other variables constant. Central Composite Design (CCD) was used for this purpose. "Custom Prediction" option of the software was used to obtain the results of the experiments. From the model, micropore area is found to be the least important factor to affect the catalytic activity, then mesopore area and then pore diameter as compared to the loading (wt.%). The catalytic activity increases with the increase in catalyst loading and relatively insensitive with the increase in mesopore surface area of the catalysts, whereas the catalytic activity increases with the increase in pore diameter (Figures 7.9 and 7.10). For 55% (theoretical) TPA loading, the TPA keggin structure exists in a distorted state (Table 7.2), which causes a reduction in surface area, pore diameter (Table 7.1) and acid strength (Table 7.3). These are responsible for lower activity in esterification.

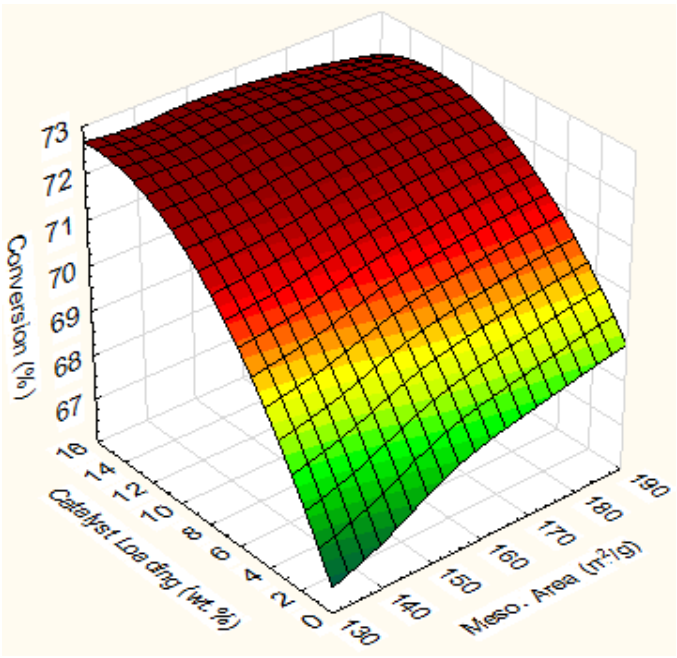

Fig. 7.9 Effects of mesopore area and loading on FFA conversion (6.55 nm pore diameter, 669.65 m^2/g micropore area, Si/Al atio 5.85)

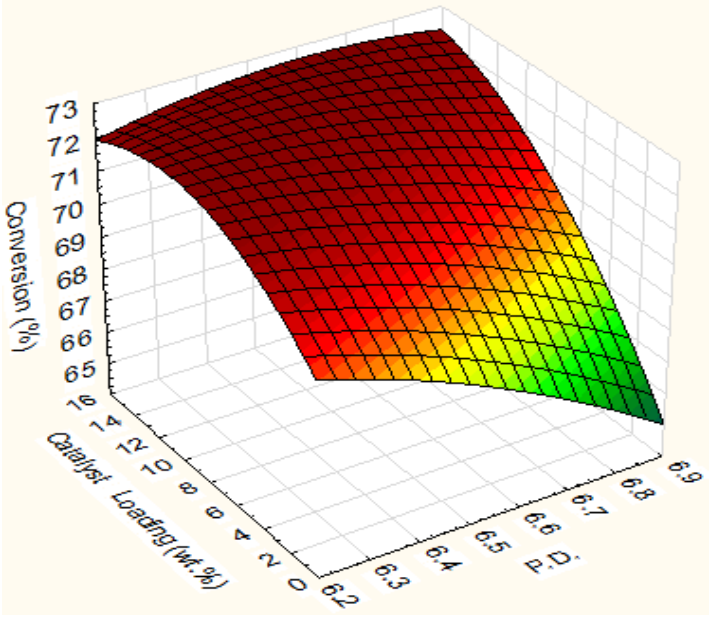

Fig. 7.10 Effects of pore diameter and loading on FFA conversion (669.65 m^2/g micropore area, 156.4 m^2/g mesopore area, Si/Al ratio 5.85)

7.4.3 Effects of reaction parameters in the esterification reaction

From the preliminary experiments, reaction temperature is found to be the most important factor affecting esterification conversion. The effects of reaction temperature on ester conversion was analyzed keeping the catalyst concentration at 5 wt% (based on the wt. of oil), 20:1 methanol to oleic acid molar ratio and 6 h of reaction time. Table 7.5 depicts that conversion increases with the increase in the reaction temperature. Esterification reaction is an endothermic reaction, thus reaction temperature has a positive impact on the FFA conversion (Sathyaselvabala et al., 2012).

Table 7.5: Effect of reaction temperature on the conversion (20:1 methanol to oleic acid molar ratio, 5 wt% catalysts, 6 h)

Reaction Temperature (°C)	Conversion (%)
65	77.3
90	82.7
120	92.7

To understand the effects of other reaction parameters at constant temperature of 120°C, the catalyst weight was varied from 5 to 15 wt%, the methanol to oleic acid molar ratio from 10:1 to 30:1 and reaction time from 2 to 10 h. A three-factor two level design was used to perform the experiments. Figures 7.11, 7.12 and 7.13 show the effects of methanol to oleic acid molar ratio, catalyst wt% and reaction time on the oleic acid conversion. These figures show the optimum region of parameter combinations for obtaining the highest conversion. From the experiments, a second-order polynomial equation is developed to fit the experimental data.

$$\text{Conversion (\%)} = -92.3 + 3.1 \times \text{Catalyst wt\%} + 7.7\times \text{Methanol ratio} + 22.2 \times \text{Time (h)} - 0.06 \times \text{Catalyst wt\%}^2 - 0.1 \times \text{Methanol to oleic acid molar ratio}^2 - 1.11 \times \text{Time (h)}^2 + 0.1 \times \text{Time}\times \text{Cat. wt\%} - 0.3 \times \text{Methanol to oleic acid molar ratio}\times \text{Time} - 0.1 \times \text{Methanol to oleic acid molar ratio} \times \text{Cat. wt\%} \quad \ldots(7.2)$$

From the above model, both linear and quadratic terms of methanol to FFA molar ratio, reaction time and their interaction are found to be the significant ($p<0.05$) factors. From this study, 13.3 wt% catalyst (based on the oleic acid) and 26:1 methanol to oleic acid molar ratio and reaction time of 7.5 h are found to be one of the optimum reaction conditions. The predicted conversion using the condition is 100% and the actual conversion (experimental) is 99.3 wt%, which validates the model well (see eqn. 7.2). Using this optimized condition, the conversion of FFA present in GSC oil obtained is 97.2%.

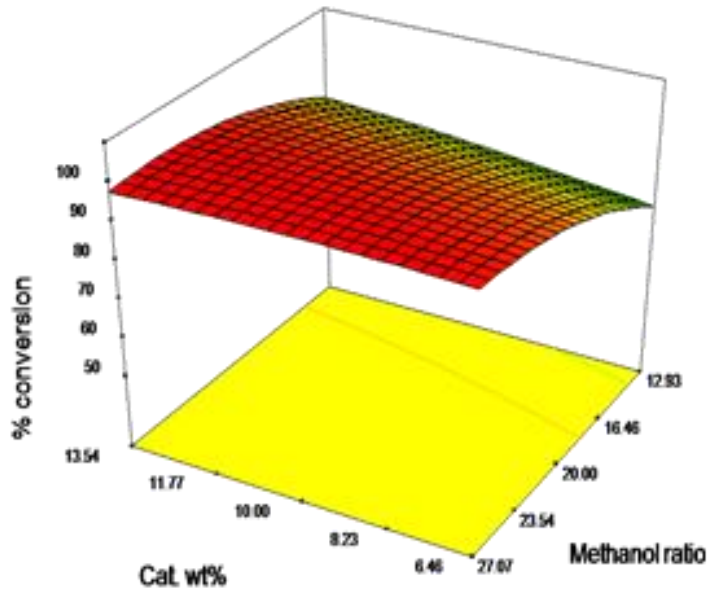

Fig. 7.11 Effects of catalyst wt% and methanol to oleic acid molar ratio on the FFA conversion (reaction temperature 120°C, 6 h)

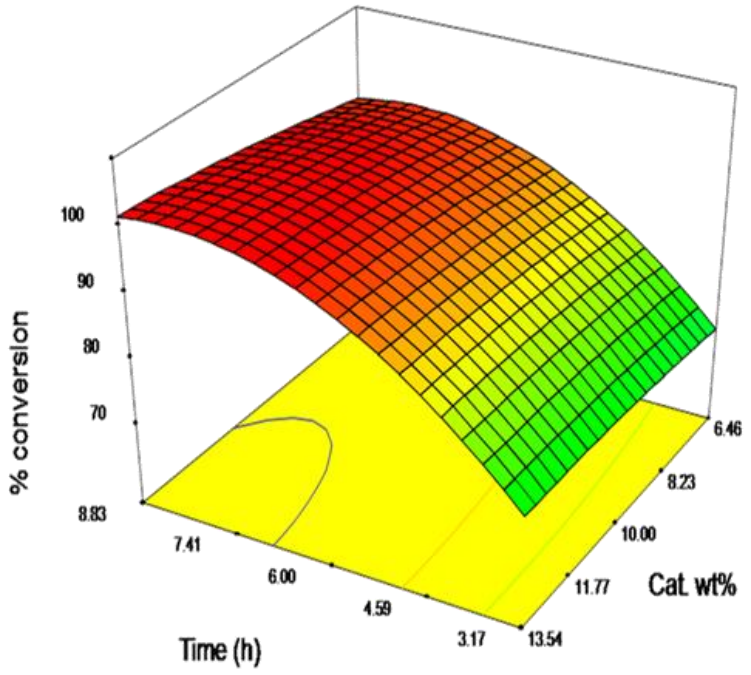

Fig. 7.12 Effects of catalyst wt% and reaction time on the FFA conversion

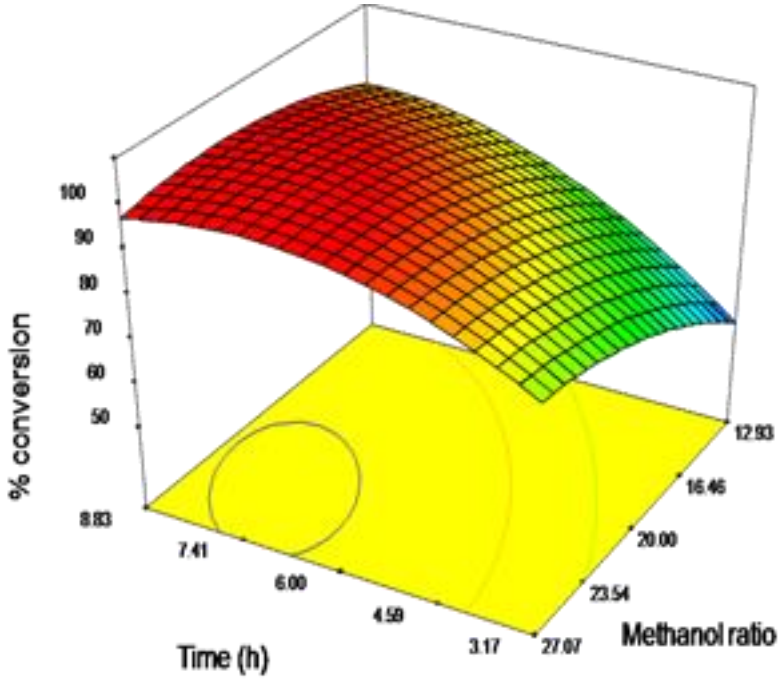

Fig. 7.13 Effects of methanol to oleic acid molar ratio and reaction time on the FFA conversion

7.4.4 Reusability of the catalysts in the esterification reaction

For the catalyst reusability study, the catalyst was separated by filtration from the reaction mixtureand was washed with methanol. It was then dried and finally regenerated by calcination, to remove the residual organic compounds. The conversion reduced from 99.3 wt% in experiment one to 96.9 % in experiment three indicating that the strong acid sites of the catalysts are still active and the catalyst is reusable after at least three reaction cycles. Additionally, the Tungsten (W) content in the product was analyzed with the help of ICP. The presence of Tungsten (W) in the product was found to be 4 ppb only.

7.4.5 Development of kinetic model and thermodynamics of the fatty acid methyl ester (FAME)

The optimized reaction condition was used for developing the kinetic model of esterification of oleic acid. In esterification reaction, free fatty acids (FFA) and methanol (M) react to produce methyl ester (ME) and water (W). It was assumed that oleic acids (OA) and methanol (M) were weakly adsorbed on the catalyst. Adsorption of different FFA on a vacant site is given by

$$OA + S \overset{K_1}{\Leftrightarrow} OA.S \qquad \ldots(7.3)$$

Adsorption of Methanol (M) on a vacant site is given by

$$M + S \overset{K_2}{\Leftrightarrow} M.S \qquad \ldots(7.4)$$

Surface reaction of OA.S and M.S leading to the formation of methyl ester (ME.S) and glycerol (G.S) on the site

$$OA.S + M.S \overset{K_{SR}}{\Longleftrightarrow} ME.S + W.S \qquad \ldots(7.5)$$

Desorption of methyl ester (ME) and water (W) is given by

$$ME.S \overset{K'_{ME}}{\Longleftrightarrow} ME + S \qquad \ldots(7.6)$$

$$W.S \overset{K'_{W}}{\Leftrightarrow} W + S \qquad \ldots(7.7)$$

If the surface reaction (eqn. 7.5) controls the rate of reaction, then the rate of reaction of OA is given by

$$-r_{OA} = -\frac{dC_{OA}}{dt} = k_{SR}C_{S.OA}.C_{M.S} - k'_{SR}C_{S.ME}.C_{W.S} \quad \ldots(7.8)$$

$$-\frac{dC_{OA}}{dt} = \frac{k_{SR}\{K_1K_2C_{OA}C_M - (K_{ME}K_WC_{ME}C_W/K_{SR})\}C_t^2}{(1 + C_{OA}K_1 + K_2C_M + K_{ME}C_{ME} + K_WC_W)^2} \quad \ldots(7.9)$$

The reaction is far away from equilibrium, as initial rate data were used. Thus, reverse reaction cane be neglected (Yadav et al., 2012).

$$-\frac{dC_{OA}}{dt} = \frac{k_rwC_{OA}C_M}{(1 + C_{OA}K_1 + K_2C_M + K_{ME}C_{ME} + K_WC_W)^2} \quad \ldots(7.10)$$

Where

$k_rw = k_{SR}K_1K_2C_t^2$; w = catalyst wt. Assuming the adsorption constants are very small (Yadav et al., 2012), then the above equation reduces to

$$-\frac{dC_{OA}}{dt} = k_rwC_{OA}C_M \quad \ldots(7.11)$$

A large excess of methanol was used in the reaction. Therefore, $C_M \cong C_{M,o}$ can be assumed constant in this reaction. Then the above equation can be written in terms of fractional conversion as,

$$\frac{dX_{OA}}{dt} = k''C_{M,o}\ \ (1 - X_{OA}) \quad \ldots(7.12)$$

Where, $k'' = k_rw$

Integrating the above equation and for constant initial triglyceride concentration, the final expression leads to

$$-\ln(1 - X_{OA}) = k't \quad \ldots(7.13)$$

Where,

$$k' = k''C_{M,o}$$

Thus, a plot of $-\ln(1 - X_{OA})$ against time at different temperatures gave the values of the reaction rate constants at different temperatures. The values of the rate constants at different temperatures were calculated and an Arrhenius plot was used to estimate the apparent activation energy of the reaction. The activation energy is comparable to values obtained from other literature (Table 7.6). The enthalpy of activation ($\Delta H^{\ddagger}$), and the entropy of activation ($\Delta S^{\ddagger}$) were estimated using Eyring equation (Eyring, 1935).

$$\ln\frac{k''}{T} = -\frac{\Delta H^{\ddagger}}{R}.\frac{1}{T} + \ln\frac{k_B}{h} + \frac{\Delta S^{\ddagger}}{R} \quad \ldots(7.14)$$

Where, k_B is the Boltzmann constant and h is the Plank constant. Gibbs energy of activation ($\Delta G^{\ddagger}$) was calculated using the following equation:

$$\Delta G^{\ddagger} = \Delta H^{\ddagger} - T.\ \Delta S^{\ddagger} \quad \ldots(7.15)$$

The positive value of entropy of activation indicates that the activation complex is formed through dissociation mechanism. Therefore, the activation complex has less ordered or less rigid structure than the reactants in the ground state, which made the rate of reaction slower (Ong et al., 2013). The positive nonzero values of Gibb's free energy indicate that the esterification reaction is non-spontaneous (Table 7.6).

Table 7.6: Activation energy and Thermodynamic data obtained from reaction kinetics

	Unit	Value	Lit. value (Tesser et al., 2009)	Lit. value (Berrios et al., 2007)	Lit. value (Su, 2013)
Activation Energy (E_a)	kJ/mol	66.3	68.9	50.7	44.9
Enthalpy of activation ($\Delta H^{\ddagger}$)	kJ/mol	63.2	-	-	-
Entropy of activation ($\Delta S^{\ddagger}$)	J/mol.K	81.4	-	-	-
($\Delta G^{\ddagger}$)	kJ/mol	40.5	-	-	-

7.5 Conclusions

This research work reveals that TPA impregnated H-Y zeolite is an effectual and reusable catalyst for esterification of oleic acid and free fatty acids. The reaction kinetics indicate that the esterification reaction is an endothermic pseudo-first order reaction with an activation energy of 66.3 kJ/mol and the reaction intermediates are unstable as compared to the reactants.

CHAPTER 8: TECHNO-ECONOMIC AND ECOLOGICAL IMPACT COMPARISON BETWEEN BIODIESEL AND COMBINED BIOFUE LPRODUCTIONPROCESSES USING HETEROGENEOUS ACID CATALYSTS

A version of this chapter will be submitted in a journal.

Contribution of the Ph.D. Candidate

Studies were conducted by Chinmoy Baroi. The content in this chapter was written by Chinmoy Baroi with discussions and suggestions provided by Dr. Ajay Dalai.

Contribution of this Chapter to the Overall Ph.D. Research

In this chapter, the techno-economic feasibility of combined biofuel production process is compared with the traditional biodiesel production process.

8.1 Abstract

In this study, the techno-economic and ecological impact of heterogeneous acid catalyzed biodiesel production process and combined biofuel production processes from green seed canola (GSC) are evaluated. The two processes are compared based on three criteria, e.g. process economics, environmental impact and process energy efficiency. Based on the assessment, it is concluded that both the processes are economically profitable, when the cost of the feedstock is $ 0.35/kg. Surprisingly, biodiesel production process depicts higher profitability as compared to that for combined biofuel production process. Additionally, biodiesel production process is more energy efficient than combined biofuel production process. However, combined biofuel production process is more environment friendly as compared to that for biodiesel production process.

8.2 Introduction

Biodiesel is a diesel substitute renewable fuel is more attractive than diesel fuel because of its low emission profile and renewability. The biodiesel production process yet to be economically attractive due to higher feedstock price. On the contrary, cheaper feedstock is only

compatible with acid-catalyzed process because of higher free fatty acid (FFA) content. Especially, solid acid catalysts can be a good choice because of easy product separation and waste minimization (Kulkarni et al., 2006).

Green seed canola oil is one of the low-grade oils available in huge quantity in North America. The raw green seed canola oil are not edible because of the presence of the higher amount of chlorophyll.The higher chlorophyll content also reduces the oxidation stability of the oil (Abraham and DeMan, 1986; Rawk and Santen, 1970). However, a method has been developed to remove the chlorophyll from the GSC oil effectively using K-10 clay as a chlorophyll adsorbent (Issariyakul and Dalai, 2010).

One of the approaches to improving the biodiesel market economy is to find useful application for the co-product i.e. glycerol. Approximately, biodiesel production generates about 10% (w/w) glycerol as the main by-product (Sdrula, 2010). Glycerol ethers, a derivative of glycerol, can be used as fuel additives that enhance fuel combustion properties and help in decreasing the cloud point of biodiesel (Klepacova et al., 2003). In a previous study, a process has been developed to produce a combined biofuel (mixture of biodiesel and glycerol-ether) from GSC oil (Baroi et al., 2014).

From an economic point of view, a process with positive or higher number in the net present value (NPV) and internal rate of return (IRR) are considered to be economically feasible (Li et al., 2011). Ecological impacts are evaluated based on the environmental impacts and process energy efficiency. An algorithm namely, waste reduction algorithm (WAR) is developed by US EPA (Young et al., 1999) to assess the environmental impact at the manufacturing stage within the overall lifecycle of the chemical production and process. The energy efficiency of the process can be evaluated based on the energy of the raw materials and the products (Trippe et al., 2013). Previous economic studies on biodiesel process show that one-step heterogeneous acid catalyzed process is profitable, safe and environment friendly process than homogeneous acid catalyzed process (Baroi and Dalai, 2015). However, no literature is found on the techno-economic and ecological impact comparison between the biodiesel and combined biofuel production processes from the green seed canola oil. This research introduces for the first time the techno-economic and ecological impact comparison between the biodiesel and combined biofuel production processes.

8.3 Development of process models

Aspen HYSYS v.8.2 is employed to obtain mass and energy balance for biodiesel and combined biofuel production processes using heterogeneous acid catalysts, and thereafter economic and ecological assessment are performed for the same systems. All the unit operations, input conditions and operating conditions are specified during process flow sheet development. Triolein, diolein, monoolein, oleic acid are selected to represent the triglycerides (TG), diglycerides (DG), monoglyceride (MG) and free fatty acids (FFA) of the GSC oil. In this paper in the process simulation, DG, MG, *tert*butyl glycerol-ether (TTBG), di-*tert*-butyl glycerol ethers (DTBG), mono-*tert*- butyl glycerol-ether (MTBG), solid catalysts, chlorophyll A and B (Ch-A and Ch-B) are inserted as hypothetical compounds. Thermodynamic group contribution method is used to develop and define the properties of DG, MG, TTBG, DTBG and MTBG as the hypothetical liquid compounds (Marrero and Gani, 2001; Reid at el., 1987) (see appendix D). Chlorophyll A and B are treated as solids and the properties of solids and thermodynamics are obtained elsewhere (Annamali et al., 1987; Chen and Cai, 2007) (see appendix D). The properties of other components (e.g. water, oleic acid, methyl oleate, glycerol, methanol) are collected from the HYSYS library. As the simulation involves polar components (glycerol and methanol), a non–random two liquid (NRTL) thermodynamic model is chosen as the base model for the simulation of the biodiesel production process. Since some of the binary interaction parameters are not provided in the databank, these parameters are estimated using the UNIFAC vapour-liquid equilibrium and UNIFAC liquid-liquid equilibrium. Plant capacity is assumed to be 8000 tonnes/year (the same as in Zhang et al., 2003; West et al., 2008). This translates to vegetable oil roughly 1000 kg/h for process configuration. Centrifuge separation methods are used to separate the pre-treatment clay and solid catalysts from the processes. Conversion reactors are used to represent the biodiesel and etherification reactors. The reactors are assumed to operate continuously. For biodiesel and combined biofuel production processes, the original data mentioned in the paper (Baroi et al., 2014) are converted to conversions for the use in this paper. The conversion from glycerol to MTBG, MTBG to DTBG, DTBG to TTBG are 100%, 94.6%, and 88.9% respectively. After the reactions, methanol is retrieved and purified using a multistage atmospheric distillation column and the purity obtained is 100%.

8.4 Process design

The biodiesel production process flowsheet is depicted in Figure 8.1. The process is described with the help of stream numbers, equipment names, and numbers mentioned in Figure 8.1. Both GSC oil (stream no. 101) and K-10 clay (stream no. 102) enter the preteater at atmospheric pressure and room temperature, where the chlorophyll is adsorbed by K-10 clay. Then the adsorbed clay is removed by gravity settling. The treated oil (stream no. 105) is mixed with solid acid catalyst (stream no. 106) and methanol (stream no. 107). The reaction mixture is then pumped through P-100 (Fig. 8.1) to obtain the desired pressure of 4187 kPa to keep the reactor mixture in the liquid phase inside the reactor and sent to the biodiesel reactor. The pressure of the reaction products are then relieved and then heated in the heater (E-100). The reaction mixture is fed to a 3-phase separator (V-101), to separate the catalyst and to strip off the methanol. The methanol is then purified in the distillation column (T-100), cooled down (E-102) and then recycled back (details of unit operations are given in Table 8.1). The mainstream is then brought down to the lower temperature and sent to an ultrafiltration membrane separator. The glycerol is separated as a retanate (stream no. 121) and the pure biodiesel is separated as a permeate (stream no. 122) through the membrane separator (Saleh et al., 2010). The reactant and product composition are given in Table 8.2.

The combined biofuel production process flowsheet is depicted in Figure 8.2. The process is described with the help of stream numbers and equipment name and numbers mentioned in Figure 8.2. Both GSC oil (stream no. 101) and K-10 clay (stream no. 102) enter the preteater at atmospheric pressure and room temperature, where the chlorophyll is adsorbed by K-10 clay. Then the adsorbed clay is removed by gravity settling. The treated oil (stream no. 105) is mixed with solid acid catalyst (stream no. 106) and methanol (stream no. 107). The reaction mixture is then pumped through P-100 (see Fig. 8.2) to obtain the desired pressure of 4187 kPa to keep the reactor mixture in the liquid phase inside the reactor and sent to the biodiesel reactor. The pressure of the reaction products are then relieved and fed to a flash separator (V-101) to strip off the methanol. The methanol is then purified in the distillation column (T-100), cooled down (E-102) and then recycled back (details of unit operations are given in Table 8.1). The mainstream is then cooled down and mixed with catalysts (stream no. 119) and TBA (stream no. 135). The mixed stream then pumped through P-101 (see Fig. 8.2) to obtain the desired pressure of 1050 kPa to keep the reactor mixture in the liquid phase inside the reactor. The pressure of the reaction

products are then relieved and fed to a 3-phase separator (V-102). The vapour and liquid stream are then cooled down in a cooler (E-103). The cold stream (stream no. 128) is then pumped to the desired pressure and sent to an ultrafiltration membrane separator. The mixture of TBA + water + methanol is separated as a permeate (stream no. 131) and the pure combined biofuelis separated as a retanate (stream no. 130) through the membrane separator (saleh et al., 2010). The TBA is recovered through pervaporation membrane (TBA separator) as retanate (Biduru et al., 2005). The permeate stream contained water and residue methanol and thrown out as waste. The reactant and product composition are given in Table 8.3.

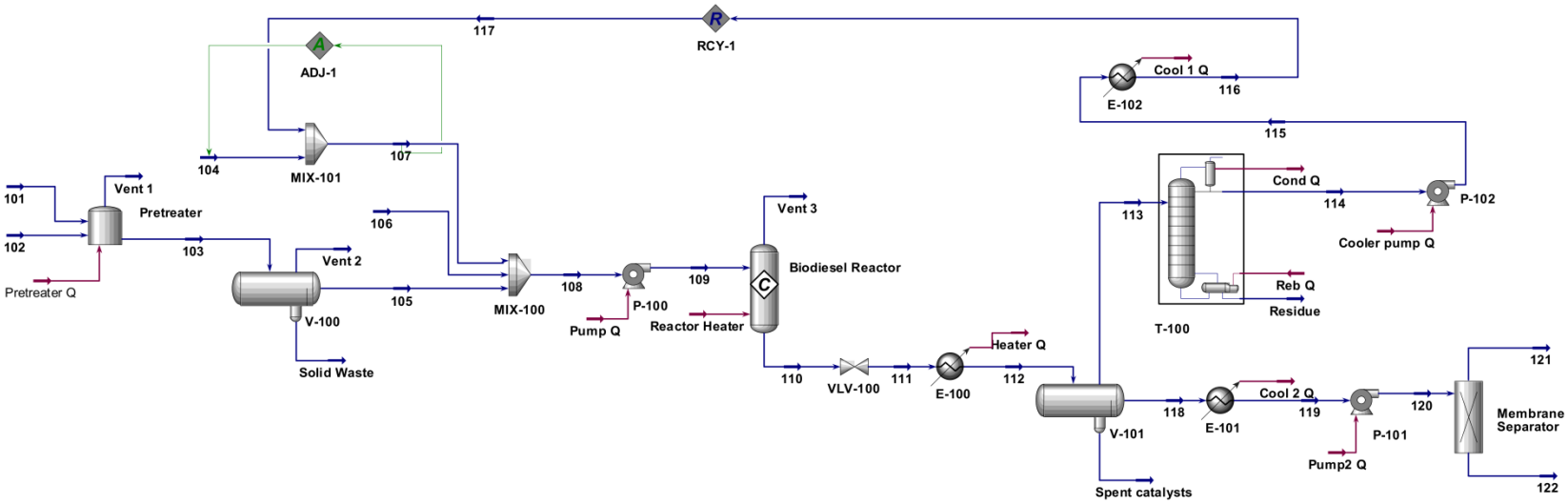

Fig. 8.1 Flowsheet for heterogeneous acid catalyzed biodiesel production process

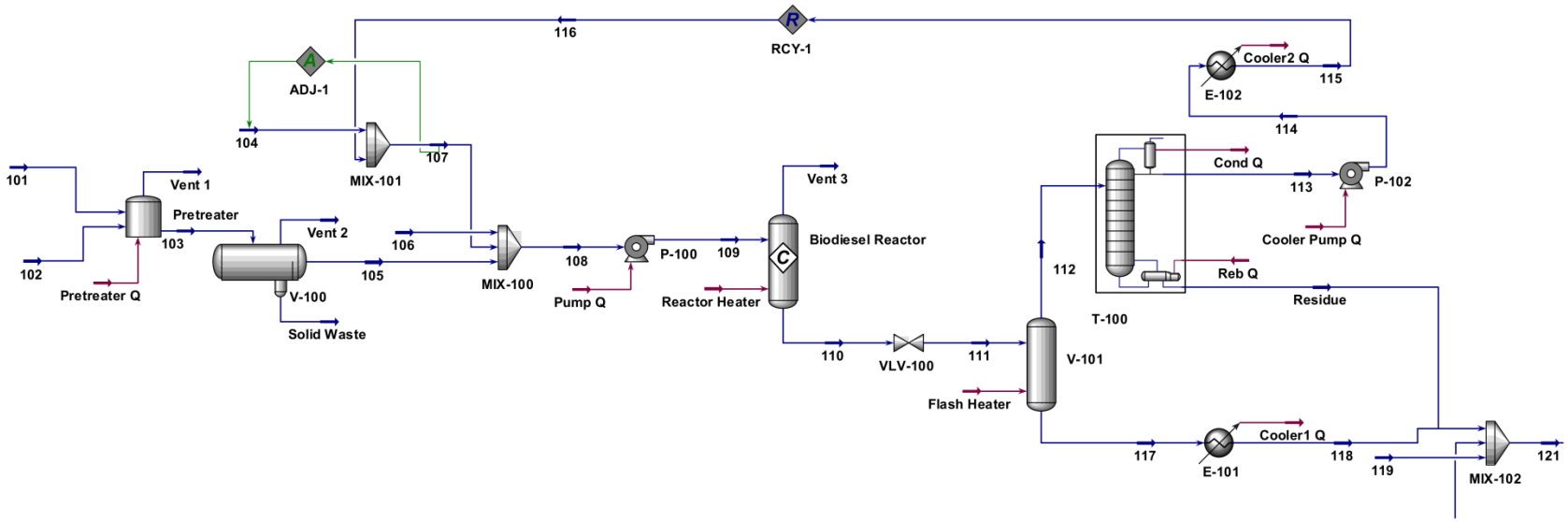

Fig. 8.2 (a) Flowsheet for combined biofuel production process

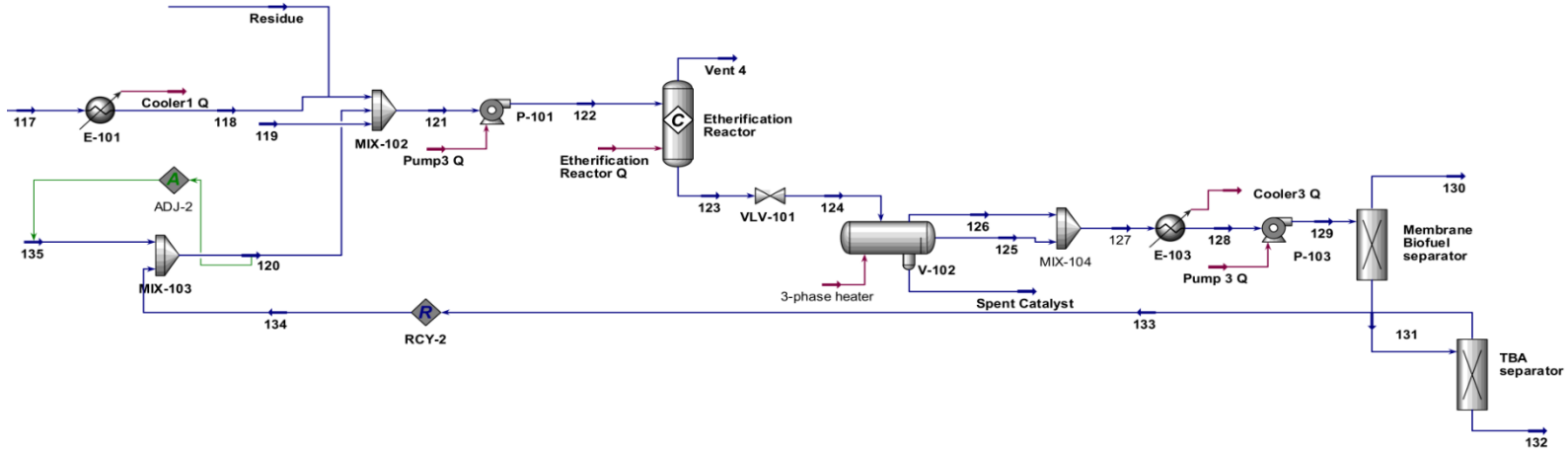

Fig. 8.2 (b) Flowsheet for combined biofuel production process

Table 8.1: Synopsis of the unit operating conditions for each process

	Biodiesel	Biofuel
Catalyst	55%TPA/H-β	55%TPA/H-β
Reactor type (Biodiesel)	CSTR	CSTR
Temperature (°C)	200	200
Pressure (kPa)	4187	4187
Alcohol to oil ratio	21.3	21.3
Residence time (h)	6.5	6.5
Reflux ratio	1	1
Condenser/reboiler pressure (kPa)	101.3/124.3	101.3/124.3
Type of trays	Packed	Packed
Distillate purity (%)	99.79	
Catalyst Removal	Gravity	Gravity
Glycerol separation	Gravity	-
Glycerol purity (%)	92.8	-
Reactor type (Etherification)	-	CSTR
Temperature (°C)	-	120
Pressure (kPa)	-	1050
TBA to glycerol ratio	-	5
Residence time (h)	-	6
Glycerol to MTBG conv.%	-	100
MTBG to DTBG conv.%	-	94.66
DTBG to TTBG conv.%	-	88.90
Biodiesel/Combined biofuelpurity, wt%	99.47	99.58

Table 8.2: Feed and product stream information for the biodiesel production process

	101	102	104	106	122	121
Temperature (°C)	25.0	25.0	25.0	25	25.31	25
Pressure (kPa)	101.3	101.3	101.3	101.3	506.3	101.3
Molar flow (kmol/h)	1.355	0.2003	5.110	1.7×10^{-2}	3.696	1.183
Mass flow (kg/h)	1100	110	163.7	36.3	1096	98.32
Component mass fraction						
Methanol	-	-	1	-	-	0.0600
GSC oil	0.9574	-	-	-	-	-
DG	-	-	-	-	-	-
MG	-	-	-	-	0.0023	-
Free Fatty Acids	0.0425	-	-	-	0.0030	-
Ch-A	0.0001	-	-	-	-	-
Ch-B	0.0000*	-	-	-	-	-
Glycerol	-	-	-	-	0.0001	0.9280
K-10 clay	-	1	-	-	-	-
Solid acid catalyst	-	-	-	1	-	-
Water	-	-	-	-	-	0.0009
FAME	-	-	-	-	0.9947	0.0111

*Very less amount

Table 8.3: Feed and product stream information for the combined biofuel production process

	101	102	104	106	119	135	130
Temperature (°C)	25.0	25.0	25.0	25	25	25	25
Pressure (kPa)	101.3	101.3	101.3	101.3	101.3	101.3	506.5
Molar flow (kmol/h)	1.355	0.2003	5.110	1.7×10^{-2}	1.4×10^{-2}	3.25	4.92
Mass flow (kg/h)	1100	110	163.7	36.3	29.7	240.9	1396
Component mass fraction							
Methanol	-	-	1	-	-	-	-
GSC oil	0.9574	-	-	-	-	-	-
DG	-	-	-	-	-	-	-
MG	-	-	-	-	-	-	0.0018
Free Fatty Acids	0.0425	-	-	-	-	-	0.0023
Ch-A	0.0001	-	-	-	-	-	-
Ch-B	0.0000*	-	-	-	-	-	-
K-10 clay		1	-	-	-	-	-
Solid acid catalysts	-	-	-	1	1	-	-
TBA	-	-	-	-	-	1	-
Water	-	-	-	-	-	-	-
FAME	-	-	-	-	-	-	0.7888
MTBG	-	-	-	-	-	-	0.0067
DTBG	-	-	-	-	-	-	0.0296
TTBG	-	-	-	-	-	-	0.1707

*Very less amount

8.5 Equipment sizing

All the equipments were sized using HYSYS sizing utility. Reactors are sized by multiplying volumetric flow rate with the residence time. The required surface areas of all the heat transfer equipments were sized using the integrated energy analysis utility. The required membrane surface area was sized considering the flux through membrane to be 35 gallon/day.m^2. The surface area was calculated based on the membrane surface area sizing procedure (Peters et al., 2011). Table 8.4 summarizes the dimensions of all relevant vessels.

Table 8.4: Equipment size for various unit operations in the process

Type	Description	Biodiesel	Biofuel
Reactor (vertical)*	Biodiesel	2.14 × 6.42	2.14 × 6.42
	Etherification	-	2.20 × 6.6
Column (vertical)*	Methanol Purification	0.61× 3.31	0.61× 3.31
Separator (horizontal)**	K-10 clay Separator	0.91 × 3.66	0.91 × 3.66
	Catalyst separator	0.61 × 3.35	0.91 × 3.66
Membrane***	Ultrafiltration (UF)	82.13	19.6
	Pervaporation	-	53.89

*Dia×Height (m)
** Dia×Length (m)
***Surface area (m^2)

8.6 Economic assessment

The plant capacity is assumed to be of 8000 tonnes/year biodiesel production. Operating hours are assumed to be 7920h/year (assuming 330 operating days/year). The processes are evaluated based on the net present value (NPV), internal rate of return (IRR) and payback period. The "study estimate" method with a range of expected accuracy from +30% to – 20% (Turton et al., 2012) is used foe economic assessment.

Table 8.5 gives the breakdown of the capital investments of two processes. The equipment prices are estimated using Bare module method (Turton et al., 2012). The bare module costs of membrane are considered to be \$20/m^2 (Arvid Lie et al., 2007). The fixed capital cost, working capital and the total capital investment are estimated using the procedure mentioned earlier (West et al, 2008).

The capital cost for the equipments (Table 8.5) depicts that biodiesel distillation column is the most expensive equipment and then reactors are the second highest expensive equipment.

Direct manufacturing expenses are estimated based on the price and consumption of each chemical and utility. The chemical and utility prices are presented in Table 8.6 and material flow information is obtained from HYSYS process flowsheet.

The operating labour cost has been estimated based on the number and types of equipments (Turton et al., 2012). Table 8.7 represents the details of the total manufacturing costs. The detailed direct and indirect manufacturing costs are estimated following the method described elsewhere (West et al, 2008). The net annual profit after tax is calculated assuming an income tax of 42%. The estimated project life is 20 years, and the estimated construction period is 2 years. Based on the net present value (NPV), and internal rate of return (IRR), it can be concluded that biodiesel production process is more economically favourable.

Table 8.5: Major equipment costs, total fixed capital costs and total capital investments (in millions) of the process

Equipment	Description	Biodiesel	Biofuel
Reactor	Biodiesel	0.27	0.27
	Etherification	-	0.28
	Pretreater	0.06	0.06
Column	Methanol Purification	0.38	0.38
	Solid/Catalyst Separator	0.03	0.04
	K-10 Separator	0.02	0.02
Pump	Reaction mixture pump	0.04	0.04
Membrane	Ultrafiltration (UF)	3.72×10^{-4}	7.48×10^{-3}
	Pervaporation	-	0.021
Total bare module cost, C_{BM}		1.28	1.61
Total module cost, C_{TM}		1.51	1.89
Fixed Capital cost, C_{FC}		1.89	2.38
Working Capital cost, C_{WC}		0.28	0.36
Total Capital Investment, C_{TCI}		2.17	2.74

Table 8.6: Condition for the economic assessment of the process

Item	Specifications	Price ($/kg)	
		Biodiesel	Biofuel
Chemicals			
Biodiesel/Biofuel		1	1.03
Glycerol		0.9	-
Methanol	99.9%	0.21	0.21
Green Seed Canola oil	raw	0.35	0.35
Solid acid catalyst	-	3.6	4.45
K-10 Clay		0.31	0.31
TBA	99.9%	-	1.47
Utilities			
Cooling water	25-30°C	$0.0001/kg	$0.0001/kg
Low-pressure steam	5 bar, 160°C	$0.03/kg	$0.03/kg
Medium pressure steam	10 bar, 184°C	$0.03/kg	$0.03/kg
High-pressure steam	41 bar, 254°C	$0.03/kg	$0.03/kg
Electricity		$16.8/GJ	$16.8/GJ

Table 8.7: Total manufacturing cost and profit after tax of the processes

	Biodiesel	Biofuel
Direct Manufacturing costs		
Total raw material cost ($ in millions)	4.86	9.14
Total utility cost ($ in millions)	0.29	0.41
Cost of operating labours ($ in millions)	0.16	0.16
Waste Treatment cost ($ in millions)	0.06	0.06
Maintenance and repair(M&R), 6% of C_{FC}	0.11	0.14
Operating supplies, 15% of M&R	0.02	0.02
Lab charges, 15% of operating labour	0.02	0.02
Patents and Royalties	0.11	0.11
Indirect Manufacturing costs		
Overhead packaging and storage	0.09	0.10
Local taxes, 1.5% C_{FC}	0.03	0.04
Insurance, 0.5% C_{FC}	0.01	0.01
Depreciation, 10%	0.19	0.24
Administrative costs	0.02	0.02
Distribution and selling	0.38	0.38
R&D	0.19	0.19
Total Manufacturing costs ($ in millions)	6.55	11.04
Revenue from sales ($ in millions)	9.86	11.98
Net annual profit ($ in millions)	3.31	0.94
Annual taxes, 42%	1.39	0.39
Net annual profit ($ in millions)	1.92	0.54
Net Present Value (NPV) (millions)	8	0.5
Internal rate of return (IRR)%	61.5	12.9

8.7 Sensitivity analysis

Figure 8.3 depicts the sensitivity analysis of biodiesel production process. It depicts that the maximum price of GSC oil: $0.6/kg, catalyst price: $12/kg and minimum selling price of biodiesel: $0.75/kg are allowable in order to run the process profitable.

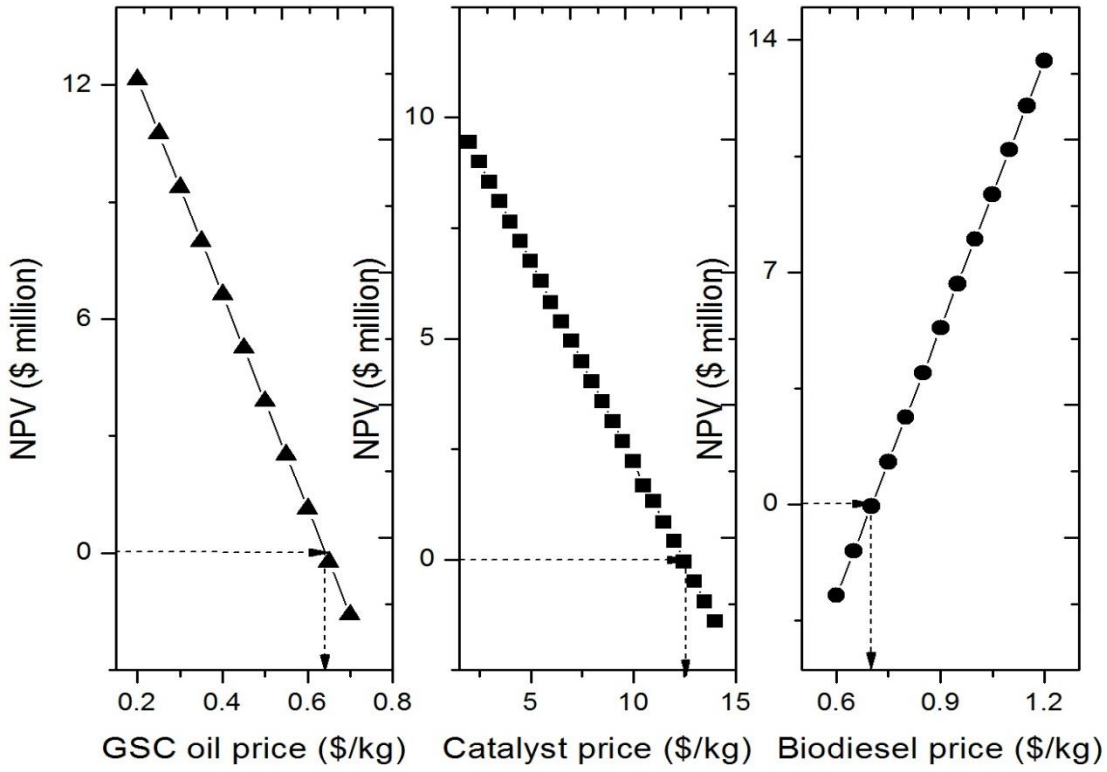

Fig. 8.3 Sensitivity analysis of biodiesel production process

Figure 8.4 depicts the sensitivity analysis of combined biofuel production process. It depicts that the maximum price of GSC oil: $0.37/kg, catalyst price: $4.6/kg and minimum selling price of biofuel: $1.02/kg are allowable in order to run the process profitable.

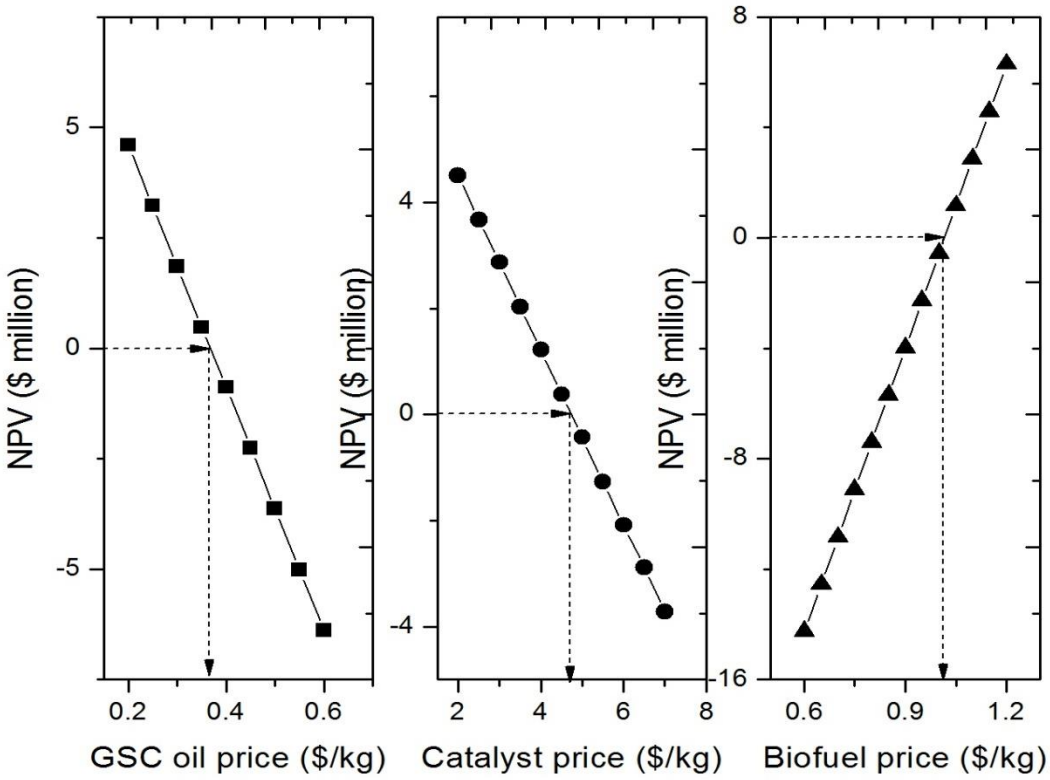

Fig. 8.4 Sensitivity analysis of combined biofuel production process

8.8 Ecological impact assessment

Ecological impact of the processes were assessed and compared based on the potential environmental impact index (PEI) and the process efficiency. The PEI index provides an indication of the chemical process environmental friendliness across the system boundary. The WAR software (www.epa.gov) is used to calculate the PEI indexes, and the PEI indexes with a lower score indicates more environmental friendliness. The impact analysis indicates that the heterogeneous acid catalyzed process is more environmentally friendly compared to that for homogeneous process (Table 8.8).

Table 8.8: Toxicity Index comparison of the two processes

	Biodiesel	Biofuel
Human Toxicity Potential by Ingestion (HTPI)	2.47	2.12
Human Toxicity Potential by Exposure (HTPE)	0.86	3.04×10^{-2}
Terrestrial Toxicity Potential (TTP)	2.47	2.12
Aquatic Toxicity Potential (ATP)	0.93	1.49
Global Warming Potential (GWP)	0.67	1.09
Ozone Depletion Potential (ODP)	7.11×10^{-6}	1.14×10^{-5}
Photochemical oxidation potential (PCOP)	21.5	5.36
Acidification Potential (AP)	21	33.6
Total (PEI/h)	49.9	45.8

The process energy efficiency is calculated by dividing the raw materials energy to product energy.

$$\text{Energy Efficiency} = \frac{\text{Energy of the products}}{\text{Energy of the raw materials+Input energy}} \times 100\% \quad \ldots(8.1)$$

The process efficiency obtained for biodiesel and combined biofuel production processes are 47.4% and 31.9% respectively. It indicates that the excess amount of energy in combined biofuel production process is utilized in the reactor, but the heating value of the combined biofuelis not improved as compared to that for biodiesel.

8.9 Discussion

All the assessment results are outlinedand compared between the two processes. Based on the relative comparison, the score 0 or 1 are assigned. Score 0 indicates unfavourable, whereas score 1 indicates favourable. The assessment comparison indicates that biodiesel production process is more favorable than combined biofuel production process (Table 8.9).

Table 8.9: Overall comparison of the processes

Assessment Criteria	Scores	
	Biodiesel	Biofuel
Profitability (profit, NPV, IRR)	1	0
Process Efficiency	1	0
Environmental Impact	0	1
Total	2	1

8.10 Conclusions

From the process simulation, economic and ecological impact assessment study it is obtained that biodiesel production process is more favourable than the combined biofuel production process. The profitability of biodiesel production process is high compared to that of combined biofuel production process. Thus, it is wise to sell the pure glycerol as a separate product rather than selling as a combined biofuel.

CHAPTER 9: CONCLUSIONS AND RECOMMENDATIONS

9.1 Conclusions

The Ph.D research reveals that silica-based solid acid catalysts are able to remove the chlorophyll while catalyzing simultaneous transesterification and esterification reactions in a single step. Therefore, solid acid catalysts allow using unrefined waste grade feedstock such as GSC oil as a direct feedstock for biodiesel production and reduce pre-treatment costs of the feedstock. Additionally the solid acid catalyzed biodiesel production process is proved to be profitable, safe and environment friendly process as compared to the homogeneous process. The research also reveals that glycerol derived after biodiesel production can be used to produce glycerol-ether. Later feasibility of a combined biofuel (mixture of biodiesel + glycerol-ether) production process indicates that combined biofuel production process is less profitable than biodiesel production process and it is worth to sell high purity glycerol as a product itself.

9.2 Recommendations

- Different TPA based heterogeneous solid acid catalysts (e.g. carbon nanotube, gamma alumina, MAS-9 supported TPA) should be tested for simultaneous esterification, transesterification and chlorophyll removal.
- The catalytic activity should be tested in a continuous flow reactor to verify the catalytic activity.
- The heterogeneous acid catalyzed biodiesel production process should be tested in the presence of co-solvents (e.g. THF) and process sustainability study should be conducted for this.
- An appropriate catalyst synthesis cost estimation method need to be established.
- In combined biofuel production process, TBA should be replaced with cheaper alcohol and the entire combined biofuel production process should be revised.

REFERENCES

Abbasi, B., H. Mahlooji, "Improving response surface methodology by using artificial neural network and simulated annealing," Expert Systems with Applications, 39, 3461–3468 (2012).

Abbaszaadeh, A., B. Ghobadian, M. R. Omidkhah and G. Najafi, "Current biodiesel production technologies: A comparative review," Energy Conversion and Management, 63, 138-148 (2012).

Abraham, V., J. M. DeMan, "Hydrogenation of canola oil as affected by chlorophyll," Journal of the American Oil Chemists' Society, 63, 1185 – 1188 (1986).

Agarwal, D., S. Sinha, A. Agarwal, "Experimental investigation of control of NOx emissions in biodiesel-fueled compression ignition engine," Renewable Energy, 31, 2356–2369 (2006).

Alba-Rubio, A. C., F. Vila, D. M. Alonso, M. Ojeda, R. Mariscal, M. L. Granados, "Deactivation of organosulfonic acid functionalized silica catalysts during biodiesel synthesis,"Applied catalysis. B, Environmental, 95, 279-287 (2010).

Annamalai, K., I. Puri, M. Jog, "Advanced Thermodynamics Engineering," 2nd edition, CRC Press, Florida, USA, pp. 715-717 (1987).

Arvid Lie, J., T. Vassbotn, M. Hagg, D. Grainger, T. Kim, "Optimization of a membrane process for CO_2 capture in the steelmaking industry," International journal of greenhouse gas control, 1, 309-317 (2007).

Atalay, B., G. Gündüz, "Isomerizaton of α-pinene over H3PW12O40 catalysts supported on natural zeolite," Chemical Engineering Journal, 168, 1311-1318 (2011).

Ataya, F., M. A. Dube, M. Ternan, "Acid-Catalyzed Transesterification of Canola Oil to Biodiesel Single- and Two-Phase Reaction Conditions," Energy and Fuels, 21, 2450 – 2459 (2007).

Atkins, P., J. de Paula, "Physical Chemistry," 8th edition,W. H. Freeman & Co, USA, pp.830 (2006).

Bahmaei, M., E. S. Sabbaghian, E. Farzadkish, "Development of a method for chlorophyll removal from canola oil using mineral acids," Journal of the American Oil Chemists' Society, 82, 679 – 684 (2005).

Baroi, C., A. K. Dalai, "TPA supported on SBA-15 as solid acid catalysts for the biodiesel production," ACS symposium series, 1092, 93-109 (2012).

Baroi, C., A. K. Dalai, "Simultaneous esterification, transesterification and chlorophyll removal from green seed canola oil using solid acid catalysts," Catalysis Today, 207, 74-85 (2013).

Baroi, C., S. Mahto, C. Niu, A. K. Dalai, "Combined biofuel production from green seed canola oil using zeolites," Applied Catalysis A, 469, 18-32 (2014).

Baroi, C., A. K. Dalai, "Process sustainability of biodiesel production process from green seed canola oil using homogeneous and heterogeneous acid catalysts," Fuel Processing Technology, (2015).

Berube, F., S. Kaliaguine, "Calcination and thermal degradation mechanisms of triblock copolymer template in SBA-15 materials," Microporous and Mesoporous Materials, 115, 469-479 (2007).

Berrios, M., J. Siles, M.A. Martı´n, A. Martı´n, "A kinetic study of the esterification of free fatty acids (FFA) in sunflower oil," Fuel, 86, 2383-2388 (2007).

Bhorodwaj, S. K.,D. K. Dutta, "Activated clay supported heteropoly acid catalysts for esterification of acetic acid with butanol," Applied Clay Science, 53, 347–352 (2011).

Biduru, S., S. Sridhar, G. S. Murthy, S. Mayor, "Pervaporation of tertiary butanol/water mixtures through chitosan membranes cross-linked with toluylene diisocyanate," Journal of Chemical Technology and Biotechnology, 80, 1416-1424 (2005).

Bokade, V. V., G. D. Yadav, "Transesterification of Edible and Nonedible Vegetable Oils with Alcohols over Heteroployacids Supported on Acid-Treated Clay," Industrial and EngineeringChemistry Research, 48, 9408 – 9415 (2009).

Bokade, V. V., G. D. Yadav, "Synthesis of biodiesel and bio-lubricant by transesterifiacation of vegetable oil with lower and higher alcohols over heteroplyacids supported by clay (K-10)," Trans IChemE-Part B, Process Safety and Environmental Protection, 85, 372–377 (2007).

Boocock, D. G. B., S. K. Konar, V. Mao, C. Lee, S. Buligan, "Fast formation of high-purity methyl esters from vegetable oils," Journal of the American Oil Chemists' Society,75, 1167-1172 (1998).

Bordoloi, A., S. B. Halligudi, "Studies in structural characterization and correlation with the catalytic activity of an efficient and stable WO*x*/SBA-15 nanocomposite catalyst," Journal of Catalysis, 257, 283-290 (2008).

Busca, G., "Acid Catalysts in industrial Hydrocarbon Chemistry," Chemical Reviews, 107, 5366-5410 (2007).

Caetano, C. S., I. M. Fonseca, A. M. Ramos, J. Vital, J. E. Castanheiro, "Esterification of free fatty acids with methanol using heteropolyacids immobilized on silica," Catalysis communications, 9, 1996–1999 (2008).

Camblor, M. A., A. Corma, S. Valencia, "Characterization of nanocrystalline zeolite Beta," Microporous and mesoporous materials, 25, 59–74 (1998).

Canakci, M., J. Van Gerpen, "Biodiesel production via acid catalysts," Transactions of the ASAE, 42, 1203-1210 (1999).

Cardoso, A. L., S. C. G. Neves, M. J. Da Silva, "Kinetic Study of Alcoholysis of the Fatty Acids Catalyzed by TinChloride(II): An Alternative Catalyst for Biodiesel Production,"Energy & Fuels, 23, 1718–1722 (2009).

Cardoso, A. L., R. Augusti, M. J. Da Silva, "Investigation on the Esterification of Fatty Acids Catalyzed by the $H_3PW_{12}O_{40}$ heteropolyacid," Journal of American Oil Chemists Society, 85, 555–560 (2008).

Chai, S. H., H. P. Wang, Y. Liang, B. Q., Xu, "Sustainable production of acrolein: gas-phase dehydration of glycerol over 12-tungstophosphoric acid supported on ZrO_2 and SiO_2," Green Chemistry, 10, 1087-1093 (2008).

Chen, M, Z. Cai, "Theoretical study on the thermodynamic properties of chlorophyll d-peptides coordinating ligand," Biochimica et biophysica acta. Bioenergetics, 1767, 603-609 (2007).

Chichova, D., P. Mäki-Arvela, T. Heikkila, N. Kumar, J. Vayrynen, T. Salmi, D.Yu.Murzin, "X-Ray Photoelectron Spectroscopy Investigation of Pd-Beta Zeolite Catalysts with Different Acidities," Topics in Catalysis, 52, 359-379 (2009).

Choi, C., J. Kim, C. Jeong, H. Kim, K. Yoo, "Transesterification kinetics of palm olein oil using supercritical methanol," Journal of Supercritical Fluids, 58, 365– 370 (2011).

Christopher, L. P., H. Kumar, V. P. Zambare, "Enzymatic biodiesel: Challenges and opportunities," Applied Energy, 119, 497–520 (2014).

Chung, K. H., H. Kim, W. J. Jang, J. K. Yoon, S. J. Kahng, J. Lee,S. Han, "Molecular Multistate Systems Formed in Two-Dimensional Porous Networks on Ag(111)," Journal of Physical Chemistry: C, 117, 302−306 (2013).

Costa, A. A., P. R. S. Braga, J. L. de Macedo, J. A. Dias, S. C. L. Dias, "Structural effects of WO_3 incorporation on USY zeolite and application to free fatty acids esterification," Microporous and mesoporous materials, 147, 142–148 (2012).

Collignon, F., P. A. Jacobs, P. Grobet, G. Poncelet, "Investigation of the Coordination State of Aluminum in β Zeolites by X-ray Photoelectron Spectroscopy," Journal of Physical Chemistry: B, 105, 6812–6816 (2001).

Damyanova, S., L. Dimitrov, R. Mariscal, J. L. G. Fierro, L. Petrov, I. Sobrados, "Immobilization of 12-molybdophosphoric and 12-tungstophosphoric acids on metal-substituted hexagonal mesoporous silica," Applied catalysis A: General, 256 183-197 (2003).

Da Silva, C. R. B., V. L. C. Gonclaves, E. R. Lachter, C. J. A. Mota, "Etherification of glycerol with benzyl alcohol catalyzed by solid acids," Journal of the Brazilian Chemical Society, 20, 201-204 (2009).

Datta, A., "Process Engineering and Design using VISUAL BASIC," Boca Raton, CRC Press, UK, pp. 130-135, 221, 307-342 (2008).

De Prado, Lui´s A. S. A., Iris L. Torriani, Inez V. P. Yoshida, "Poly(n-alkylsilsesquioxane)s: Synthesis, characterization, and modification with poly(dimethylsiloxane)," Journal of polymer science. Part: A, Polymer chemistry, 48, 1220-1229 (2010).

Devassy, B. M., S. B. Halligudi, "Zirconia-supported heteropoly acids: Characterization and catalytic behavior in liquid-phase veratrole benzoylation," Journal of Catalysis, 236, 313-323 (2005).

Didi, M. A., B. Makhoukhi, A. Azzouz, D. Villemin, "Colza oil bleaching through optimized acid activation of bentonite. A comparative study," Applied Clay Science, 42, 336–344 (2009).

Di Serio, M., R. Tesser, L. Pengmei and E. Santacesaria, "Heterogeneous Catalysts for Biodiesel Production," Energy and Fuels, 22,207 -217 (2008).

Dufaud, V., F. Lefebvre, G. P. Niccolai, M. Aouine, "New insights into the encapsulation and stabilization of heteropolyacids inside the pore walls of mesostructured silica materials," Journal of Materials Chemistry, 19, 1142–1150 (2009).

Dufaud, V., F. Lefebvre, "Inorganic Hybrid Materials with Encapsulated Polyoxometalates," Materials, 3, 682-703 (2010).

Eckey, E. W., L. P. Miller, "Vegetable fats and oils," Reinhold Publishing Corporation, Newyork, USA, pp.1-5 (1954).

Encinar, J. M., J. F. Gonzalez, E. Sabio, M. J. Ramiro, "Preparation and Properties of Biodiesel from *Cynara cardunculus* L. Oil," Industrial and Engineering Chemistry Research, 38, 2927-2931 (1999).

Eyring, H., "The Activated Complex in Chemical Reactions," Journal of Chemical Physics, 3, 107-115 (1935).

Fischer, K., "Neues Verfahren zur maßanalytischen Bestimmung des Wassergehaltes von Flüssigkeiten und festen Körpern,"Angewandte Chemie, 48, 394–396 (1935).

Fogler, H. S., "Elements of Chemical Reaction Engineering," 4th edition, PRENTICE HALL, Massachusetts, USA, pp. 832-833, 839-841 (2006).

Frusteri, F., L. Frusteri, C. Cannilla, G. Bonura, "Catalytic etherification of glycerol to produce biofuels over novel spherical silica supported Hyflon® catalysts," Bioresource Technology, 118, 350–358 (2012).

Gagea, B. C., Y. Lorgouilloux, Y. Altintas, P. A. Jacobs, J. A. Martens, "Bifunctional conversion of *n*-decane over HPW heteropoly acid incorporated into SBA-15 during synthesis," Journal of Catalysis, 265, 99–108 (2009).

Gan, S., H. K. Ng, P. H. Chan, F. L. Leong, "Heterogeneous free fatty acids esterification in waste cooking oil using ion-exchange resins," Fuel Processing Technology, 102, 67–72 (2012).

Gangadharan, P., R. Singh, F. Cheng, H. Lou, "Novel Methodology for Inherent Safety Assessment in the Process Design Stage," Industrial and EngineeringChemistry Research, 52, 5921-5933 (2013).

Galarneau, A., H. Cambon, F. D. Renzo, F. Fajula, "True Microporosity and Surface Area of Mesoporous SBA-15 Silicas as a Function of Synthesis Temperature,"Langmuir, 17, 8328–8335 (2001).

Gerpen, J.V., G. Knothe, "Chapter 4: Biodiesel production" in "Biodiesel Handbook," AOCS Press., USA, pp. 26-38 (2005).

González, M. D., Y. Cesteros, P. Salagre, "Comparison of dealumination of zeolites beta, mordenite and ZSM-5 by treatment with acid under microwave irradiation," Microporous and mesoporous materials, 144, 162-170 (2011).

Gu, Y., A. Azzouzi, Y. Pouilloux, F. Jerome, J. Barrault, "A green route to silica nanoparticles with tunable size and structure," Green chemistry, 10, 183-190 (2008).

Guler, C., F. Tunc, "Chlorophyll adsorption on acid-activated clay," Journal of the American Oil Chemists' Society, 69, 948-950 (1993).

Gunay, M. E., R. Yildirim, "Knowledge extraction from catalysis of the past: A case of selective CO oxidation over noble metal catalysts between 2000 and 2012," ChemCatChem, 5, 1395 – 1406 (2013).

Guo, Y., K. Li, X. Yu, J. H. Clark, "Mesoporous $H_3PW_{12}O_{40}$-silica composite: Efficient and reusable solid acid catalyst for the synthesis of diphenolic acid from levulinic acid," Applied Catalysis B: Environmental, 81, 182–191 (2008).

Haber, J., L. Matachowski, D. Mucha, J. Stoch, P. Sarv, "New Evidence on the Structure of Potassium Salts of 12-Tungstophosphoric Acid, $K_xH_{3-x}PW_{12}O_{40}$,"Inorganic Chemistry, 44, 6695-6703 (2005).

Haber, J.,K. Pamin, L. Matachowski, D. Mucha, "Catalytic performance of the dodecatungstophosphoric acid on different supports," Applied Catalysis A: General, 256, 141–152 (2003).

Hara, M., "Biodiesel Production by Amorphous Carbon Bearing SO_3H, COOH and Phenolic OH Groups, a Solid Brønsted Acid Catalyst," Topics in Catalysis, 53, 805-810 (2010).

Herrera, J. E., J. H. Kwak, J. Z. Hu, Y. Wang, C. H. F. Peden, "Effects of Novel Supports on the Physical and Catalytic Properties of Tungstophosphoric Acid for Alcohol Dehydration Reactions," Topic in Catalysis, 49, 259 – 267 (2008).

Hoffmann, G., "The chemistry and technology of edible oils and fats and their higher fat products," Academic Press, London, UK, pp. 9-10(1989).

http://www.epa.gov/nrmrl/std/war/sim_war.htm accessed 8 August, 2014, 8.27 pm

Huang, S., F. Chen, S. Liu, Q. Zhu, X. Zhu, W. Xin, Z. Feng, C. Li, Q. Wang, L. Xu, "The influence of preparation procedures and tungsten loading on the metathesis activity of ethene and 2-butene over supported WO_3 catalysts,"Journal of molecular catalysis. A: Chemical, 267, 224-233 (2007).

Inumaru, K., T. Ishihara, Y. Kamiya, T. Okuhara, S. Yamanaka, "Water-Tolerant, Highly Active Solid Acid Catalysts Composed of the Keggin-Type Polyoxometalate $H_3PW_{12}O_{40}$ Immobilized in Hydrophobic Nanospaces of Organomodifiesd Mesoporous Silica," Angewandte Chemie International Edition, 46, 7625 – 7628 (2007).

Issariyakul, T., A. K. Dalai, "Biodiesel Production from Greenseed Canola Oil," Energy and Fuels, 24, 4652–4658 (2010).

Izumi, Y., "Hydration/hydrolysis by solid acids," Catalysis Today, 33, 371 – 409 (1997).

Kafuku, G., M. K. Lam, J. Kansedo, K. T. Lee, M. Mbarawa, "*Croton megalocarpus* oil: A feasible non-edible oil source for biodiesel production," Bioresource Technlogy, 101, 7000-7004 (2010).

Katadaa, N., M. Niwa, "Analysis of Acidic Properties of Zeolitic and Non-Zeolitic Solid Acid Catalysts Using Temperature-Programmed Desorption of Ammonia," Catalysis surveys from Asia, 8, 161-170 (2004).

Khder, A. E. R., "Preparation, characterization and catalytic activity of tin oxide-supported 12-tungstophosphoric acid as a solid catalyst," Applied Catalysis A: General, 343, 109 – 116 (2008).

Kiss, A. A., A. C. Dimian, G. Rothenberg, "Solid Acid Catalysts for Biodiesel Production - Towards Sustainable Energy," Advanced Synthesis and Catalysis, 348, 75-81 (2006).

Klepacova, K., D. Mravec, E. Hajekova, M. Bajus, "Etherification of glycerol for diesel fuels," Petroleum and Coal, 45, 54–57 (2003).

Kozhevnikov, I. V., "Sustainable heterogeneous acid catalysis by heteropoly acids," Journal of Molecular Catalysis, 262, 86 – 92 (2007).

Kozhevnikov, I. V., "Heterogeneous acid catalysis by heteropoly acids: Approaches to catalyst deactivation," Journal of Molecular Catalysis A: Chemical, 305, 104–111 (2009).

Kulkarni, M. G., R. Gopinath, L. C. Meher, A. K. Dalai, "Solid acid catalyzed biodiesel production by simultaneous esterification and transesterification," Green Chemistry, 8, 1056 – 1062 (2006).

Kulkarni, M.G., A. K. Dalai, "Waste Cooking Oil ─ An Economical Source for Biodiesel: A Review," Industrial and Engineering Chemistry Research, 45, 2901-2913 (2006).

Lavarez, M., M. J. Ortiz, J. L. Ropero, M. E. Nin, R. Rayon, F. Tzompantzi, R. Gomez, "Evaluation of Sulfated Aluminas Synthesized via the Sol-Gel Method in the Esterification of Oleic Acid with Ethanol," Chemical Engineering Communication, 196, 1152–1162 (2009).

Legagneux, N., J. Basset, A. Thomas, F. Lefebvre, A. Goguet, J. S´a*b*, C. Hardacre, "Characterization of silica-supported dodecatungstic heteropolyacids as a function of their dehydroxylation temperature," Dalton transactions, 12, 2235-2240 (2009).

Leng, Y., J. Wang, D. Zhu, Y. Wu, P. Zhao, "Sulfonated organic heteropolyacid salts: Recyclable green solid catalysts for esterifications," Journal of Molecular Catalysis A: Chemical, 313, 1–6 (2009).

Li, X., B. Li, J. Xu, Q. Wang, X. Pang, X. Gao, Z. Zhou, J. Piao, "Synthesis and characterization of Ln-ZSM-5/MCM-41 (Ln = La, Ce) by using kaolin as raw material," Applied clay science, 50, 81–86 (2010).

Li, X., A. Zanwar, A. Jayswal, H. Lou, Y. Huang, "Incorporating Exergy Analysis and Inherent Safety Analysis for Sustainability Assessment of Biofuels," Industrial and Engineering Chemistry Research, 50, 2981-2993 (2011).

Li, S., C. L. Guenther, M. S. Kelley, D. A. Dixon, "Molecular Structures, Acid−Base Properties, and Formation of Group 6 Transition Metal Hydroxides," The Journal of Physical Chemistry: C, 115, 8072-8103 (2011).

Liao, X., S. G. Wang, X. Xiang, Y. Zhu, X. She, Y. Wang, "SO_3H-functionalized ionic liquids as efficient catalysts for the synthesis of bioadditives," Fuel Processing Technology, 96, 74–79 (2012).

Lichtenthaler, H. K., "Chlorophylls and Carotenoids: Pigments of Photosynthetic Biomembranes," Methods in Enzymology, 148, 350–382 (1987).

Lin, Y. C., Yang, P. M., Chen, S. C., Tu, Y. T., J. F., Lin, "Biodiesel production assisted by 4-allyl-4-methylmorpholin-4-ium`bromine ionic liquid and a microwave heating system," Applied Thermal Engineering, 61, 570-576 (2013).

Lopez, D. E., J. G. Goodwin Jr., D. A. Bruce and S. Furuta, "Esterification and transesterificationusing modified-zirconia catalysts," Applied Catalysis A: General, 339, 76 – 83 (2008).

Lopez-Salinas, E., J. G. Hernandez-Cortez, E. Torres-Garcia, J. Navarrete, A. Gutierrez-Carrillo, T. Lopez, P. P. Lottici, D. Bersani, "Thermal stability of 12-tungstophosphoric acid supported on zirconia," Applied catalysis. A: General, 193, 215-225 (2000).

Lotero, E., Y. Liu, D. E. Lopez, K. Suwannakarn, D. A. Bruce, J. G. Goodwin, "Synthesis of Biodiesel via Acid Catalysis,"Industrial and Engineering Chemistry Research,44, 5353 – 5363 (2005).

Manna, J. S., S. Basu, M. K. Mitra, S. Mukherjee, G. C. Das, "Study on the biostability of chlorophyll a entrapped in silica gel nanomatrix," Journal of materials science. Materials in electronics, 20, 1068–1072 (2009).

Marchetti, J. M., A. F. Errazu, "Technoeconomic study of supercritical biodiesel production plant," Energy conversion and Management, 49, 2160 – 2164 (2008).

Marrero, J., R. Gani, "Group-contribution based estimation of pure component properties," Fluid Phase Equilibria, 183-184, 183-208 (2001).

Matachowski, L., A. Zieba, M. Zembala, A. Drelinkiewicz,"A Comparison of Catalytic Properties of $Cs_xH_{3-x}PW_{12}O_{40}$ Salts of Various Cesium Contents in Gas Phase and Liquid Phase Reactions," Catalysis Letters, 133, 49–62 (2009).

McCormick, R. L., S. K. Boonrueng, A. M. Herring, "In situ IR and temperature programmed desorption-mass spectrometry study of NO absorption and decomposition by silica supported 12-tungstophosphoric acid," Catalysis Today, 42, 145-157 (1998).

Melero, J. A., L. F. Bautista, J. Iglesias, G Morales, R. Sa´nchez-Va´zquez, I. Sua´rez-Marcos, "Biodiesel Production Over Arenesulfonic Acid-Modified Mesostructured

Catalysts: Optimization of Reaction Parameters Using Response Surface Methodology," Topics in Catalysis, 53, 795-804 (2010).

Melero, J. A., G. Vicente, M. Paniagua, G. Morales, P. Mu˜noz, "Etherification of biodiesel-derived glycerol with ethanol for fuel formulation over sulfonic modified catalysts," Bioresource Technology, 103, 142-151 (2012).

Mihailova, B., V. Valtchev, S. Mintova, A.C. Faust, N. Petkov, T. Bein, "Interlayer stacking disorder in zeolite beta family: a Raman spectroscopic study," Physical chemistry chemical physics, 7, 2756-2763 (2005).

Ming, H., C. Wei, L. X. Mei, D. X. Yan, "Immobilization of 12-phosphotungstic heteropolyacid on amine-functionalized SiO_2 for tetrahydrofuran polymerization," Chinese Science Bulletin, 55, 2652-2656 (2010).

Mokaya, R., W. Jones, M. E. Davies, M. E. Whittle, "Chlorophyll adsorption by alumina-pillared acid-activated clays," Journal of the American Oil Chemists' Society, 70, 241-244 (1993).

Moller, K., B. Yilmaz, R. M. Jacubinas, U. Muller, T. Bein, "One-Step Synthesis of Hierarchical Zeolite Beta via Network Formation of Uniform Nanocrystals," Journal of the American Chemical Society, 133, 5284-5295 (2011).

Molnar, A., T. Beregszasi, A. Fudala, B. Torok, M. Rozsa-Tarjani, I. Kiricsi, "Preparation, characterization and application of new, supported, superacidic heteropolyacid caesium salts," Special publication, 216, 25 – 30 (1998).

Moradi, G.R.,S. Dehghani, F. Khosravian, A. Arjmandzadeh, "The optimized operational conditions for biodiesel production from soybean oil and application of artificial neural networks for estimation of the biodiesel yield," Renewable Energy, 50, 915-920 (2013).

Morales-Pacheco, P., J. M. Domínguez, L. Bucio, F. Alvarez, U. Sedran, M. Falco, "Synthesis of FAU(Y) and MFI(ZSM5)-nanosized crystallites for catalytic cracking of 1,3,5-triisopropylbenzene," Catalysis Today, 166, 25-38 (2011).

Mozgawa, M., "The influence of some heavy metals cations on the FTIR spectra of zeolites," Journal of Molecular Structure, 555, 299-304 (2000).

Nandiwalea, K. Y., S. K. Sonara, P. S. Niphadkara, P. N. Joshi, S. S. Deshpandea, V. S. Patil, V. V. Bokadea, "Catalytic upgrading of renewable levulinic acid to ethyl

levulinate biodiesel using dodecatungstophosphoric acid supported on desilicated H-ZSM-5 as catalyst," Applied Catalysis A: General, 460– 461, 90– 98 (2013).

Narasimharao, K., D. R. Brown, A. F. Lee, A. D. Newman, P. F. Siril, S. J. Tavener, K. Wilson, "Structure–activity relations in Cs-doped heteropolyacid catalysts for biodiesel production," Journal of Catalysis,248, 226–234 (2007).

Naskar, M. K., D. Kundu, M. Chatterjee, "Synthesis of ZSM-5 Zeolite Particles Using Triethanol Amine as Structure-Directing Agent," Journal of the American Ceramic Society, 95, 449-452 (2012).

Niwa, M., N. Katada, "Measurements of acidic property of zeolites by temperature programmed desorption of ammonia," Catalysis surveys from Japan, 1, 215-226 (1997).

NOAA. Chemical Reactivity Worksheet; NOAA's office of Response and Restoration

Ohrenberg, A., C. von Tçrne, A. Schuppert, B. Knab, "Application of Data Mining and Evolutionary Optimization inCatalyst Discovery and High-Throughput Experimentation –Techniques, Strategies, and Software," QSAR & Combinatorial Science, 24, 29-37 (2005).

Olejniczak, Z., B. Sulikowskia, A. Kubacka, M. Gasior, "Heterogenization of 12-tungstophosphoric acid on stabilized zeolite Y," Topics in catalysis, 11/12, 391-400 (2000).

Ong, L. K., A. Kurniawan, A. C. Suwandi, C. X. Lin, X. S. Zhao, S. Ismadji, "Transesterification of leather tanning waste to biodiesel at supercriticalcondition: Kinetics and thermodynamics studies," The Journal of supercritical fluids, 75, 11-20 (2013).

Okuhara, T., H. Watanabe, T. Nishimura, K. Inumaru, M. Misono, "Microstructure of Cesium Hydrogen Salts of 12-Tungstophosphoric Acid Relevent to Novel Acid Catalysis," Chemistry of Masterials, 12, 2230 – 2238 (2000).

Okuhara, T., T. Nakato, "Catalysis by porous heteropoly compounds," Catalysis Surveys from Japan, 2, 31–44 (1998).

Pamin, K., A. Kubacka, Z. Olejniczak, J. Haber, B. Sulikowski, "Immobilization of dodecatungstophosphoric acid on dealuminated zeolite Y: a physicochemical study," Applied catalysis A: General, 194–195, 137–146 (2000).

Papai, I., A. Goursot, F. Fajula, "Density Functional Calculations on Model Clusters of Zeolite-β," Journal of Physical Chemistry, 98, 4654–4659 (1994).

Park, J. R., B. K. Kwak, D. S. Park, T. Y. Kim, Y. S. Yun, J. Yi, "Effect of acid type in WO_Xclusters on the esterification of ethanol with acetic acid," Korean Journal of Chemical Engineering, 29, 1695-1699 (2012).

Patel, A., N. Narkhede, "12-Tungstophosphoric Acid Anchored to Zeolite Hβ: Synthesis, Characterization, and Biodiesel Production by Esterification of Oleic Acid with Methanol," Energy and Fuels, 26, 6025−6032 (2012).

Perez-Ramirez, J. C., H. Christensen, K. Egeblad, C. H. Christensen, J. C. Groen, "Hierarchical zeolites: enhanced utilisation of microporous crystals in catalysis by advances in materials design," Chemical Society Reviews, 37, 2530-2542 (2008).

Peters, M., D. Glasser, D. Hildebrandt, S. Kauchali., "Membrane Process Design Using Residue Curve Maps," 1st Edition, John Wiley & Sons Inc., USA, pp. 8-9 (2011).

Prabhakarn, A., J. A. Fereiro, C. Subrahmanyam, "Esterification of Methacrylic acid with Ethylene glycol over Heteropolyacid supported on ZSM-5," Journal of Korean Chemical Society, 55, 14-18, (2011).

Rawks, R., P. J. V. Santen, "A possible role for singlet oxygen in the initiation of fatty acid autoxidation," Journal of the American Oil Chemists' Society, 47, 121 – 125 (1970).

Reid, R. C., J. M. Prausnitz, B. E. Poling, "The Properties of Gases and Liquids," 4th editition, Mc-Graw-Hill Book Company, Virginia, USA, pp.14-20 (1987).

Reyes, J. F., M.A. Sepúlveda, "PM-10 emissions and power of a Diesel engine fueled with crude and refined Biodiesel from salmon oil," Fuel, 85, 1714–1719 (2006).

Rothenberg, G., "Data mining in catalysis: Separating knowledge from garbage," Catalysis Today, 137, 2–10 (2008).

Sabah, E., "Decolorization of vegetable oils: Chlorophyll-a adsorption by acid-activated sepiolite," Journal of colloid and interface science, 310, 1-7 (2007).

Saleh, J., A. Y. Tremblay, M. A. Dube, "Glycerol removal from biodiesel using membrane separation technology," Fuel, 89, 2260-2266 (2010).

Satish kumar, G., M. Vishnuvarthan, M. Palanichamy, V. Murugesan, "SBA-15 supported HPW: Effective catalytic performance in the alkylation of phenol," Journal of Molecular Catalysis A: Chemical, 260, 49-55 (2006).

Satterfield, C. N., "Mass Transfer in Heterogeneous Catalysis," M.I.T Press, Massachusetts, USA, pp.16–19 (1970).

Sathyaselvabala, V., S. Ponnusamy, P. M. Periyaraman, D. K. Selvaraj, V. Thangaraj, S. Subramanian, "Two step biodiesel production from *Calophyllum inophyllum* oil: Studies on thermodynamic and kinetic modelling of modified β-zeolite catalysed pre-treatment," The Canadian Journal of Chemical Engineering, 90, 1178-1185 (2012).

Sawant, D. P., J. Justus, V. V. Balasubramanian, K. Ariga, P. Srinivasu, S. Velmathi, S. B. Halligudi, A. Vinu, "Heteropoly Acid Encapsulated SBA-15/TiO_2 Nanocomposites and Their Unusual Performance in Acid-Catalysed Organic Transformations," Chemistry - A European Journal, 14, 3200-3212 (2008).

Sdrula, N., "A study using classical or membrane separation in the biodiesel process," Desalination, 250, 1070-1072 (2010).

Shetty, S., S. Pal, D. G. Kanhere, A. Goursot, "Structural, Electronic, and Bonding Properties of Zeolite Sn-Beta: A Periodic Density Functional Theory Study," Chemistry - A European Journal, 12, 518-523 (2006).

Shi, C., R. Wang, G. Zhu, S. Qiu, J. Long, "Synthesis, Characterization, and Catalytic Properties of SiPW-X Mesoporous Silica with Heteropolyacid Encapsulated into Their Framework," European Journal of Inorganic Chemistry, 23, 4801-4807 (2005).

Shi, W., J. Zhao, X. Yuan, S. Wang, X. Wang, M. Huo, "Effects of Brønsted and Lewis Acidities on Catalytic Activity of Heteropolyacids in Transesterification and Esterification Reactions," Chemical Engineering Technology, 35, 347-352 (2012).

Shimizu, K., K. Nimi, A. Satsuma, "Polyvalent-metal salts of heteropolyacid as catalyst for Fridel-Crafts alkylation reactions," Applied Catalysis A: General, 349, 1–5 (2008).

Soleimani, R., N. A. Shoushtari, B. Mirza, A. Shahid, "Experimental investigation, modeling and optimization of membrane separation using artificial neural network

and multi-objective optimization using genetic algorithm," Chemical engineering research and design, 91, 883–903 (2013).

Srilatha, K., B. L. A. Prabhavathi Devi, N. Lingaiah, R. B. N. Prasad, P. S. Sai Prasad, "Biodiesel production from used cooking oil by two-step heterogeneous catalyzed process," Bioresource Technology, 119, 306–311 (2012a).

Srilatha, K., B. L. A. Prabhavathi Devi, N. Lingaiah, R. B. N. Prasad, P. S. Sai Prasad, N. Lingaiah, "Preparation of biodiesel from rice bran fatty acids catalyzed by heterogeneous cesium-exchanged 12-tungstophosphoric acids," Bioresource Technology, 116, 53–57 (2012b).

Srilatha, K., N. Lingaiah, P. S. Sai Prasad, B.L.A. Prabhavathi Devi, R. B. N. Prasad, "Kinetics of the esterification of palmitic acid with methanol catalyzed by 12-tungstophosphoric acid supported on ZrO_2," Reaction Kinetics, Mechanisms and Catalysis, 104, 211-226 (2011).

Srilatha, K., T. Issariyakul, N. Lingaiah, P. S. Sai Prasad, J. Kozinski, A. K. Dalai, "Efficient Esterification and Transesterification of Used Cooking Oil Using12-Tungstophosphoric Acid (TPA)/Nb_2O_5 Catalyst," Energy and Fuels, 24, 4748–4755 (2010).

Srilatha, K., N. Lingaiah, B. L. A. Prabhavathi Devi, R. B. N. Prasad, S. Venkateswar, P. S. Sai Prasad, "Esterification of free fatty acids for biodiesel production over heteropoly tungstate supported on niobia catalysts," Applied Catalysis A: General, 365, 28–33 (2009).

Srivastava, A., R. Prasad, "Triglycerides-based diesel fuels," Renewable and Sustainable Energy Reviews, 4, 111 – 133 (2000).

Su, C. H., "Kinetic study of free fatty acid esterification reaction catalyzed by recoverable and reusable hydrochloric acid," Bioresource Technology, 130, 522-528 (2013).

Sun, L., Q. Zhao, G. Zhu, Y. Zhou, T. Wang, Y. Shan, K. Yang, Z. Liang, L. Zhang, Y. Zhang, "Octyl-functionalized hybrid magnetic mesoporous microspheres for enrichment of low-concentration peptides prior to direct analysis by matrix-assisted laser desorption/ionization time-of-flight mass spectrometry," Rapid Communications in Mass Spectrometry, 25, 1257-1265 (2011).

Sunita, G., B. M. Devassy, A. Vinu, D. P. Sawant, V. V. Balasubramanian, S. B. Halligudi, "Synthesis of biodiesel over zirconia-supported isopoly and heteropoly tungstate catalysts," Catalysis Communications, 9, 696–702 (2008).

Talley, T. M., J. R. Talburt, Y. Chan, "Data Engineering-Mining, Information and Intelligence," Springer, Newyork, USA, pp. 1-16(2010).

Tesser, R., L. Casale, D. Verde, M. Di Serio, E. Santacesaria, "Kinetics of free fatty acids esterification: Batch and loop reactor modeling," Chemical Engineering Journal, 154, 25-33 (2009).

Thomas, A. C. Dablemont, J. M. Basset, F. C. R. Lefebvre, "Comparison of $H_3PW_{12}O_{40}$ and $H_4SiW_{12}O_{40}$ heteropolyacids supported on silica by 1H MAS NMR," Chimie, 8, 1969–1974 (2005).

Thommes, M., R. Kohn, M. Froba, "Sorption and Pore Condensation Behavior of Nitrogen, Argon, and Krypton in Mesoporous MCM-48 Silica Materials,"Journal of Physical Chemistry: B, 104, 7932-7943 (2000).

Thouvenot, R., M. Fournier, R. Franck, C. Rochhiccioli-deltcheff, "Vibrational Investigations of Polyoxometalates. 3. Isomerism in Molybdenum (V1) and Tungsten (V1) Compounds Related to the Keggin Structure," Inorganic Chemistry, 23, 598-605 (1984).

Towler, G., R. Sinnott, "Principles, Practice and Economics of Plant and Process design," 2nd edition, Elsevier, UK, pp. 1077-1083 (2013).

Turton, R., R. C. Bailie, W. B. Whiting, J. A. Shaeiwitz, D. Bhattacharyya, "Analysis, Synthesis, and Design of Chemical Processes," 4th edition, Prentice Hall, Upper Saddle River, New Jersey, USA, pp. 164-310 (2012).

Trakarnpruk, W., "Supported cesium polyoxotungstates as catalysts for the esterification of palm fatty acid distillate," Mendeleev Communications,23, 46–48 (2013).

Trippe, F., M. Frohling, F. Schultmann, E. Henrich, A. Dalai, "Comprehensive techno-economic assessment of dimethyl ether (DME) synthesis and Fischer–Tropsch synthesis as alternative process steps within biomass-to-liquid production," Fuel Processing Technology, 106, 577-586 (2013).

Tropecelo, A. I., M. H. Casimiro, I. M. Fonseca, A. M. Ramos, J. Vital, J. E. Castanheiro, "Esterification of free fatty acids to biodiesel over heteropolyacids immobilized on mesoporous silica," Applied catalysis A: General, 390, 183-189(2010).

Uchida, S., K. Inumaru, M. Misono, "States and Dynamic Behavior of Protons and Water Molecules in $H_3PW_{12}O_{40}$Pseudoliquid Phase Analyzed by Solid-State MAS NMR," Journal of Physical Chemistry: B, 104, 8108-8115 (2000).

Veljkovic, V. B., J. M. Avramovic, O. S. Stamenkovic, "Biodiesel production by ultrasound-assisted transesterification: State of the art and the perspectives," Renewable and Sustainable Energy Reviews, 16, 1193-1209 (2012).

Wagner, T., S. Haffer, C. Weinberger, D. Klaus, M. Tiemann, "Mesoporous materials as gas sensors,"Chemical Society Review, 42, 4036-4053 (2013).

Wang, X., K. S. K. Lin, J. C. C. Chen, S. Cheng, "Preparation of ordered large pore SBA-15 silica functionalized with aminopropyl groups through one-pot synthesis," Chemical Communications, 23, 2762-2763 (2004).

Wang, X., K. S. K. Lin, J. C. C. Chen, S. Cheng, "Direct Synthesis and Catalytic Applications of Ordered Large Pore Aminopropyl-Functionalized SBA-15 Mesoporous Materials," 109, 1763-1769 (2005).

Wang,J., L. Yan, G. Qian, K. Yang, H. Liu, X. Wang, "Heteropolyacid encapsulated into mesoporous silica framework for an efficient preparation of 1,1-diacetates from aldehydes under a solvent-free condition," Tetrahedron Letter, 47, 8309-8312 (2006).

Wessendorf, R., Erdol, K. Erdgas, "Derivatives of glycerol as components of fuels," Petrochemie, 48, 138-142 (1995).

West, A. H., D. Posarac, N. Ellis, "Assessment of four biodiesel production processes using HYSYS.Plant," Bioresource Technology, 99, 6587-6601 (2008).

Wong, M. S., W. V. Knowles, "Surfactant-templated mesostructured materials: synthesis and compositional control" in "Nanoporous Materials, Science and Engineering, Series on Chemical Engineering", Lu G. Q. and X. S. Zhao, eds., Imperial College Press, UK, pp.125 (2006).

Wu, Y., X. Ye, X. Yang, X. Wang, W. Chu, H. Yucai, "Heterogenization of Heteropolyacids: A General Discussion on the Preparation of Supported Acid

Catalysts," Industrial and Engineeringand Chemistry Research, 35, 2546-2560 (1996).

Xiao, L., J. Mao, J. Zhou, X. Guo, S. Zhang, "Enhanced performance of HY zeolites by acid wash for glycerol etherification with isobutene," Applied catalysis. A: General, 393, 88–95 (2011).

Xu, L., W. Li, J. Hu, X. Yang, Y. Guo, "Biodiesel production from soybean oil catalyzed by multifuncitionalized Ta_2O_5/SiO_2-[$H_3PW_{12}O_{40}$/R] (R = Me or Ph) hybrid catalyst," Applied Catalysis B: Environmental, 90, 587-594 (2009a).

Xu, L., W. Li, J. Hu, K. Li, X. Yang, F. Ma, Y. Guo, X. Yu, Y. Guo, "Transesterification of soybean oil to biodiesel catalyzed by mesostructured Ta_2O_5-based hybrid catalysts functionalized by both alkyl-bridged organosilica moieties and Keggin-type heteropoly acid," Journal of Material Chemistry, 19, 8571–8579 (2009b).

Xu, L., X. Yang, X. Yu, Y. Guo,Maynurkader, "Preparation of mesoporous polyoxometalate–tantalum pentoxide composite catalyst for efficient esterification of fatty acid," Catalysis Communications, 9, 1607–1611 (2008).

Yadav, G. D., N. S. Asthana and V. S. Kamble, "Cesium-substituted dodecantungstophosphoric acid on K-10 clay for benzoylation of anisole with benzoyl chloride," Journal of Catalysis, 217, 88 -99 (2003).

Yadav, G. D., "Synergism of clay and heteropoly acids as nano-catalysts for the development of green processes with potential industrial applications," Catalysis Surveys from Asia, 9, 117-137 (2005).

Yadav, G. D., H. N. Manyar, "Novelties of synthesis of acetoveratrone using heteropoly acid supported on hexagonal mesoporous silica," Microporous and Mesoporous Materials, 63, 85-96 (2003).

Yadav, G. D., P. A. Chandan, N. Gopalswami, "Green etherification of bioglycerol with 1-phenyl ethanolover supported heteropolyacid," Clean Technology Environment Policy, 14, 85-95 (2012).

Yamazoe, S., Y. Hitomi, T. Shishido, T. Tanaka, "XAFS Study of Tungsten L_1- and L_3-Edges: Structural Analysis of WO_3 Species Loaded on TiO_2 as a Catalyst for Photo-oxidation of NH_3," Journal of Physical Chemistry, 112, 6869-6879 (2008).

Yang, L., Y. Qi, X. Yuan, J. Shen, J. Kim, "Direct synthesis, characterization and catalytic application of SBA-15 containing heteropolyacid $H_3PW_{12}O_{40}$," Journal of Molecular Catalysis A: Chemical, 229, 199 – 205 (2005).

Yang, X-L, R. Gao, W-L Dai, K. Fan, "Influence of Tungsten Precursors on the Structure and Catalytic Properties of WO_3/SBA-15 in the Selective Oxidation of Cyclopentene to Glutaraldehyde," Journal of Physical Chemistry: C, 112, 3819-3826 (2008).

Yori, J. C., J. M. Grau, V. M. Benı´tez, J. Sepu´lveda, "Hydroisomerization-cracking of *n*-octane on heteropolyacid $H_3PW_{12}O_{40}$ supported on ZrO_2, SiO_2 and carbon: Effect of Pt incorporation on catalyst performance," Applied catalysis. A: General, 286, 71-78 (2005).

Young, D. M., H. Cabezas, "Designing sustainable processes with simulation: the waste reduction (WAR) algorithm," Computers & chemical engineering, 23, 1477-1491 (1999).

Young, D., R. Scharp, H. Cabezas, "The waste reduction (WAR) algorithm: environmental impacts, energy consumption, and engineering economics,"Waste Management, 20, 605-615 (2000).

Yu, Y., G. Xiong, C. Li, F. Xiao, "Characterization of aluminosilicate zeolites by UV Raman spectroscopy," Microporous and mesoporous materials, 46, 23-34 (2001).

Yun, H. S., M. Kuwabara, H. S. Zhou, I. Honma, "One-step synthesis of mesoporous PWA/SiO_2 composite materials using triblock copolymer templates," Journal of materials science, 39, 2341–2347 (2004).

Zhang, R., C. Yang, "A novel polyoxometalate-functionalized mesoporous hybrid silica: synthesis and characterization," Journal of Materials Chemistry, 18, 2691–2703 (2008).

Zhang, W., Y. Leng, D. Zhu, Y. Wu, J. Wang, "Phosphotungstic acid salt of triphenyl (3-sulfopropyl) phosphonium: An efficient and reusable solid catalyst for esterification," Catalysis Communications,11, 151–154 (2009).

Zhang, X., C. Yuan, M. Li, B. Gao, X. Wang, X. Zheng, "Synthesis and characterization of mesoporous, tungsten-containing molecular sieve composites," Journal of Non-Crystalline Solids, 355, 2209–2215 (2009).

Zhang, Y., M. A. Dube, D. D. McLean, M. Kates, "Biodiesel production from waste cooking oil: 1. Process design and technological assessment," Bioresource Technology, 89, 1-16, (2003).

Zhang, Q., H. Y. Wang, X. Jia, B. Liu, Y. Yang, "One-dimensional metal oxide nanostructures for heterogeneous catalysis," Nanoscale, 5, 7175-7183 (2013).

Zhao, W., C. Yi, B.Y.J. Hu, X. Huang, "Etherification of glycerol and isobutylene catalyzed over rare earth modified Hβ-zeolite," Fuel Processing Technology, 112, 70–75 (2013).

Zhao, Q.,H. Wang, H. Zheng, Z. Sun, W. Shi, S. Wang, X. Wang, Z. Jiang, "Acid–base bifunctional HPA nanocatalysts promoting heterogeneous transesterification and esterification reactions,"Catalysis Science and Technology, 3, 2204-2209 (2013).

Zheng, S., M. Kates, M. A. Dube, D. D. McLean, "Acid-catalyzed production of biodiesel from waste frying oil," Biomass & bioenergy, 30, 267–272 (2006).

Zheng, J., Y. Yi, W. Wang, K. Guo, J. Ma, R. Li, "Synthesis of bi-phases composite zeolites MFZ and its hierarchical effects in isopropylbenzene catalytic cracking," Microporous and Mesoporous Materials, 171, 44–52 (2013).

Zheng, J., Q. Zeng, Y. Yi, Y. Wang, J. Ma, B. Qin, X. Zhang, W. Sun, R. Li, "The hierarchical effects of zeolite composites in catalysis," Catalysis Today, 168,124–132 (2011).

Zieba, A., L. Matachowski, J. Gurgul, E. Bielanska, A. Drelinkiewicz, "Transesterification reaction of triglycerides in the presence of Ag-doped $H_3PW_{12}O_{40}$," Journal of Molecular Catalysis A: Chemical, 316, 30–44 (2010).

Zieba, A., L. Matachowski, E. Lalik, A. Drelinkiewicz, "Methanolysis of Castor Oil Catalysed by Solid Potassium and Cesium Salts of 12-Tungstophosphoric Acid," Catalysis Letters, 127, 183–194 (2009).

APPENDIX A: ADDITIONAL DATA USED FOR MODEL VALIDATION (FOR LITERATURE REVIEW STUDY)

Example	Catalysts	Feedstock	Reaction conditions	Experimental Results	Model Prediction
1	25% TPA/SBA-15, 300°C	Triolein, no FFA present	25% TPA loading, 4.13 wt% cat. 39:1 methanol ratio, 10 h, 200°C	97.2% yield[a]	98.8% yield
2	45% TPA/H-Y, 250°C	Oleic acid	10.2% TPA loading, 13.6 wt% cat. 26:1 methanol ratio, 7.5 h, 120°C	99.9% conv. of FFA[b]	99.9% conv.
3	45% TPA/H-Y, 250°C	GSC oil and 4.25% FFA	10.2% TPA loading, 13.6 wt% cat. 26:1 methanol ratio, 7.5 h, 120°C	97.64% conv. of FFA[b]	97.37% conv.
4	10% TPA/Al_2O_3, 300°C	GSC oil and 4.25% FFA	10% TPA loading, 3 wt% cat. 6:1 methanol ratio, 10 h, 200°C	62.5% yield[c]	63.52% yield

References:

[a]Baroi, C., A. K. Dalai**,**"TPA supported on SBA-15 as solid acid catalysts for the biodiesel production," ACS symposium series, 1092, 93-109 (2012).

[b]Baroi, C., A. K. Dalai**, "**Esterification of free fatty acids (FFA) of Green Seed Canola (GSC) oilusing H-Y zeolite supported 12-Tungstophosphoric acid (TPA)," Applied Catalysis A: General,485, 99-107(2014).

[c]Kulkarni, M. G., R. Gopinath, L. C. Meher, A. K. Dalai, "Solid acid catalyzed biodiesel production by simultaneous esterification and transesterification," Green Chemistry, 8, 1056 – 1062 (2006).

APPENDIX B: CALIBRATION CURVES OF HPLC, GC

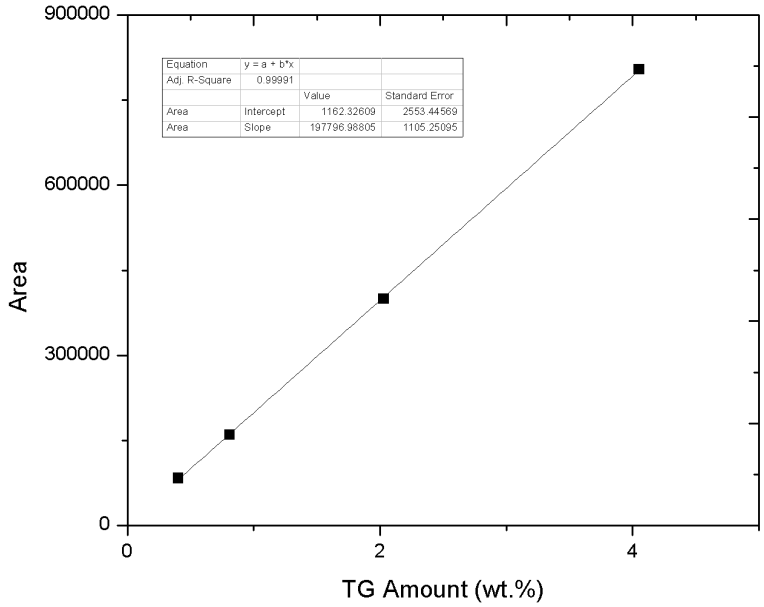

Fig. B.1 Calibration curve for TG (HPLC 1100)

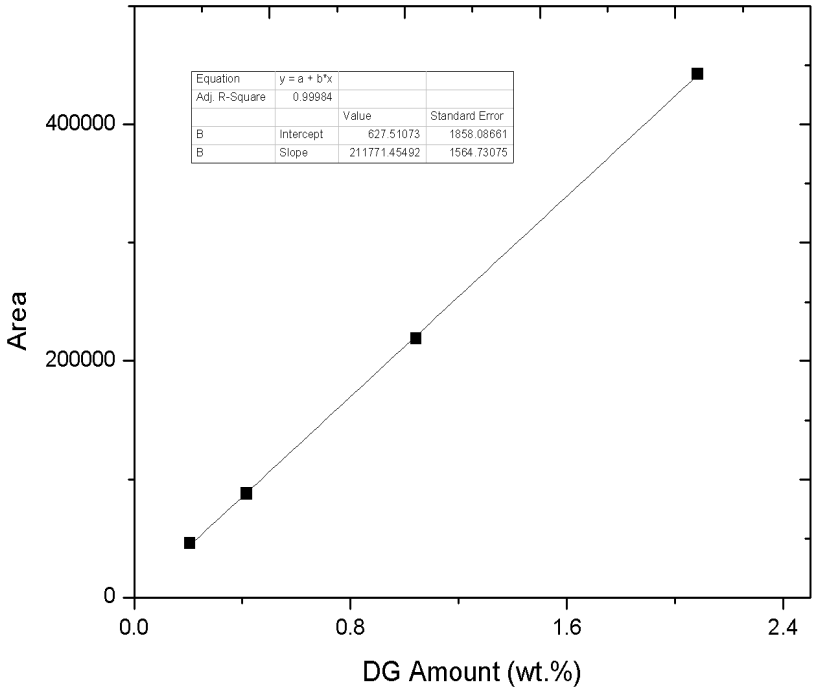

Fig. B.2 Calibration curve for DG (HPLC 1100)

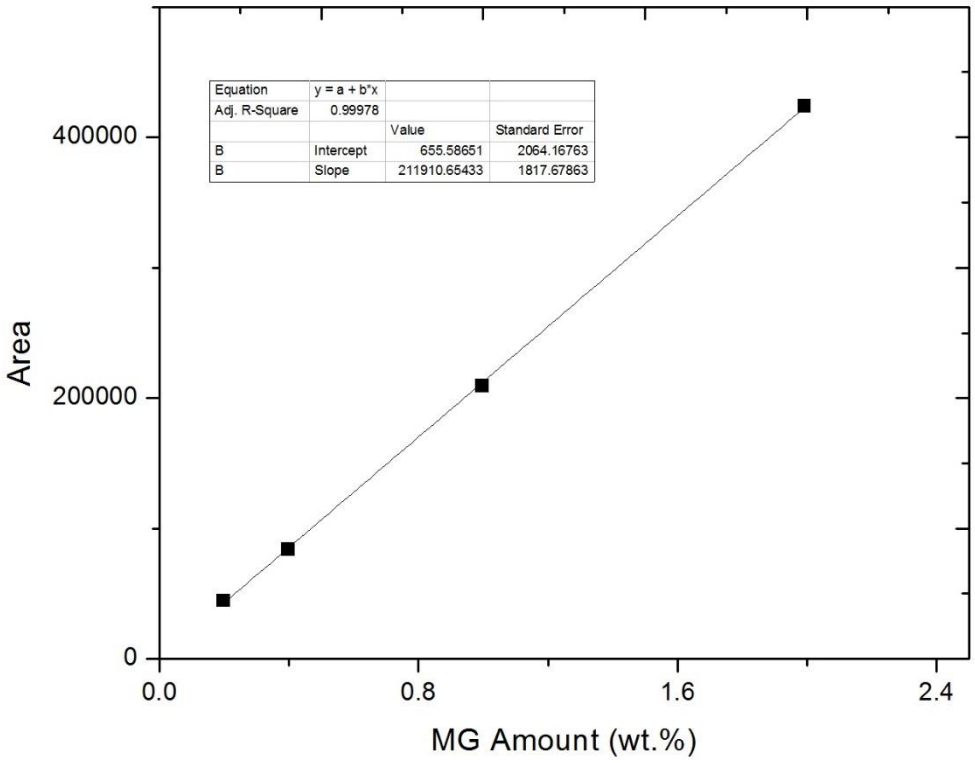

Fig. B.3 Calibration curve for MG (HPLC 1100)

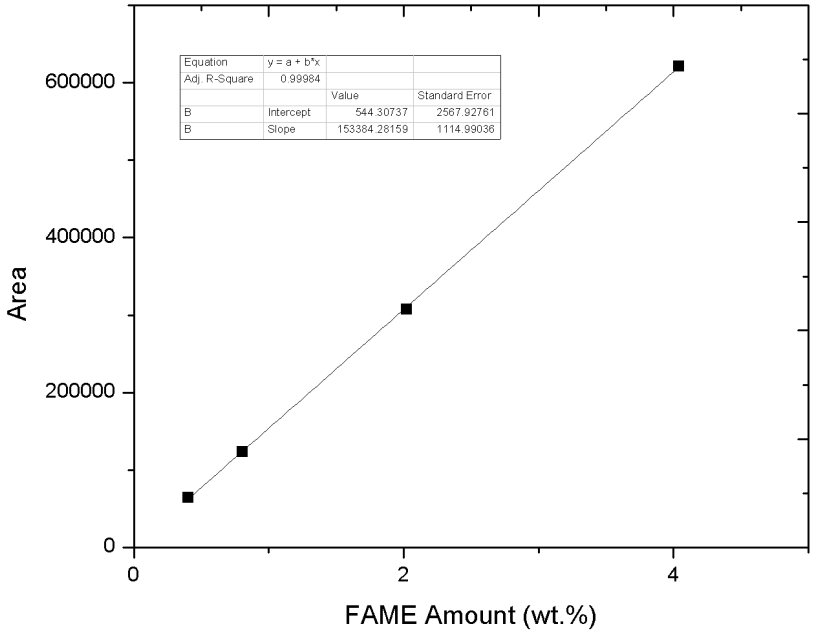

Fig. B.4 Calibration curve for FAME (HPLC 1100)

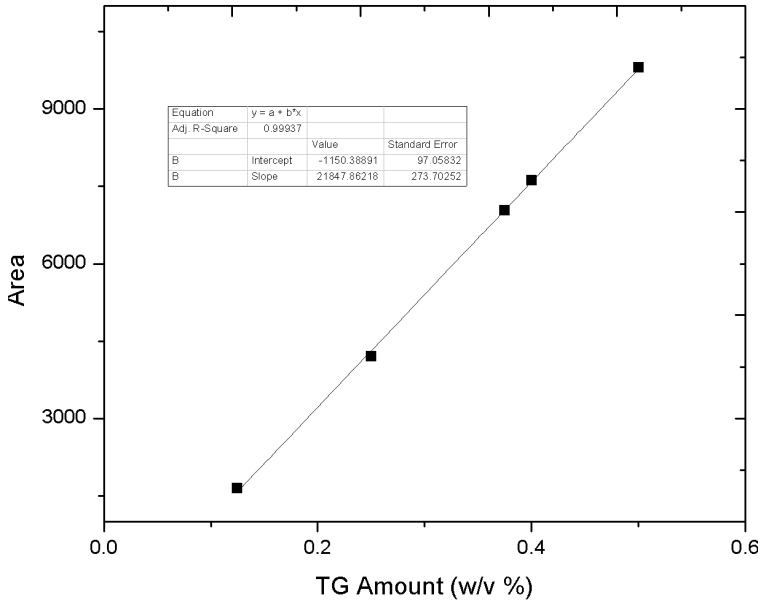

Fig. B.5 Calibration curve for TG (HPLC 1200)

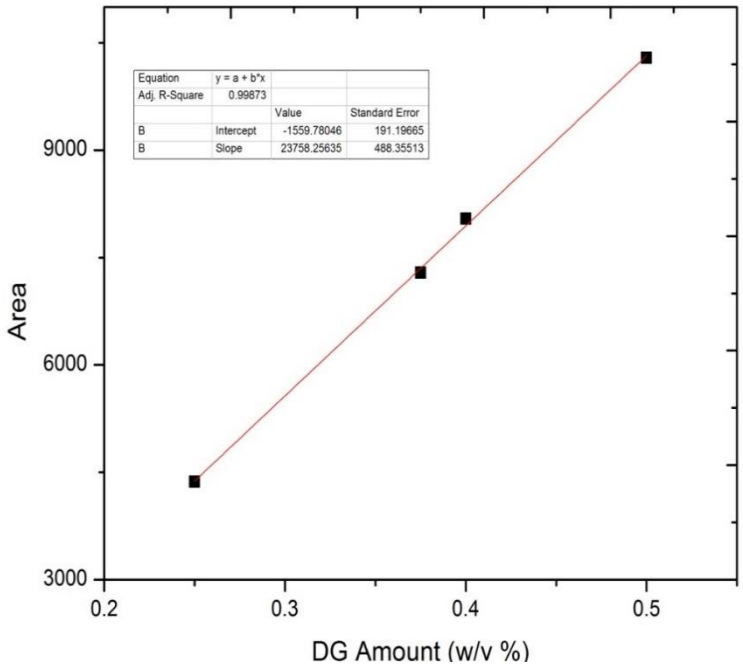

Fig. B.6 Calibration curve for DG (HPLC 1200)

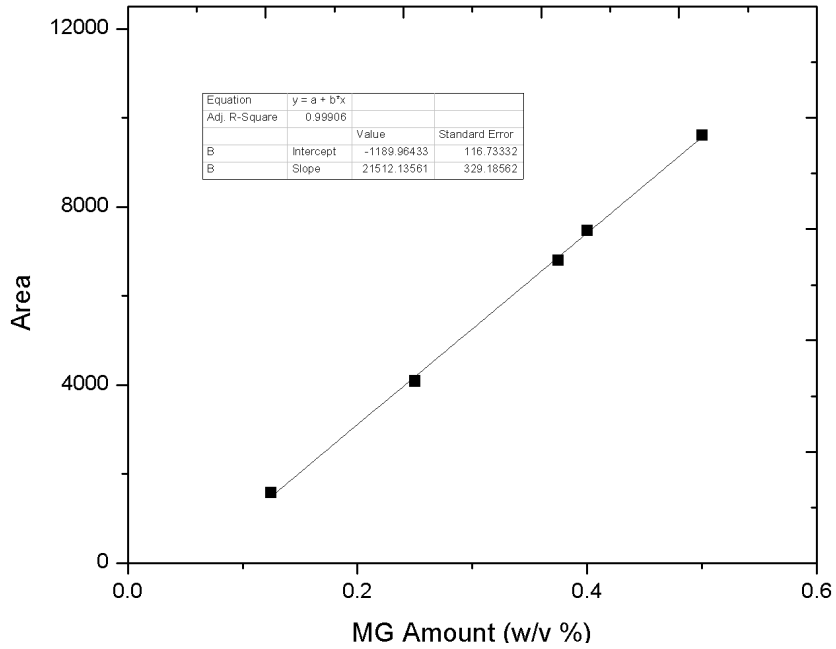

Fig. B.7 Calibration curve for MG (HPLC 1200)

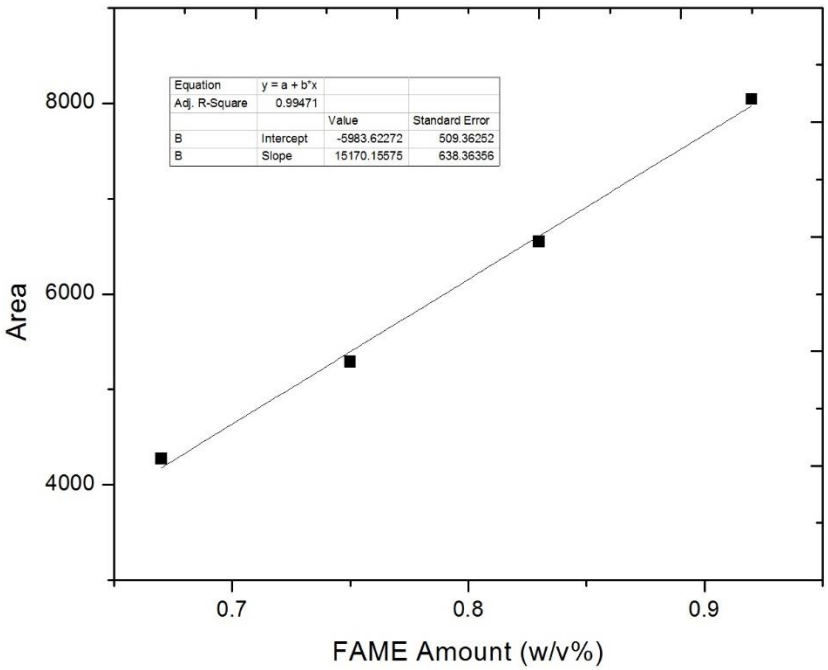

Fig. B.8 Calibration curve for FAME (HPLC 1200)

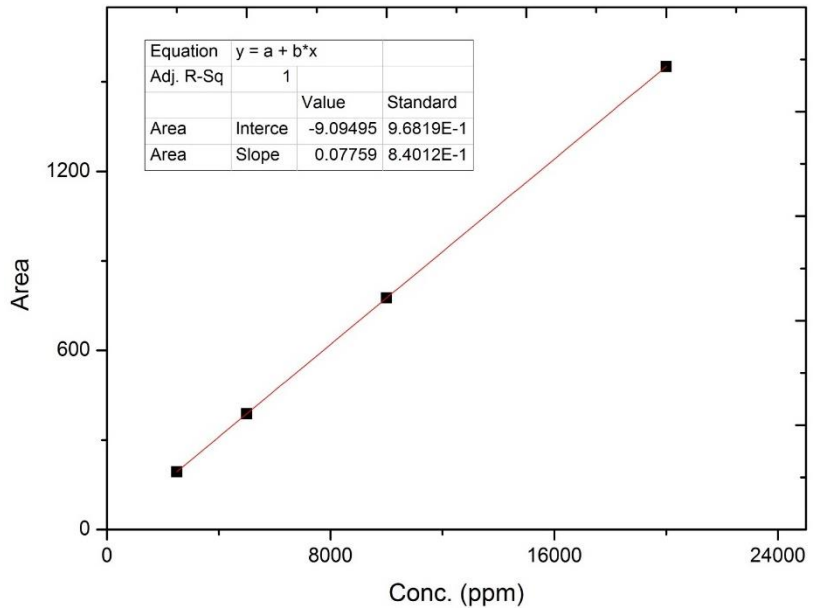

Fig. B.9 Calibration curve for Glycerol (GC HP 5890)

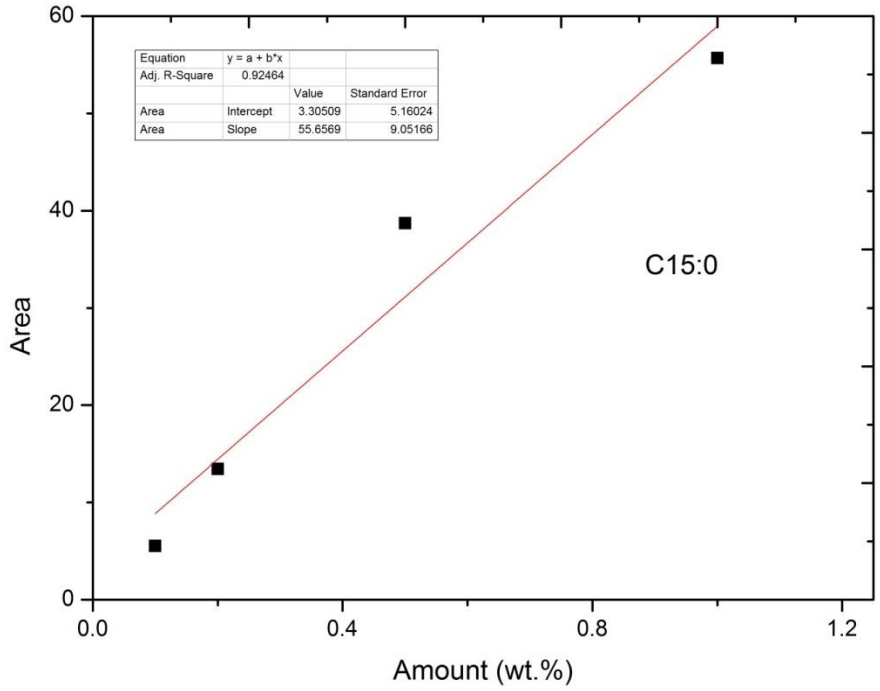

Fig. B.10 Calibration curve for FAME (GC Agilent 7890)

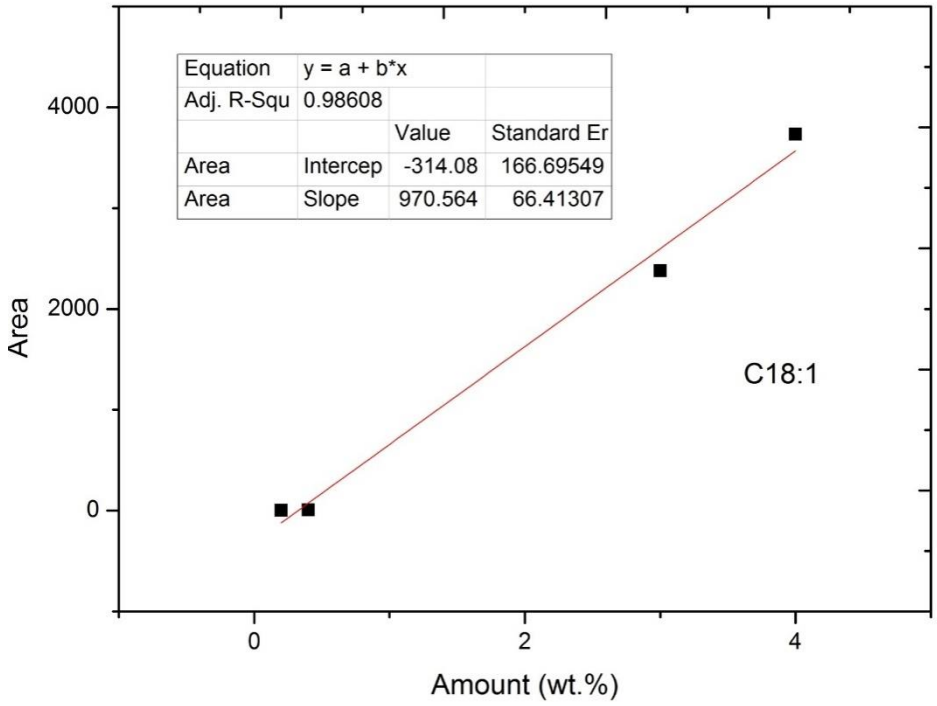

Fig. B.11 Calibration curve for FAME (GC Agilent 7890)

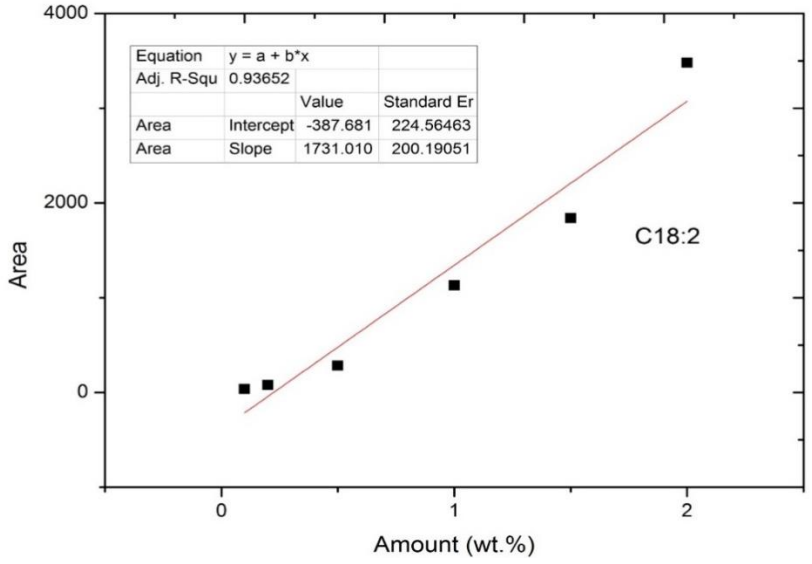

Fig. B.12 Calibration curve for FAME (GC Agilent 7890)

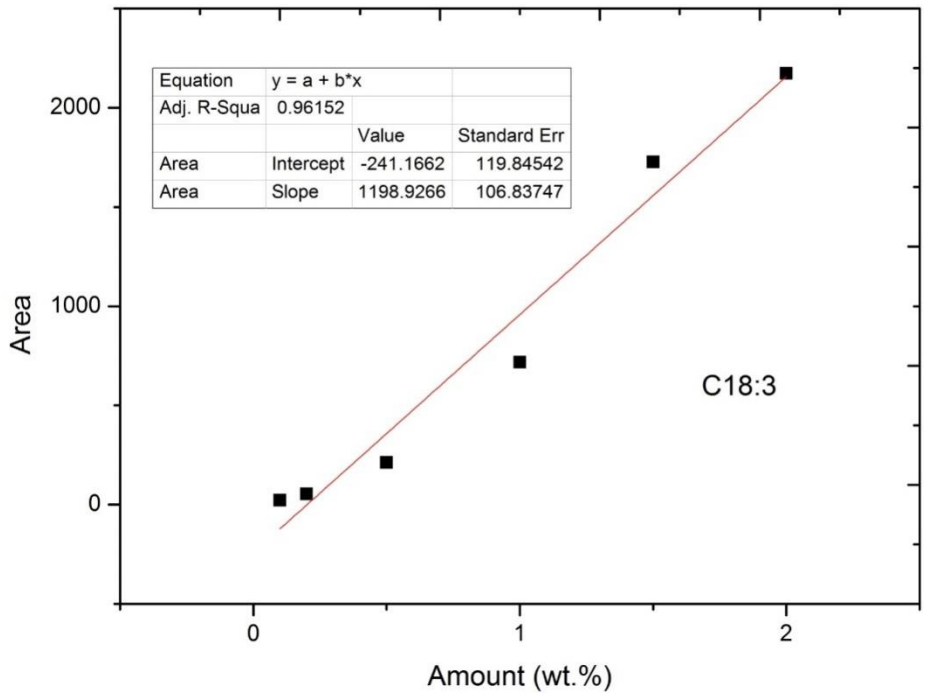

Fig. B.13 Calibration curve for FAME (GC Agilent 7890)

APPENDIX C: Confirmation of absence of external and internal mass-transfer limitations

Table C.1: Confirmation of absence of external and internal mass-transfer limitations

Chapters	Mixing intensity (Reynolds no.)	External mass-transfer		Internal mass-transfer	
		Mass transfer flux ($mol/m^2.s$)	Reaction rate ($mol/m^2.s$)	Effective diffusivity (m^2/s)	Weisz – Prater criteria
4	35186	6.27×10^{-4}	1.4×10^{-12}	1.67×10^{-12}	9.42×10^{-5}
6 (transesterification)	35186	5.82×10^{-4}	1×10^{-10}	1.67×10^{-12}	9.22×10^{-3}
6 (etherification)	5018	9.1×10^{-4}	9.3×10^{-10}	7.26×10^{-13}	3.75×10^{-4}
7	35186	1.37×10^{-4}	1.7×10^{-12}	5.59×10^{-12}	1.29×10^{-3}

APPENDIX D: THERMODYNAMIC PROPERTIES OF DIFFERENT CHEMICAL COMPOUNDS

Table D.1: Thermodynamic properties of liquid compounds

Compound	Density (kg/m^3)	Boiling Point (°C)	Critical Temp. (°C)	Critical Pressure. (bar)	Molar volume (cm^3/mole)	Accentric Factor (ω)
DG	934	485.4	657.4	4.59	2240	1.97
MG	970	391	582.8	11.54	1247	1.11
MTBG	1000	164.9	277	38.58	481.5	0.14
DTBG	940	411.2	577	24.12	626.5	0.96
TTBG	880	481.3	655	16.71	812.5	1.44

Table D.2: Thermodynamic properties of solid compounds

Sample	Molecular weight	Density (kg/m^3)	Particle size (μm)	Surface area (m^2/g)	Area/volume ratio
K-10 clay	549.1	2500	25	270	-
β zeolite	1941	2000	22	268	-
Ch-A	892	892	5	-	200
Ch-B	906	1500	5	-	200